Experimental and Theoretical Investigation of Optical Properties on Cyanostyrene Based Donor-Acceptor Systems

Thesis Submitted to the **University of Calicut** for the Award of

Doctor of Philosophy in **Chemistry**

by

Femina C

Under the supervision of

Dr. Reji Thomas

DEPARTMENT OF CHEMISTRY

FAROOK COLLEGE (AUTONOMOUS), KOZHIKODE

KERALA, INDIA – 673632

September 2025

DECLARATION

I hereby declare that the work presented in the thesis entitled "**Experimental and Theoretical Investigation of Optical Properties on Cyanostyrene Based Donor-Acceptor Systems**" is based on the original work done by me under the supervision of Dr. Reji Thomas and Dr. Sajith P. K., Assistant Professors, Department of Chemistry, Farook college (Autonomous), Kozhikode, Kerala and has not been included in any other thesis submitted previously for the award of any degree. The contents of the thesis are undergone plagiarism check using 'iTHENTICATE' software at C.H.M.K. Library, University of Calicut, and the similarity index found within the permissible limit. I also declare that the thesis is free from AI generated contents.

Femina C

U.O.No. 9362/2018/Admn

Research Supervisor: Dr. Reji Thomas

Dr. Reji Thomas
Assistant Professor
Department of Chemistry
Farook College (Autonomous)
Farook College (P.O)
Kozhikode - 673 632

Research Co-Supervisor: Dr. Sajith P K

Dr. P.K. Sajith
Assistant Professor
Department of Chemistry
Farook College, Kozhikode - 673632

Farook College
13-04-2026

FAROOK COLLEGE (AUTONOMOUS) CALICUT 673 632 P. O. FAROOK COLLEGE

CERTIFICATE

This is to certify that the work embodied in the thesis entitled "**Experimental and Theoretical Investigation of Optical Properties on Cyanostyrene Based Donor-Acceptor Systems**" submitted by **Femina C** to the University of Calicut for the award of the degree of Doctor of Philosophy in Chemistry under the Faculty of Sciences, is an authentic record of precise research work carried out at the Department of Chemistry, Farook College (Autonomous), Kozhikode, under our supervision and guidance. The contents of the thesis have been checked for plagiarism using the software 'iTHENTICATE' and the similarity index falls under permissible limit of University of Calicut. We also declare that the thesis is free from AI generated contents. We further certify that the contents of this thesis have not been submitted elsewhere for any degree or diploma. We also clarify that the corrections/suggestions recommended by the adjudicators have been incorporated in the thesis.

Farook College

13-04-2026

Research Supervisor: Dr. Reji Thomas

Dr. Reji Thomas
Assistant Professor
Department of Chemistry
Farook College (Autonomous)
Farook College (P.O)
Kozhikode - 673 632

Research Co-Supervisor: Dr. Sajith P K

Dr. P K. Sajith
Assistant Professor
Department of Chemistry
Farook College, Kozhikode - 673632

FAROOK COLLEGE (AUTONOMOUS) CALICUT 673 632 P.O. FAROOK COLLEGE

ACKNOWLEDGEMENT

Looking back on my adventurous Ph.D. journey, a lengthy path marked by challenges, trials, learning, and moments of fulfilment, I realize that reaching this milestone would not have been possible without the unwavering support, guidance, and encouragement of many individuals who have played a vital role in shaping my academic and personal growth. This acknowledgement is a humble attempt to thank them all, and I sincerely apologize for any names that may have been unintentionally left out.

I owe immense gratitude and sincere thanks to Dr. Reji Thomas, my research supervisor, for his constant guidance, support, patience, and motivation, and for providing a stimulating research environment throughout my Ph.D. journey. His strong research culture and commitment to academic excellence greatly influenced me and his expertise in research skills helped to shape and refine my own experimental abilities. His guidance and encouragement have been invaluable, significantly contributing to my personal and academic growth.

I would like to express my deepest gratitude to my co-supervisor Dr. Sajith PK for the invaluable support and guidance provided throughout my research journey. His mentorship in both theoretical studies and practical aspects of my work has greatly enriched my academic growth. I am also deeply grateful for his understanding and encouragement during challenging times and moments of difficulties along the journey. His patience, empathy, and unwavering support helped me regain confidence and persevere.

I would like to express my gratitude to Doctoral Committee members, Prof. M. T. Ramesan, Prof. N. K. Renuka, Prof. Mohamed Shahin T, and Prof. V. M. Abdul Mujeeb, for their valuable advice and comments for improving the research work.

I take this opportunity to thank the current and former principals of Farook College, Calicut. Dr Ayisha Swapna K.A., the principal of the College, Dr Naseer K.M and Prof. E P Imbichikoya, the former principals of the College, for their support in the completion of the work. I extend my sincere gratitude to Dr. Kavitha, head of the department, for providing me all necessary assistance for pursuing my research. I also thank the former heads of the Department of Chemistry Prof. PEM Abdul Rasheed and Dr. Abdul Rahim for their immense support during the journey.

I am also gratefully acknowledging all the faculty members in the department of chemistry for their support in my research journey. I also thank all the non-teaching staff of the Department of Chemistry. I extend my heartfelt gratitude to the office staff of Farook College for their assistance and support.

I would also like to make a special acknowledgement to my research collaborators for their insightful comments, valuable recommendations, and support throughout this journey. I am especially grateful to Dr. Shanthil M, Assistant Professor, Government Victoria College, Palakkad; Rajadurai Vijay Solomon, Department of Chemistry, Madras Christian College (Autonomous); Prof. Norifumi Yamamoto, Department of Applied Chemistry, Faculty of Engineering, Chiba Institute of Technology, Japan; Dr. Aijaz A Dar, Department of Chemistry, university of Kashmir for their contributions, which enriched the quality and depth of my research.

I extend my sincere thanks to Dr. Jatish Kumar, IISER Tirupati, for providing access to the photophysical measurement facilities and for his gracious arrangements that ensured a pleasant and comfortable stay during my IISERT visit. I also express my thanks to Mr. Alex P. A. (IISER, Trivandrum) for single crystal X-ray diffraction measurements and structure solving, Prof. Ratheesh K Vijayaraghavan (IISER Kolkata), Prof. Prakash P. Neelakandan (INST, Mohali) and Dr. Chinna Ayya Swamy P. (NIT Calicut) for various photophysical measurements.

I sincerely acknowledge the support of the present and former Heads of the Department of Chemistry, University of Calicut, in facilitating access to the experimental facilities. I also extend my special thanks to Dr. Fazalurahman K., for his contribution in expanding the photoluminescence emission measurement facilities. My wholehearted thanks to Dr. Deepak Joshy, Ms. Arifa K V, Ms. Nimisha, Mr. Jay, research scholars from University of Calicut, for their immense support in conducting various photophysical measurements. My deepest gratitude to Dr. Sonia M, IISER Tirupati, Ms. Afrin A, NIT Calicut for helping me various photophysical measurements.

I am greatly thankful to the Department of Science and Technology (DST) under the Women Scientist Scheme-A (WOS-A) for their generous financial support. I deeply appreciate their continued encouragement and commitment to empowering women in science and research.

My heartfelt gratitude is extended to all my past and present colleagues, especially Thufail, Farhan, Hadiya, Athira, Remya Miss, Nizamka, Rajeena Miss, Shanavas Sir and Sumayya miss for all the memorable moments and experiences we shared throughout the journey.

Above all, I wish to convey my profound gratitude to my family. I am especially grateful to my parents, 'Umma' and 'Uppa', for their unwavering love and support, for selflessly devoting their time to caring for my children during my absence, and for sustaining our family with strength and resilience while I was fully engaged in the challenges and demands of my research. I thank my siblings and in-laws for their support during the journey. I extend my sincere gratitude to my kids, Farana Faishah and Nazafarin, for their patience, resilience and understanding throughout this journey. They gracefully endured my frequent absences, long hours of work, and the emotional strains associated with the challenges of research. Their understanding and strength, despite being the innocent witnesses of my struggles, have been a silent source of motivation that carried me forward.

I am deeply indebted to my husband, Mr. Navas, for his unwavering support, understanding, and constant encouragement, which sustained me through the highs and lows of this research journey and the most challenging periods of my work.

Thank God for everything…

Femina C

ABSTRACT

Luminescent materials based on π-conjugated molecules have gained significant attention owing to their unique photophysical properties and the tunability of these properties through structural modulation. Majority of the luminophores of this class are highly emissive in the solution state while weakly emissive or non-emissive in the solid state. In this context the molecules showing aggregation induced emission found relevant for various solid state lighting applications. Among various molecules showing aggregation induced emission properties, the molecules based on intramolecular charge transfer (ICT) are found strongly emissive in both solution state and solid state. In this scenario the design and synthesis of organic π-conjugated molecules showing ICT is relevant due to their scope for active component in various optoelectronic devices and sensors with switchable photoluminescence. However, there are several strategies have emerged towards the design and synthesis of D-π-A systems with intense photoluminescence, a detailed experimental and theoretical structure-property correlation is necessary towards the design of molecules with enhanced photoluminescence and its multimode switching. Herein, this thesis pertains to the design and synthesis of cyanostyrene based organic fluorophores with strong emission and multi-stimuli responsive nature. This work details the synthesis of novel anthracene-cyanostilbene D-π-A compounds, and their structural and optoelectronic properties. The structure-property correlations are examined through structural data obtained from X-ray diffraction in conjunction with density functional theory (DFT) and time-dependent density functional theory (TD-DFT) calculations. Furthermore, a systematic comparative theoretical study using the DFT method was undertaken in α and β cyanostilbene derivatives to model the non-linear optical properties of these molecules. This thesis elaborate a promising and rational strategy towards the design of molecules with potential for applications in organic optoelectronics and sensing.

Dr. Reji Thomas
Assistant Professor
Department of Chemistry
Farook College (Autonomous)
Farook College (P.O)
Kozhikode - 673 632

സംഗ്രഹം

സംയോജിത π-തന്മാത്രകളെ അടിസ്ഥാനമാക്കിയുള്ള പ്രകാശദീപ്തി പുറപ്പെടുവിക്കുന്ന വസ്തുക്കൾ അവയുടെ പ്രത്യേകതരം പ്രകാശഭൗതിക ഗുണങ്ങൾ കാരണവും ഘടനാപരമായ മാറ്റങ്ങളിലൂടെ ഈ ഗുണങ്ങളെ ക്രമീകരിക്കാനുള്ള കഴിവ് കാരണവും വലിയ ശ്രദ്ധ നേടിയിട്ടുണ്ട്. ഈ വിഭാഗത്തിൽപ്പെട്ട മിക്ക പ്രകാശദീപ്തി പുറപ്പെടുവിക്കുന്ന വസ്തുക്കളും ലായനി രൂപത്തിൽ വളരെ ഉയർന്ന പ്രകാശദീപ്തിയുള്ളവയാണ്, എന്നാൽ ഖരരൂപത്തിൽ അവയ്ക്ക് പ്രകാശദീപ്തി വളരെ കുറവായിരിക്കും അല്ലെങ്കിൽ തീരെ പ്രകാശദീപ്തി ഉണ്ടായിരിക്കില്ല. ഈ സാഹചര്യത്തിൽ, അഗ്രഗേഷൻ ഇൻഡ്യൂസ്ഡ് എമിഷൻ എന്ന പ്രതിഭാസം കാണിക്കുന്ന തന്മാത്രകൾക്ക് ഖരരൂപത്തിലുള്ള പ്രകാശോപകരണങ്ങളിൽ വളരെയധികം പ്രസക്തിയുണ്ട്. അഗ്രഗേഷൻ ഇൻഡ്യൂസ്ഡ് എമിഷൻ ഗുണങ്ങളുള്ള തമാത്രകളുടെ ഗണത്തിൽപ്പെടുന്ന, ഇൻട്രാമോളികുലാർ ചാർജ് ട്രാൻസ്ഫർ അടിസ്ഥാനമാക്കിയുള്ള തന്മാത്രകൾ ലായനി രൂപത്തിലും ഖരരൂപത്തിലും ഒരുപോലെ ശക്തമായി പ്രകാശം പുറത്തുവിടുന്നവയായി കാണപ്പെടുന്നു. അതിനാൽ, ഇൻട്രാമോളികുലാർ ചാർജ് ട്രാൻസ്ഫർ കാണിക്കുന്ന ഓർഗാനിക് π-സംയോജിത തന്മാത്രകളുടെ രൂപകൽപ്പനയും നിർമ്മാണവും വളരെ പ്രധാനമാണ്, കാരണം ഇവയ്ക്ക് പ്രകാശത്തെ നിയന്ത്രിക്കാൻ കഴിയുന്ന വിവിധ ഓപ്റ്റോഇലക്ട്രോണിക് ഉപകരണങ്ങളിലും സെൻസറുകളിലും സജീവ ഘടകങ്ങളായി പ്രവർത്തിക്കാൻ സാധിക്കും. ശക്തമായ പ്രകാശദീപ്തി ഉള്ള D-π-A സിസ്റ്റങ്ങൾ രൂപകൽപ്പന ചെയ്യാനും നിർമ്മിക്കാനും നിരവധി മാർഗ്ഗങ്ങൾ നിലവിലുണ്ടെങ്കിലും, പ്രകാശദീപ്തി വർദ്ധിപ്പിക്കാനും വിവിധ രീതികളിൽ നിയന്ത്രിക്കാനും കഴിയുന്ന തന്മാത്രകൾ ഉണ്ടാക്കാൻ, വിശദമായ പരീക്ഷണാത്മകവും സൈദ്ധാന്തികവുമായ ഘടന- ഗുണവിശേഷതാ ബന്ധം മനസ്സിലാക്കേണ്ടത് അത്യാവശ്യമാണ്. ഈ പ്രബന്ധത്തിൽ, ശക്തമായ പ്രകാശദീപ്തി, വിവിധ ഉത്തേജനങ്ങളോട് പ്രതികരിക്കാനുള്ള കഴിവ് എന്നിവയുള്ള സയനോസ്റ്റെറീൻ ഘടനയെ അടിസ്ഥാനമാക്കിയുള്ള പ്രതിദീപ്തി പുറപ്പെടുവിക്കുന്ന വസ്തുക്കളുടെ രൂപകൽപ്പനയും നിർമ്മാണവുമാണ് ചർച്ച ചെയ്യുന്നത്. ഈ പഠനം പുതിയ ആന്ത്രാസീൻ- സയനോസ്റ്റിൽബീൻ D-π-A സംയുക്തങ്ങളുടെ നിർമ്മാണവും അവയുടെ ഘടനാപരവും പ്രകാശ-ഇലക്ട്രോണിക് ഗുണങ്ങളും വിശദമാക്കുന്നു. എക്സ്-റേ ഡിഫ്രാക്ഷൻ വഴി ലഭിച്ച ഘടനാപരമായ വിവരങ്ങളും ഡെൻസിറ്റി ഫങ്ഷണൽ തിയറിയും (DFT), ടൈം-ഡിപെൻഡന്റ് ഡെൻസിറ്റി ഫങ്ഷണൽ തിയറിയും സംയോജിപ്പിച്ച് ഘടന-ഗുണവിശേഷത ബന്ധങ്ങൾ പരിശോധിക്കുന്നു. കൂടാതെ, ഈ തന്മാത്രകളുടെ നോൺ-ലീനിയർ ഓപ്റ്റിക്കൽ ഗുണങ്ങൾ മനസ്സിലാക്കാൻ, സയനോസ്റ്റെറീൻ വിഭാഗത്തിൽപ്പെടുന്ന തന്മാത്രകളുടെ ആൽഫ, ബീറ്റ വകഭേദങ്ങൾ ഡെൻസിറ്റി ഫങ്ഷണൽ തിയറി ഉപയോഗിച്ച് ഒരു വ്യവസ്ഥാപിതമായ താരതമ്യ സൈദ്ധാന്തിക പഠനം നടത്തുന്നു. ഓർഗാനിക് കാർബണിക തമാത്രകളെ അടിസ്ഥനാക്കിയുള്ള ഓപ്റ്റോഇലക്ട്രോണിക് ഉപകരണങ്ങൾ, സെൻസിംഗ് തുടങ്ങിയ മേഖലകളിലെ ഉപയോഗങ്ങൾക്കായി തന്മാത്രകൾ രൂപകൽപ്പന ചെയ്യുന്നതിനുള്ള വളരെ യുക്തിസഹവും പ്രതീക്ഷ നൽകുന്നതുമായ മാർഗരേഖകൾ ഈ പ്രബന്ധം മുന്നോട്ട് വയ്ക്കുന്നു.

Dr. Reji Thomas
Assistant Professor
Department of Chemistry
Farook College (Autonomous)
Farook College (P.O)
Kozhikode - 673 632

TABLE OF CONTENTS

LIST OF ABBREVIATIONS

NMR	Nuclear Magnetic Resonance
XRD	X-Ray Diffraction
HRMS	High-Resolution Mass Spectroscopy
DCM	Dichloromethane
SCXRD	Single Crystal X-Ray Diffraction
PXRD	Powder X-Ray Diffraction
UV	Ultraviolet
PL	Photoluminescence
D–π–A	Donor–π–Acceptor
ICT	Intramolecular Charge Transfer
AIE	Aggregation Induced Emission
AIEE	Aggregation Induced Enhanced Emission
CT	Charge Transfer
IR	Infrared
MFC	Mechanofluorochromism
TICT	Twisted Intramolecular Charge Transfer
NLO	Non-Linear Optical
DSE	Dual State Emission
CCDC	Cambridge Crystallographic Data Centre
ACQ	Aggregation Caused Quenching
DMF	Dimethylformamide
THF	Tetrahydrofuran
TBAH	Tetrabutylammonium Hydroxide
DFT	Density Functional Theory
TD-DFT	Time-dependent density functional theory
MESP	Molecular Electrostatic Potential
QTAIM	Quantum Theory of Atoms in Molecules
NCI	Non-Covalent Interaction
FMO	Frontier Molecular Orbital
RDG	Reduced Density Gradient
vdW	van der Waals

PREFACE

The thesis discusses the experimental and theoretical investigation of cyanostyrene based donor-acceptor systems with unique photophysical properties in both solution and solid states. The organic π-conjugated systems are the most relevant area of research owing to their unique optoelectronic and advanced material applications. The possibility for structural modification through extension of conjugation and incorporation of functional groups makes them more attractive for new generation optoelectronic devices and sensors. Recognizing the versatility and functional potential of donor–π–acceptor (D–π–A) incorporated organic π-conjugated systems, the focus of the thesis is directed towards the design and study of such type of D–π–A based systems. The major class of the D–π–A systems explored in this category includes carbazole, triphenylamine, pyrene, and other polyaromatic hydrocarbons. Although there are several donor-acceptor systems have been explored which showing excellent photoluminescence behaviour, the donor-acceptor system with anthracene-cyanostilbene moiety is limited in the literature. The cyanostilbene-based molecules in which the cyanostilbene moiety plays the role of acceptor unit along with anthracene donor part. The predominance of these class of compounds are due to their strong π-conjugation with satisfactory intramolecular charge transfer (ICT) characteristics, and unique aggregation-induced emission (AIE) behaviour. The combination of these features endow them with response to the external stimuli, such as light, temperature, solvent polarity, and mechanical force etc. making them ideal candidates for multi-responsive systems. Furthermore, the facile molecular engineering was made promising due to their structural versatility, which enables the construction of a wide array of optoelectronic functional materials tailored for specific applications. Aggregation caused quenching (ACQ) and aggregation induced emission (AIE) are the two important class of phenomena which determine the material applications of these luminogens. The emission is diminished or quenched at the aggregated state is termed as ACQ. The ACQ effect restricts the practical applications in the areas of optoelectronics, where it requires high emission in the solid or aggregated state. The planar disc like compounds often shows ACQ. So the major strategy to overcome this problem is design a system with twisted geometry. Later Tang and coworkers made this possible and achieved the breaking discovery, which challenge the ACQ phenomena. These are compounds non-emissive or less emissive in the solution state and become highly emissive in the aggregated or at the solid state due to the restricted intramolecular rotation (RIR). Following this observation, various research group

synthesized many systems based on different organic chromophores like cyanostyrenes, pyrene, carbazole etc.

However, there are various design strategies have emerged to satisfy the dual state emission (DSE) characteristics, a detailed study with design and synthesis of D-π-A system exploring both experimental and theoretical aspects are necessary to understand the real mechanism behind the dual state emissive nature and enhanced photoluminescence behaviour. Therefore a detailed study on synthesis, structural, and optoelectronic properties as well as theoretical studies based on combination of density functional theory (DFT) and time-dependent density functional theory (TD-DFT) calculations are relevant. Furthermore, a systematic comparative theoretical study of various cyanostilbene derivatives using the DFT method was also necessary for the synthesis of materials with enhanced optical properties and applications in future optoelectronics.

The general introduction to organic π-conjugated materials and their design strategies for various optoelectronic applications are the content of **Chapter 1**.This chapter gives the overview of the relevant class of π-conjugated compounds and their aggregation induced emission, stimuli-responsive emission behaviours.

The **Chapter 2** explains the various experimental details and computational methods adopted for the spectral analysis, photophysical studies, diffraction analysis and theoretical studies.

In **Chapter 3**, discuss the synthesis and photophysical properties of highly emissive donor-acceptor systems based on anthracene and cyanostilbene, carrying hexyl (**CS-3.1**) and dodecyl (**CS-3.2**) chains. The molecules showed strong emission in the solution state attributed to the intramolecular charge transfer (ICT). The ICT band in these molecules showed solvatochromic redshift with an increase in the dielectric constant of the solvents. The study explored the solid state emission properties of **CS-3.1** and compared with that of dodecyloxy derivative **CS-3.2**. Both the **CS-3.1** and **CS-3.2** showed strong emission in the solid state attributed to the molecular aggregation. Interestingly, the molecule **CS-3.1** showed a stimuli responsive dual mode luminescence switching under applied stress and ethyl acetate vapours. Owing to the rigid molecular packing, **CS-3.1** showed a higher quantum yield (Φ_F = 0.43) in the solid state in comparison to polycrystalline **CS-3.2** (Φ_F = 0.37). The analysis of single crystal structural data of **CS-3.1** has shown that the molecules possess a twisted geometry and

the adjacent molecular pairs comprise a J-aggregate, with arrangement along the molecular short axis. A comparative study of powder X-ray diffractograms showed that both **CSB-1** and **CSB-2** adopt similar molecular packing with different interplanar distances along the molecular long axis.

Chapter 4 discusses the synthesis and photophysical studies of four anthracene-incorporated cyanostilbene derivatives with donor–π–acceptor (D–π–A) architectures. The study also investigate the effect of a phenyl π-spacer on the donor-acceptor systems. Compounds without the spacer (**CS-4.1a**, **CS-4.1b**) showed low quantum yields (Φ_F = 0.05 – 0.25) in various solvents, negative solvatochromism, aggregation-induced enhanced emission (AIEE), and red-shifted mechanofluorochromism. In contrast, those with the spacer (**CS-4.2a**, **CS-4.2b**) exhibited high quantum yields (Φ_F = 0.75 – 0.85), positive solvatochromism, aggregation-induced emission (AIE), and blue-shifted mechanofluorochromism, highlighting the key role of the spacer in modulating photophysical properties.

The **Chapter 5** includes the quantum mechanical study of the synthesized compounds in the *chapter* 3 and 4, which involves the systematic analysis of intermolecular interactions contributing to supramolecular aggregation of compounds using Hirshfeld surface and noncovalent interaction (NCI) analysis. Further, quantum chemical calculations reveal the presence of two distinct conformers- *syn* and *anti*- for compounds **2** and **3**, which are energetically comparable in both the ground and excited states. The blue-shifted absorption observed for compound **2** is supported by frontier molecular orbital analysis and further corroborated by molecular electrostatic potential calculations. Compound **3** exhibits conformational flexibility between *syn* and *anti* conformers in both ground and excited states, attributed to a more energetically accessible transition state compared to analogue **2**. The presence of the *anti* conformer in the first excited state for both compounds **2** and **3** is confirmed by the close agreement between quantum chemically predicted emission wavelengths and experimental data, whereas emission from the *syn* form is absent in compound **2** but remains possible in compound **3**. Thus, the quantum chemical studies presented in this chapter offer valuable insights into the structure–activity relationships of compounds **2** and **3**, highlighting how conformational preferences, electronic properties, and intermolecular interactions influence their photophysical behavior and supramolecular aggregation.

The content of **Chapter 6** explains the designing and comparative study of ten donor-π-acceptor (D-π-A) type cyanostilbene derivatives (**P_1** – **P_{10}**) with different π linkers and their structural and optoelectronic properties arising from the positional variations of -CN group (α and β- variations) through the utilization of density functional theory (DFT) and time-dependent DFT (TDDFT) methods. The topological analyses of the electron density are used to explain the relatively high stability of α isomer compared to that of β. Frontier molecular orbital analysis reveals that seventeen molecules tend to show a reduced HOMO-LUMO gap, and most of them showed a greater nonlinear optical (NLO) character compared to the parent molecule. TDDFT calculations indicate that β isomers show higher absorption maxima compared to their α counterparts. Amongst all the scrutinized molecules, the absorption maximum extended up to 602 nm for **P_9** and it possesses the highest first-order hyperpolarizability.

The thesis concludes an overall summary of the findings from previous chapters. This research demonstrates a promising and rational approach for creating bright, emissive materials with the potential for diverse applications in organic electronics and other devices. Furthermore, this study sheds light on positional isomers and their reactivity, absorption spectra, and NLO properties of D-π-A type architecture that can be suitably tuned by appropriating the π-bridge for practical applications.

Chapter 1

Introduction

1.1 Abstract

This chapter of the thesis provides a brief introduction to the optoelectronic properties of π-conjugated compounds and the structural aspects of that decides the optoelectronic properties of these molecules. The introduction discuss the key concepts such as aggregation induced emission (AIE), Intramolecular charge transfer and stimuli responsive emission that are emerged important parameters in the designing of materials for organic electronics and photonics. The aggregation induced emission is a unique phenomenon wherein the photoluminescence enhances in the solid state of molecules that are weakly emissive or non-emissive in solution. The AIE systems offers scope for potential applications in solid state lighting, sensing, imaging etc. The intramolecular charge transfer (ICT) describes the electronic transition of charge between a donor and acceptor moiety within a molecule, significantly affecting its optoelectronic properties. Both AIE and ICT plays an important role in deciding solid state luminescence properties in the solution as well as solid state, where these concepts contributed to the molecular designs presented in these thesis. The introduction further discusses the molecular design and design strategies in cyanostilbene derivatives, wherein the designs combine the electron deficient nature of the cyano group with the electron rich stilbene backbone or stilbenes functionalized with donor units such as carbazole, triphenylamine etc. These types of donor-π-acceptor have been extensively explored for optoelectronic and energy harvesting applications. The unique structure of cyanostilbene or cyanostyryl based compounds allows efficient charge separation and easily modifiable solid state structure that facilitate strong and tunable photoluminescence in the solid state. The chapter details the main concepts that governs the design of photoluminescent π-systems with a relevance to cyanostilbene based donor-acceptor systems. This introductory chapter enlist the pioneering studies in the field of cyanostilbene based π-conjugated materials and discuss the upcoming trends in the field of cyanostilbene/cyanostyrene based photoluminescence materials, a prospective candidate for next-generation energy and display technologies.

1.2 Organic π–conjugated based optoelectronics

Organic π–conjugated luminophores are one of the most relevant topics of modern optoelectronics on account of their unique photophysical properties and scope for their tunabilty through structural modifications.[1–3] Recent years have seen substantial attention in π-conjugated organic luminescent materials, which represents pivotal class of compounds in organic optoelectronic research.[4–7] Benefitting their excellent properties such as structural diversity, stability at high temperatures, and impressive photoelectric properties, these materials have evolved into a advanced area of research, supported by innovations in both design and device applications.[8,9] Along with their excellent luminescent properties and finely tunable optical and electronic qualities have enabled them to use in many fields including the applications in the fields such as organic light-emitting diodes (OLEDs),[10] organic field-effect transistors (OFETs),[11] chemical sensors,[12,13] bioimaging agents,[14] and various biomedical devices.[9] Although traditional π-conjugated organic and polymeric systems often display limited complexity in optoelectronic properties, which highlights the increasing demand for materials with enhanced functionality and environmental capability.[15] To overcome these limitations researchers have focused on the incorporation of diverse luminophores, advanced molecular design strategies, and innovative device fabrication techniques aimed at tuning and enhancing photophysical behaviours.[16] In particular, π-conjugated stimuli-responsive luminescent materials has emerged as a rapidly expanding boundary. These smart materials exhibit dynamic optical changes in response to external stimuli such as pH, light, temperature,[17] or mechanical stress, enabling specific control over their luminescent nature.[17–19] The ability to manipulate these responses in a controlled and reversible manner has positioned such compounds as promising candidates for next-generation intelligent optoelectronic systems. Ongoing research progress in this area establishing continues a strong foundation for the creation of multifunctional, adaptable materials capable for meeting the upcoming demands of advanced sensing, display, and therapeutic technologies. Additionally, these compounds have found extensive use in the fabrication of OLEDs, chemosensors, organic solar cells, photoswitches, bioimaging, etc.[20–22] underscoring the, great potential applications of organic luminophores in the hot areas of material chemistry.

Conventional π-conjugated luminophores typically exhibit relatively simple photophysical behavior with respect to their functional derivatives. As a result, mixture of luminophores are employed to obtain basic optoelectronic performances on newly designed

molecular structures. Over the past few decades, substantial advances have been achieved in the design and synthesis of π-conjugated oligomers due to their promising applications in optoelectronic devices.[23–25] Several crystal structures of these conjugated systems have been reported and extensively investigated for their solid state optical properties. However, the number of compounds for which the established systematic and quantitative structure–property correlations have been remains relatively limited. This challenge is most evident when slight modifications in molecular architecture, such as variations in substituent position or conformational flexibility, which can cause pronounced changes in intermolecular packing, which can greatly influence photophysical behavior. Gaining a clearer understanding of these correlations is vital for the rational design of materials, as it makes it possible to predict and fine-tune functional properties through targeted molecular engineering. Consequently, there is a pressing need for integrated research that combines thorough structural analysis with comprehensive optical characterization to bridge the gap between molecular design and material performance.

In recent years, considerable scientific effort has been devoted to enhancing the stimuli-responsive functions of π-conjugated luminophores, with the aim of making these materials more advanced, versatile, and suitable for real-world applications.[26–28] The stimuli-responsive luminescent molecules are smart materials in which we can tune the photophysical properties in a controlled manner. Numerous novel stimuli-responsive materials with different π-conjugated structures with optoelectronic properties are emerging constantly.[29–31] Among the various targets pursued in this field, the development of multi-responsive systems, materials capable of responding to more than one external stimulus, has emerged as a particularly promising direction. Achieving such functionality demands the deliberate design and engineering of molecular architectures that capable of incorporating multiple responsive elements within a single framework. To this purpose, variety of chemical modification strategies have been employed to precisely regulate the electronic structures, conjugation lengths, and intermolecular interactions of luminophores in a controlled manner. These methods make it possible to adjust the luminescent properties such as emission wavelength, intensity, and lifetime in response to different environmental factors such as temperature, pH, mechanical stress, solvent polarity, and light irradiation. Furthermore, the core luminescent structures can be tailored through rational molecular design, facilitating their incorporation into larger supramolecular assemblies, nanostructures, or polymeric matrices. The flexibility not only enhances their stimuli-responsive behavior but also broadens their applicability in diverse

photophysical contexts, including optical sensors, data storage, anti-counterfeiting materials, and bioimaging platforms. As research in this area continues to evolve, the development of multi-responsive luminophores holds key building blocks for the next generation of intelligent materials for advanced optoelectronic applications (see Figure 1.1).

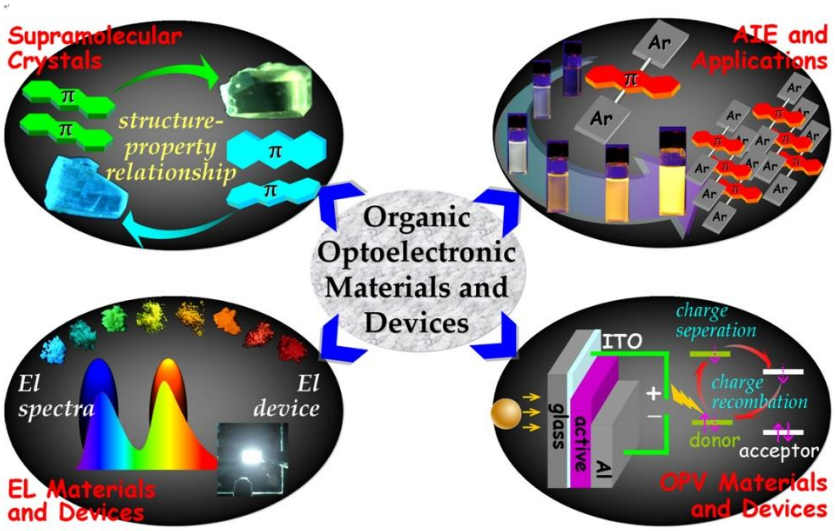

Figure 1.1 Organic π–conjugated luminophores with their wide variety of areas.

The π-conjugated systems featuring donor–π–acceptor (D–π–A) architectures, such as triphenylamine (TPAs), tetraphenylethene (TPE), oligo(phenylene ethynylene)s (OPEs), oligo(phenylene vinylene)s (OPVs), and cyanostilbene derivatives, have emerged as an important class of materials in optoelectronics due to their tunable electronic structures and excellent charge-transport and light-emission properties.[32–36] These molecular systems contain a conjugated π-bridge connecting electron-rich donor moieties to electron-deficient acceptor units, promoting efficient intramolecular charge transfer (ICT) and intensifying the overall polarizability of the molecule. TPAs featuring the planar triarylamine core and strong electron-donating properties, are widely used as hole-transport layers in devices such as OLEDs, dye-sensitized solar cells (DSSCs), and perovskite solar cells (PSCs).[37–41] Other systems like OPEs and OPVs also possess rigid linear backbones and extended conjugation. Through their synthetic tunability, these systems allow precise modulation of HOMO–LUMO energy levels, absorption wavelengths, and charge carrier mobilities.[42,43] Addition to this versatile feature cyanostilbene derivatives exhibit notable aggregation-induced emission (AIE) characteristics, making them highly effective in solid-state luminescent applications, molecular sensors, and stimuli-responsive systems. The tunable and flexible nature of these D–π–A systems enable precise management of optoelectronic properties through structural

modification, such as adjusting their conjugation length or introducing functional substituents. These modifications enabling the materials to be tailored for specific applications (see Figure 1.2).[44]

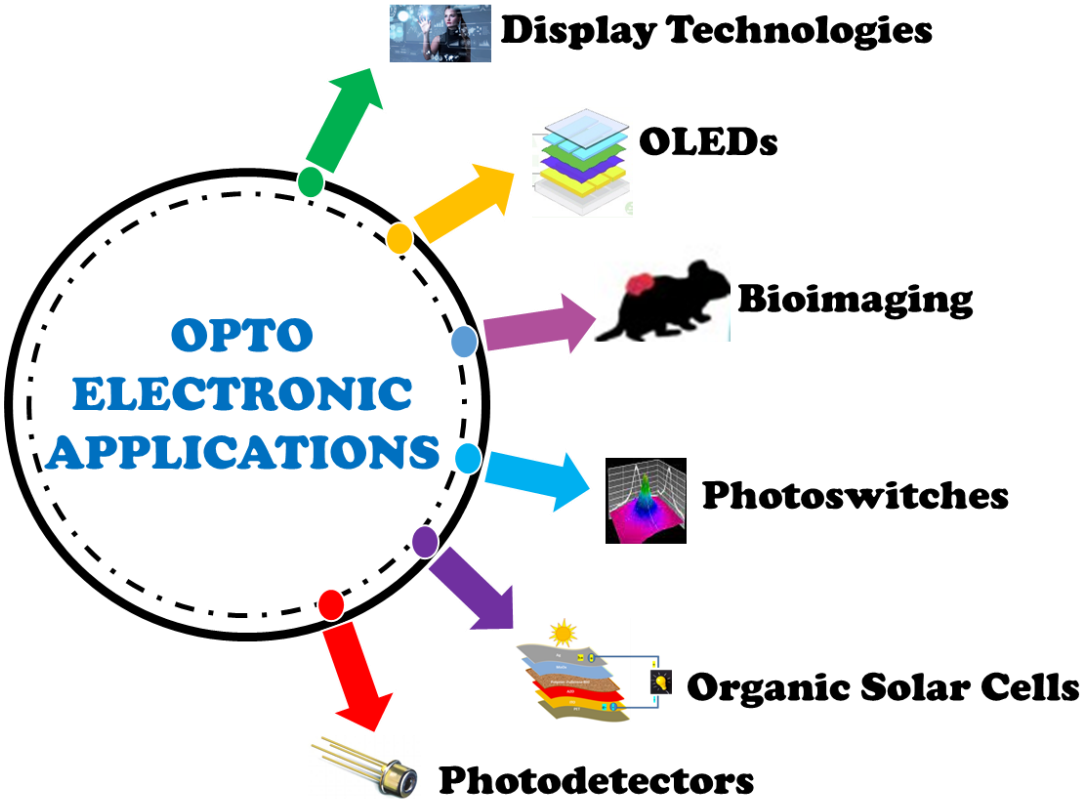

Figure 1.2 Various applications in the field of optoelectronics.

Recognizing the versatility and functional potential of donor–π–acceptor (D–π–A) organic π-conjugated systems, our current research is directed toward the design and study of cyanostilbene-based molecules, due to their exceptional potential in the development of multifunctional optoelectronic materials.[45] Cyanostilbenes are attractive due to their strong π-conjugation, robust ICT characteristics, and unique AIE behaviour.[46] These features endow them with high sensitivity to external stimuli such as light, temperature, solvent polarity, and mechanical stress, making them ideal candidates for multi-responsive systems.[47] Furthermore, their structural versatility facilitates straightforward molecular engineering, allowing the design of diverse optoelectronic materials that can be tailored for precise applications such as OLEDs, sensors, data storage devices, and smart materials.[48–50] The intrinsic π-conjugated framework of cyanostilbenes not only supports efficient electronic communication across the molecule but also facilitates ordered packing in the solid state, crucial for optimizing device

performance. Therefore, cyanostilbene-based D–π–A systems represent a promising and versatile platform for advancing next-generation organic optoelectronic technologies.

Stilbene is a well-known π- conjugated molecule with activity towards light, that has been studied in many areas of chemistry.[51] Its characteristic cis-trans photo isomerization feature make it an attractive fluorescent chromophore with unique photophysical behavior. Owing to their low quantum yield in the solution state, stilbene molecule is observed as the perfect molecule in luminophore research. To meet the diverse and evolving requirements of modern materials science, extensive efforts have focused on the structural modification and synthetic optimization of stilbene-based derivatives.[52] Stilbenes, characterized by their rigid conjugated backbone and inherent luminescent properties, serve as versatile molecular scaffolds for the development of advanced functional materials. Through strategic structural modifications, such as the introduction of various substituents at specific positions on the aromatic rings, the extension of π-conjugation, and the incorporation of heteroatoms, researchers have refined the photophysical and electronic characteristics of stilbenes.[53,54] These modifications allow for precise control over key properties, including emission wavelength, fluorescence quantum yield, thermal stability, and environmental responsiveness, thereby expanding their applicability across a wide range of optoelectronic and photonic devices.

Derived from stilbene, cyanostilbene composed of extended π-conjugated backbone covalently linked to a –CN group. One of the most advantages of the cyanostilbene is its straightforward synthesis, which requires only easily accessible chemical synthons. Structurally derived from the stilbene scaffold and functionalized with one or more cyano (–CN) groups, cyanostilbenes exhibit highly tunable photophysical behaviors that are intimately governed by their solid-state organization. The positional isomerism of the cyano substituent, whether located at the *ortho*, *meta*, or *para* position on the aromatic ring (see Figure 1.3), plays a pivotal role in modulating the nature and strength of intermolecular interactions such as π–π stacking, dipole–dipole coupling, and hydrogen bonding. Among these, α-Cyanostilbene (π-conjugated molecule with –CN group connected at the α-position of the ethylinic bond) and β-Cyanostilbene (with –CN group connected at the β-position of the ethylinic bond) are two important classes of positional isomers that show greater application potential in terms of functionalization. Despite their structural similarities, these isomers exhibit distinct packing motifs and solid-state morphologies, resulting in significantly different optical properties. This underscores the importance of rational molecular design and crystal engineering in the development of next-generation luminescent materials, where even subtle variations in

molecular architecture can lead to dramatic differences in material performance. Structural diversity in cyanostilbenes arises from their tunable ability to undergo substitution at either the aromatic ring or the double bond.[45,55]

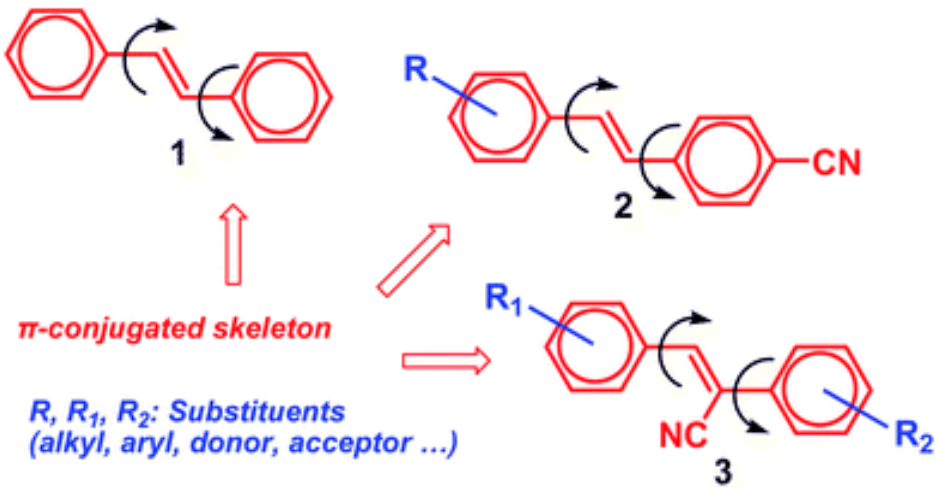

Figure 1.3 Chemical structures of (1) stilbene, (2) 4-cyanostilbene, and (3) α/β-cyanostilbenes. The arrows represent the intramolecular rotation of the aromatic groups. (Reproduced with permission from reference 45, Copyright RSC 2013)

1.3 Cyanostilbenes in luminescent molecular design

Since the first discovery of stilbene by Laurent, extensive research has focused on the structural, photophysical, photochemical, and biological properties of suitably substituted stilbenoid systems. This sustained curiosity stems from their synthetic versatility, which allows for the incorporation of various π-conjugated spacers, alkyl chains, heteroaromatic rings, and electron-donating or electron-withdrawing groups. These modifications enable fine-tuning of their optical and electronic characteristics, establishing stilbenoid as promising candidates for a wide range of applications in materials science, photoelectronic, and biomedical fields.[56–59] Subsequent structural modifications of stilbenoid systems have led to significant enhancement of their emissive properties in the solution and solid state. These enhanced photophysical characteristics have expanded their utility across a range of advanced applications, including organic electronics, self-assembling systems, liquid crystalline materials, organogels, sensors, fluorescent probes, and other functional materials.

Cyanostilbenes occupy a prominent position in the field of molecular design and functional material development due to their unique combination of a conjugated π-framework and the presence of electron-withdrawing cyano (–CN) substituents. The stilbene core provides an extended π-conjugation system that facilitates efficient charge delocalization and enhances

optical responsiveness, making cyanostilbenes ideal candidates for applications in photonic and electronic devices. The incorporation of cyano groups into the stilbene backbone introduces a strong electron-accepting character, which not only modifies the electronic structure of the molecule but also significantly influences the molecular dipole moment and solid-state packing behavior. These cyano substituents serve as key sites for non-covalent interactions like dipolar interactions and hydrogen bonding, which are crucial in directing molecular self-assembly and determining crystalline morphology. Additionally, the tunability of cyano group positioning (*ortho*, *meta*, or *para*) enables precise control over both molecular conformation and intermolecular interactions, which directly affect the photophysical properties such as fluorescence, AIE, and mechanofluorochromism (MFC). As a result, cyanostilbenes have emerged as versatile scaffolds in the rational design of luminescent materials advanced applications, where their structural features can be systematically manipulated to achieve targeted optical and electronic functionalities.[60–65]

The derivatives of cyanostilbene show remarkable changes in color, when subjected to the mechanical force in the solid state through grinding, shearing, pressing etc. Such MFC responses are accompanied by distinctive emission characteristics and have promising applications in material chemistry. This class of materials have shown wide applications in the hot areas of material chemistry like optoelectronics, organic light emitting diodes (OLED), sensors, bioimaging etc.[66] Cyanostilbene derivatives exhibit unique properties like Aggregation Induced Enhanced Emission (AIEE), solvatochromic, mechanochromic, thermochromic properties.[20,67,68] AIEE active molecules are those which are non-emissive or weakly emissive in solution state and which are more emissive in solid or aggregate state. Owing to their excellent AIEE properties cyanostilbenes are widely used in the field of organic optoelectronic.[69–73] These molecules typically exhibit strong self-assembling properties and demonstrate excellent performance in optical devices. Consequently, the design and synthesis of new systems derived from such materials are crucial for investigating their luminescent behavior and unlocking their potential applications.

1.4 Aggregation-induced emission (AIE) versus aggregation-caused quenching (ACQ)

Luminescence, encompassing both fluorescence and phosphorescence, refers to the spontaneous emission of light from excited electronic states following the absorption of ultraviolet or visible light. This phenomenon has garnered significant interest across a wide

range of disciplines, including chemistry, physics, materials science, medicine, and biology, due to its broad applicability in areas such as imaging, sensing, diagnostics, and optoelectronic device development. The fundamental principles of fluorescence and phosphorescence have explored by many studies, particularly focusing on the photophysical properties of organic luminescent materials. The photophysical studies are typically conducted in dilute solutions, where it is generally assumed that intermolecular interactions are negligible. However, it has been observed that many organic materials display significantly different photophysical behaviors in dilute versus concentrated solutions, highlighting the critical influence of molecular aggregation on their emission characteristics.[74,75]

It is widely recognized that luminescence frequently diminishes or is completely quenched at high concentrations, this type of "concentration quenching," primarily attributed to the formation of molecular aggregates, a process widely recognized as Aggregation-Caused Quenching (ACQ).[76–78] The ACQ effect poses a significant challenge for various practical applications, particularly in areas requiring high luminescence efficiency in the solid or aggregated state, such as in optoelectronic devices, sensors, and bioimaging platforms. The ACQ effect presents an even greater challenge in applications such as OLEDs and light-emitting electrochemical cells, where the solid state luminophores are used. In these environments, the tendency of organic molecules to aggregate is heightened, often leading to more pronounced quenching of emission.[79,80] Such limitation in the efficiency and performance highlights the necessity of addressing ACQ in the development of solid-state luminescent materials. (see Figure 1.4).

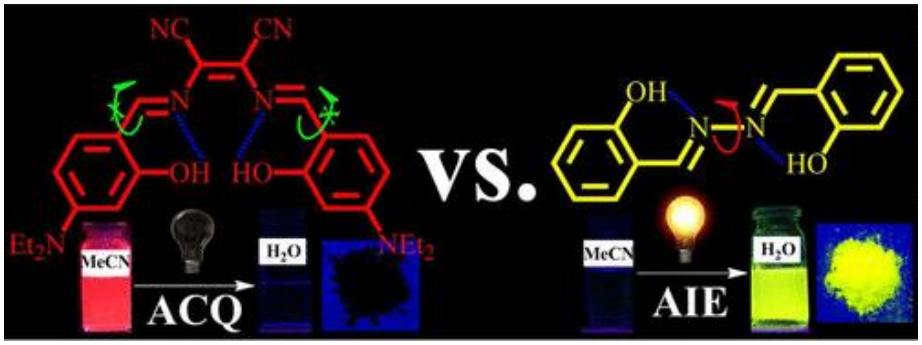

Figure 1.4 Comparison of fluorescence behaviors: Aggregation Caused Quenching vs. Aggregation Induced Emission. (Reproduced with permission from reference 75, Copyright 2016 American Chemical Society).

Tang and co-workers made a groundbreaking discovery that challenged the widely observed phenomenon of aggregation-caused quenching (ACQ), revealing an exactly opposite

behavior in certain molecular systems. They investigated 1-methyl-1,2,3,4,5-pentaphenylsilole (see Figure 1.5), a compound that exhibited no detectable fluorescence in dilute ethanol solution. Interestingly, when the same compound was studied in concentrated solutions or in the solid state, it displayed remarkably strong fluorescence. This phenomenon was attributed to the dynamic intramolecular rotations (IRs) of the five peripheral phenyl rings in the silole structure. In dilute solutions, these phenyl rotors remain highly mobile, enabling the molecule to dissipate its excited-state energy through nonradiative decay pathways, thereby quenching luminescence. However, upon aggregation, the molecules are packed in a constrained environment that significantly restricts the freedom of intramolecular rotations. Additionally, due to the unique propeller-like geometry of silole, the molecules are sterically hindered from engaging in face-to-face π–π stacking interactions, which often contribute to ACQ in planar aromatic systems. This dual restriction, suppression of intramolecular rotations (RIR) and avoidance of π–π stacking, suppresses nonradiative transitions and favors radiative decay, resulting in a pronounced enhancement of fluorescence in the aggregated state. Tang et al. termed this phenomenon "aggregation-induced emission" (AIE).[81] Since its discovery, AIE has garnered substantial attention across various scientific domains, including the development of efficient OLEDs, the design of sensitive luminescent probes, and the advancement of high-contrast bioimaging agents, establishing itself as a pivotal concept in modern photophysics and materials chemistry.[81–83]

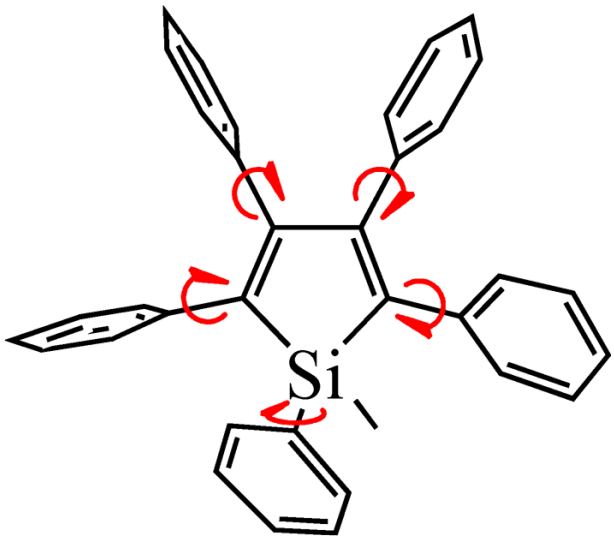

Figure 1.5 Chemical structure of AIE-active 1-methyl-1,2,3,4,5- pentaphenylsilole. (Reproduced with permission from reference 75, Copyright 2016 American Chemical Society).

Later on, Park and his co-workers also observed the similar phenomenon on α-Cyanostilbene-based compounds, an organic gelator called CN-TFMBE showing strong aggregation-induced enhanced emission (AIEE) phenomenon.[62] In this particular type of molecules, the intramolecular rotations are restricted and which is well accepted, as it provide driving force for the AIEE effect. The AIEE phenomenon is further substantiated by fluorescence microscopy imaging. Notably, due to the cooperative effect of π-π stacking interactions among the rigid cyano-substituted stilbene core structures of luminescent compounds are capable of functioning as gelators even in the absence of side groups. Additionally, the molecular polarity generated by the four terminal groups contribute to strong intermolecular interactions, thereby facilitating the distinction and enhancement of the AIEE effect. Given the pronounced AIEE efficiency observed in these compounds, the α-cyanostilbene structural motif has emerged as a key design framework for the progress of multi-responsive soft smart materials as well as advanced organic light-emitting systems.

To advance the development of new luminophoric materials whose aggregated forms exhibit enhanced emission compared to their solution state, researchers have identified two novel photoluminescence (PL) phenomena: AIE and AIEE. The first one AIEE mechanism, a chromophoric material that already exhibits fluorescence in solution becomes significantly more emissive upon aggregation. A compelling example is a cyclophane-functionalized poly(p-phenyleneethynylene), which displays notable photoluminescence in solution but exhibits a 3.5-fold increase in quantum yield upon aggregation, demonstrating its enhanced light-emitting capability in the condensed phase.[84] In contrast, the second one is AIE, refers to materials that are virtually less emissive in dilute solution but shows high luminescent nature at the aggregated state. A well-studied AIE-active compound is hexaphenylsilole, which exhibits a remarkable transition from a weakly emissive state (quantum yield of 0.2 %) in solution to a strongly luminescent state in its aggregated form, achieving increased quantum yield value (23 %).[85]

Systematic experimental investigations and theoretical analyses have elucidated that the restriction of intramolecular motions (RIM), including rotational (RIR), vibrational (RIV), and stretching movements, plays a pivotal role in the aggregation-induced emission (AIE) phenomenon. In solution, active intramolecular motions provide nonradiative pathways for excited-state energy dissipation. However, upon aggregation, these motions are significantly hindered by spatial constraints, effectively suppressing nonradiative decay channels and

thereby enhancing radiative decay processes. The solid-state photoluminescence of molecules is critically determined by the nature of the aggregates they form.

In addition to the primary mechanism of restriction of intramolecular motions (RIM), several secondary photophysical processes contribute to the AIE phenomenon, further enriching the design strategies and functional versatility of AIE-active materials. One such mechanism is excited-state intramolecular proton transfer (ESIPT), in which a proton relocates within a molecule upon excitation, forming a tautomeric structure with distinct photophysical properties.[86] In certain AIEgens, aggregation stabilizes the ESIPT state, enhancing emission intensity by suppressing nonradiative decay. Another contributing process is twisted intramolecular charge transfer (TICT), which involves the formation of a twisted geometry between donor and acceptor segments in the excited state.[87] While the TICT state often leads to fluorescence quenching in dilute solutions due to efficient nonradiative decay, aggregation can restrict this twisting, thereby suppressing energy loss and restoring fluorescence. J-aggregation, characterized by the head-to-tail alignment of chromophores, is another aggregation mode that facilitates red-shifted, narrow-band emission and contributes to enhanced luminescence in the solid state. Finally, crystallization-induced emission (CIE), a subtype of AIE, arises when molecular crystallization limits intramolecular motion and enforces rigid packing, resulting in significantly increased emission efficiency. Together, these mechanisms broaden the scope of AIE by offering multiple pathways to achieve high-performance luminescence in aggregated and condensed phases. Moreover, AIE systems can be tailored to exhibit room-temperature phosphorescence (RTP), particularly in rigid matrices or crystalline phases, where intersystem crossing and long-lived triplet emission are enhanced by the suppression of nonradiative pathways and oxygen quenching. Another notable mechanism is Aggregation-Induced Delayed Fluorescence (AIDF), which merges the principles of AIE and thermally activated delayed fluorescence (TADF), enabling the up-conversion of triplet excitons into singlet states via efficient reverse intersystem crossing (RISC), thereby achieving high-efficiency delayed emission in solid-state devices. Additionally, certain chiral AIEgens exhibit Circularly Polarized Luminescence (CPL), where the aggregation of chiral luminophores amplifies emission anisotropy, finding use in advanced optical materials and 3D displays. Furthermore, AIE-active materials also exhibit mechano-luminescence (ML), light emission induced by mechanical stimuli such as grinding or stretching, due to changes in molecular packing and excited-state dynamics, presenting novel opportunities in stress sensing and damage detection systems. Stimuli-responsive emission is

a key functional extension of AIE, enabling materials to change their luminescence behavior in response to external stimuli. This property greatly enhances the utility of AIEgens in smart materials**,** sensors, and dynamic devices. Such luminogenic systems are highly responsive to a variety of external stimuli, including mechanical stress, temperature fluctuations, pH changes, exposure to toxic vapors, and photonic irradiation. Leveraging these responsive characteristics, numerous stimuli-responsive AIE-active smart materials have been rationally designed and synthesized, exhibiting mechanochromic**,** thermochromic, vapochromic, and photochromic behaviors. These multifunctional systems offer dynamic and reversible emission changes, making them highly promising for applications in sensing, data storage, display technologies, and environmental monitoring. Collectively, these photophysical processes and functional phenomena greatly expand the application potential of AIE materials across optoelectronics, bioimaging, security, sensing, and smart material design, making AIE a foundational principle in next-generation luminescent systems.

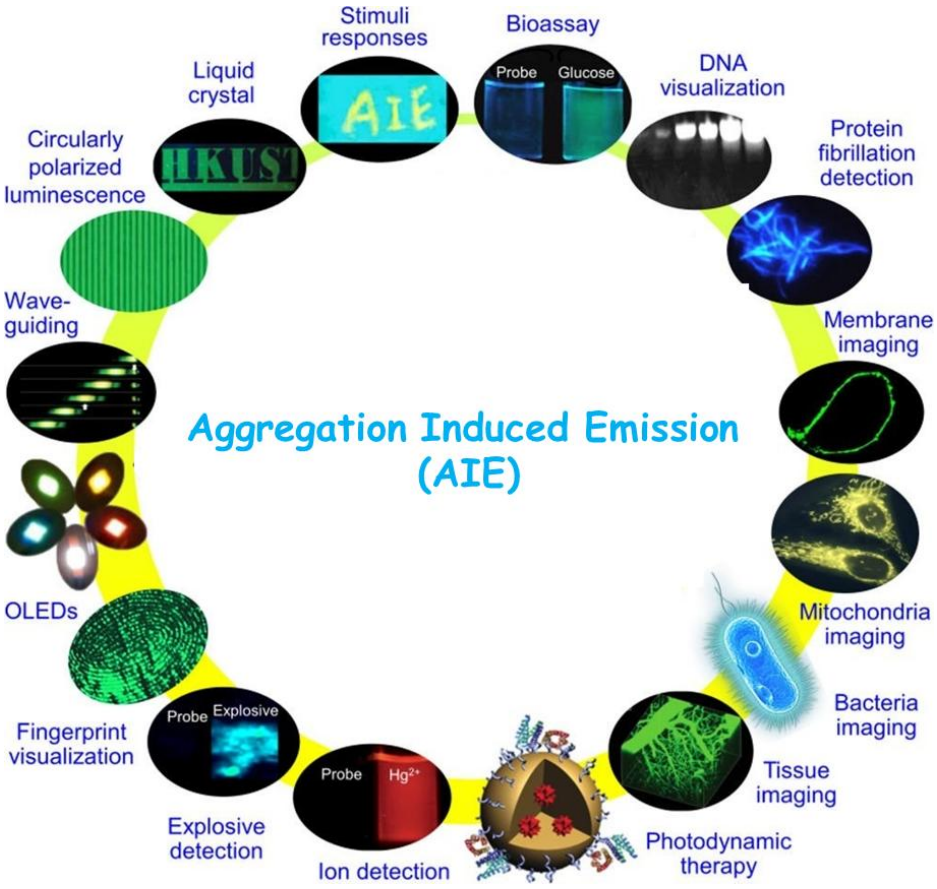

Figure 1.6 Common structural frameworks of AIE luminogens and their diverse applications in advanced technologies. (Reproduced with permission from reference 74, Copyright 2015 American Chemical Society).

In recent years, there are several studies reported molecules with enhanced emission in the solid state, originating from molecular structural factors and molecular aggregation. Intramolecular contributions to fluorescence enhancement are often linked to conformational changes within the chromophore itself. In solution, many chromophores adopt twisted or non-planar conformations that inhibit radiative decay pathways, resulting in weak emission. However, upon aggregation in the solid state, these molecules often adopt more planar configurations, which facilitate π-conjugation and promote radiative transitions, thereby enhancing fluorescence. Beyond these intramolecular factors, intermolecular interactions play a decisive role as well. The mode of molecular packing within aggregates, particularly in π-conjugated systems, profoundly influences emission properties. Two common aggregate morphologies are H-aggregates and J-aggregates, each exhibiting distinct optical behaviors. H-aggregates, characterized by a parallel alignment of molecules with strong face-to-face π–π interactions, often suppress fluorescence by favoring nonradiative decay pathways. These aggregates typically show blue-shifted absorption spectra relative to the monomeric form. Conversely, J-aggregates, which involve a head-to-tail arrangement of molecules, tend to enhance fluorescence efficiency. This configuration supports coherent excitonic coupling and results in a bathochromic (red) shift in the absorption spectrum, often associated with intensified emission. Understanding and manipulating these aggregation-induced effects provide valuable strategies for designing high-performance luminescent materials in optoelectronic, sensing, and imaging applications.[88]

With a solid understanding of the fundamental mechanisms underlying Aggregation Induced Emission (AIE), researchers can now rationally design and synthesize novel luminogenic systems that exploit the unique properties of AIE for a wide array of functional applications. The knowledge gained from AIE studies suggest that that active intramolecular motions dissipate excitons energy while the restricted intramolecular motion (RIM) promotes radiative decay, where these concepts guide the development of novel materials optoelectronic and sensing applications. Moving beyond trial-and-error approaches, this mechanistic insight enables designing of tailored molecular systems with precise control over light emission in addition to enhanced performance and minimized deficiencies. The possibility to incorporate the tailor made properties through proper structural modifications provide the scope for many previously inaccessible applications within the reach. The adoption of AIE principles has driven significant advancements in areas such as bioimaging, chemosensing, optoelectronics,

and stimuli-responsive systems.[89] Any strategy that effectively activates the RIM process holds potential for developing innovative bio- and chemosensing platforms. AIE-active luminogens (AIEgens) have been employed as "turn-on" or "light-up" fluorescent biosensors, DNA visualizers, and molecular probes for monitoring biological phenomena such as protein fibrillation.[90–92] Their ability to emit strongly in aggregated states has enabled high-resolution imaging of organelles, cells, microorganisms, and tissues across molecular to macroscopic levels. Nanostructured AIE materials, including highly emissive AIE dots, have become prominent tools in bioimaging, offering superior brightness and photostability. Multifunctional AIEgen-based systems have also been constructed for integrated biomedical imaging, diagnostics, and therapeutic applications. Beyond biological applications, the AIE materials have been employed in platforms capable of chemosensing such as metal ions, explosives etc. Furthermore these class of compounds are used in fingerprint detection, environmental monitoring, water quality assessment, public safety, and forensic science etc. (see Figure 1.6).[92]

1.4.1 Donor-π-Acceptor (D-π-A) cyanostyrenes/cyanostilbenes with AIE

The modulation of π-systems through incorporation of a Donor-π-Acceptor (D-π-A) architecture represents an intelligent strategy in contemporary molecular design.[93,94] This approach involves incorporation of electron-donating and electron-withdrawing groups at opposite ends of a π-conjugated system, allowing effective intramolecular charge transfer. Cyanostilbene, due to its electron-deficient nature, functions effectively as an acceptor moiety and can be strategically coupled with appropriate donor units and π-linkers to construct tailored D-π-A frameworks. These systems exhibit promising hole and electron transport capabilities, which can be finely tailored by modifying the donor groups or the π-conjugated spacers. The inherent push–pull electronic effect in D-π-A structures facilitates directional electron movement from donor to acceptor, enhancing charge separation and making such systems highly attractive for applications in optoelectronic devices. The cyano group, owing to its inherent electron-withdrawing nature, is frequently utilized in combination with electron-donating moieties to construct donor–acceptor (D–A) type molecules featuring intramolecular charge transfer (ICT) characteristics (see Figure 1.7). Cyano-containing fluorophores, particularly cyanostyrene and cyanostilbene derivatives, have garnered significant attention for their strong solid-state emission.[95] However, these derivatives typically exhibit weak fluorescence in solution, primarily due to torsion-induced nonradiative deactivation pathways. Since high-efficiency emission in solution often requires enhanced molecular rigidity and

optimized donor–acceptor interactions, the strategic incorporation of cyano groups within rigid D–A frameworks presents a promising approach for the development of bright dual-state emissive luminogens (DSEgens).[96–98]

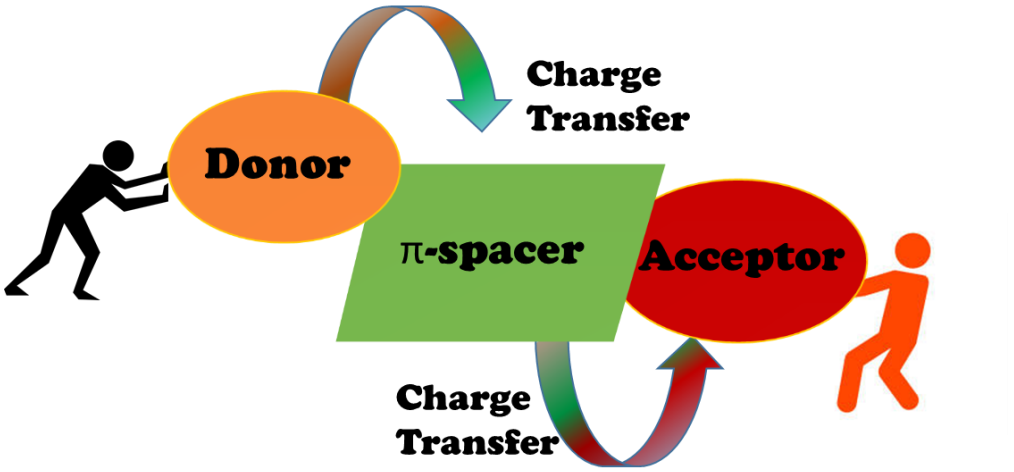

Figure 1.7 Intramolecular charge transfer (ICT) interaction with donor-π-acceptor (D-π-A) architecture.

In a recent study, Z. Huang et al. reported the synthesis of two novel compounds by incorporating pyrene and triphenylamine units into a cyanostyrene skeleton, resulting in materials exhibiting dual-state emission (DSE) behavior, referred to as DSEgens (see Figure 1.8). These compounds demonstrated high quantum yield values in both solution and solid states, highlighting their efficient luminescent properties. In addition to their strong photophysical performance, the compounds exhibited mechanochromic fluorescence (MCF) behavior and were successfully employed for bioimaging applications in living HeLa cells. This study underscores the potential of cyanostyrene/cyanostilbene-based DSEgens as multifunctional materials for applications in information storage and biological imaging. [99,100] In a noteworthy study, Shubhra Kanti Bhaumik and co-workers developed amphiphilic cyanostilbene systems incorporating donor–acceptor functionalities, which exhibited multivalent heparin binding and demonstrated modulation of luminescent properties within their co-assembled structures.[101] In a separate investigation, Majumder et al. synthesized a series of cyanostilbene-based compounds bearing multiple donor–acceptor substituents. These compounds displayed low quantum yields in solution but exhibited pronounced AIE behavior in the aggregated state, attributed to the formation of nanostructures, and the DLS and the SEM studies confirmed the formation of the nanostructures.[102] Additionally, C. Arivazhagan and colleagues reported two distinct molecular designs incorporating phenothiazine as the electron

donor and triarylborane and cyanostilbene as acceptor units. The resulting series of phenothiazine–triarylborane–cyanostilbene derivatives exhibited notable polymorphism and mechanochromic fluorescence (MCF) behavior in select donor–acceptor combinations, underscoring the critical role of structural variation in modulating solid-state emission properties.[103]

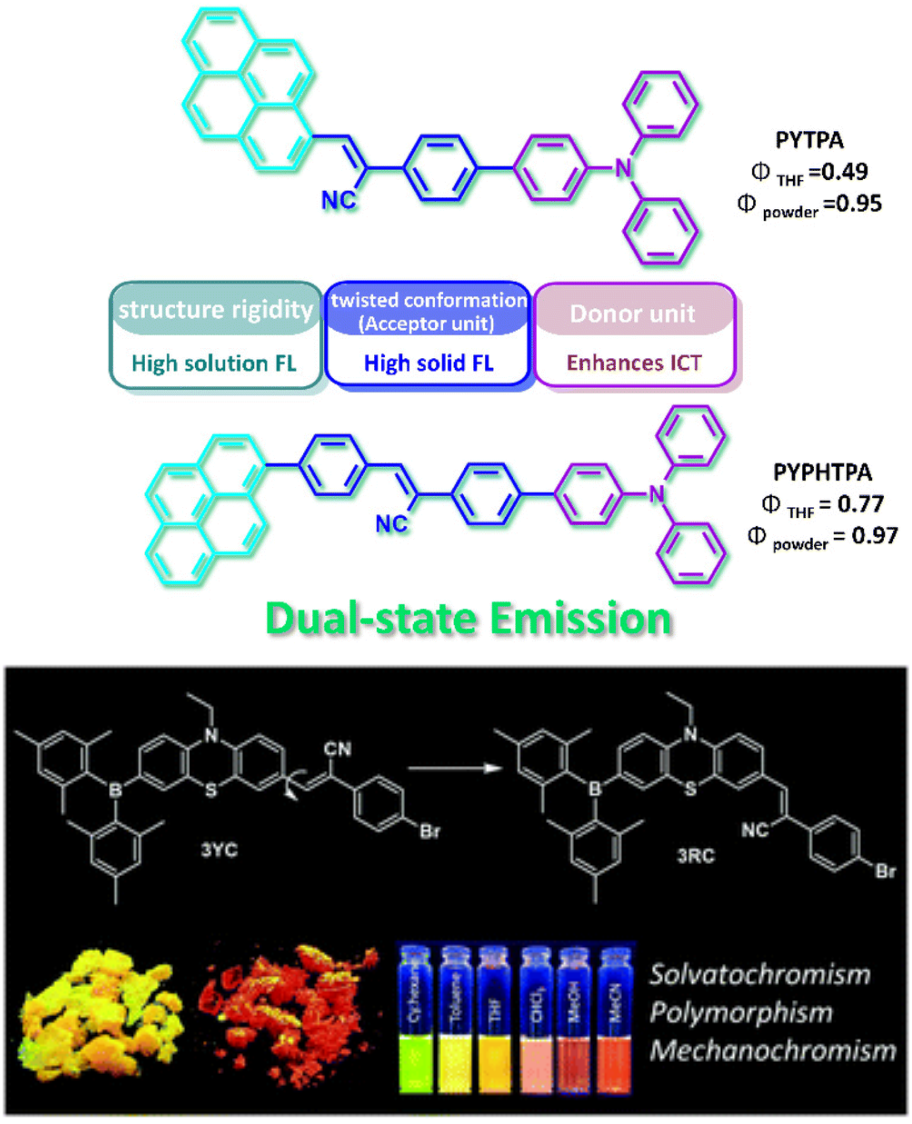

Figure 1.8 Organic luminogens with solid state dual state emissive (DSE) nature. (Reproduced with permission from reference 99, Copyright 2022 RSC and reference 103, Copyright 2018 RSC).

1.5 Tuning Molecular Structures for Efficient Non-Linear Optical (NLO) Activity

Nonlinear optical (NLO) materials have become a central focus in modern science and technology because of their wide-ranging applications in optoelectronics, telecommunications, data storage, signal processing, and laser technologies. The discovery of the first Ruby laser ignited renewed interest in nonlinear optics, paving the way for both computational design and experimental development of advanced NLO materials.[104] Today, researchers are actively exploring both organic and inorganic systems with higher-order nonlinearities, as these materials are essential for frequency doubling (second-harmonic generation), optical switching, electro-optic modulation, photonic circuits, and ultrafast signal transmission (see Figure 1.9) . To enhance their nonlinear optical response, several strategies have been developed, such as metal–ligand coordination frameworks, the push–pull (donor–acceptor) mechanism, and the incorporation of diradical character into molecular systems. These approaches provide powerful design principles for tailoring materials that meet the growing demands of next-generation optoelectronic devices.

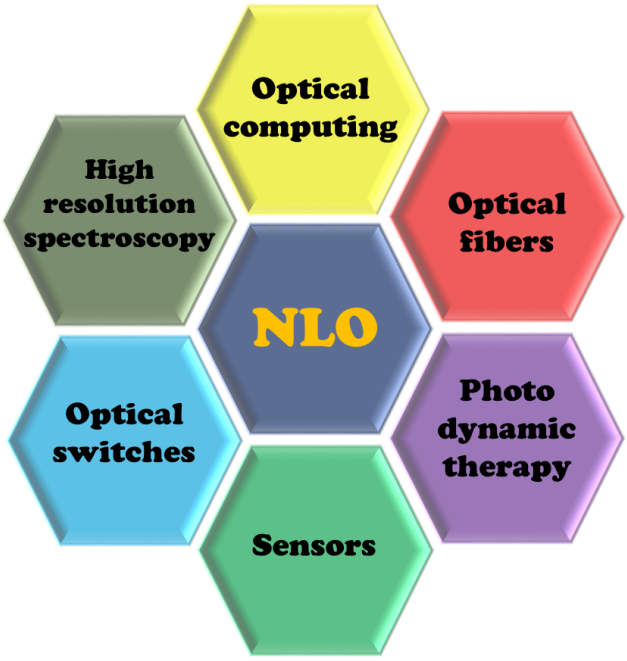

Figure 1.9 Applications of nonlinear optical materials in various fields.

Among various design strategies, the donor–π–acceptor (D–π–A) framework has proven particularly powerful for enhancing the NLO response of organic molecules. In this approach, an electron-donating group (D) and an electron-accepting group (A) are connected

through a π-conjugated bridge, which facilitates intramolecular charge transfer under an external electric field or light excitation. This charge transfer significantly increases molecular polarizability and hyperpolarizability, which are directly related to NLO activity. By tuning the strength of the donor and acceptor groups and optimizing the π-bridge length and conjugation, materials with superior nonlinear responses can be achieved. Together, these approaches are driving the development of next-generation materials with potential applications in high-speed optical communication, integrated photonic devices, laser frequency conversion, and advanced information processing systems.

Systems based on D–π–A architecture have emerged as promising candidates for organic non-linear optical (NLO) materials due to their strong optical non-linearity. NLO materials play an indispensable role in advancing optoelectronic technologies, where high-performance electro-optic conversion is critical. The design and synthesis of novel compounds exhibiting significant NLO responses remain a major challenge, primarily because organic materials with large NLO responses are essential for efficient optoelectronic applications. Among various structural motifs, D–π–A architectures are particularly effective for optimizing molecular NLO properties.[105] Their characteristic push–pull electronic arrangement enhances charge transfer and molecular non-linearity, resulting in high non-linear susceptibilities and the formation of efficient NLO-phores. Recent studies confirm the effectiveness of this design strategy.[106]

In one of the such studies, Shivani et al. investigated the non-linear optical behavior of fluorene–amine derivatives constructed with different D–π–A dyads featuring linear and non-linear π-conjugation pathways.[107] Their findings highlighted a significant enhancement in both first hyperpolarizability and intrinsic hyperpolarizability upon modulation of the π-conjugation pathway. In a related study, the same group examined how variations in the π-conjugation length of fluorene derivatives influence NLO responses.[108] They found that increasing the π-conjugation length improves the NLO response up to a certain limit, beyond which further extension does not yield significant benefits. Fine-tuning structural features such as tuning of length and nature of π-linkers of the NLO-phores can lead to the control of frontier molecular orbital energy levels (HOMO–LUMO gap) and light absorption/emission properties. These optimizations are essential for practical applications including optical communications and optoelectronic devices.[109,110]

1.6 Stimuli responsive emissions in organic fluorophores

Numerous examples in nature demonstrate intelligent responses to external stimuli, governed by subtle molecular mechanisms that rely on weak non-covalent interactions.[27,111–113] These interactions, such as hydrogen bonding, van der Waals forces, electrostatic forces, and π–π stacking, enable biological systems to undergo reversible structural and functional changes in response to environmental factors. A classic example is found in the bioluminescence of fireflies, where the molecule luciferin emits visible light in the presence of ATP, oxygen, and the enzyme luciferase, where this chemically triggered emission illustrates how nature uses stimulus-responsive pathways with high precision. Such natural systems have inspired the

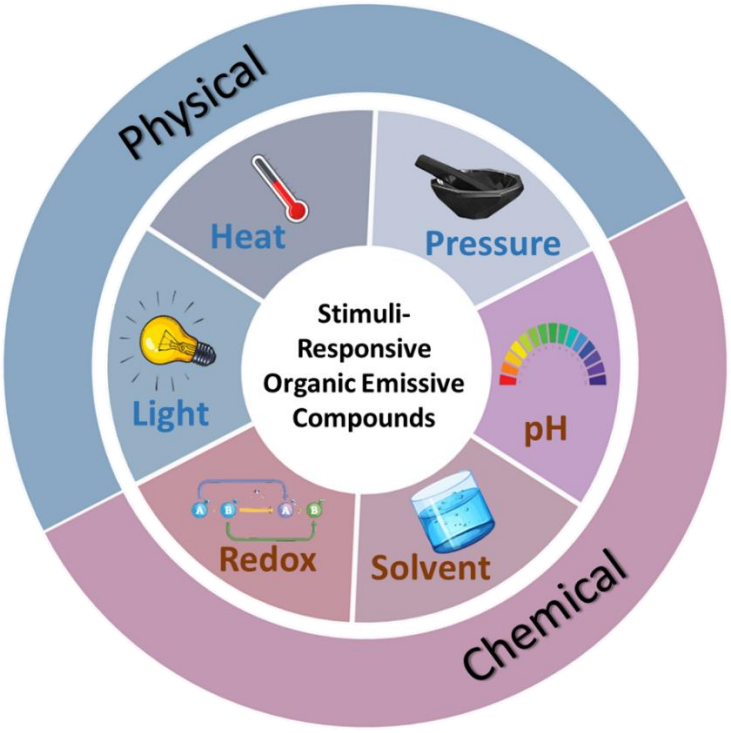

Figure 1.10 Classification of stimulants with respect to stimulus origin.

design of synthetic materials capable of mimicking natural systems is particularly relevant in the growing field of smart materials.

In material science, stimuli-responsive materials are engineered to undergo reversible changes in their properties, such as color, fluorescence, conductivity, or shape, when exposed to external stimuli. These stimuli are generally categorized into physical (e.g., temperature, light, pressure, stress, moisture, electric or magnetic fields) and chemical (e.g., pH, redox agents, metal ions, or specific analytes), which is shown in the Figure 1.10. Among these π-conjugated systems are of particular interest due to their tunable electronic structures,

flexibility in molecular design, and sensitivity to their environment. Organic π-conjugated molecules often display pronounced photophysical responses when external stimuli perturb the molecular packing, intermolecular interactions, or charge transfer dynamics. This makes them perfect candidates for developing smart optical sensors, responsive coatings, and data storage materials.

Extensive investigations into the solid-state emission of stimuli-responsive π-conjugated materials have revealed that changes in aggregate structure are often at the heart of their photoluminescence behavior. These structural changes influence a wide range of photophysical properties, including absorption, reflection, and most significantly, emission. Among these, stimuli-induced modulation of photoluminescence, such as fluorescence and phosphorescence, has drawn particular interest due to its high sensitivity and direct applicability in device fabrication and environmental sensing.

Stimuli-responsive materials have garnered significant attention due to their wide-ranging applications across advanced technologies. These smart materials are capable of undergoing reversible changes in their physical or chemical properties in response to external stimuli, making them highly valuable in fields such as switchable optoelectronics, environmental and biological sensing, targeted drug delivery, soft robotics, and adaptive systems.[27,114–116] In optoelectronic devices, these materials can enable tunable light emission or conductivity, while in sensors, they provide selective and sensitive detection of chemical or physical changes. Moreover, in biomedical applications, stimuli-responsive carriers can be designed to release therapeutic agents in a controlled manner at specific sites, thereby enhancing drug efficacy and reducing side effects. In robotics, such materials enable the development of soft actuators and artificial muscles that respond dynamically to external triggers, offering flexibility and adaptability that traditional materials cannot achieve.[117]

The underlying mechanism of such stimuli-responsive emission is frequently attributed to structural transformations within the aggregated states of the molecules. These transformations often manifest as reversible or irreversible transitions between different aggregate forms, typically crystal-to-crystal or crystal-to-amorphous phase transitions, triggered by the applied stimuli. Such phase changes can significantly alter molecular packing and intermolecular interactions, thereby modulating the electronic states and radiative decay pathways of the luminophores.[118,119]

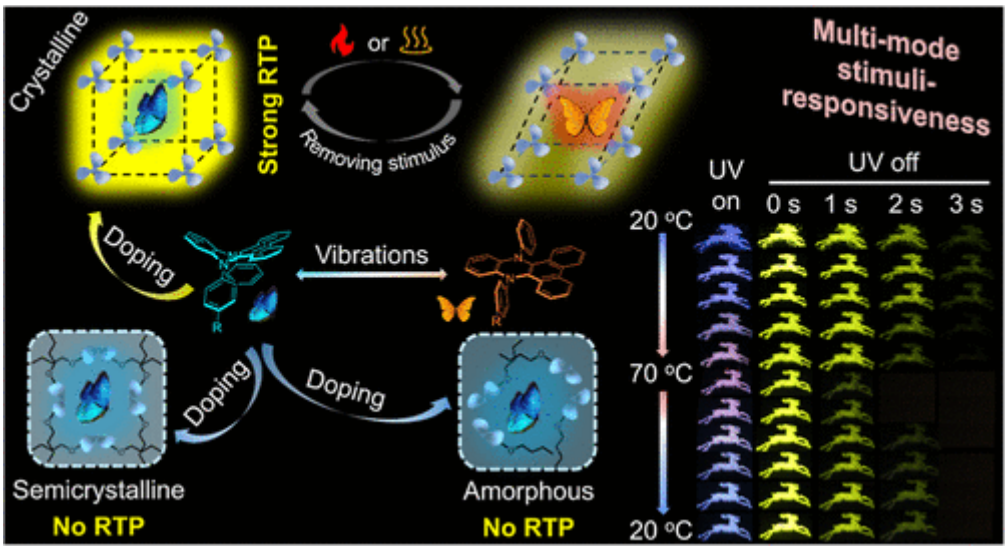

Figure 1.11 Systems exhibiting multimode stimuli-responsiveness with the luminescence behavior. (A creative common licensed publication with reference 27)

A growing body of both theoretical and experimental research underscores the critical influence of molecular packing on their solid-state luminescent behaviour. Specifically, the efficiency of emission and the ability to undergo emission switching in response to external stimuli are strongly dictated by how these molecules organize in the aggregated state. One of the key advantages of π-conjugated systems is their inherent propensity for self-assembly, which allows for precise modulation of their supramolecular architecture through subtle changes in their molecular design and intermolecular interactions (see Figure 1.11). This structural adaptability opens up avenues for tuning their photophysical and optoelectronic properties, making them ideal candidates for responsive material systems.[27]

Extensive investigations into the underlying mechanisms of stimuli-responsive luminescence in these systems have revealed that the nature of aggregation, including the degree of crystallinity, packing motif, and intermolecular forces, plays a pivotal role in determining their emission characteristics. Whether through pressure, temperature, solvent vapour, or mechanical force, external stimuli can induce significant changes in the molecular packing arrangements, leading to observable shifts in emission intensity or colour. These findings highlight the importance of aggregate structure in the rational design of smart luminescent materials.

A key strategy in the molecular design of such systems involves incorporating flexible side chains and functional groups that promote weak, yet dynamic, intermolecular interactions. Flexibility in the molecular backbone and peripheral substituents enhances the ability of the molecules to undergo conformational or packing changes in response to stimuli, thereby enabling reversible switching of their photophysical properties in the solid state. To achieve precise modulation of emission characteristics under different environmental triggers, a diverse array of π-conjugated chromophoric systems has been explored. Among the various molecular architectures developed, one of the most versatile classes of these systems is the donor–π–acceptor (D–π–A) architecture, which allows for efficient intramolecular charge transfer (ICT) and sensitivity to external perturbations. Among this the systems based on triphenylamine (TPAs), tetraphenylethene (TPE), oligo(phenylene ethynylene)s (OPEs), oligo(phenylene vinylene)s (OPVs), pyrene derivatives and cyanostilbene derivatives have emerged as leading platforms. These compounds are especially prominent due to their strong π-conjugation, ease of functionalization, and favourable aggregation-induced emission (AIE) or aggregation-modulated emission behaviours. These chromophores serve as the backbone for the design of smart materials capable of exhibiting stimuli-responsive luminescence, with potential applications in data storage, sensors, anti-counterfeiting technologies, and optoelectronic devices. By understanding the relationship between molecular structure, packing behavior on photophysical properties, researchers can continue to push the boundaries of functional organic materials.

Noteworthy examples within this class of stimuli responsive material classes are highlighted in in the forthcoming paragraphs. The tetraphenylethene (TPE) derivatives have garnered considerable attention due to their aggregation-induced emission enhancement (AIEE) and sensitivity to various external stimuli. Notably, Tang and co-workers reported two AIE luminogens capable of reversible tricolor emission, driven by changes in molecular packing triggered by mechanical force, temperature shifts, and solvent vapor exposure. Building on this, the introduction of weak intermolecular interactions into propeller-like molecules has been shown to yield materials with morphology-dependent multicolor emission.[120,121] In another study, Tang and co-workers reported a pair of triazole-functionalized tetraphenylethene (TPE) derivatives synthesized via a copper-catalyzed Click reaction. The pure *E* and *Z* isomers were successfully separated, both exhibiting aggregation-induced emission (AIE) characteristics and multicolor emission switching in response to various external stimuli. Notably, both isomers demonstrated multiple chromic behaviors, with the *E*

isomer displaying more pronounced chromic responses, superior molecular organization, and higher crystallinity compared to the *Z* isomer. These chromic properties are closely linked to the unique structural features of the AIE luminogens. The propeller-like geometry of the TPE molecules promotes loose molecular packing, which can contribute to the tenability of the solid state structure. This structural adaptability facilitates phase transitions and morphological transformations, making these molecules promising candidates for advanced "smart" materials. Such materials hold potential for a broad range of high-tech applications, including miniature photonic devices, chemical sensors, biological probes, security inks, logic gates, optical displays, and information storage systems.[122]

Xiong et al. synthesized a vinylpyridine-substituted TPE system exhibiting multistimuli-responsive emission switching (Figure 1.12). The compound displayed emission changes in response to mechanical stress, hydrostatic pressure, and upon protonation. SCXRD revealed a highly twisted molecular conformation and a packing structure featuring shrinkable voids, enabling deformation under applied pressure. [123]

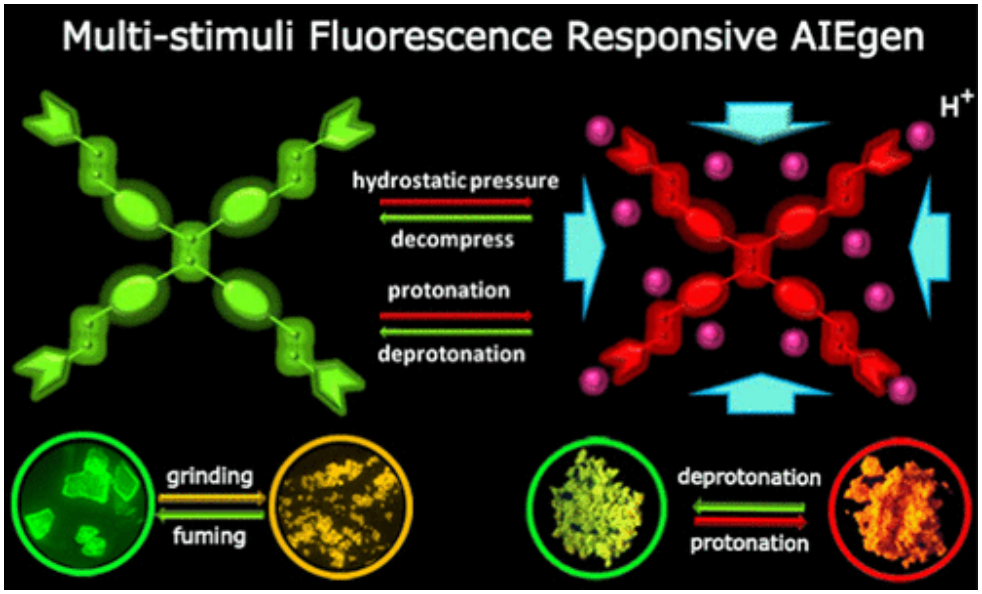

Figure 1.12 Functionalization of TPE with vinyl pyridine offers an effective multistimuli-responsive luminescence switching. (Reproduced with permission from reference 123, Copyright 2018 American Chemical Society).

The family of oligo(phenylenethynylene) (OPE) systems has garnered significant interest as optoelectronic materials, owing to their notable electrical and photophysical properties. Often referred to as "molecular wires," these compounds feature an extended conjugated bond architecture that facilitates efficient charge transport. OPE based molecules

are also investigated for their solid-state emissive behavior and potential as single-molecule conductors. This interest arises from the ability of these molecules to undergo free rotation around the triple bond, leading to varying degrees of molecular planarity. Deviations from planarity influence the extent of conjugation, which in turn affects the electronic energy levels of the system. A study by Bunz and coworkers validated the occurrence of thermochromic luminescence in an octyloxy-substituted phenyleneethynylene polymer. The work reports the emission switching is attributed to changes in molecular planarity within the liquid crystalline state.[124] Kulkarni and coworkers conducted a related study on a dimethoxy-substituted oligo(phenyleneethynylene) system, demonstrating that the fluorescence spectra and emission color could be controlled by the cooling rate. The study also investigated the impact of surface morphology on emission behavior. The cooling rate-dependent variation in emission color was attributed to preferential surface wetting during cooling and the associated molecular planarization.[125]

Another important class within this category comprises triphenylamine (TPA)-based donor–acceptor π-conjugated systems. TPA serves as a widely utilized electron-donating unit in π-conjugated architectures for optoelectronic applications, owing to its tunable electronic properties and effective charge transport capabilities. Its characteristic propeller-like, non-planar geometry—arising from three phenyl rings connected to a central nitrogen atom—provides a favorable balance between resonance stabilization and steric hindrance, which helps minimize molecular aggregation. In a representative study, Quinton et al. synthesized TPA-based compounds incorporating an electron-withdrawing tetrazine unit linked through various spacers. They systematically investigated the electrochemical and photophysical properties of these derivatives and further demonstrated their potential application in the development of photovoltaic solar cells.[126] In another study, Sivakumar and co-workers synthesized yellow-emitting organic phosphors and conducted a complete investigation of their photophysical and electrochemical properties. The work highlighted notable solid-state bathochromic emission behavior, attributed to AIE and π–π stacking interactions. Additionally, the study examined the solvatochromic responses of the compounds and supported the experimental findings through density functional theory (DFT) and time-dependent DFT (TD-DFT) calculations.[127]

Pyrene, a key member of the polycyclic aromatic hydrocarbon family characterized by its fused four-ring benzene system, exhibits strong blue fluorescence with high quantum yield and notable charge carrier mobility. Owing to these advantageous properties, pyrene-based chromophores have found widespread application as luminescent materials in OLEDs and

biological probes, as well as in hole-transport layers for organic photovoltaics and perovskite solar cells. In a notable study, Feng and coworkers investigated the pyrene based systems which exhibit a clear correlation between the number of TPA-OMe moieties and improved photophysical properties, including increased molar absorption coefficients, enhanced photoluminescence efficiency, and larger two-photon absorption cross-sections, while maintaining a stable emission peak. Investigations into their excited-state dynamics suggest that both charge transfer (CT) and charge separation (CS) states play key roles in modulating emission behavior. Specifically, short-lived CS states, favored by higher TPA-OMe content and low-polarity solvents, promote efficient charge recombination and stronger emission. In contrast, long-lived CS states dominate in high-polarity environments or in molecules with fewer TPA-OMe units, leading to suppressed emission. These findings highlight the importance of molecular design and solvent polarity in tuning the performance of artificial light-harvesting systems.[128]

For instance, cyanostilbene derivatives—a subset of D–π–A molecules—exhibit mechanochromic luminescence, where their emission color changes upon mechanical stress due to phase transitions from crystalline to amorphous states. Similarly, many D–π–A chromophores exhibit solvatochromism, showing bathochromic shifts in emission as solvent polarity increases. The key to such tunability lies in the regulation of weak interactions within the system, allowing for finely controlled, stimulus-triggered photophysical responses. Through deliberate molecular engineering, researchers can manipulate these interactions to produce materials that are not only responsive and reversible, but also robust and functional across a wide range of conditions. These innovations are opening new avenues for next-generation applications in flexible electronics, bioimaging, optical memory devices, and environmental sensors.

1.6.1 Cyanostilbene-Based Luminescent Switches

Cyanostilbene-based π–conjugated systems have gained remarkable attention in recent years owing to their strong solid–state emission, facile synthesis, and tunable photophysical properties. Unlike many conventional luminogens, cyanostilbenes and styrene derivatives exhibit intriguing dual characteristics: they are often weakly emissive in solution but display pronounced emission enhancement in the aggregated or solid state. Importantly, in solution these molecules demonstrate notable stimuli-responsive behavior, with their fluorescence being sensitive to external factors such as solvent polarity, pH, temperature, and concentration.

This solution-state stimuli responsiveness is primarily governed by their ICT character, arising from the strong electron-donating and electron-withdrawing substituents across the stilbene framework. The balance between locally excited states and ICT states plays a crucial role in dictating their emission efficiency and color, leading to environment-dependent luminescence. Furthermore, in the solid state, restriction of intramolecular motion enhances their radiative decay pathways, giving rise to intense fluorescence that can also respond dynamically to external stimuli such as pressure, heat, and mechanical force. Consequently, cyanostilbene derivatives represent a versatile class of stimuli-responsive fluorophores, combining ICT-driven solution behavior with AIE in the condensed phase, making them attractive for sensing, optoelectronics, and smart material.

Recent efforts have focused on designing cyanostilbene-based AIEgens with multifunctional luminescence. Athira et al. reported the synthesis of two cholesterol-functionalized cyanostyrene–phenothiazine D–π–A systems that display strong fluorescence in both solution and solid states. The molecules show good quantum yields in nonpolar solvents due to TICT and exhibit AIE in the solid state. Flexible alkyl chains from phenothiazine and cholesterol enable mechanochromic luminescence switching under shear stress, with emission recovery upon methanol vapor exposure. Powder X-ray diffraction confirms that the reversible crystalline–amorphous phase transition underlies the observed emission switching.[129] In another work Liang et al. developed chiral AIE-active luminogens by integrating BINOL with cyanostilbene (CS) units. These materials exhibited internal charge transfer in low-water environments and strong aggregation-induced emission upon nano-aggregate formation. (see Figure 1.13) The CS cis–trans isomerization and D–π–A architecture with benzothiazole groups enabled adaptive luminescence responsive to light and polarity. While weak circularly polarized luminescence (CPL) appeared in aggregates and polymer films, significantly amplified and sign-inverted CPL signals emerged in nematic liquid crystals. Furthermore, CPL intensity, emission color, and handedness could be tuned by light irradiation and medium polarity.[130]

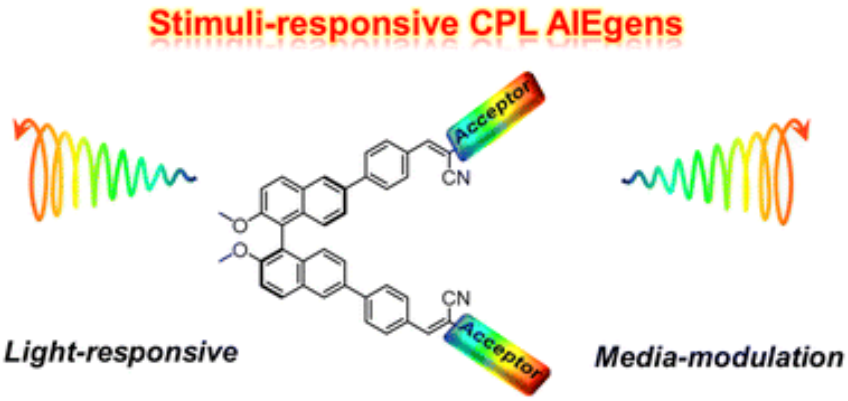

Figure 1.13 stimuli-responsive CPL-active materials. (Reproduced with permission from reference 130, Copyright 2024 RSC).

In another study, Zhang et al. reported the synthesis of two cruciform cyanostilbene-based AIEgens that exhibited reversible photochromic luminescence, arising from E/Z isomerization in solution and [2+2] cycloaddition in the solid state. Furthermore, their emission properties could be tuned by concentration in polymer films, and the materials displayed distinct mechanochromic luminescence.[131] Chen et al. proposed a structure-driven strategy for dual-state luminescence was demonstrated using benzimidazole as an electron donor and pyridine as an acceptor to construct D–A-type cyanopyridine ethylene derivatives. Theoretical studies revealed energy-close isomers with planar conformations in dilute solutions, suppressing nonradiative decay and yielding high fluorescence efficiency (Φ up to 42.7%). In the solid state, distorted cyanobenzene structures, π–π stacking suppression, and intermolecular hydrogen bonding further restricted molecular motion, enabling strong emission (Φ up to 27.4%). Such dual-state emitters show promise for applications in information encryption and temperature sensing.[132]

Xue et al. developed the system of carbazole-based D–π–A–π–D luminogens have been developed as efficient dual-state emitters (DSEgens) with intramolecular charge transfer characteristics and multi-stimuli responsiveness. These systems demonstrate high sensitivity toward trace water and picric acid in organic media, along with reversible mechanofluorochromism marked by significant emission shifts. Such findings underscore the potential of rationally designed DSEgens for multifunctional sensing across both molecular and aggregated states.[133] In another work by the team they explored the carbazole–cyanostyrene derivatives with varied terminal substituents have been explored to tune emission behavior through electronic structure modulation. While most derivatives exhibited typical aggregation-induced emission (AIE), the N,N-dimethylamino-substituted analogue functioned

as a DSEgen, showing efficient luminescence in both solution and solid states (see Figure 1.14). This compound further demonstrated sensitivity toward trace water and picric acid, along with reversible MFC, highlighting electronic tuning as a viable strategy for designing multifunctional DSE materials.[61]

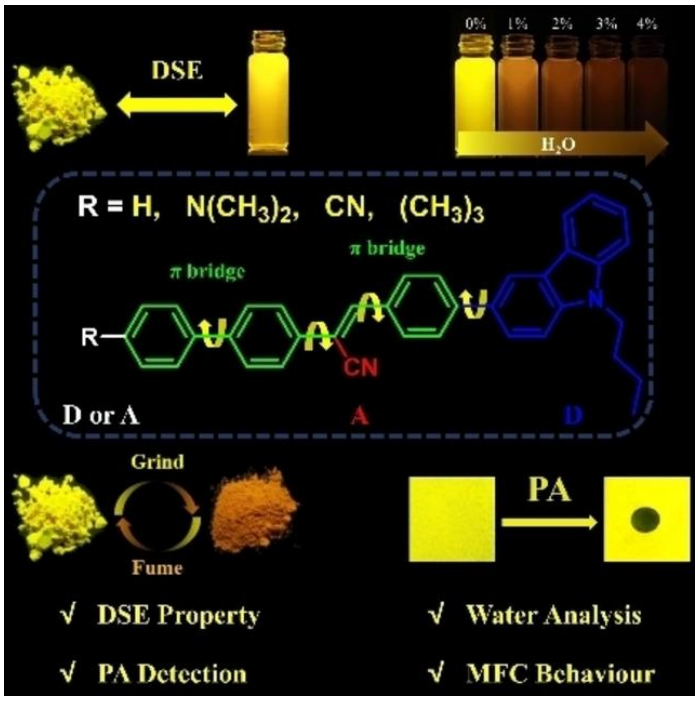

Figure 1.14 DSE materials with efficient emission in solution and solid state. (Reproduced with permission from reference 61, Copyright 2022 Wiley-VCH).

In conclusion, cyanostyrene-based compounds offer remarkable advantages of facile synthesis and structural tunability, making them highly attractive platforms for stimuli-responsive luminescent materials. Subtle substitution on the cyanostyrene core enables the construction of twisted or non-planar architectures, as well as donor–acceptor (D–A) type systems, thereby achieving efficient emission in both the states. The ability to realize reversible luminescence switching through such structural design underscores the versatility of cyanostilbene derivatives and highlights their continued potential in the development of multifunctional optoelectronic materials.

1.7 References

(1) Nowsherwan, G. A.; Ali, Q.; Ali, U. F.; Ahmad, M.; Khan, M.; Hussain, S. S. Advances in Organic Materials for Next-Generation Optoelectronics: Potential and Challenges. *Organics*. 2024, pp 520–560.

(2) Meti, P.; Yang, J.-W.; Gong, Y.-D. Aggregation Induced Emission Properties of Cruciform-Type Conjugated Pyrazine Molecules with Four Pendent Donor Groups. *Dye. Pigment.* **2021**, *192*, 109419.

(3) Huang, Z.; Yang, J.; Cheng, J.; Zhou, L.; Zhao, C.; Shen, S.; Baryshnikov, G.; Ågren, H.; Zou, Q.; Zhu, L. Molecular Engineering of Red Aggregation-Induced Emission Luminogens with Small Conjugated Structures. *Chem. Mater.* **2024**, *36* (17), 8546–8554.

(4) Coghi, P.; Coluccini, C. Literature Review on Conjugated Polymers as Light-Sensitive Materials for Photovoltaic and Light-Emitting Devices in Photonic Biomaterial Applications. *Polymers*. 2024.

(5) Lou, X.-Y.; Wang, J.; Zhang, G.; Yang, Y.-W. Pyrene-Armed Pillararene Nanostructure-Facilitated Enhanced Fluorescence and Self-Driven Gelation. *ACS Appl. Nano Mater.* **2022**, *5* (10), 13720–13728.

(6) Datta, S.; Xu, J. Recent Advances in Organic Molecular-to-Supramolecular Self-Assembled Room-Temperature Phosphorescent Materials for Biomedical Applications. *ACS Appl. Bio Mater.* **2023**, *6* (11), 4572–4585.

(7) Basabe-Desmonts, L.; Reinhoudt, D. N.; Crego-Calama, M. Design of Fluorescent Materials for Chemical Sensing. *Chem. Soc. Rev.* **2007**, *36* (6), 993–1017.

(8) Mateo-Alonso, A. π-Conjugated Materials: Here, There, and Everywhere. *Chem. Mater.* **2023**, *35* (4), 1467–1469.

(9) Barman, D.; Narang, K.; Parui, R.; Zehra, N.; Khatun, M. N.; Adil, L. R.; Iyer, P. K. Review on Recent Trends and Prospects in π-Conjugated Luminescent Aggregates for Biomedical Applications. *Aggregate* **2022**, *3* (5), e172.

(10) Wei, Q.; Zhang, J.; Ge, Z. AIE-Active Emitters and Their Applications in OLEDs. In *Handbook of Aggregation-Induced Emission*; 2022; pp 1–26.

(11) Mei, J.; Diao, Y.; Appleton, A. L.; Fang, L.; Bao, Z. Integrated Materials Design of Organic Semiconductors for Field-Effect Transistors. *J. Am. Chem. Soc.* **2013**, *135* (18), 6724–6746.

(12) Ni, F.; Li, N.; Zhan, L.; Yang, C. Organic Thermally Activated Delayed Fluorescence Materials for Time-Resolved Luminescence Imaging and Sensing. *Adv. Opt. Mater.* **2020**, *8* (14), 1902187.

(13) Wang, D.; Tang, B. Z. Aggregation-Induced Emission Luminogens for Activity-Based Sensing. *Acc. Chem. Res.* **2019**, *52* (9), 2559–2570.

(14) Cheng, H.-B.; Li, Y.; Tang, B. Z.; Yoon, J. Assembly Strategies of Organic-Based Imaging Agents for Fluorescence and Photoacoustic Bioimaging Applications. *Chem. Soc. Rev.* **2020**, *49* (1), 21–31.

(15) Palani, P.; Karpagam, S. Conjugated Polymers – a Versatile Platform for Various Photophysical, Electrochemical and Biomedical Applications: A Comprehensive Review. *New J. Chem.* **2021**, *45* (41), 19182–19209.

(16) Elgiddawy, N.; Elnagar, N.; Korri-Youssoufi, H.; Yassar, A. π-Conjugated Polymer Nanoparticles from Design, Synthesis to Biomedical Applications: Sensing, Imaging, and Therapy. *Microorganisms*. 2023.
(17) Abdollahi, A.; Roghani-Mamaqani, H.; Razavi, B.; Salami-Kalajahi, M. The Light-Controlling of Temperature-Responsivity in Stimuli-Responsive Polymers. *Polym. Chem.* **2019**, *10* (42), 5686–5720.
(18) Mrinalini, M.; Prasanthkumar, S. Recent Advances on Stimuli-Responsive Smart Materials and Their Applications. *Chempluschem* **2019**, *84* (8), 1103–1121.
(19) Yan, D.; Wang, Z.; Zhang, Z. Stimuli-Responsive Crystalline Smart Materials: From Rational Design and Fabrication to Applications. *Acc. Chem. Res.* **2022**, *55* (7), 1047–1058.
(20) G. R., S.; Pandey, M.; Chakravarthy, A. S. J. Review on New Horizons of Aggregation Induced Emission: From Design to Development. *Mater. Chem. Front.* **2021**, *5* (4), 1541–1584.
(21) Goshisht, M. K.; Tripathi, N. Fluorescence-Based Sensors as an Emerging Tool for Anion Detection: Mechanism, Sensory Materials and Applications. *J. Mater. Chem. C* **2021**, *9* (31), 9820–9850.
(22) Islam, A.; Shah, S. H.; Haider, Z.; Imran, M.; Amin, A.; Haider, S. K.; Li, M.-D. Biological Interfacial Materials for Organic Light-Emitting Diodes. *Micromachines*. 2023.
(23) Sun, Y.; Davis, E. Nanoplatforms for Targeted Stimuli-Responsive Drug Delivery: A Review of Platform Materials and Stimuli-Responsive Release and Targeting Mechanisms. *Nanomaterials*. 2021.
(24) Vassalini, I.; Alessandri, I.; de Ceglia, D. Stimuli-Responsive Phase Change Materials: Optical and Optoelectronic Applications. *Materials*. 2021.
(25) Ekbote, A.; Han, S. H.; Jadhav, T.; Mobin, S. M.; Lee, J. Y.; Misra, R. Stimuli Responsive AIE Active Positional Isomers of Phenanthroimidazole as Non-Doped Emitters in OLEDs. *J. Mater. Chem. C* **2018**, *6* (8), 2077–2087.
(26) Zhang, L.; Wang, Z.; Zhang, R.; Yang, H.; Wang, W.-J.; Zhao, Y.; He, W.; Qiu, Z.; Wang, D.; Xiong, Y.; Zhao, Z.; Tang, B. Z. Multi-Stimuli-Responsive and Cell Membrane Camouflaged Aggregation-Induced Emission Nanogels for Precise Chemo-Photothermal Synergistic Therapy of Tumors. *ACS Nano* **2023**, *17* (24), 25205–25221.
(27) Zhang, Z.; Wang, Q.; Zhang, X.; Mei, J.; Tian, H. Multimode Stimuli-Responsive Room-Temperature Phosphorescence Achieved by Doping Butterfly-like Fluorogens into Crystalline Small-Molecular Hosts. *JACS Au* **2024**, *4* (5), 1954–1965.
(28) Kundu, S.; Das, S.; Dutta, A.; Patra, A. Three in One: Stimuli-Responsive Fluorescence, Solid-State Emission, and Dual-Organelle Imaging Using a Pyrene-Benzophenone Derivative. *J. Phys. Chem. B* **2022**, *126* (3), 691–701.
(29) Qin, X.; Li, Y. Strategies To Design and Synthesize Polymer-Based Stimuli-Responsive Drug-Delivery Nanosystems. *ChemBioChem* **2020**, *21* (9), 1236–1253.
(30) Figueira-Duarte, T. M.; Müllen, K. Pyrene-Based Materials for Organic Electronics. *Chem. Rev.* **2011**, *111* (11), 7260–7314.
(31) Kim, F. S.; Ren, G.; Jenekhe, S. A. One-Dimensional Nanostructures of π-Conjugated Molecular Systems: Assembly, Properties, and Applications from Photovoltaics,

Sensors, and Nanophotonics to Nanoelectronics. *Chem. Mater.* **2011**, *23* (3), 682–732.
(32) Elbashier, E.; Wagner, P.; Officer, D. L.; Gordon, K. C. Impact of the Acceptor Group on the Properties of Triphenylamine-Donor–Acceptor Dyes: An Experimental and Computational Study. *J. Phys. Chem. A* **2025**, *129* (4), 1026–1041.
(33) Fernández, Z.; Sánchez, L.; Santhosh Babu, S.; Fernández, G. Oligo(Phenyleneethynylene)s: Shape-Tunable Building Blocks for Supramolecular Self-Assembly. *Angew. Chemie Int. Ed.* **2024**, *63* (18), e202402259.
(34) Albano, G.; Pescitelli, G.; Di Bari, L. Chiroptical Properties in Thin Films of π-Conjugated Systems. *Chem. Rev.* **2020**, *120* (18), 10145–10243.
(35) Balsukuri, N.; Manav, N.; Lone, M. Y.; Mori, S.; Das, A.; Sen, P.; Gupta, I. Donor-Acceptor Architectures of Tetraphenylethene Linked Aza-BODIPYs: Synthesis, Crystal Structure, Energy Transfer and Computational Studies. *Dye. Pigment.* **2020**, *176*, 108249.
(36) Luan, T.-X.; Xing, L.-B.; Lu, N.; Li, X.-L.; Kong, S.; Yu, W. W.; Li, P.-Z.; Zhao, Y. Donor–Acceptor-π-Acceptor–Donor-Type Photosensitive Covalent Organic Framework for Effective Photocatalytic Aerobic Oxidation. *J. Am. Chem. Soc.* **2025**, *147* (15), 12704–12714.
(37) Bhuin, S.; Bhattacharya, S.; Chakravarty, M. Acceptor–Donor–Acceptor-Linked Triphenylamine and Phenothiazine Motifs as Cousin Molecules: The Methyl Effect on Stimuli-Responsiveness, Crystallochromism, and Dual-State Emission. *New J. Chem.* **2021**, *45* (45), 21236–21247.
(38) Ersoy, G.; Henary, M. Roadmap for Designing Donor-π-Acceptor Fluorophores in UV-Vis and NIR Regions: Synthesis, Optical Properties and Applications. *Biomolecules*. 2025.
(39) Derkowski, W.; Kumar, D.; Gryber, T.; Wagner, J.; Morawiak, M.; Kochman, M. A.; Kubas, A.; Data, P.; Lindner, M. V-Shaped Donor–Acceptor Organic Emitters. A New Approach towards Efficient TADF OLED Devices. *Chem. Commun.* **2023**, *59* (19), 2815–2818.
(40) Prachumrak, N.; Sudyoadsuk, T.; Thangthong, A.; Nalaoh, P.; Jungsuttiwong, S.; Daengngern, R.; Namuangruk, S.; Pattanasattayavong, P.; Promarak, V. Improvement of D–π–A Organic Dye-Based Dye-Sensitized Solar Cell Performance by Simple Triphenylamine Donor Substitutions on the π-Linker of the Dye. *Mater. Chem. Front.* **2017**, *1* (6), 1059–1072.
(41) Cao, H.; Li, T.; Zhao, L.; Qiang, Y.; Zheng, X.; Dai, S.; Chen, Y.; Zhu, Y.; Zhao, L.; Cai, R.; Sun, Z.; Li, F.; Yang, Y.; Zhang, L.; Yip, H.-L.; Yu, Z. Triphenylamine-Based Hole-Transporting Ligands for 2D/3D FAPbI3 Perovskite Solar Cells. *ACS Energy Lett.* **2025**, *10* (4), 2017–2025.
(42) Jagtap, S. P.; Mukhopadhyay, S.; Coropceanu, V.; Brizius, G. L.; Brédas, J.-L.; Collard, D. M. Closely Stacked Oligo(Phenylene Ethynylene)s: Effect of π-Stacking on the Electronic Properties of Conjugated Chromophores. *J. Am. Chem. Soc.* **2012**, *134* (16), 7176–7185.
(43) Syamakumari, A.; Schenning, A. P. H. J.; Meijer, E. W. Synthesis, Optical Properties, and Aggregation Behavior of a Triad System Based on Perylene and Oligo(p-Phenylene Vinylene) Units. *Chem. – A Eur. J.* **2002**, *8* (15), 3353–3361.

(44) Liu, G.-C.; Huang, T.-H.; Wang, H.-W.; Hsu, C.-H.; Chou, P.-T.; Hung, W.-Y.; Wong, K.-T. Exciplex-Forming Cohost Systems with 2,3-Dicyanopyrazinophenanthrene-Based Acceptors to Achieve Efficient Near Infrared OLEDs. *Chem. – A Eur. J.* **2023**, *29* (21), e202203660.

(45) Zhu, L.; Zhao, Y. Cyanostilbene-Based Intelligent Organic Optoelectronic Materials. *J. Mater. Chem. C* **2013**, *1* (6), 1059–1065.

(46) Wang, X.; Ding, Z.; Ma, Y.; Zhang, Y.; Shang, H.; Jiang, S. Multi-Stimuli Responsive Supramolecular Gels Based on a D–π–A Structural Cyanostilbene Derivative with Aggregation Induced Emission Properties. *Soft Matter* **2019**, *15* (7), 1658–1665.

(47) Ma, Y.; Cametti, M.; Džolić, Z.; Jiang, S. Responsive Aggregation-Induced Emissive Supramolecular Gels Based on Bis-Cyanostilbene Derivatives. *J. Mater. Chem. C* **2016**, *4* (46), 10786–10790.

(48) Chung, J. W.; Yoon, S.-J.; An, B.-K.; Park, S. Y. Correction to "High-Contrast On/Off Fluorescence Switching via Reversible E–Z Isomerization of Diphenylstilbene Containing the α-Cyanostilbenic Moiety." *J. Phys. Chem. C* **2017**, *121* (46), 26139.

(49) Externbrink, M.; Riebe, S.; Schmuck, C.; Voskuhl, J. A Dual PH-Responsive Supramolecular Gelator with Aggregation-Induced Emission Properties. *Soft Matter* **2018**, *14* (30), 6166–6170.

(50) Lu, H.; Qiu, L.; Zhang, G.; Ding, A.; Xu, W.; Zhang, G.; Wang, X.; Kong, L.; Tian, Y.; Yang, J. Electrically Switchable Photoluminescence of Fluorescent-Molecule-Dispersed Liquid Crystals Prepared via Photoisomerization-Induced Phase Separation. *J. Mater. Chem. C* **2014**, *2* (8), 1386–1389.

(51) Xu, F.; Sheng, J.; Stindt, C. N.; Crespi, S.; Danowski, W.; Hilbers, M. F.; Buma, W. J.; Feringa, B. L. All-Visible-Light-Driven Stiff-Stilbene Photoswitches. *Chem. Sci.* **2024**, *15* (18), 6763–6769.

(52) Wang, H.; Zhao, C.; Burešová, Z.; Bureš, F.; Liu, J. Cyano-Capped Molecules: Versatile Organic Materials. *J. Mater. Chem. A* **2023**, *11* (8), 3753–3770.

(53) An, B.-K.; Gierschner, J.; Park, S. Y. π-Conjugated Cyanostilbene Derivatives: A Unique Self-Assembly Motif for Molecular Nanostructures with Enhanced Emission and Transport. *Acc. Chem. Res.* **2012**, *45*, 544.

(54) Saltiel, J.; Waller, A.; Sun, Y. P.; Sears, D. F. J. Cis-Stilbene Fluorescence in Solution. Adiabatic 1c*.Fwdarw.1t* Conversion. *J. Am. Chem. Soc.* **1990**, *112* (11), 4580–4581.

(55) Martínez-Abadía, M.; Robles-Hernández, B.; Villacampa, B.; de la Fuente, M. R.; Giménez, R.; Ros, M. B. Cyanostilbene Bent-Core Molecules: A Route to Functional Materials. *J. Mater. Chem. C* **2015**, *3* (13), 3038–3048.

(56) Zhu, L.; Li, X.; Zhang, Q.; Ma, X.; Li, M.; Zhang, H.; Luo, Z.; Ågren, H.; Zhao, Y. Unimolecular Photoconversion of Multicolor Luminescence on Hierarchical Self-Assemblies. *J. Am. Chem. Soc.* **2013**, *135* (13), 5175–5182.

(57) Jana, P.; Paramasivam, M.; Khandelwal, S.; Dutta, A.; Kanvah, S. Perturbing the AIEE Activity of Pyridine Functionalized α-Cyanostilbenes with Donor Substitutions: An Experimental and DFT Study. *New J. Chem.* **2020**, *44* (1), 218–230.

(58) M, J. H.; Giri, A.; Kundu, S.; Kumar, V.; Sk, B.; Patra, A. Pyrene-Cyanostyrene-Pyridine Triad: Multi-Stimuli Responsive Fluorescent Emitter and Mitochondrial Imaging. *Chem. Phys. Impact* **2021**, *3*, 100036.

(59) Afrin, A.; Chinna Ayya Swamy, P. Symphony of Light: AIE and MFC in Carbazole-Based Cyanostilbenes. *J. Mater. Chem. C* **2024**, *12* (6), 1923–1944.
(60) Li, B.; Zhang, J.; Wang, J.; Chen, X. Aggregation-Induced Emission-Active Cyanostilbene-Based Liquid Crystals: Self-Assembly, Photophysical Property, and Multiresponsive Behavior. *Molecules*. 2024.
(61) Xue, J.; Tang, F.; Wang, C.; Yang, J.; Ding, A. Tuning Electronic Structures of Carbazole-Cyanostyrene Molecules to Achieve Dual-State Emission for Trace Water Analysis, Picric Acid Sensing, and Reversible Mechanofluorochromism. *ChemPhotoChem* **2022**, *6* (12), e202200184.
(62) An, B.-K.; Kwon, S.-K.; Jung, S.-D.; Park, S. Y. Enhanced Emission and Its Switching in Fluorescent Organic Nanoparticles. *J. Am. Chem. Soc.* **2002**, *124* (48), 14410–14415.
(63) An, B.-K.; Lee, D.-S.; Lee, J.-S.; Park, Y.-S.; Song, H.-S.; Park, S. Y. Strongly Fluorescent Organogel System Comprising Fibrillar Self-Assembly of a Trifluoromethyl-Based Cyanostilbene Derivative. *J. Am. Chem. Soc.* **2004**, *126* (33), 10232–10233.
(64) Xie, W.; Li, Y.; Li, F.; Shen, F.; Ma, Y. Amplified Spontaneous Emission from Cyano Substituted Oligo(p-Phenylene Vinylene) Single Crystal with Very High Photoluminescent Efficiency. *Appl. Phys. Lett.* **2007**, *90* (14), 141110.
(65) Li, Y.; Li, F.; Zhang, H.; Xie, Z.; Xie, W.; Xu, H.; Li, B.; Shen, F.; Ye, L.; Hanif, M.; Ma, D.; Ma, Y. Tight Intermolecular Packing through Supramolecular Interactions in Crystals of Cyano Substituted Oligo(Para-Phenylene Vinylene): A Key Factor for Aggregation-Induced Emission. *Chem. Commun.* **2007**, No. 3, 231–233.
(66) Park, S. K.; Kim, J. H.; Yoon, S.-J.; Kwon, O. K.; An, B.-K.; Park, S. Y. High-Performance n-Type Organic Transistor with a Solution-Processed and Exfoliation-Transferred Two-Dimensional Crystalline Layered Film. *Chem. Mater.* **2012**, *24* (16), 3263–3268.
(67) Jimenez, E. R.; Rodríguez, H. Aggregation-Induced Emission: A Review of Promising Cyano-Functionalized AIEgens. *J. Mater. Sci.* **2020**, *55* (4), 1366–1387.
(68) Li, J.; Wang, J.; Li, H.; Song, N.; Wang, D.; Tang, B. Z. Supramolecular Materials Based on AIE Luminogens (AIEgens): Construction and Applications. *Chem. Soc. Rev.* **2020**, *49* (4), 1144–1172.
(69) Huang, G.; Chang, X.; Jiang, Y.; Lin, B.; Li, B. S.; Tang, B. Z. Multi-Stimuli Responsive Cyanostilbene Derivatives: PH, Amine Vapor Sensing and Mechanoluminescence. *Mater. Chem. Front.* **2020**, *4* (6), 1720–1728.
(70) Hang, C.; Wu, H.-W.; Zhu, L.-L. π-Conjugated Cyanostilbene-Based Optoelectric Functional Materials. *Chinese Chem. Lett.* **2016**, *27* (8), 1155–1165.
(71) Yu, H.; Wu, W.; Zhao, H.; Chen, K.; Li, S.; Tan, M.; Wang, T.; Huang, X.; Wang, N.; Hao, H. Cyanostyrene Derivative with Multi-Stimuli Responsive Properties: Multicolor- and High-Color-Contrast Switching in Response to Force, Heat and Light. *Dye. Pigment.* **2023**, *220*, 111727.
(72) Katla, J.; Kumari, B.; Kanvah, S. Small Molecule Organogels from AIE Active α-Cyanostilbenes. In *Handbook of Aggregation-Induced Emission*; 2022; pp 255–276.
(73) Gawade, V. K.; Jadhav, R. W.; Bhosale, S. V. AIE-Based & Organic Luminescent Materials: Nanoarchitectonics and Advanced Applications. *Chem. – An Asian J.* **2024**,

19 (21), e202400682.

(74) Mei, J.; Leung, N. L. C.; Kwok, R. T. K.; Lam, J. W. Y.; Tang, B. Z. Aggregation-Induced Emission: Together We Shine, United We Soar! *Chem. Rev.* **2015**, *115* (21), 11718–11940.

(75) Ma, X.; Sun, R.; Cheng, J.; Liu, J.; Gou, F.; Xiang, H.; Zhou, X. Fluorescence Aggregation-Caused Quenching versus Aggregation-Induced Emission: A Visual Teaching Technology for Undergraduate Chemistry Students. *J. Chem. Educ.* **2016**, *93* (2), 345–350.

(76) Thomas, S. W.; Joly, G. D.; Swager, T. M. Chemical Sensors Based on Amplifying Fluorescent Conjugated Polymers. *Chem. Rev.* **2007**, *107* (4), 1339–1386.

(77) Menon, A.; Galvin, M.; Walz, K. A.; Rothberg, L. Structural Basis for the Spectroscopy and Photophysics of Solution-Aggregated Conjugated Polymers. *Synth. Met.* **2004**, *141* (1), 197–202.

(78) Lemmer, U.; Heun, S.; Mahrt, R. F.; Scherf, U.; Hopmeier, M.; Siegner, U.; Go¨bel, E. O.; Mu¨llen, K.; Ba¨ssler, H. Aggregate Fluorescence in Conjugated Polymers. *Chem. Phys. Lett.* **1995**, *240* (4), 373–378.

(79) Liu, Y.; Wang, L.; Xu, L.; Song, Y. From Aggregation-Caused Quenching to Aggregation-Induced Delayed Fluorescence: The Impact of the Effect of Substituents. *J. Mater. Chem. C* **2023**, *11* (39), 13403–13417.

(80) Hong, Y.; Lam, J. W. Y.; Tang, B. Z. Aggregation-Induced Emission: Phenomenon, Mechanism and Applications. *Chem. Commun.* **2009**, No. 29, 4332–4353.

(81) Luo, J.; Xie, Z.; Lam, J. W. Y.; Cheng, L.; Chen, H.; Qiu, C.; Kwok, H. S.; Zhan, X.; Liu, Y.; Zhu, D.; Tang, B. Z. Aggregation-Induced Emission of 1-Methyl-1,2,3,4,5-Pentaphenylsilole. *Chem. Commun.* **2001**, No. 18, 1740–1741.

(82) Zhao, Z.; Zhang, H.; Lam, J. W. Y.; Tang, B. Z. Aggregation-Induced Emission: New Vistas at the Aggregate Level. *Angew. Chemie Int. Ed.* **2020**, *59* (25), 9888–9907.

(83) Han, T.; Yan, D.; Wu, Q.; Song, N.; Zhang, H.; Wang, D. Aggregation-Induced Emission: A Rising Star in Chemistry and Materials Science. *Chinese J. Chem.* **2021**, *39* (3), 677–689.

(84) Deans, R.; Kim, J.; Machacek, M. R.; Swager, T. M. A Poly(p-Phenyleneethynylene) with a Highly Emissive Aggregated Phase. *J. Am. Chem. Soc.* **2000**, *122* (35), 8565–8566.

(85) Zhao, Z.; He, B.; Tang, B. Z. Aggregation-Induced Emission of Siloles. *Chem. Sci.* **2015**, *6* (10), 5347–5365.

(86) Takeda, Y. Modulating the Photophysical Properties of Twisted Donor–Acceptor–Donor π-Conjugated Molecules: Effect of Heteroatoms, Molecular Conformation, and Molecular Topology. *Acc. Chem. Res.* **2024**, *57* (15), 2219–2232.

(87) Chiang, Y.-C.; Lai, Z.-L.; Chen, C.-M.; Chang, C.-C.; Liu, B. Construction of Emission-Tunable Nanoparticles Based on a TICT-AIEgen: Impact of Aggregation-Induced Emission versus Twisted Intramolecular Charge Transfer. *J. Mater. Chem. B* **2018**, *6* (18), 2869–2876.

(88) Ma, S.; Du, S.; Pan, G.; Dai, S.; Xu, B.; Tian, W. Organic Molecular Aggregates: From Aggregation Structure to Emission Property. *Aggregate* **2021**, *2* (4), e96.

(89) Fan, G.; Yan, D. Positional Isomers of Cyanostilbene: Two-Component Molecular

Assembly and Multiple-Stimuli Responsive Luminescence. *Sci. Rep.* **2014**, *4* (1), 4933.
(90) Naghibi, S.; Chen, T.; Jamshidi Ghahfarokhi, A.; Tang, Y. AIEgen-Enhanced Protein Imaging: Probe Design and Sensing Mechanisms. *Aggregate* **2021**, *2* (3), e41.
(91) Wang, S.; Zhou, K.; Lyu, X.; Li, H.; Qiu, Z.; Zhao, Z.; Tang, B. Z. The Bioimaging Story of AIEgens. *Chem. Biomed. Imaging* **2023**, *1* (6), 509–521.
(92) Qian, J.; Tang, B. Z. AIE Luminogens for Bioimaging and Theranostics: From Organelles to Animals. *Chem* **2017**, *3* (1), 56–91.
(93) Solodukhin, A. N.; Luponosov, Y. N.; Mannanov, A. L.; Savchenko, P. S.; Bakirov, A. V; Shcherbina, M. A.; Chvalun, S. N.; Paraschuk, D. Y.; Ponomarenko, S. A. Branched Electron-Donor Core Effect in D-π-A Star-Shaped Small Molecules on Their Properties and Performance in Single-Component and Bulk-Heterojunction Organic Solar Cells †. *Energies*. 2021.
(94) Rana, S.; Vaidyanathan, S.; Patel, S. Aggregation Induced Emission (AIE) Based Donor–π–Acceptor Fluorophores: An Approach to Fabricate Acidochromic Sensors and White Light Emitting Diodes. *J. Mater. Chem. C* **2024**, *12* (35), 14148–14164.
(95) Zeng, C.; Cao, Z.; He, Y.; Ye, T.; Gao, Y.; Li, D.; Liu, Q.; Zhou, W.; Fang, W. Multi-Stimuli-Responsive Fluorescence of Bibranched Bromo-Substituted Cyanostilbene Derivative with Aggregation Induced Emission Enhancement and Green Light-Emitting Diode. *Results Opt.* **2022**, *8*, 100264.
(96) Zeng, C.; Yang, T.; Wang, Z.; Chen, K.; Ge, Q.; Peng, W.; Zhang, J.; Liu, J.; Zhang, T.; Sun, M. Functional-Group-Regulated Stimuli-Responsive Banana-Shaped α-Cyanostilbene Derivatives: Dual-State Emission, AIEE, Acidochromism and Their Applications in Anti-Counterfeiting, Fingerprint Recognition and OLEDs. *J. Lumin.* **2024**, *269*, 120452.
(97) Bonnot, M.; Ibrahim, N.; Allain, M.; Frère, P. Designing Dual-State and Aggregation-Induced Emissive Luminogens from Lignocellulosic Biosourced Molecules. *Molecules*. 2024.
(98) Belmonte-Vázquez, J. L.; Amador-Sánchez, Y. A.; Rodríguez-Cortés, L. A.; Rodríguez-Molina, B. Dual-State Emission (DSE) in Organic Fluorophores: Design and Applications. *Chem. Mater.* **2021**, *33* (18), 7160–7184.
(99) Huang, Z.; Tang, F.; He, F.; Kong, L.; Huang, J.; Yang, J.; Ding, A. Pyrene and Triphenylamine Substituted Cyanostyrene and Cyanostilbene Derivatives with Dual-State Emission for High-Contrast Mechanofluorochromism and Cell Imaging. *Org. Chem. Front.* **2022**, *9* (19), 5118–5124.
(100) Zhang, G.; Yao, S.; Miao, M.; Yan, J.; Chen, F.; Yang, J. Dual-State Emission of Anthracene and Triphenylamine Functionalized E-Cyanostilbene Derivative with Mechanochromic Property. *Chem. Pap.* **2025**, *79* (8), 5533–5541.
(101) Bhaumik, S. K.; Kumar, N.; Banerjee, S. Efficient Energy Transfer in Heparin-Based Co-Assemblies of Donor–Acceptor Cyanostilbenes. *J. Mater. Chem. C* **2023**, *11* (20), 6573–6579.
(102) Majumder, R.; Dey, S.; Jana, D.; Ghorai, B. K. Donor-Acceptor Cyanostilbene Based Nano-AIEgens: Synthesis and Properties. *Results Chem.* **2023**, *5*, 100856.
(103) Arivazhagan, C.; Malakar, P.; Jagan, R.; Prasad, E.; Ghosh, S. Dimesitylboryl-Functionalised Cyanostilbene Derivatives of Phenothiazine: Distinctive Polymorphism-

Dependent Emission and Mechanofluorochromism. *CrystEngComm* **2018**, *20* (23), 3162–3166.

(104) Bano, R.; Asghar, M.; Ayub, K.; Mahmood, T.; Iqbal, J.; Tabassum, S.; Zakaria, R.; Gilani, M. A. A Theoretical Perspective on Strategies for Modeling High Performance Nonlinear Optical Materials. *Front. Mater.* **2021**, *Volume 8-2021*.

(105) Sagir, M.; Mushtaq, K.; Khalid, M.; Khan, M.; Tahir, M. B.; Braga, A. A. C. Exploration of Linear and Third-Order Nonlinear Optical Properties for Donor–π-Linker–Acceptor Chromophores Derived from ATT-2 Based Non-Fullerene Molecule. *RSC Adv.* **2023**, *13* (45), 31855–31872.

(106) List, N. H.; Zaleśny, R.; Murugan, N. A.; Kongsted, J.; Bartkowiak, W.; Ågren, H. Relation between Nonlinear Optical Properties of Push–Pull Molecules and Metric of Charge Transfer Excitations. *J. Chem. Theory Comput.* **2015**, *11* (9), 4182–4188.

(107) Shivani; Mishra, A.; Kaur, P.; Singh, K. Synthesis and Nonlinear Optical Behavior of Thermally Stable Chromophores Based on 9,9-Dimethyl-9H-Fluoren-2-Amine: Improving Intrinsic Hyperpolarizability through Modulation of "Push–Pull." *ACS Omega* **2022**, *7* (43), 39045–39060.

(108) Shivani; Mishra, A.; Kaur, P.; Singh, K. Perpetual Extension of Conjugation of Fluorene-Based Donor–Acceptor Dyads Yield Diminished Nonlinear Optical Response. *J. Phys. Chem. C* **2023**, *127* (2), 1260–1272.

(109) Shimizu, A.; Ishizaki, Y.; Horiuchi, S.; Hirose, T.; Matsuda, K.; Sato, H.; Yoshida, J. HOMO–LUMO Energy-Gap Tuning of π-Conjugated Zwitterions Composed of Electron-Donating Anion and Electron-Accepting Cation. *J. Org. Chem.* **2021**, *86* (1), 770–781.

(110) Park, J.; Lee, J. H.; Lim, B.; Lee, N. K.; Sim, G.; Ryu, S.; Kim, I.; Hwang, H.; Lee, J. Fine Tuning of the HOMO–LUMO Gap of 6-(Thiophen-2-Yl) Indolizino[3,2-c]Quinolines and Their Self-Assembly to Form Fluorescent Organic Nanoparticles: Rational Design and Theoretical Calculations. *ChemPhotoChem* **2021**, *5* (1), 58–67.

(111) Lin, X.; Wang, X.; Li, R.; Wang, Z.; Liu, W.; Chen, L.; Chen, N.; Sun, S.; Li, Z.; Hao, J.; Lin, B.; Xie, L. Development of a New Multiple Stimuli-Responsive Fluorescent Material Using the Minus Strategy Based on the Structure of Tetraphenyl-1,3-Butadiene. *ACS Omega* **2022**, *7* (13), 10994–11001.

(112) Xiang, X.; Zhan, Y.; Yang, W. Tetraphenylethene Functionalized Quinoxaline Derivative Exhibiting Aggregation-Induced Emission and Multi-Stimuli Responsive Fluorescent Switching. *Tetrahedron* **2022**, *104*, 132600.

(113) Hariharan, P. S.; Gayathri, P.; Kundu, A.; Karthikeyan, S.; Moon, D.; Anthony, S. P. Synthesis of Tunable, Red Fluorescent Aggregation-Enhanced Emissive Organic Fluorophores: Stimuli-Responsive High Contrast off–on Fluorescence Switching. *CrystEngComm* **2018**, *20* (5), 643–651.

(114) Anthony, S. P. Organic Solid-State Fluorescence: Strategies for Generating Switchable and Tunable Fluorescent Materials. *Chempluschem* **2012**, *77* (7), 518–531.

(115) Hu, L.; Duan, Y.; Xu, Z.; Yuan, J.; Dong, Y.; Han, T. Stimuli-Responsive Fluorophores with Aggregation-Induced Emission: Implication for Dual-Channel Optical Data Storage. *J. Mater. Chem. C* **2016**, *4* (23), 5334–5341.

(116) Wang, J.; Liu, M.; Zhang, X.; Wang, X.; Xiong, M.; Luo, D. Stimuli-Responsive Linkers

and Their Application in Molecular Imaging. *Exploration* **2024**, *4* (4), 20230027.

(117) Akhtar, N.; Biswas, O.; Manna, D. Stimuli-Responsive Transmembrane Anion Transport by AIE-Active Fluorescent Probes. *Org. Biomol. Chem.* **2021**, *19* (34), 7446–7459.

(118) Fernandes, R. S.; Dey, N. Polarity-Independent Temperature-Induced Reversible Fluorescence Switching of Organic Nanoparticles: Application to Intracellular Temperature Imaging. *ACS Appl. Nano Mater.* **2023**, *6* (7), 5168–5176.

(119) Xie, Y.; Li, Z. Recent Advances in the Z/E Isomers of Tetraphenylethene Derivatives: Stereoselective Synthesis, AIE Mechanism, Photophysical Properties, and Application as Chemical Probes. *Chem. – An Asian J.* **2019**, *14* (15), 2524–2541.

(120) Huang, G.; Jiang, Y.; Yang, S.; Li, B. S.; Tang, B. Z. Multistimuli Response and Polymorphism of a Novel Tetraphenylethylene Derivative. *Adv. Funct. Mater.* **2019**, *29* (16), 1900516.

(121) Shi, J.; Chang, N.; Li, C.; Mei, J.; Deng, C.; Luo, X.; Liu, Z.; Bo, Z.; Dong, Y. Q.; Tang, B. Z. Locking the Phenyl Rings of Tetraphenylethene Step by Step: Understanding the Mechanism of Aggregation-Induced Emission. *Chem. Commun.* **2012**, *48* (86), 10675–10677.

(122) Wang, J.; Mei, J.; Hu, R.; Sun, J. Z.; Qin, A.; Tang, B. Z. Click Synthesis, Aggregation-Induced Emission, E/Z Isomerization, Self-Organization, and Multiple Chromisms of Pure Stereoisomers of a Tetraphenylethene-Cored Luminogen. *J. Am. Chem. Soc.* **2012**, *134* (24), 9956–9966.

(123) Xiong, J.; Wang, K.; Yao, Z.; Zou, B.; Xu, J.; Bu, X.-H. Multi-Stimuli-Responsive Fluorescence Switching from a Pyridine-Functionalized Tetraphenylethene AIEgen. *ACS Appl. Mater. Interfaces* **2018**, *10* (6), 5819–5827.

(124) Miteva, T.; Palmer, L.; Kloppenburg, L.; Neher, D.; Bunz, U. H. F. Interplay of Thermochromicity and Liquid Crystalline Behavior in Poly(p-Phenyleneethynylene)s: Π−π Interactions or Planarization of the Conjugated Backbone? *Macromolecules* **2000**, *33* (3), 652–654.

(125) Gupta, R.; Thomas, R.; Kulkarni, G. U. Tunable Solid State Fluorescence Behavior of a Methoxy Substituted Oligo(Phenyleneethynylene): Influence of Cooling Rate and Surface Crystallization. *J. Mater. Chem.* **2012**, *22* (36), 19139–19145.

(126) Quinton, C.; Alain-Rizzo, V.; Dumas-Verdes, C.; Clavier, G.; Vignau, L.; Audebert, P. Triphenylamine/Tetrazine Based π-Conjugated Systems as Molecular Donors for Organic Solar Cells. *New J. Chem.* **2015**, *39* (12), 9700–9713.

(127) Kajjam, A. B.; Giri, S.; V., S. Triphenylamine-Based Donor–π–Acceptor Organic Phosphors: Synthesis, Characterization and Theoretical Study. *Mater. Chem. Front.* **2017**, *1* (3), 512–520.

(128) Wang, X.; Kong, W.; Jiang, T.; Xie, Z.; Zhang, J.; Ma, L.; Redshaw, C.; Zhao, Z.; Feng, X. Pyrene-Based Light-Harvesting Antenna Molecules. *J. Phys. Chem. Lett.* **2025**, *16* (10), 2468–2478.

(129) Athira, P.; Nelliyulla Kappumchalil, R.; Sachin, A. R.; Yoosuf, M.; Thomas, R.; Gopakumar, G. Intramolecular Charge Transfer and Stimuli-Responsive Emission in Cholesterol-Appended Phenothiazine–Cyanostyryl-Based Donor–Acceptor Systems. *J. Phys. Chem. A* **2024**, *128* (20), 3935–3946.

(130) Liang, J.; Fu, S.; Wu, Q.; Wang, P.; Liu, X.; Wang, L.; Liu, Y. Stimuli-Responsive Chiral Aggregation-Induced Emission Luminogens and Their Circularly Polarized Luminescence. *J. Mater. Chem. C* **2024**, *12* (47), 19140–19147.
(131) Zhang, Z.; Liu, X.; Feng, Y.; Yu, Z.-Q.; Wang, L.; Ren, X.-K.; Liu, Y. Aggregation-Mediated Photo-Responsive Luminescence of Cyanostilbene Based Cruciform AIEgens. *J. Mater. Chem. C* **2021**, *9* (3), 975–981.
(132) Chen, Y.; Sahoo, S. R.; Baryshnikov, G. V; Gao, L.; Zhu, Z.; Wu, H. Solution and Solid-State Fluorescence Emission from Cyanostyrene Molecules with Multiple Nitrogen Atoms. *Phys. Chem. Chem. Phys.* **2024**, *26* (42), 26816–26822.
(133) Xue, J.; Tang, F.; Ding, A.; He, F.; Huang, J.; Kong, L.; Yang, J. α-Cyanostilbene Functionalized Carbazole Derivatives Exhibiting Dual-State Emission and Multi-Stimuli Responsive Fluorescent Switching. *J. Lumin.* **2022**, *250*, 119119.

Chapter 2

Experimental and Computational Methods

2.1 Synthesis and Characterization

All starting materials and solvents were obtained from commercial sources and used without further purification. Detailed synthetic procedures for each compound are provided in the respective experimental sections of the following chapters. The synthesized compounds were characterized using ^{1}H NMR and ^{13}C NMR spectroscopy in $CDCl_3$ with TMS as internal standard. The mass spectral data were obtained from Electron Spray Ionization Mass Spectroscopy (ESI-MS), Model-Micromass QTof MicroTM and a Maxis Impact. The CHNS/O data were recorded on a Thermo Scientific FLASH 2000 HT analyzer. The average particle size in the solutions was obtained using a Malvern Panalytical Zetasizer Nano S90 instrument.

2.1.1 Crystallization Techniques

In this thesis, the crystals of the compounds were obtained by the slow evaporation of dilute solution of respective compounds. The single crystals of the compounds pertaining to different chapters were obtained either at room temperature or at 4 °C. The solvents were used either in the form single or mixtures depending on the solubility of the compounds. Specifically, the crystals described in **Chapter 3** were predominantly grown from dilute ethyl acetate/hexane mixtures. The crystals of compounds discussed in in **Chapter 4** were crystallized from ethyl acetate/hexane mixture or pure dichloromethane.

2.1.2 X-ray Diffraction Analysis

X-ray diffraction is a powerful technique for determining the structural arrangement of atoms in crystalline materials, and it is fundamentally based on **Bragg's law**. According to this principle, constructive interference occurs when X-rays are incident on the parallel crystal planes at specific angles, satisfying the condition:

$$n\lambda = 2dsin\theta$$

where 'n' is the order of reflection, 'λ' is the wavelength of the incident X-rays, d'' is the interplanar spacing, and 'θ' is the angle of incidence. The resulting diffraction pattern is unique for each crystalline material and provides detailed information about its atomic arrangement. Thus, analysis of the diffraction data allows precise determination of the molecular and crystal structures of the compounds under investigation.

2.1.2.1 Powder X-ray diffraction analysis

The powder X-ray diffraction (PXRD) provides valuable information related to crystallinity, molecular packing and phase nature through the analysis of peak position, peak intensity, and peak width at half maxima. The PXRD is used as an important tool in this thesis to analyses the stimuli responsive nature of the compounds. The correlation of the diffraction patterns enables the exploration of subtle structural variations, giving a comprehensive understanding of stimuli responsive emission originating from change in molecular packing. The PANalytical Aeris (Cu Kα radiation, λ = 1.5406 Å) operated at 40 kV and 15 mA, was employed to record diffraction patterns presented in various chapters of this thesis. The diffraction data were collected over a 2θ range of 5°–60 °, with step sizes of 0.05 ° for the PANalytical Aeris system.

2.1.2.2 Single-Crystal X-ray Diffraction Studies

Single-crystal X-ray diffraction (SCXRD) is one of the most powerful and reliable techniques for the determination of molecular structures. Unlike powder X-ray diffraction, which provides information on the bulk crystalline phase, SCXRD enables the direct elucidation of the three-dimensional arrangement of atoms within a single, well-formed crystal. This technique provides precise information about bond lengths, bond angles, torsional parameters, and overall molecular geometry. Beyond the molecular structure itself, SCXRD also reveals crucial details regarding intermolecular interactions such as hydrogen bonding, π–π stacking, and van der Waals contacts. These interactions govern the overall molecular packing in the crystal lattice, which in turn influences the physical, optical, and mechanical properties of the material.

2.1.2.2.1 Data Collection

For single-crystal X-ray diffraction studies, good-quality crystals were carefully selected under an Olympus SZ-61 stereozoom microscope equipped with a polarizing filter. Crystals with well-defined morphology and dimensions in the range of 0.1 to 0.4 mm were chosen for data collection to ensure optimal diffraction quality and minimize absorption effects. The selected crystal was mounted on a glass fiber fixed to a copper pin and placed on the goniometer head of the diffractometer. It was carefully aligned with the incident X-ray beam using an optical microscope with crosshairs and a monitor for precise centering. Preliminary diffraction tests were performed to assess crystal quality, including stability, mosaic spread, and diffraction intensity. Suitable crystals were then used for systematic data collection by rotating the

goniometer to capture reflections over multiple orientations. When necessary, a low-temperature device was employed to minimize thermal vibrations, reduce disorder, and prevent solvent loss, thereby enhancing data accuracy.

The X-ray diffraction intensity data for single-crystal measurements were collected using two different diffractometers, depending on the availability and suitability of the samples. A Bruker D8 Quest Eco diffractometer, operating at 50 kV and 30 mA, and equipped with a Photon-III detector, was employed for routine data acquisition. In addition, a Bruker D8 Venture diffractometer, operating at 50 kV and 40 mA with a Photon-II CMOS detector, was used for selected crystals to achieve higher sensitivity and resolution. Both instruments utilized Cu Kα radiation (λ = 1.54184 Å) or Mo Kα radiation (λ = 0.71073 Å**)** depending on the crystal size, quality, and absorption characteristics.

The single-crystal X-ray diffraction data for all compounds, except compound **2b** (Chapter 4), were collected at room temperature (298 K). For compound **2b**, data collection was carried out at 130 K under a stream of liquid nitrogen to improve crystal stability and reduce thermal motion. All measurements were performed using Mo Kα radiation (λ = 0.71073 Å) with a fixed crystal-to-detector distance of 4.5 cm. The data collection strategy was designed and monitored using the APEX-III program suite.[1] Data integration, Lorentz and polarization corrections, and merging of frames were performed with SAINT.[1] Absorption corrections were applied to the merged data using SADABS, and the dataset was averaged with SORTAV, available in the WINGX program suite.[2]

The crystal structures were solved by direct methods using SHELXS-2014 [3]and refined by full-matrix least-squares procedures with SHELXL-2014,[4] both integrated into the WINGX program.[5] Hydrogen atoms bonded to carbon were located from difference Fourier maps and refined isotropically, except in cases involving disorder. The ORTEP plots of all compounds were generated at the 50 % probability level using ORTEP-3. Molecular packing diagrams and intermolecular interaction analyses were carried out using Mercury (version 4.2.0),[6] while additional geometric and interaction parameters were evaluated with PLATON.[7]

2.1.3 UV-Visible absorption and photoluminescence spectroscopy

UV-visible absorption spectroscopy is a widely used technique to investigate the electronic transitions of molecules, particularly π–π* and n–π* transitions. These transitions provide

insights into the electronic structure, conjugation, band gap, and light–matter interactions of the compounds under study. In the chapter 3, UV-visible spectroscopic measurements were performed using a Cary Bio 50 UV-visible spectrometer. The instrument records the absorption of light across the ultraviolet and visible regions, allowing the determination of absorption maxima (λ_{max}), molar extinction coefficients, and optical band gaps. Where as in Chapter 4 UV-visible spectroscopic studies were carried out on Cary 5000 is a high-performance UV-Vis-NIR spectrophotometer with superb photometric performance in the 175-3300 nm range. Such information is crucial for correlating the structural features of the compounds with their photophysical and stimuli-responsive properties**.**

Photoluminescence spectroscopy (P L) is a method used to determine the electronic structure of matter. It is a contactless non-destructive method. The intensity of emitted photons and their spectral positions provide valuable information regarding the electronic structure of the materials under investigation. The fluorescence spectra presented in Chapter 3 and chapter 4 were obtained using a Horiba Jobin Yvon Fluorolog-3-11 spectrofluorimeter. The fluorescence lifetime and the steady state fluorescence studies were conducted on Jobin Yvon Fluorolog-3-11 spectrofluorimeter, FLS1000-xS-t fluorescence lifetime spectrometer and an Edinburgh FLS-1000 photoluminescence spectrometer attached with an integrating sphere. All the fluorescence spectra were recorded with a quartz cuvette of path length 1 cm at a slit width of 1 nm. Absolute fluorescence quantum yield of the compounds in both solid and solution states was recorded on an Edinburg FLS-1000 photoluminescence spectrometer attached with an integrating sphere (chapter 3) and LQE-100 LED Photo-Luminescence Quantum Yield Measurement system (chapter 4).

2.2 Computational chemistry

The primary objective of computational chemistry is to harmonize theoretical approaches with experimental data to achieve a deeper understanding of chemical systems. This integration allows for a synergistic relationship where advanced spectroscopic techniques enhance theoretical modeling, while theoretical predictions, in turn, validate or support experimental observations. Computational chemistry relies primarily on two foundational approaches: classical mechanics and quantum mechanics. Methods derived from quantum mechanics, known as electronic structure methods, are central to this field and are categorized into ab initio, semi-empirical, and density functional theory (DFT) methods. In the context of this study, DFT methods were employed, and a brief overview of each is provided in the following section.

2.2.1 Basis set

Electronic structure calculations begin with the construction of a trial wave function for the system under study. The choice of this trial wave function is the first and most crucial step in solving the Schrödinger equation. To build such a function, one relies on a basis set, a collection of mathematical functions used to approximate the true wave function of the system. In computational chemistry, two main types of basis functions are most commonly employed for this purpose. They are Slater-type orbitals (STOs; χ^{STO}) and Gaussian-type orbitals (GTOs; χ^{GTO}). The mathematical expressions for STOs and GTOs are presented below (Eq. 1.1 and Eq. 1.2, respectively).

$$\chi^{STO}(r,\varphi,\phi) = Nr^{n-1}e^{(-\xi r)}Y_m^l(\varphi,\phi) \qquad \text{(Eq. 2.1)}$$

$$\chi^{GTO}(r,\varphi,\phi) = Nr^{2n-2-l}e^{(-\xi r^2)}Y_m^l(\varphi,\phi) \qquad \text{(Eq. 2.2)}$$

where N is the normalization constant, r is the distance of orbital from the nucleus, n, l, and m refers to principal, azimuthal, and magnetic quantum numbers, ξ is orbital exponent, and $Y_m^l(\varphi,\phi)$ term represent the angular part of the wave function.

The STOs closely resemble hydrogen-like atomic orbitals, making them highly effective for representing the electronic configurations of atoms. However, their main drawback lies in the high computational cost, which becomes especially prohibitive for large systems. To address this limitation, Boys introduced GTOs in 1950. Although a single GTO does not accurately reproduce the shape of an STO, a linear combination of three or more GTOs can closely approximate its behavior. When an orbital is expressed as a combination of multiple GTOs, it is referred to as a contracted Gaussian-type orbital (CGTO), where each individual GTO is termed a primitive Gaussian-type orbital (PGTO).

Basis sets in computational chemistry are further classified according to the number of functions used to represent each atomic orbital. A minimal basis set assigns one function per orbital, such as STO-3G, where each function is formed from three primitive Gaussians; this offers fast but low-accuracy calculations. To improve flexibility**,** double-zeta (DZ) and triple-zeta (TZ) basis sets use two and three functions per orbital, respectively, providing better accuracy at higher computational cost. A more efficient approach is the split-valence basis set, developed by Pople, in which core orbitals are described minimally while valence orbitals, the ones involved in bonding, are expanded with double- or triple-zeta functions. For example, in the 6-31G basis set for fluorine, the 1s core orbital is represented by one function built from

six primitives, while each valence orbital (2s, 2p) is described by two functions, one from three primitives and one from a single primitive. This balanced treatment of core and valence orbitals makes split-valence sets widely used in practical quantum chemical calculations.

2.2.2 Density functional theory (DFT)

DFT is a quantum mechanical method that offers a significant simplification over traditional wave function-based approaches by focusing on electron density as the central variable. Unlike methods such as Hartree-Fock (HF), which require solving the complex many-body wave function dependent on 3N spatial coordinates for a system of N electrons, DFT reduces this complexity by relying solely on the electron density, which depends only on three spatial coordinates regardless of the number of electrons. This reduction transforms a computationally intensive 3N-dimensional problem into a far more manageable three-dimensional one, making DFT a highly efficient and practical tool for studying the electronic structure of atoms, molecules, and solids. Despite this simplification, DFT can still provide accurate results, especially when suitable exchange-correlation functionals are used, and has become one of the most widely employed methods in computational chemistry for investigating molecular properties, reaction mechanisms, and material behavior. Hohenberg and Kohn proposed two fundamental theorems about DFT, which are known as the foundations of DFT.

2.2.2.1 Hohenberg-Kohn theorem

Hohenberg and Kohn proposed two fundamental theorems about DFT, which are known as foundations of DFT. According to their first theorem, the ground state energy of a system (E^0) is a functional of electron density (ρ(r)).[8-10]

$$E^0 = E[\rho_0\,(r)] \qquad \text{(Eq. 2.3)}$$

Here, the ρ_0 should satisfy the condition when N is the total number of electrons.

$$N = \int \rho_0(r) d^3r \qquad \text{(Eq. 2.4)}$$

The second Hohenberg-Kohn theorem states that "the electron density that minimizes the energy of the overall functional is the true electron density corresponding to the full solutions of the Schrödinger equation". The variational principle is applied in DFT also. For a trial $\rho\,(r)$, the energy calculated (E) is always greater than or equal to E^0.

$$E[\rho\,(\mathrm{r})] > E[\rho_0(r)] \geq E^0 \qquad \text{(Eq. 2.5)}$$

It may be noted that, the true functional that relates the ρ (r) to the ground state remains unknown. Hence, the DFT calculations use approximate functionals.

2.2.2.2 Kohn-Sham approach

Kohn and Sham (K-S) introduced a formalism that forms the foundation of modern molecular Density Functional Theory (DFT) calculations. In this approach, the ground-state electron density of a system is determined by assuming that the many-electron system can be treated as an equivalent system of non-interacting electrons. The DFT energy $E[\rho(r)]$ calculated by a trial density $\rho(r)$ can be written as,

$$E[\rho(r)] = T_s[\rho(r)] + E_{ne}[\rho(r)] + J[\rho(r)] + E_{XC}[\rho(r)] \qquad \text{(Eq. 2.6)}$$

where T_s represents the kinetic energy functional for non-interacting electrons, while E_{ne} and J denote the potential energy functional for nuclear-electron interaction and classical electron-electron repulsion respectively. The term E_{XC} refers to the exchange-correlation functional, which accounts for all corrections arising from non-classical electron-electron interactions.

2.2.2.3 Exchange-correlation functional

The exchange-correlation functional E_{XC}, can be expressed as,

$$E_{XC}[\rho(r)] = \Delta T[\rho(r)] + \Delta V[\rho(r)] \qquad \text{(Eq. 2.7)}$$

$\Delta T[\rho(r)]$ represents the kinetic correlation energy while $\Delta V[\rho(r)]$ corresponds to the potential correlation energy and exchange energy. Together, these exchange-correlation energy, which provide the necessary corrections for electron–electron interactions beyond the classical description. It is important to note that the overall accuracy of the Kohn–Sham method strongly depends on the quality of the chosen exchange–correlation functional, $E_{XC}[\rho(r)]$.

The exact form of the exchange–correlation functional, $E_{XC}[\rho(r)]$ is unknown because the explicit functional depends of the exchange-correlation potential energy on the the ρ (r) in real systems has not been determined. Hence, various approximations are employed to obtain practical forms of the exchange-correlation functional.

2.2.3 Time-dependent density functional theory (TDDFT)

TD-DFT has emerged as one of the most widely used and well-established theoretical methods for the investigation of excited-state properties in molecular systems.[8] It provides an efficient and relatively accurate framework for calculating key spectroscopic parameters such as excitation energies, absorption wavelengths, and oscillator strengths. The method combines the strengths of ground-state DFT with a time-dependent formalism, thereby extending the applicability of DFT beyond ground-state properties to a wide range of excited-state phenomena. A major advantage of TDDFT lies in its favourable balance between computational cost and accuracy. In practice, its computational demand is comparable to that of single-excitation-based wavefunction methods, such as configuration interaction singles (CIS) or the random phase approximation (RPA), while often offering improved reliability. The excitation energies in TDDFT are obtained as poles of the frequency-dependent linear response of the electronic density matrix to an external perturbation. This linear response framework makes TDDFT particularly well suited for describing excited states dominated by single-electron excitations, which are common in many organic and inorganic chromophores.[9, 10]

The most general result in the time-dependent setting is given by the Runge–Gross theorem (RGT). For a chosen initial state, the theorem demonstrates that the particle density as a function of time is uniquely determined by the external potential, establishing a one-to-one relationship between them. The potential is fixed by the density up to an additive function that depends only on time, and this correspondence holds regardless of the type of particle-particle interaction, even in the non-interacting limit.[11]

This result provides the conceptual foundation of TDDFT. By ensuring that the density can serve as the basic variable, the RGT makes it possible to construct the TDKS system, a fictitious non-interacting model designed to reproduce the exact density of the interacting system. In this way, the theorem establishes the formal justification, while the TDKS scheme delivers a practical framework for calculations.

Furthermore, TDDFT provides a natural route for evaluating excited-state response properties, as the derivatives of higher-energy states with respect to external perturbations can be systematically derived within the formalism. Despite its broad success, the accuracy of TDDFT is strongly dependent on the choice of the underlying exchange-correlation functional.

Numerous benchmark studies have been conducted to evaluate the performance of different functionals, although such assessments are often less comprehensive and less systematic than would be ideal for drawing general conclusions.

In practical applications, vertical excitation energies are typically calculated within the adiabatic approximation, wherein the exchange–correlation kernel is assumed to be time-independent. Within this approximation, excitation energies, oscillator strengths, and transition dipole moments are routinely computed for a series of low-lying excited states, often focusing on at least the five lowest excited states for each symmetry class. These calculated properties not only enable the prediction of electronic absorption spectra but also provide valuable insight into the nature of electronic transitions and the photophysical behavior of molecular systems.

2.2.3.1 Oscillator strength

When atoms or molecules interact with electromagnetic radiation, three main processes can occur. In spontaneous emission, an excited atom gives off radiation and falls to a lower energy level. In absorption, the system takes in energy from incoming radiation and moves to a higher state. In stimulated emission, an external radiation field can trigger the atom to release photons while dropping to a lower state. The probability of these processes can be described through measurable transition rates.

From the classical side, the electromagnetic field appears in the Hamiltonian through the time-dependent vector potential. If the radiation field is weak, only terms that are linear in this potential need to be kept. The state of the system can be written as a combination of the eigenstates of the unperturbed Hamiltonian. A useful way to describe how strong a transition is comes from the oscillator strength. This is a dimensionless number that tells us how likely it is for an atom or molecule to absorb or emit radiation in a particular transition. In quantum mechanics, it is related to the dipole matrix element between the two states.

The oscillator strength for a transition from state 'i' to state 'j' is written as

$$f_{ij} = \frac{2m_e\omega_{ij}}{3\hbar e^2}|\langle \mathrm{j}|\mathrm{r}|\mathrm{i}\rangle|^2 \qquad \text{(Eq. 2.8)}$$

Where

- m_e is the electron mass,

- e is the electron charge,
- $\hbar$ is the reduced Planck constant,
- ω_{ij} is the angular frequency of the transition,
- and $\langle j|r|i\rangle$ is the dipole matrix element or the transition dipole moment (transition between the initial 'i' and the final 'j' state)

The oscillator strength is directly proportional to the transition dipole moment. It indicates how probable a transition is between two quantum states, depending on the magnitude of the dipole moment. A large oscillator strength means the transition is strong and appears clearly in spectra, while small values correspond to weak transitions. The total sum of oscillator strengths over all transitions equals the number of electrons in the system (Thomas–Reiche–Kuhn sum rule).

2.2.4 Theoretical analyses

A wide range of theoretical analyses have been developed to extract detailed chemical information regarding atomic characteristics and bonding properties within molecular systems, based on computational solutions of the Schrödinger equation. In the present study, several advanced analytical methods are employed to gain deeper insights into the electronic structure and interatomic interactions of the investigated systems. These include molecular electrostatic potential (MESP) analysis, which provides a visualization of charge distribution and potential reactive sites; Non-covalent interaction (NCI) analysis is a method that provides a topological examination of weak interactions within molecular systems based on the electron density and its derivatives. The non-linear optical (NLO) properties were investigated theoretically with DFT calculations. This approach provides insights into the electronic structure and molecular responses responsible for the observed NLO behaviour. Each of these methodologies contributes complementary insights and is briefly outlined in the following sections.

2.2.4.1 Molecular electrostatic potential (MESP) analysis

The MESP is a physically measurable property of a molecule, which can be experimentally determined using diffraction techniques.[12] Theoretically, it is rigorously calculated from the electron density distribution**,** ($\rho(r)$) according to the following equation (Eq. 2.9).[12]

$$V(r) = \sum_A^N \frac{Z_A}{|r-R_A|} - \int \rho\,(r') \frac{d^3r'}{|r-r'|} \qquad \text{(Eq. 2.9)}$$

The electrostatic potential $V(r)$ represent the potential at any point in three-dimensional space defines by the position vector 'r' of a molecule. In this expression Z_A and R_A represents the

nuclear charge and position vector of nucleus A, and $\rho\ (r')$ corresponds to the electron density at 'r'. In Eq. 2.9, the first term describes the nuclear potential whereas the second term accounts for the electronic contributions. The combination of these two terms provides a complete description of the influence of both nuclei and electrons in a particular region of a molecular system.

For a neutral molecule, the $V(r)$ is typically positive near the nucleus and negative in electron-rich regions. The most positive value of the potential in a region, V_{max}, indicates the electron-deficient site, while the most negative value potential (V_{min}) corresponds to the electron-rich site. Consequently, molecular electrostatic potential (MESP) analysis serves as a powerful tool to identify regions associated with lone pairs, π-bonds, electrophilic and nucleophilic sites, as well as noncovalent interactions. Thus, MESP provides an essential link between the electronic distribution of chemical entities and their chemical reactivity and physical properties. In **Chapters 5** and **6**, MESP analysis was employed to visualize the electron density distribution within the molecules. This approach was particularly useful for identifying regions associated with lone pairs and for interpreting the nature of various non-covalent interactions, such as hydrogen bonding and π–π stacking. By mapping the electrostatic potential onto the molecular surface, MESP analysis provided valuable insights into reactive sites and intermolecular interaction patterns.

2.2.4.2 Non-covalent interaction (NCI) analysis

Instead of focusing on strong covalent bonds, NCI[13] identifies and visualizes weak interactions such as hydrogen bonding, van der Waals forces, π–π stacking, and steric repulsion. The NCI analysis was carried out using Multiwfn software[14] based on the wave functions obtained at the corresponding level of theory. The isodensity surfaces and the scatterplots of reduced density gradient (RDG) are plotted using the VMD program[15] and gnuplot,[16] respectively. The RDG (s*(r)*) is a function of the electron density *ρ(r)*, defined by the following equation.[17]

$$s(r) = \frac{1}{2(3\pi^2)^{1/3}} \frac{|\nabla\rho(r)|}{\rho(r)^{4/3}} \qquad \text{(Eq. 2.10)}$$

The weak interactions can be detected by analyzing the reduced density gradient (RDG), which highlights regions of space where electron density is low but non-negligible, precisely the regions where non-covalent interactions occur. The resulting NCI plots or isosurfaces use colour coding to distinguish between attractive interactions (e.g., hydrogen bonds), weak dispersive interactions, and repulsive steric effects. By doing so, NCI analysis offers a detailed and intuitive understanding of how non-covalent forces contribute to molecular stability,

recognition, and function. In **Chapter 5**, NCI analysis was used to gain insights into the attractive interactions that contribute to the stability of the aggregates and their associated emission quenching. In **Chapter 6**, NCI analysis was applied to evaluate the stability of the isomers by examining the various weak interactions present between them.

2.2.4.3 Quantum theory of atoms in molecules (QTAIM) analysis

Bader's Quantum Theory of Atoms in Molecules (QTAIM) [18, 19] analyzes the topology of electron density,$\rho(r)$, in a chemical system. The distribution of $\rho(r)$is characterized by critical points, where the first derivative of $\rho(r)$becomes zero, representing extrema in the electron density-minima, maxima, or saddle points. There are four types of critical points, labeled as (3, -3), (3, -1), (3, +1), and (3, +3). These labels are defined by two parameters: ω, the number of nonzero eigenvalues of the Hessian matrix of $\rho(r)$, and σ, the sum of the signs of these eigenvalues. Here the (3, -3) critical point corresponds to a nuclear critical point, the (3, -1) critical point is a bond critical point (bcp), the (3, +1) critical point is a ring critical point and the (3, +3) critical point is a cage critical point. A bcp is located at the boundary between the atomic basins of two neighboring atoms. Its presence indicates a connection between the $\rho(r)$ of these atoms. This connection, represented by a gradient path linking the two atoms, is called a bond path. The molecular graph of a chemical system is a visual representation showing all critical points along with the network of bond paths, illustrating the bonding and structural framework of the molecule.

In this thesis, the bcp's are used in **chapter 6** to analyze the occurrence and nature of intramolecular noncovalent interactions also to interpret the nature of such interactions through the appearance of (3,-1) bcp's. In QTAIM analysis, the $\rho(r)$ at a bcp gives important insight into the nature of the bond. The $\rho(r)$value indicates the bond's strength: typically, a value greater than 0.20 au corresponds to a covalent bond, while a value below 0.10 au is associated with closed-shell interactions such as ionic, hydrogen, or dihydrogen bonds.

2.2.4.4 Nonlinear optics (NLO)

Nonlinear optics (NLO) is a rapidly developing field of research with profound implications for photonics, optoelectronics, high-speed communication, data storage, and biomedical imaging. Unlike linear optics, where the induced polarization in a medium is directly proportional to the applied electric field, nonlinear optical phenomena arise when the response of matter becomes a nonlinear function of the incident field intensity. This occurs typically

under the influence of high-power laser sources, leading to effects such as harmonic generation, multi-photon absorption, and nonlinear refractive index modulation.

The fundamental relationship governing NLO[20] processes is expressed through the expansion of the polarization vector 'P' in powers of the applied electric field 'E'

$$P = \varepsilon_0\left(\chi^{(1)}E + \chi^{(2)}E^2 + \chi^{(3)}E^3 + \cdots\right) \quad \text{(Eq. 2.11)}$$

where ε_0 is the vacuum permittivity, $\chi^{(1)}$is the linear susceptibility, and $\chi^{(2)}$, $\chi^{(3)}$….are the second- and third-order nonlinear optical susceptibilities. The coefficients $\chi^{(n)}$ determine the strength of the nonlinear response, with $\chi^{(2)}$governing second-order effects such as second-harmonic generation (SHG), and $\chi^{(3)}$describing third-order processes like third-harmonic generation and two-photon absorption. At the molecular level, these macroscopic susceptibilities are directly related to microscopic properties such as the molecular polarizability α, first hyperpolarizability β, and second hyperpolarizability γ, which are defined as higher-order derivatives of the dipole moment (μ) with respect to the applied field:

$$\mu = \mu_0 + \alpha E + \frac{1}{2}\beta E^2 + \frac{1}{6}\gamma E^3 + \cdots \quad \text{(Eq. 2.12)}$$

Here, μ_0 is the permanent dipole moment, α, describes the linear response, β corresponds to the first hyperpolarizability (second-order NLO response), and γ represents the second hyperpolarizability (third-order NLO response). These molecular quantities form the theoretical foundation for predicting and understanding nonlinear optical phenomena.

Computational chemistry provides a powerful framework for evaluating these parameters with high precision. Method based on DFT can be employed to compute α, β, and γ values. By enabling the estimation of NLO coefficients before experimental synthesis, computational calculations significantly reduce costs, accelerate material screening, and provide valuable insight into structure-property relationships. The First hyperpolarizability (β), and the second hyperpolarizability (γ) are calculated in the **chapter 6** using the equations,

$$\beta_0 = [(\beta_{xxx}+\beta_{xyy}+\beta_{xzz})^2 + (\beta_{yyy}+\beta_{yzz}+\beta_{yxx})^2 + (\beta_{zzz}+\beta_{zxx}+\beta_{zyy})^2]^{1/2} \quad \text{(Eq. 2.13)}$$

$$\gamma = 1/5\ [\gamma_{xxxx}+\gamma_{yyyy}+\gamma_{zzzz}+2(\gamma_{xxyy}+\gamma_{yyzz}+\gamma_{xxzz})] \quad \text{(Eq. 2.14)}$$

Thus, the synergy between NLO theory and computational modeling forms a cornerstone in the rational design of novel photonic and optoelectronic materials. This combined approach

not only facilitates the discovery of efficient NLO systems but also deepens our understanding of how molecular and electronic structures influence macroscopic nonlinear responses.

2.3 References

(1) Bruker, APEX2, SAINT and SADABS, **2006**.

(2) Blessing, R. H; Outlier Treatment in Data Merging, *J. Appl. Crystallogr*., **1997**, 30, 421–426.

(3) Sheldrick, G. M.; A short history of SHELX, *Acta Crystallogr. Sect. A Crystallogr*, **2008**, 64, 112– 122.

(4) Sheldrick, G. M.; Crystal structure refinement with SHELXL, *Acta Crystallogr. Sect. C Struct. Chem.*, **2015**, 71, 3–8.

(5) Farrugia, L. J.; *J. Appl. Crystallogr*., **2012**, 45, 849– 854.

(6) Macrae, C. F.; Edgington, P. R.; McCabe, P.; Pidcock, E.; Shields, G. P.; Taylor, R.; Towler, M.; and Van De Streek, J.; *J. Appl. Crystallogr*., **2006**, 39, 453– 457.

(7) Spek, A. L.; *J. Appl. Crystallogr*., **2003**, 36, 713.

(8) Dreuw, A.; Head-Gordon, M. *Chem. Rev*. **2005**, 105, 4009−4037.

(9) Bartolotti, L.J.; *Phys. Rev. A* 24, 1661 (**1981**); 26, 2243 (1982).

(10) Chakravarty, S.; Fogel, M.B.; and Kohn, W.; *Phys. Rev. Lett*. 43, 775 (**1979**).

(11) Density-functional theory for time-dependent systems, E. Runge and E.K.U. Gross, *Phys. Rev. Lett*. 52, 997 (**1984**).

(12) Politzer, P.; Murray, J. S. The Fundamental Nature and Role of the Electrostatic Potential in Atoms and Molecules. *Theor Chem Acc* **2002**, *108*, 134–142.

(13) Johnson, E. R.; Keinan, S.; Mori-Sánchez, P.; Contreras-García, J.; Cohen, A. J.; Yang, W. Revealing Noncovalent Interactions. *J. Am. Chem. Soc.* **2010**, *132* (18), 6498–6506.

(14) Lu, T.; Chen, F. Multiwfn: A Multifunctional Wavefunction Analyzer. *J. Comput. Chem.* **2012**, *33* (5), 580–592.

(15) Humphrey, W.; Dalke, A.; Schulten, K. VMD: Visual Molecular Dynamics. *J. Mol. Graph.* **1996**, *14* (1), 33–38.

(16) Williams, T.; Kelley, C. *Gnuplot 4.5: An Interactive Plotting Program*, 2011, http://gnuplot.info.

(17) Johnson, E. R.; Keinan, S.; Mori-Sánchez, P.; Contreras-García, J.; Cohen, A. J.; Yang, W. Revealing Noncovalent Interactions. *J. Am. Chem. Soc.* **2010**, *132*, 6498–6506.

(18) Bader, R. F. W. Atoms in Molecules. *Acc. Chem. Res.* **1985**, *18* (1), 9–15.

(19) Bader, R. F. W. A Quantum Theory of Molecular Structure and Its Applications. *Chem. Rev.* **1991**, *91*, 893–928.

(20) Thanthiriwatte, K. S.; Nalin de Silva, K. *J. Mol. Struct. (THEOCHEM)* **2002**, 617, 169−175.

Chapter 3

Anthracene Incorporated Cyanostilbene Based Donor-Acceptor Systems: Intramolecular Charge Transfer and Aggregation Induced Emission

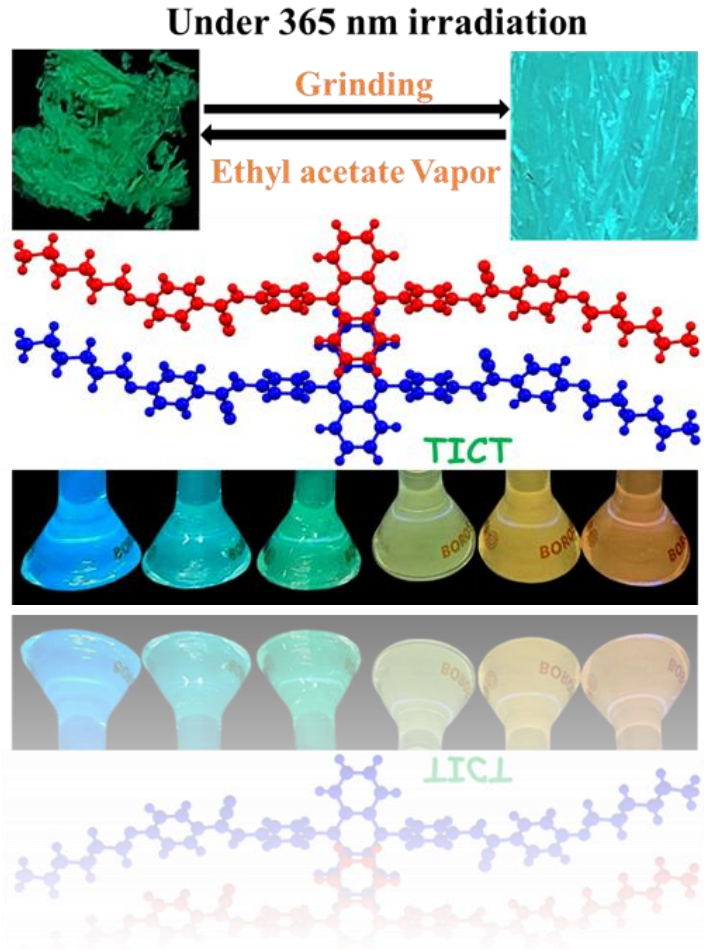

3.1 Abstract

Cyanostilbene systems are highly attractive due to their fascinating fluorescence properties in the solid state. Herein, the synthesis and photophysical properties of highly emissive donor-acceptor systems based on anthracene and cyanostilbene, carrying hexyl (**CS-3.1**) and dodecyl (**CS-3.2**) chains is presented. The molecules showed strong emission in the solution state attributed to the intramolecular charge transfer (ICT). The ICT band in these molecules showed solvatochromic redshift with an increase in the dielectric constant of the solvents. The study explored the solid state emission properties of **CS-3.1** and compared with that of dodecyloxy derivative **CS-3.2**. Both the **CS-3.1** and **CS-3.2** showed strong emission in the solid state attributed to the molecular aggregation. Interestingly, the molecule **CS-3.1** showed a stimuli responsive dual mode luminescence switching under applied stress and ethyl acetate vapours. Owing to the rigid molecular packing, **CS-3.1** showed a higher quantum yield (Φ = 0.43) in the solid state in comparison to polycrystalline **CS-3.2** (Φ = 0.37). The analysis of single crystal structural data of **CS-3.1** has shown that the molecules possess a twisted geometry and the adjacent molecular pairs comprise a J-aggregate, with arrangement along the molecular short axis. A comparative study of powder X-ray diffractograms showed that both **CS-3.1** and **CS-3.2** adopt similar molecular packing with different interplanar distances along the molecular long axis. The present study provides a detailed structure-property correlation of two novel compounds with the potential for various optoelectronic applications.

***<u>Publication based on this chapter</u>**

Femina, C.; Shanthil, M.; Sajith, P. K.; Thomas, R. Anthracene-Incorporated Cyanostilbene Based Donor–Acceptor Systems: Intramolecular Charge Transfer and Aggregation Induced Emission. *New J. Chem.* **2023**, *47* (29), 13810–13819.

3.2 Introduction

Conjugated organic molecules with strong solid state emission, have got much attention for their possible applications in various fields such as electronics,[1,2] optics,[3] memory[4,5] and sensing.[6] Among a range of molecules investigated, the anthracene-based molecules with substantial charge carrier mobility and high quantum efficiency,[7,8] widely used in various optoelectronic devices such as organic field-effect transistors (OFETs),[9] organic light-emitting transistors (OLETs),[10] and organic light-emitting diodes (OLEDs) etc.[11,12] The planar structure and strong π-π interaction of anthracene may favour or unfavour its use depending on the applications.[13,14] Although the π-π stacking improves the charge carrier mobility in anthracene systems, it leads to the quenching of fluorescence in the aggregated state. In addition to their incredible optical properties, anthracene derivatives have got high thermal and photostability compliant for various device applications.[15] These types of special properties make anthracene moieties indispensable for the development of optoelectronic devices which call for excellent luminescent properties.[11] However, the anthracene based molecules are good candidates for optoelectronic devices, most of the compounds faces aggregation induced quenching due to closely spaced anthracene chromophores in the solid state.[16] In this scenario, the design strategies which involve the structural modifications, such as the extension of π-conjugation and control over the π-overlap are relevant. In recent days there are several reports, which adopt design strategies to obtain unquenched solid state emission[17] that rely on various phenomena such as aggregation-induced emission (AIE),[13,18,19] charge transfer (CT),[20,21] restriction of intramolecular rotation,[22] excited state intramolecular proton transfer (ESIPT) etc.[23] These types of materials are known to show solid state emission with high quantum yield and improved lifetime. These class of materials with strong emission in the solid state are potential candidates for the aforementioned applications, especially, in OLEDs, which requires high photoluminescent quantum yield in the solid state.

Aggregation is a common phenomenon, which is observed in most of the systems having π-π stacking and often results in aggregation caused quenching (ACQ).[17] In spite of the possibility for quenching of emission due to π-π stacking certain molecules showed aggregation induced emission or sometimes aggregation induced enhanced emission (AIEE) in the solid state as a result of π-π interactions with slipped molecular arrangement.[24] Nowadays, cyanostilbene based solid state emissive materials received paramount interest attributed to their AIE properties.[25,26] Though the cyanostilbene systems are faintly emissive in the solution state, they are one of the most promising candidates for designing molecules with aggregation-

induced emission in the solid state.[24] In addition to the enhanced emission, in the solid state these class of molecules are known to show switchable emission in response to various stimuli such as pressure,[27–29] temperature,[30] pH[31], solvent, etc.[32–34]

Among various cyanostilbene systems explored, most of them are non-emissive or less emissive in the solution state, consequently, it is relevant to develop systems that are emissive in both solid and solution states with switchable properties. A design strategy that relies on charge transfer (CT) and aggregation capabilities of molecules is promising to develop highly luminescent molecules equipped with switchable emission properties. Recently, Kanvah et al. reported a series of anthracene appended cyanostilbenes carrying trifluoromethane units, where this study focused on gelling properties of the molecules.[35] In another study Tonga reported the effect of π-conjugation and AIE effect on cyanostilbene incorporated with anthracene, naphthalene and pyrene systems[13] and they showed that the steric hindrance due to cyano group and vinylenes enable the polyaromatic hydrocarbons to achieve the twisted conformation and thereby the AIE. One of the recent reports by Tang et al. illustrated the effect of solvatochromism and mechanochromism of two luminogens in terms of the AIEE activity and polymorphism.[36] Hence a detailed study focusing on the mechanistic aspects of the emission of these class of compounds is important.

3.3 Scope of the present investigation

The systematic study focusing on the structural aspects that contribute to the photophysical characteristics of compounds showing highly emissive both in solution and solid state is relevant and critical to address the demands in the field of advanced materials. With an aim to explore the structure property relationship on photophysical properties two anthracene appended cyanostilbene derivatives were designed and synthesized. The new molecular design expected to show intramolecular charge transfer and thereby strong emission in the solid state and solution state. This chapter tries to demonstrate the stimuli responsive emission tuning in both solution and solid states and substantiates the underlying mechanism behind the photophysical properties of the molecules with the support of structural data obtained from single crystal X-ray diffraction.

3.4 Experimental section

All the chemicals and reagents required for the synthesis of anthracene derivatives **CS-3.1** and **CS-3.2** were purchased from commercial supplies and used without further purification. All the compounds were synthesized by following the reported procedures with modifications and

the synthesized compounds were characterized using ^{1}H NMR and ^{13}C NMR spectroscopy in $CDCl_3$ with TMS as internal standard (see **Figure 3.1** to **Figure 3.10**). The CHNS data were recorded on a Thermo Scientific FLASH 2000 HT analyzer. The mass spectral data were obtained from a Thermo Fischer Scientific Exactive mass spectrometer. UV-visible spectroscopic studies were carried out on Carey Bio 50 UV-visible spectrometer. Steady state fluorescence and fluorescence lifetime studies were conducted on a Jobin Yvon Fluorolog-3-11 spectrofluorimeter. All the fluorescence spectra were recorded with a quartz cuvette of path length 1 cm at a slit width of 1 nm. Absolute fluorescence quantum yield of the compounds in both solid and solution states were recorded on Edinburg FLS-1000 photoluminescence spectrometer attached with an integrating sphere. The average particle size in solutions was obtained using Panalytical Zetasizer Nano S90. The single crystal X-ray diffraction data were measured on a Bruker AXS Kappa Apex2 diffractometers. The powder X-ray diffraction intensities were measured on a Panalytical Aeris Research diffractometer.

3.4.1 Synthesis of the compounds CS-3.1 and CS-3.2

The synthesis of compounds **CS-3.1** and **CS-3.2** are summarized in Scheme 3.1. Both **CS-3.1** and **CS-3.2** were prepared from 9,10-dibromoanthracene following a Suzuki coupling with 4-formyl phenylboronic acid resulting in 4,4'-(anthracene-9,10-diyl) dibenzaldehyde. The target molecules with varying alkyl chains were synthesized by a Knoevenagel condensation between 4,4'-(anthracene-9,10-diyl)dibenzaldehyde and corresponding 2-(4-alkyloxyphenyl)acetonitrile (see Scheme 3.1) . Initially, the photochemical properties of **CS-3.1** are investigated by detailed spectroscopic studies. Further, the effect of alkyl chain variation on the photophysical properties is assessed by comparing **CS-3.1** and **CS-3.2** in the solid state.

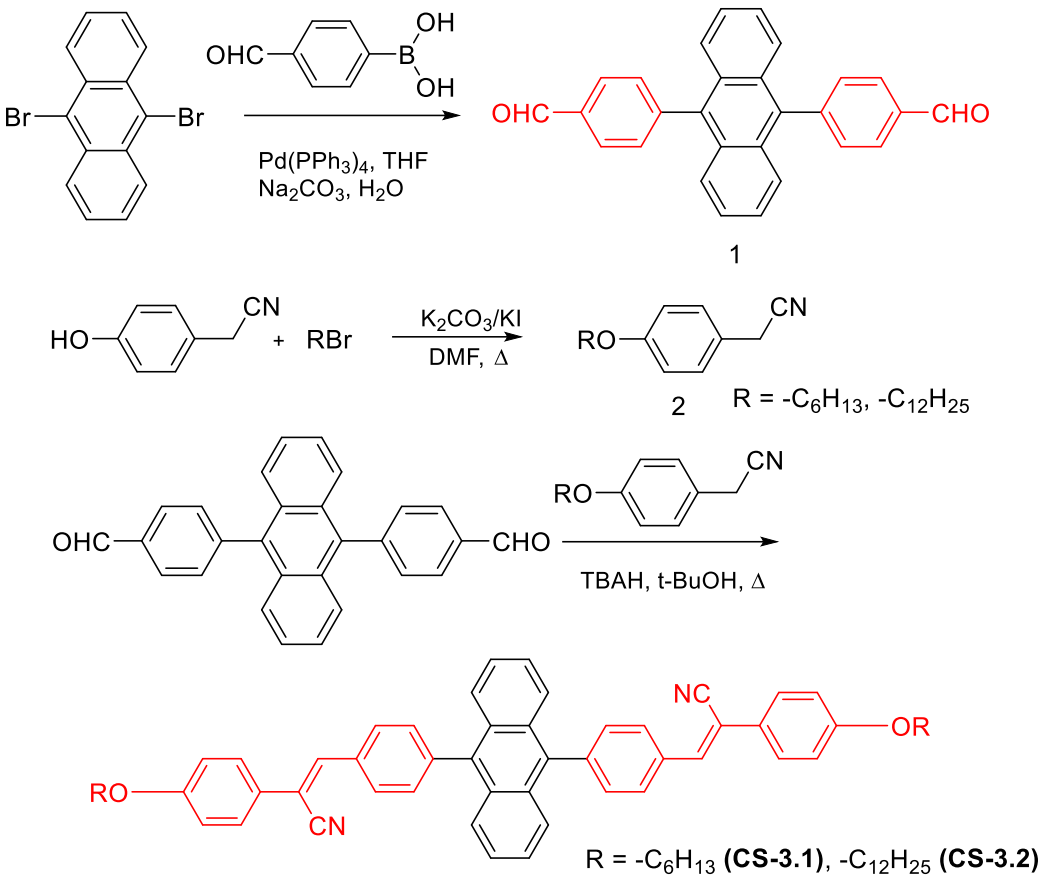

Scheme 3.1. Synthesis of anthracene appended cyanostilbene derivatives with varying alkyloxy chains.

3.4.1.1 Synthetic procedures of the compounds

Synthesis of 4,4'-(anthracene-9,10-diyl)dibenzaldehyde, 1

Compound **1** was synthesized by adopting the previously reported procedures with suitable modifications.[43] A mixture of 9,10-dibromoanthracene (3.08 g, 9.17 mmol), 4-formylphenylboronicacid (4.44 g, 29.61 mmol), aqueous solution of Na_2CO_3 (2 M, 25 mL) and $Pd(PPh_3)_4$ (0.61 g, 0.53 mmol) was added to dry THF 25 mL and the mixture was thoroughly degassed and refluxed for 48 hour under argon atmosphere. The reaction mixture was brought to room temperature and the organic phase was extracted with dichloromethane (3 x 30 mL) and washed with water. The collected organic fraction was dried over anhydrous sodium sulphate and the crude product was purified using column chromatography over silica gel using dichloromethane. The product was characterized using ^{1}H NMR and ^{13}C NMR spectroscopy (see Figure 3.1 and 3.2).

Colourless solid, Yield: 54.52 %,^{1}H NMR (400 MHz, $CDCl_3$) δ (ppm) 10.15 (s, 2H), 8.09 (d, J =8.1 Hz, 4H), 7.63 – 7.60 (m, 4H), 7.55 (dd, J = 6.8, 3.3 Hz, 4H), 7.31 (dd, J = 6.8, 3.2 Hz,

4H).^{13}C NMR (400 MHz, $CDCl_3$) δ (ppm) 192.15, 145.94, 136.16, 135.79, 132.13, 129.91, 129.40, 126.52, 125.70. FT-IR (KBr): ν_{max} 3050, 2913, 2737, 1935, 1700, 1693, 1700, 1603 cm^{-1}.

General method for the synthesis of 2-(4-alkyloxyphenyl)acetonitrile, ***2***

4-alkyloxy substituted phenylacetonitriles were prepared by adopting the previously reported procedure.[44,45] A suspension of K_2CO_3 (4.05 g, 29.2 mmol) in dimethylformamide(DMF) (15mL) was purged with argon for 15 minutes and heated to 80 ºC, and 2-(4-hydroxyphenyl)acetonitrile (1.47 g, 11.0 mmol) was added. 1-bromoalkane (14.2 mmol) was slowly added over 10 minutes and stirred at 80 ºC for 4 hours. The reaction mixture was evaporated and the organic phase was extracted with ethyl acetate and washed with water (3 x 50). The organic phase was evaporated and column chromatographed over silica gel using ethyl acetate/hexane (0.5:9.5) to obtain the target compound. The products were characterized using ^{1}H NMR and ^{13}C NMR spectroscopy (see Figure 3.3 to Figure 3.6).

2-(4-(hexyloxy)phenyl)acetonitrile, 2a: Colourless liquid, Yield: 76 %, ^{1}H NMR (400 MHz, $CDCl_3$) δ (ppm) 7.22 (d, 2H, J = 8.7 Hz), 6.89 (d, 2H, J = 8.7 Hz), 3.94 (t, 2H, J = 6.6 Hz), 3.68, 1.91 – 1.65 (m), 1.45 (m, J = 14.3, 8.8, 4.6, 2.8 Hz), 1.38 – 1.30 (m), 0.97 – 0.78 (m). ^{13}C NMR (400 MHz,$CDCl_3$) δ (ppm) 159.00, 129.12, 121.57, 118.35, 115.16, 77.43, 77.12, 76.80, 68.22, 31.66, 29.25, 25.78, 22.92, 22.69, 14.12. FT-IR (KBr): ν_{max} 3037, 2930, 2857, 2250, 1614, 1513, 1419 cm^{-1}.

2-(4-(dodecyloxy)phenyl)acetonitrile, 2b: Colourless solid, Yield: 79 %, ^{1}H NMR (400 MHz, $CDCl_3$) δ (ppm) 7.14 (d, 2H J = 8.8 Hz), 6.81 (d, 2H, J = 8.7 Hz), 3.87 (t, 2H, J = 6.6 Hz), 3.60, 1.75 – 1.64 (m), 1.37 (p, J = 6.7 Hz), 1.19, 0.81 (t, 3H J = 6.8 Hz).^{13}C NMR (400 MHz, $CDCl_3$) δ (ppm) 158.93, 77.05, 76.73, 68.16, 31.93, 29.67, 29.60, 29.36, 29.21, 26.02, 22.82, 22.70. FT- IR (KBr): ν_{max} 3062, 3042, 2955, 2916, 2848, 2246, 1617, 1517, 1406 cm^{-1}.

Synthesis of compounds **CS-3.1** *and* **CS-3.2**

A mixture of 4,4'-(anthracene-9,10-diyl)dibenzaldehyde (1.3 g, 3.44 mmol) and 2-(4-(hexyloxy)phenyl)acetonitrile (1.5 g, 6.9 mmol) in tert-butyl alcohol (20 mL) was stirred at 50 °C. Tetrabutylammonium hydroxide (TBAH, 1 M solution in methanol, 0.69 mL) was slowly dropped into the mixture and stirred for 2 hours.[46] The resulting precipitate was filtered and purified by column chromatography using dichloromethane as eluent. The structures of **CS-3.1** and **CS-3.2** were confirmed by ^{1}H and^{13}C NMR, and mass spectrometry (see Figure 3.7 to

Figure 3.10). Further, the compound **CS-3.1** was characterized using single-crystal X-ray diffraction.

Compound **CS-3.1**:Yield: 67%,^{1}H NMR (400 MHz, $CDCl_3$) δ (ppm) 8.12 (d, J = 8.2 Hz), 7.73 – 7.67 (m), 7.59, 7.37 (dd, J = 6.9, 3.2 Hz), 7.25, 7.00 (d, J = 8.9 Hz), 4.03 (t, J = 6.6 Hz), 1.86 – 1.78 (m), 1.51 – 1.45 (m), 1.37 (dt, J = 7.3, 3.7 Hz), 0.95 – 0.90 (m). ^{13}C NMR (400 MHz, $CDCl_3$) δ (ppm) 159.92, 141.64, 139.26, 136.66, 133.37, 132.20, 129.82, 129.26, 127.47, 126.94, 125.46, 118.33, 115.23, 111.27, 68.37, 32.01, 29.10, 25.72, 22.83, 14.21. IR (KBr): ν_{max} 3061, 3041, 2923, 2852, 2214, 1607, 1513 cm^{-1}. HRMS (ESI) m/z 784.40 [M^+]. The CHNS analysis of the compound **CS-3.1** gave the following results, C 84.35% H 6.29% and N 3.58%. The calculated values are C 85.74% H 6.6% and N 3.57% for $C_{56}H_{52}N_2O_2$.

Compound **CS-3.2**:Yield: 57%,^{1}H NMR (400 MHz, $CDCl_3$) δ (ppm) 8.13 (d, J = 8.2 Hz), 7.74 – 7.68 (m), 7.61 (d, J = 3.0 Hz), 7.38 (dd, J = 6.8, 5.3 Hz), 7.01 (d, J = 8.9 Hz), 4.03 (t, J = 6.6 Hz), 1.86 – 1.78 (m), 1.48 (q, J = 7.1, 6.2 Hz), 1.29 (q, J = 10.6, 8.7 Hz), 0.91 – 0.87 (m). ^{13}C NMR (400 MHz,$CDCl_3$) δ (ppm) 160.62, 141.54, 139.64, 136.89, 133.86, 131.97, 130.06, 129.25, 127.58, 126.78, 125.44, 118.85, 114.81, 111.77, 68.55, 32.25, 29.49, 29.22, 26.44, 23.20, 14.47. IR (KBr): ν_{max} 3063, 3050, 2922, 2850, 2215, 1608, 1614, 1391 cm^{-1}. HRMS (ESI) m/z 952.59 [M^+]. The CHNS analysis of the compound **CS-3.2** gave the following results, C 85.54% H 7.61% and N 2.85% and the calculated values are C 85.67% H 8.04% and N 2.94% for $C_{68}H_{76}N_2O_2$.

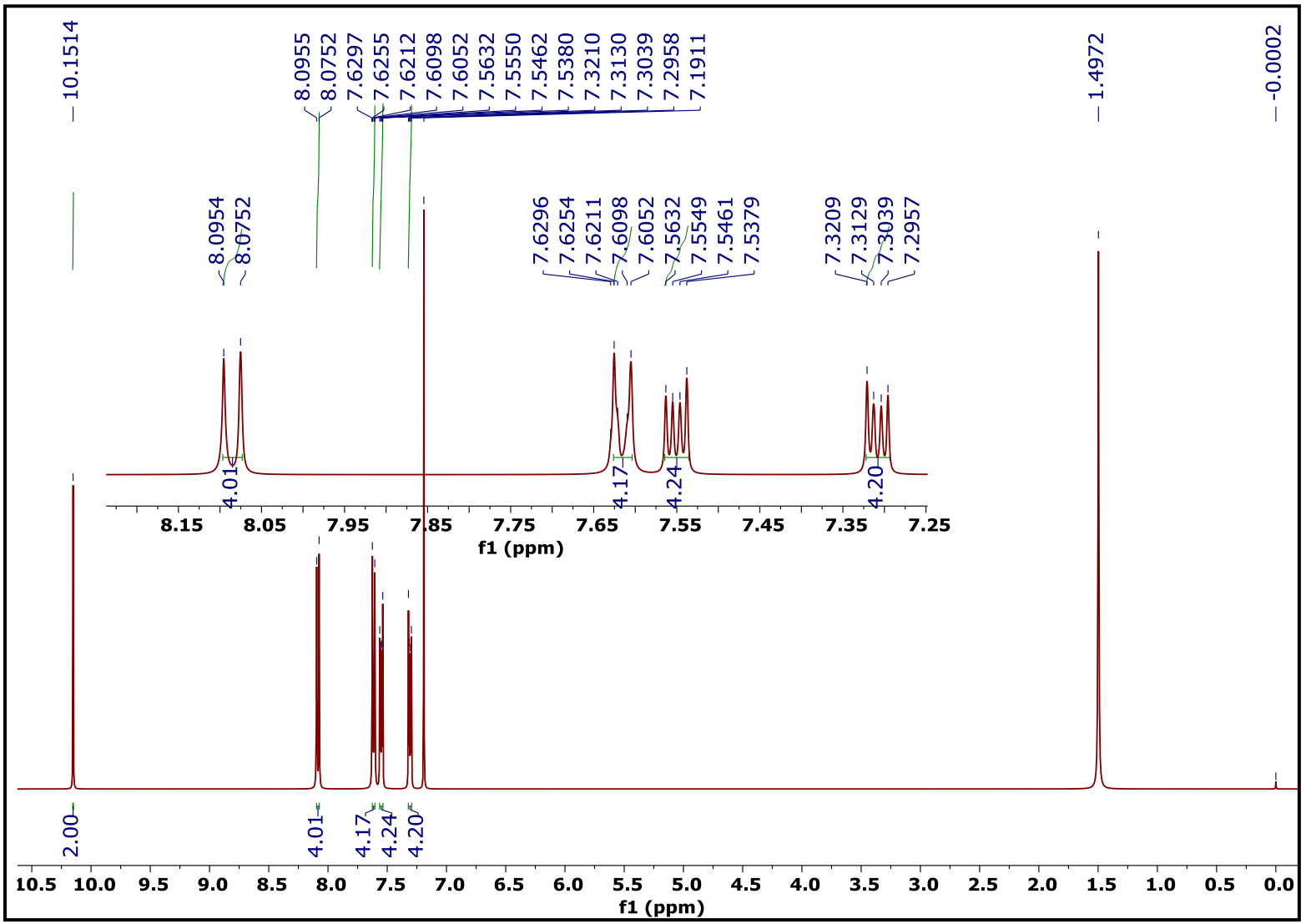

Figure 3.1 ^{1}H NMR spectra of Compound **1** (400 MHz, $CDCl_3$).

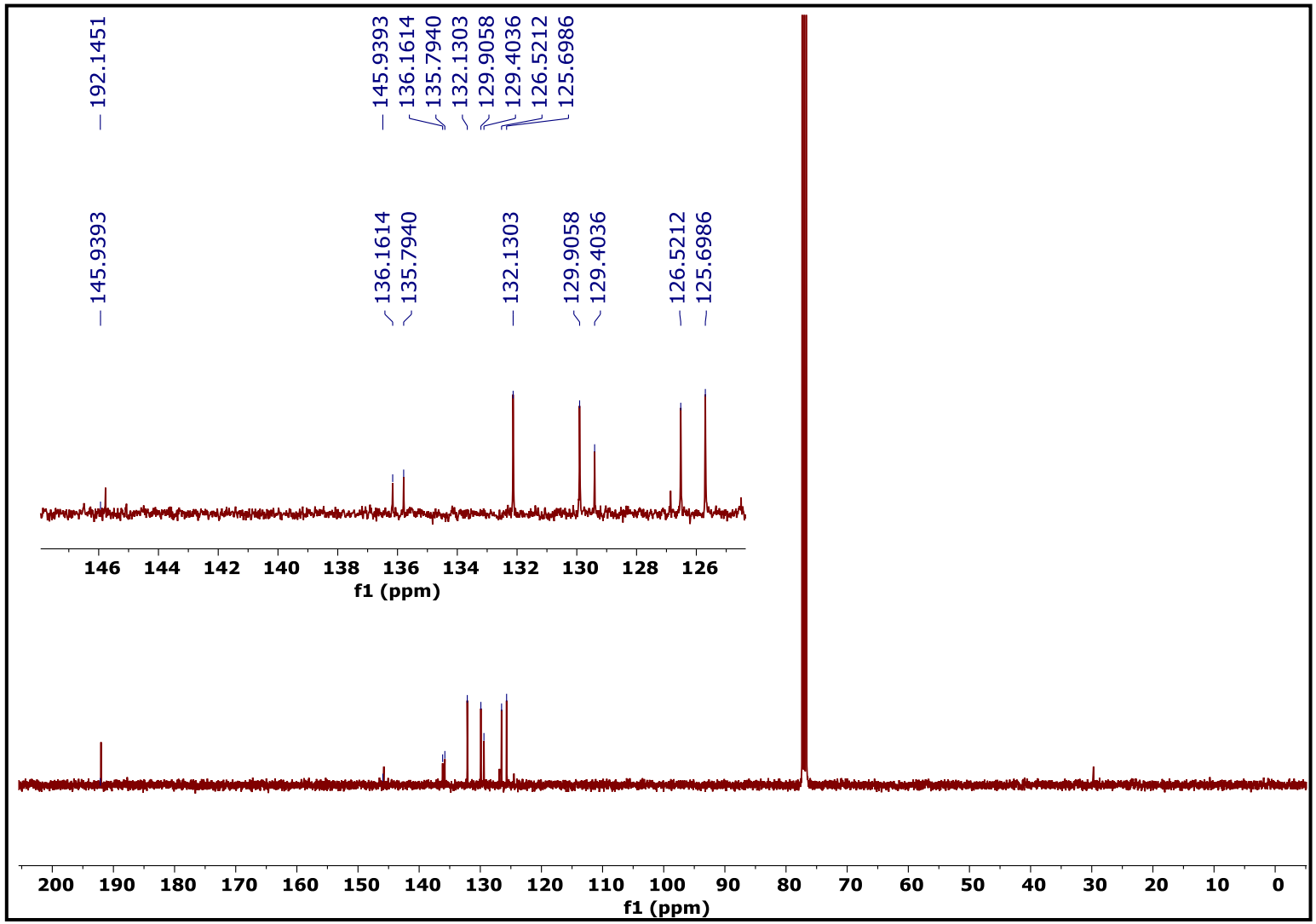

Figure 3.2 ^{13}C NMR spectra of Compound **1** (400 MHz, $CDCl_3$).

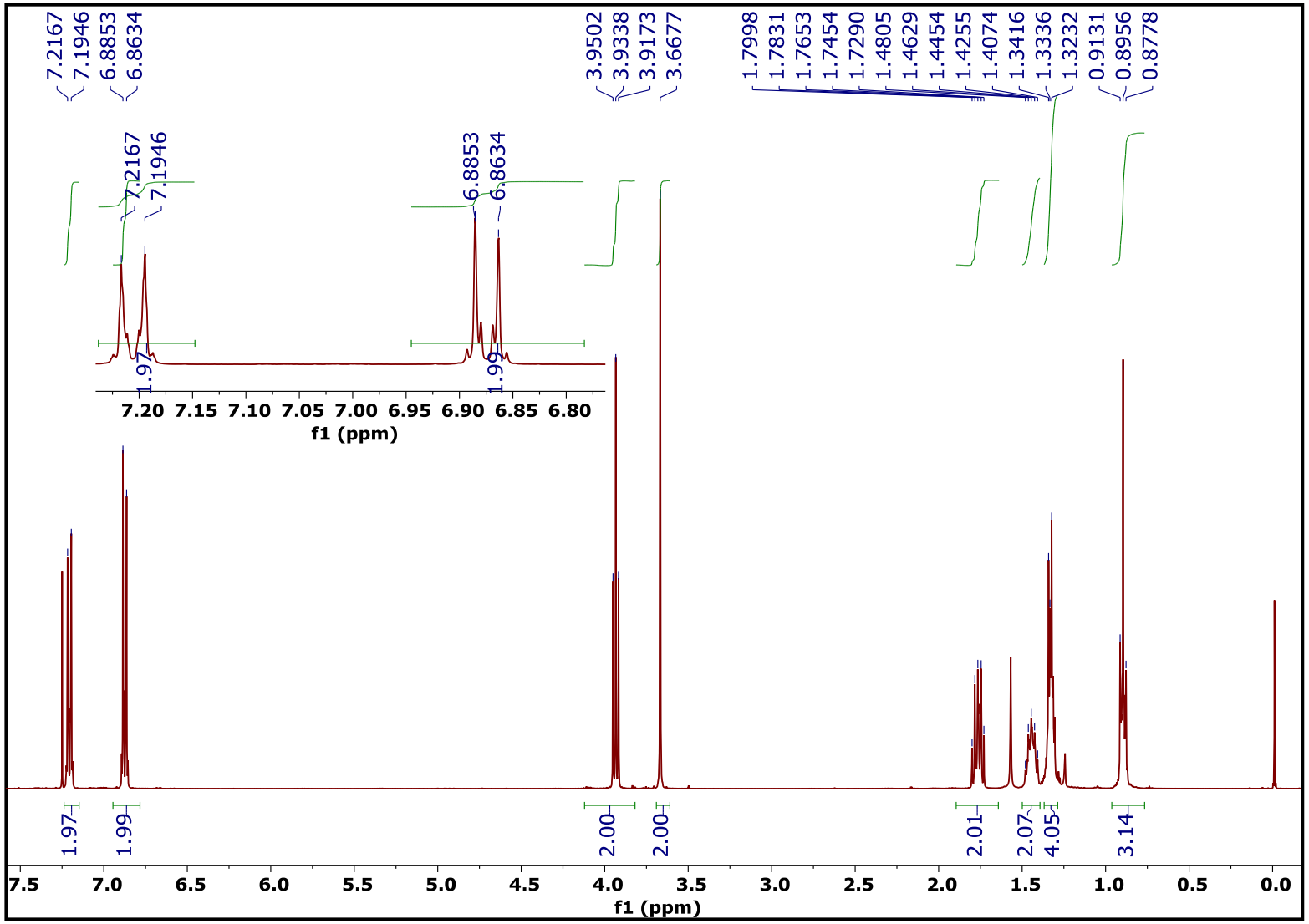

Figure 3.3 ^{1}H NMR spectra of Compound **2a** (400 MHz, $CDCl_3$).

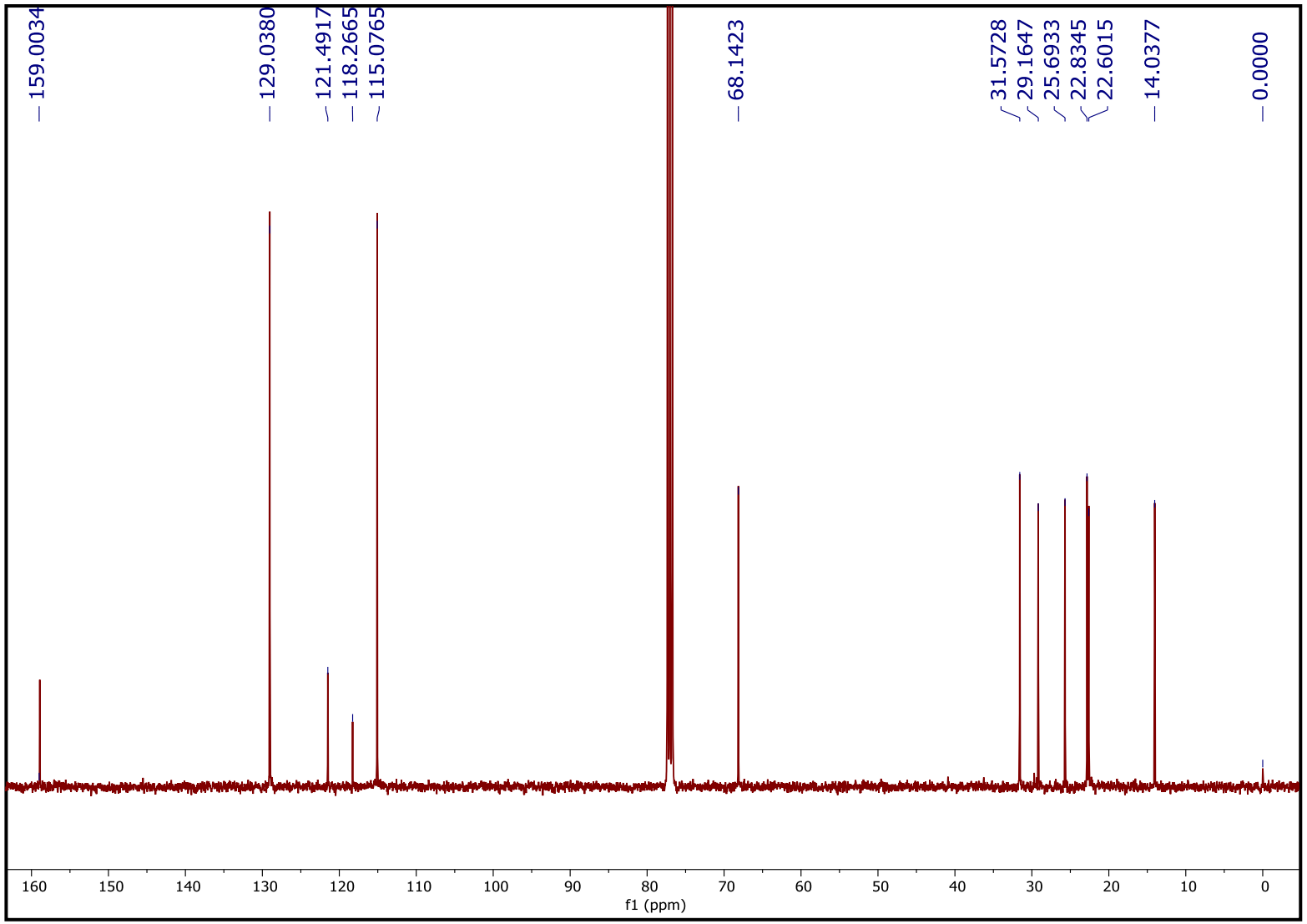

Figure 3.4 ^{13}C NMR spectra of Compound **2a** (400 MHz, $CDCl_3$).

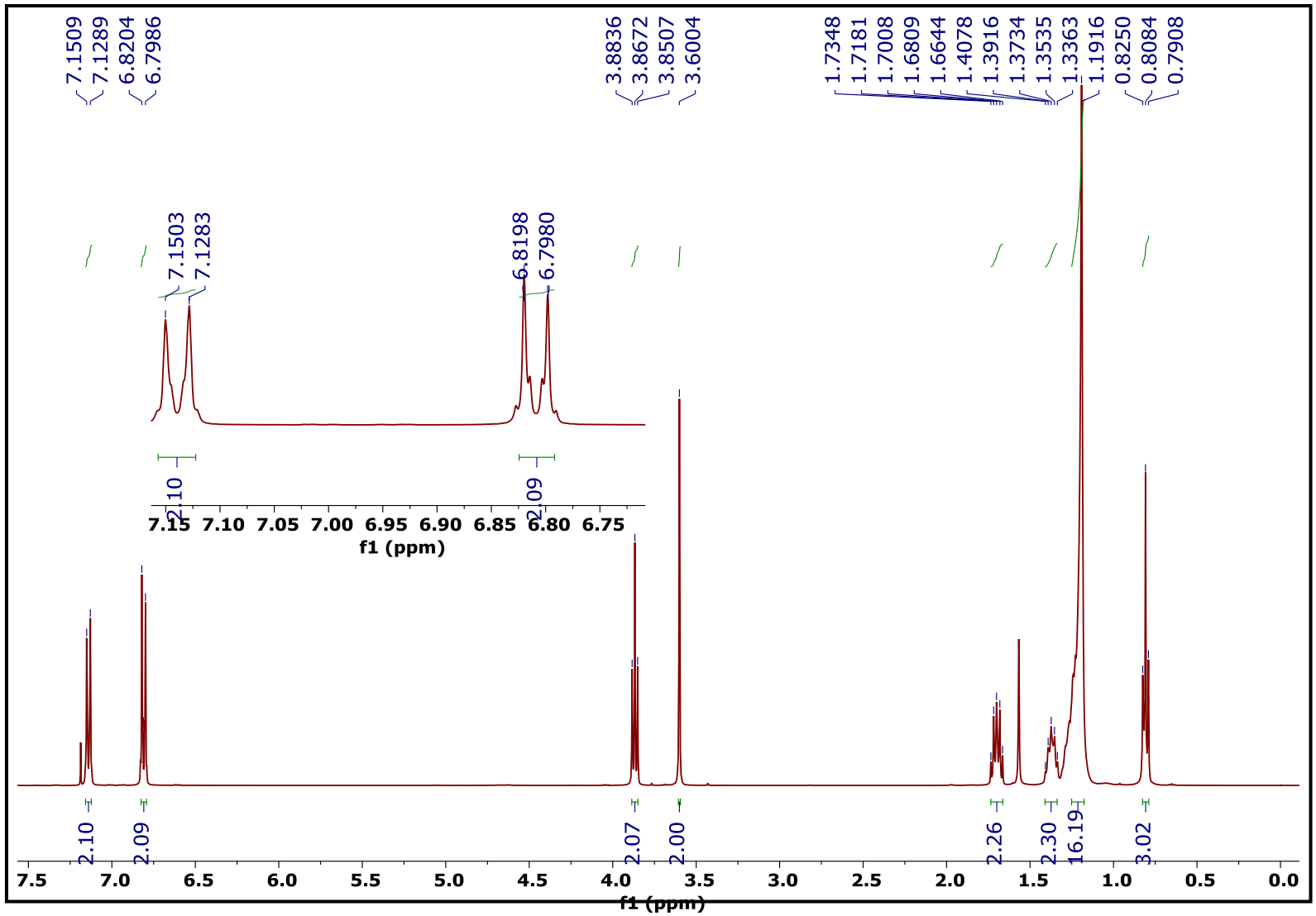

Figure 3.5 ^{1}H NMR spectra of Compound **2b** (400 MHz, $CDCl_3$).

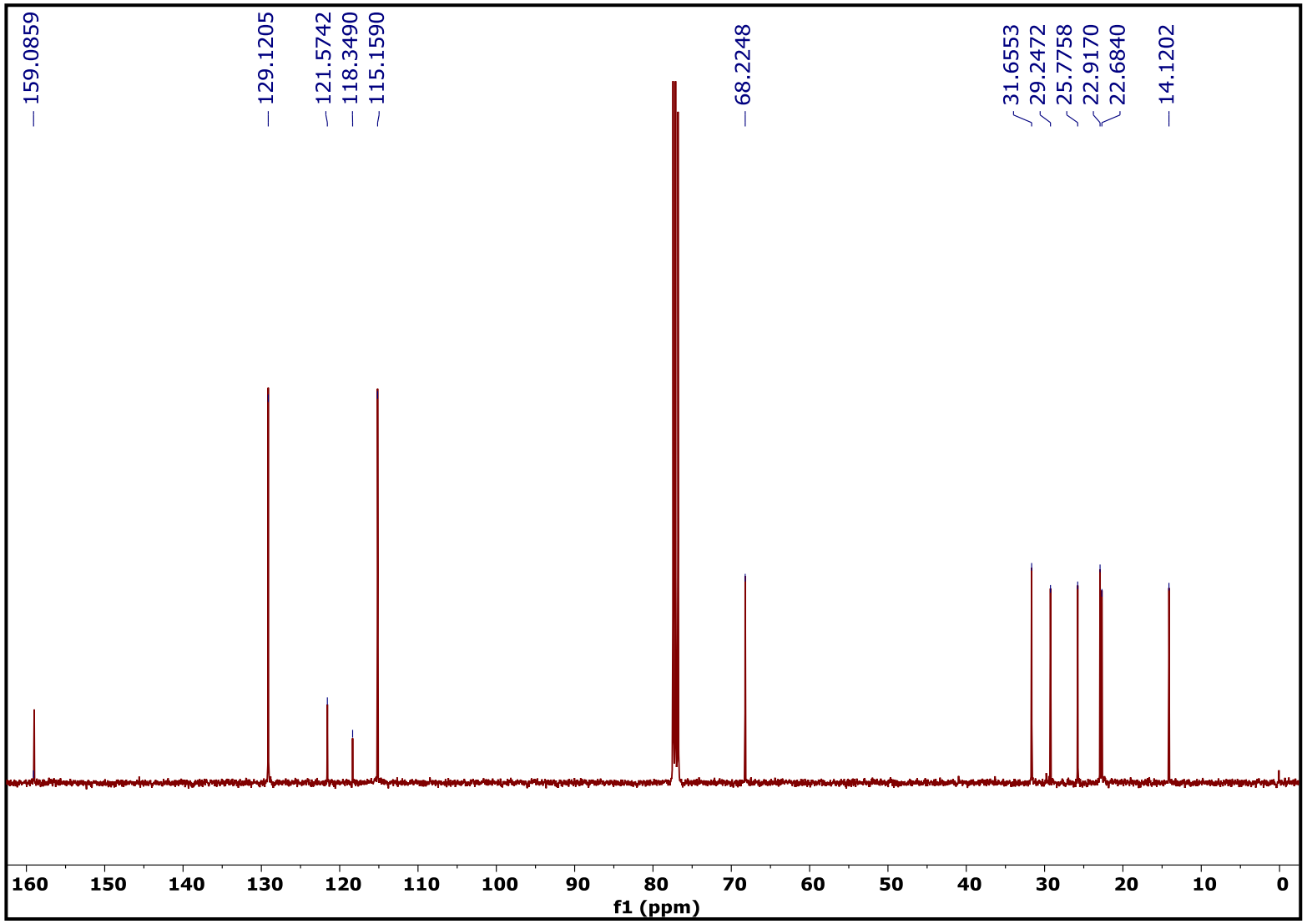

Figure 3.6 ^{13}C NMR spectra of compound **2b** (400 MHz, $CDCl_3$).

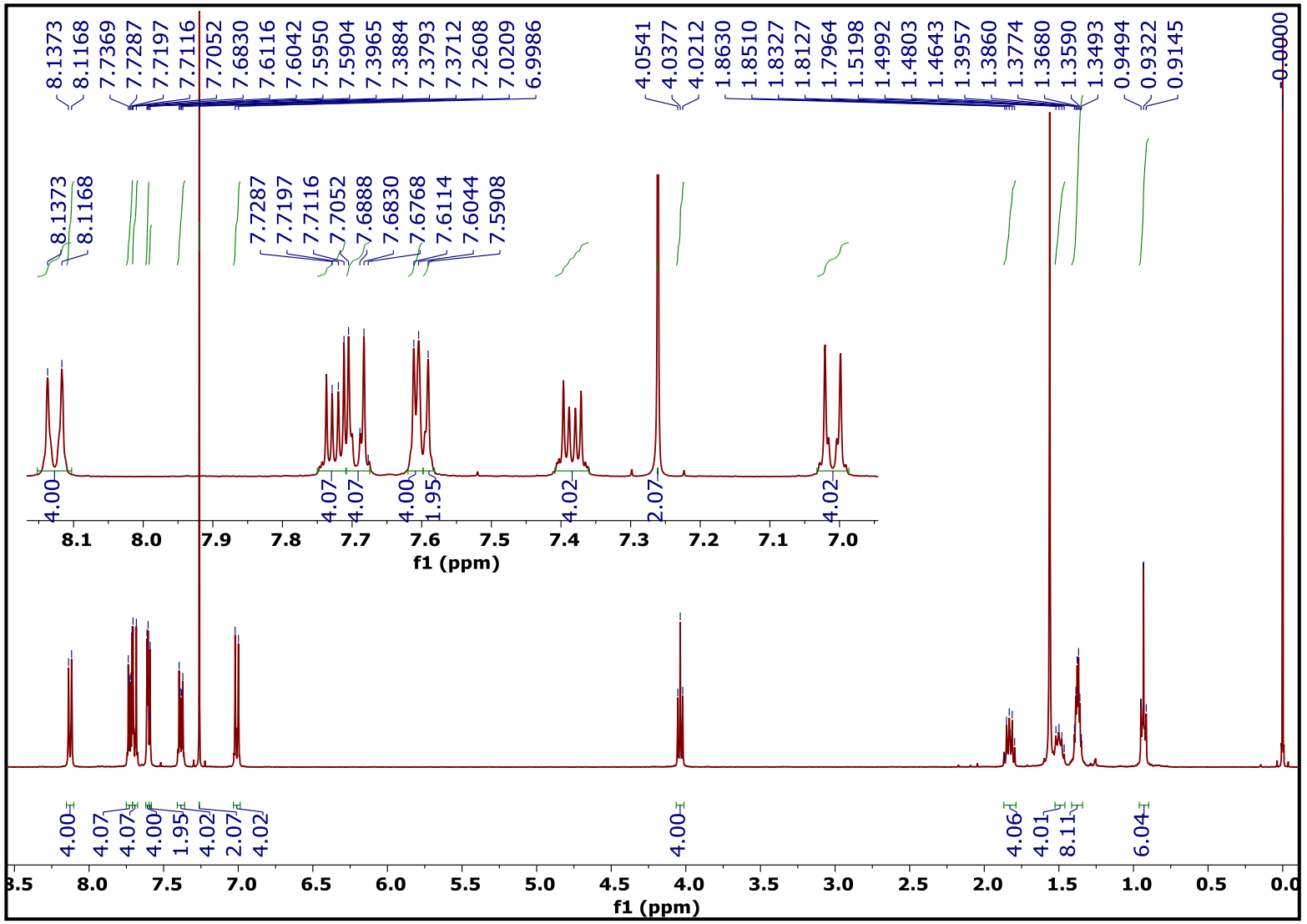

Figure 3.7 ^{1}H NMR spectra of compound **CS-3.1** (400 MHz, $CDCl_3$).

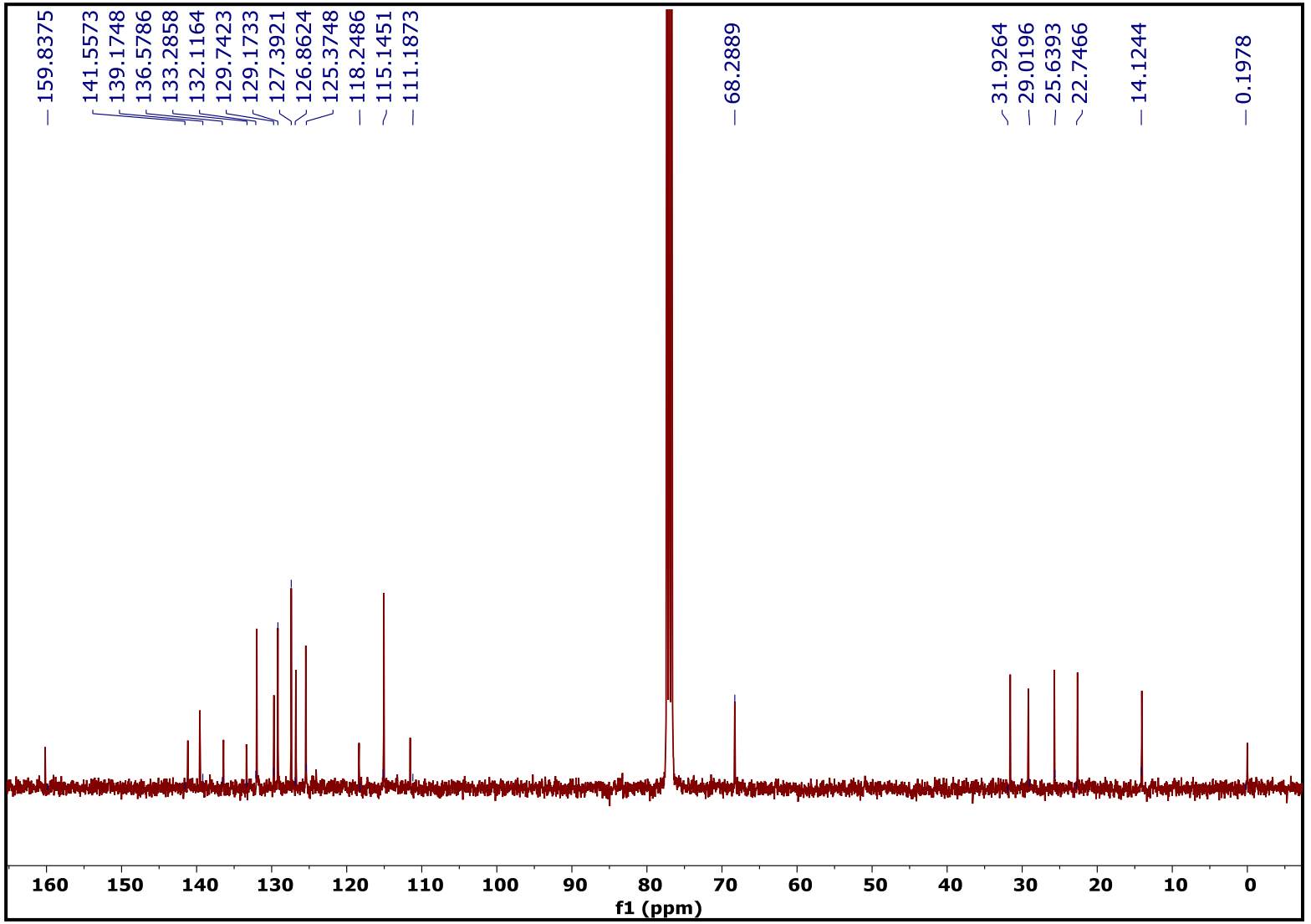

Figure 3.8 ^{13}C NMR spectra of compound **CS-3.1** (400 MHz, $CDCl_3$).

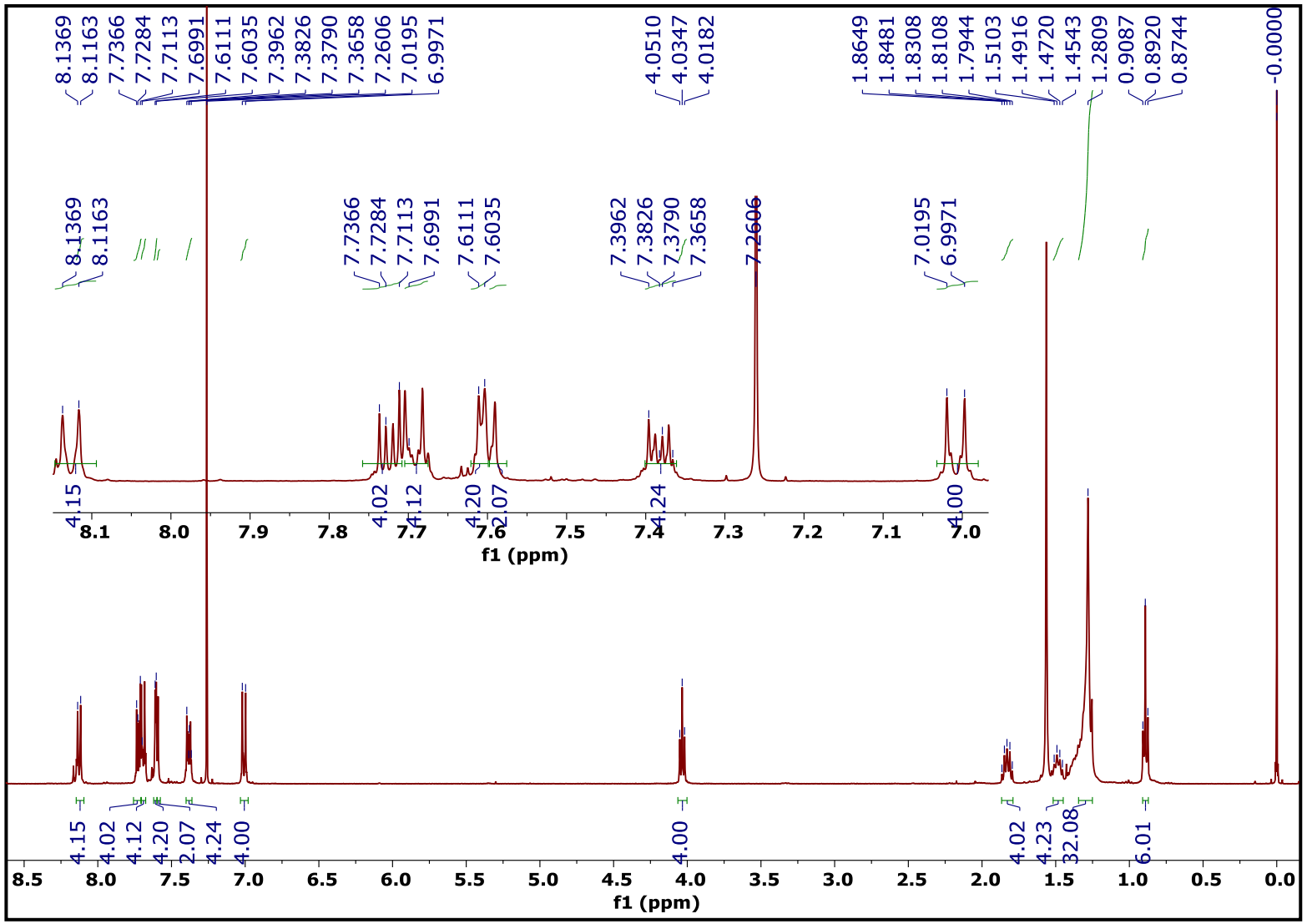

Figure 3.9 ^{1}H NMR spectra of compound **CS-3.2** (400 MHz, $CDCl_3$).

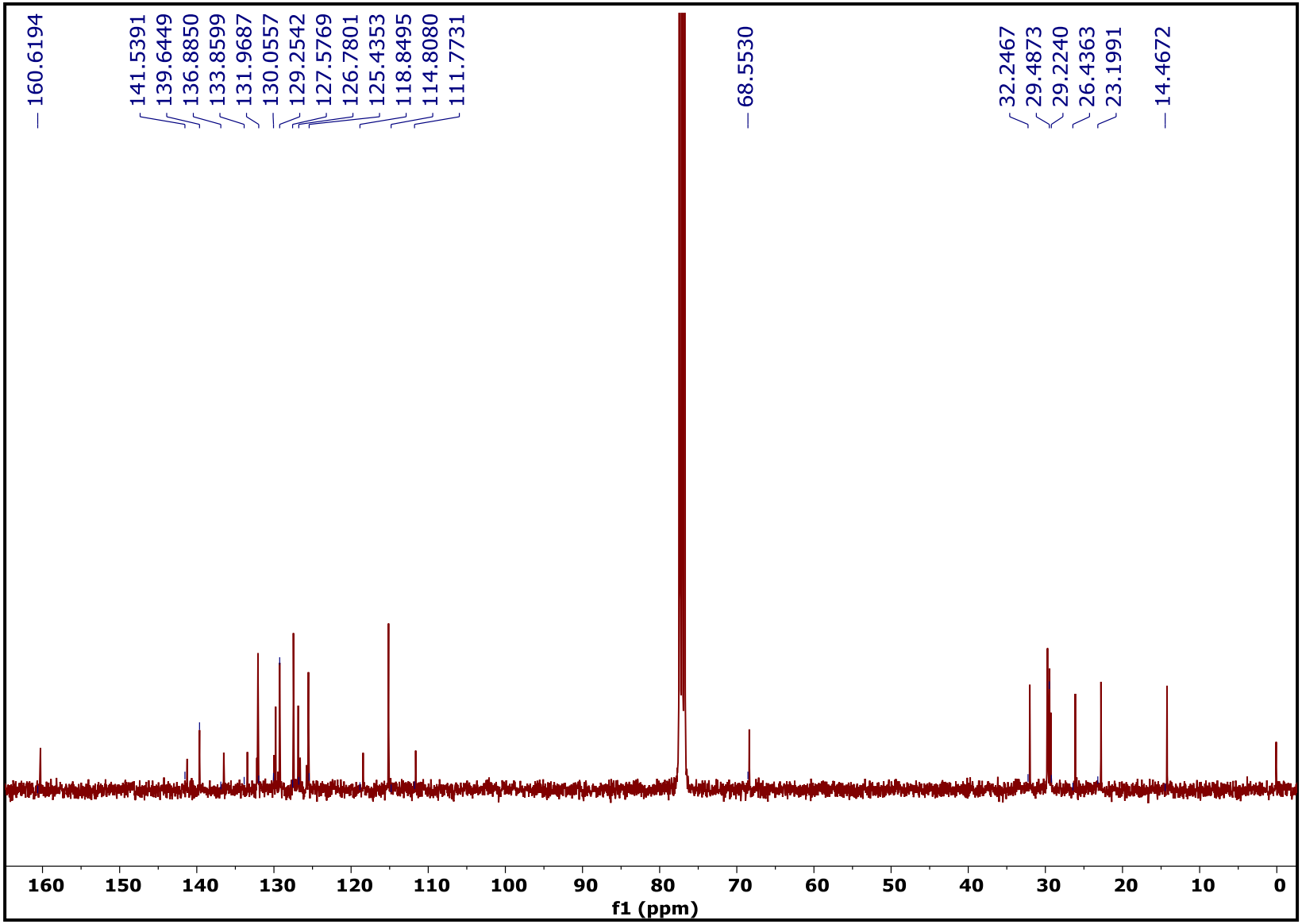

Figure 3.10 ^{13}C NMR spectra of compound **CS-3.2** (400 MHz, $CDCl_3$).

3.5 Results and discussion

This chapter investigates the synthesis of two anthracene appended cyanostilbene derivatives **CS-3.1** and **CS-3.2**, with the possibility of intramolecular charge transfer and aggregation capabilities to form programmed organization of molecules driven by an alkyl chain in condensed state. The rationale behind the design of these systems is to synthesize a strongly emissive fluorophore with stimuli responsive emission in both solid and solution states.

3.5.1 Photophysical properties of CS- 3.1

Anthracene with cyanostyryl substitution increases the conjugation, and it is evident in the steady-state photophysical properties of the compound **CS-3.1** in solution. The UV-Visible spectrum of the compound **CS-3.1** is recorded from $1x10^{-6}$ M solution in toluene. The absorption spectrum shows structured and vibronic bands at 340, 370, and 400 nm (see Figure 3.11), mainly originating from the π -π* transitions. The fluorescence spectra of the compound **CS-3.1** (Figure 3.11, emission curve) showed an emission maximum of 470 nm and exhibited a bright blue emission colour in toluene. The significant stock shift observed in the 470 nm peak probably indicates the existence of an excited state intramolecular charge transfer (ICT) band.

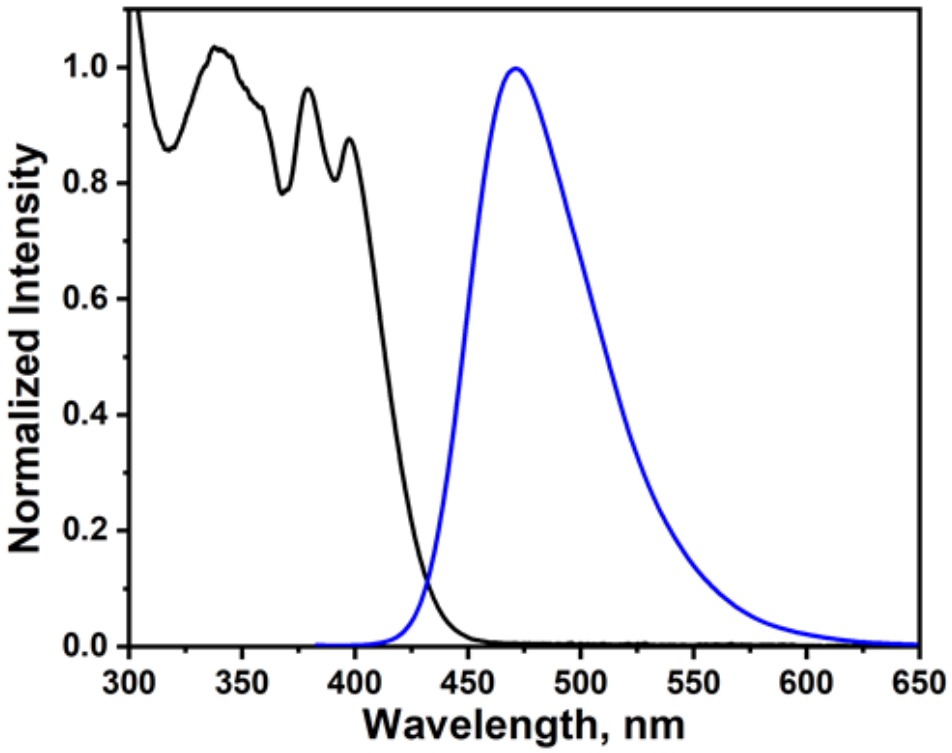

Figure 3.11. UV-Vis absorption (black curve) and emission spectra (blue curve) of **CS-3.1** in toluene (10^{-6} molar).

3.5.2 Solvatochromism

To explore the solvent dependence of optical properties of the compound **CS-3.1**, we have recorded the absorption spectra in solvents of different dielectric constants (see Figure 3.12). The absorption spectra did not show any significant shift with a change in the nature of the solvents, indicating that **CS-3.1** showed only a minor dipole change in the ground state. Then, we recorded the emission spectra of the compound in various solvents. It is noteworthy that the charge transfer band has shown a solvatochromic redshift from 470 nm to 525 nm (Figure 3.13a) along with a change in emission colour from blue to orange under 370 nm irradiation (see Figure 3.13b) when the solvent is changed from toluene to DMSO. The combination of electron donor anthracene and acceptor cyanostyryl group linked through the π-system readily offers intramolecular charge transfer in **CS-3.1**. The solvent-dependent redshift observed in the solution spectra of **CS-3.1** can be attributed to the interaction between the change in dipole moment due to the intramolecular charge transfer and the solvent dipole moment.

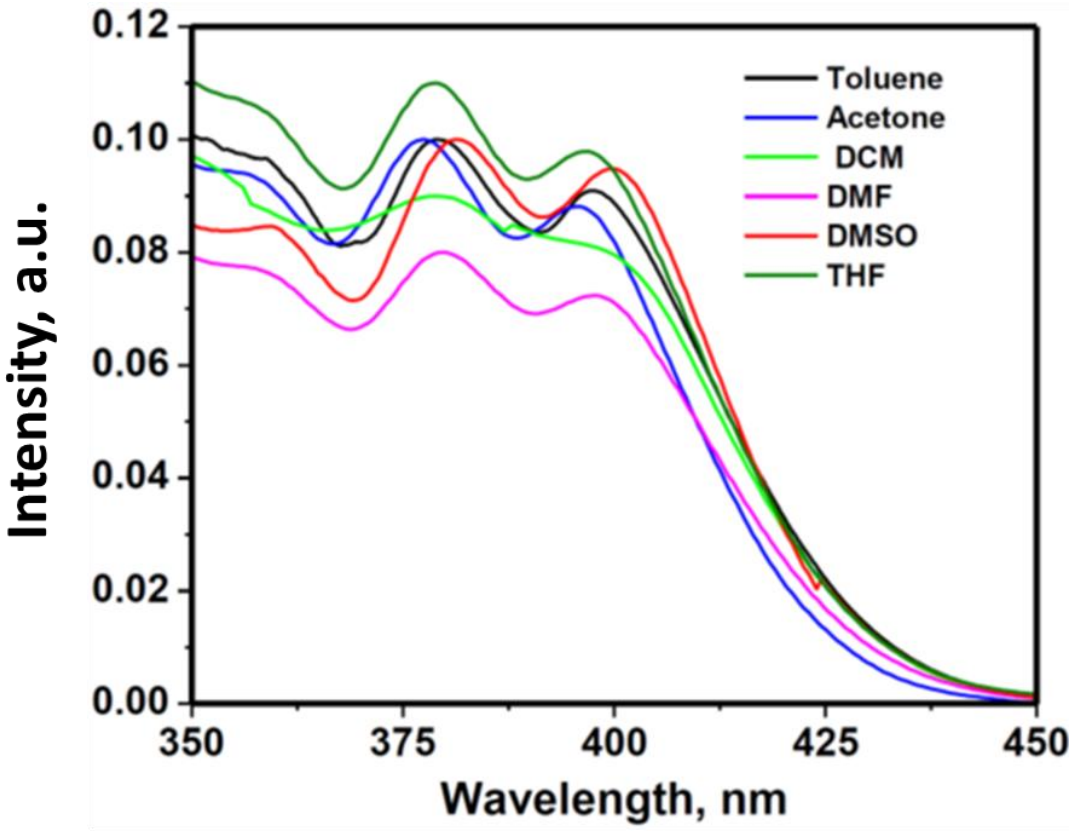

Figure 3.12 UV-Vis absorption spectra of the **CS-3.1** from solvents of different polarity ($1x10^{-6}$ M).

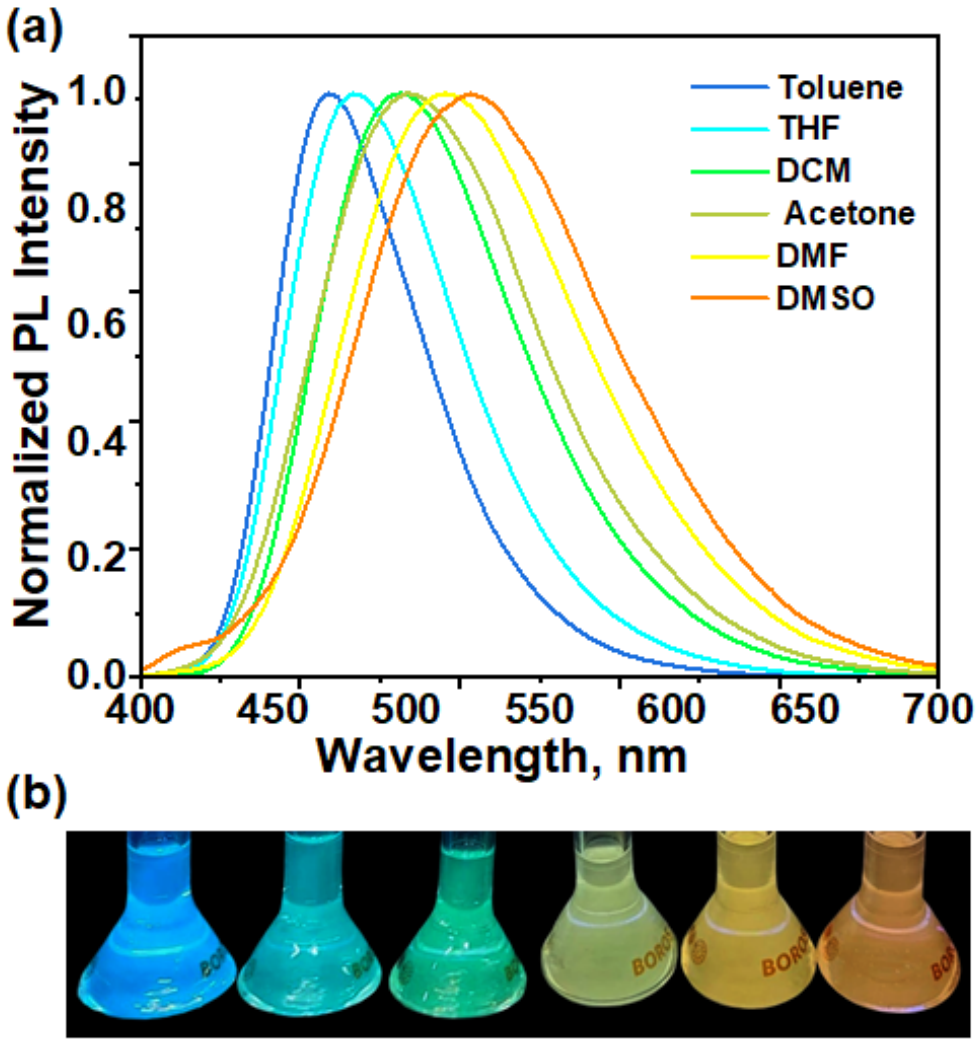

Figure 3.13 (a) Normalized fluorescence spectra of **CS-3.1** in different solvents ($1x10^{-6}$ M) recorded by exciting at 370 nm. (b) Solvatochromic effect on emission colour of **CS-3.1** (toluene to DMSO) under 370 nm.

3.5.3 Calculation of change in dipole moment between excited and ground state.

The difference in dipole moment ($\mu_e - \mu_g$) is calculated by using molecular microscopic solvent polarity parameter method proposed by Reichardt and developed by Ravi et al.[47]

Microscopic solvent polarity function ' E_T^N 'is given by the equation

$$E_T^N = \frac{E_T(solvent) - 30.7}{32.4}$$

The graph is plotted between E_T^N against stokes shift is shown below. Where m is the slope of the graph (see Figure 3.14).

The difference in the excited state and ground state dipole moment value is estimated using the equation.[48]

$$\mu_e - \mu_g = \sqrt{\frac{m \times 81}{\left(\frac{62}{a}\right)^3 \times 11307.6}}$$

$\mu_e and\ \mu_g$ are the dipole moments in the excited state and ground state, respectively. The van der Waals radius (a) is calculated from the van der Waals Volumes. The method developed by Abraham and co-workers is used for this purpose.[49]

A correlation of the optical property of the **CS-3.1** to the polarity of various solvents was investigated by plotting stokes shift against molecular microscopic solvent polarity (E_T^N) function (see Figure 3.14). From plot it can be inferred that, unlike the ground state the excited state is largely affected by the solvent polarity. Thus, it is clear that the molecule in the excited state possesses a notable increase in dipole moment (Δμ=6.6 D) in comparison to that in ground state, which is consistent with the characteristics of charge transfer states.

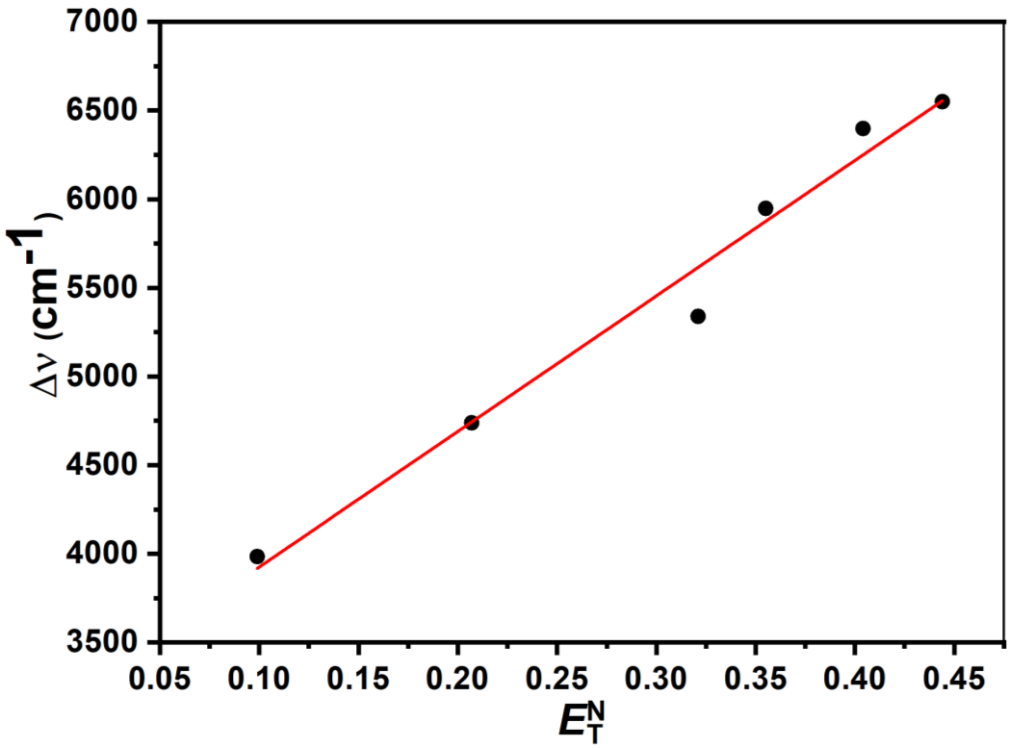

Figure 3.14 The Stokes shift (Δυ, cm^{-1}) of **CS-3.1** vs. solvent polarity parameter (E_T^N). Concentration: $1x10^{-6}$M; λex: 370 nm; 293 K.

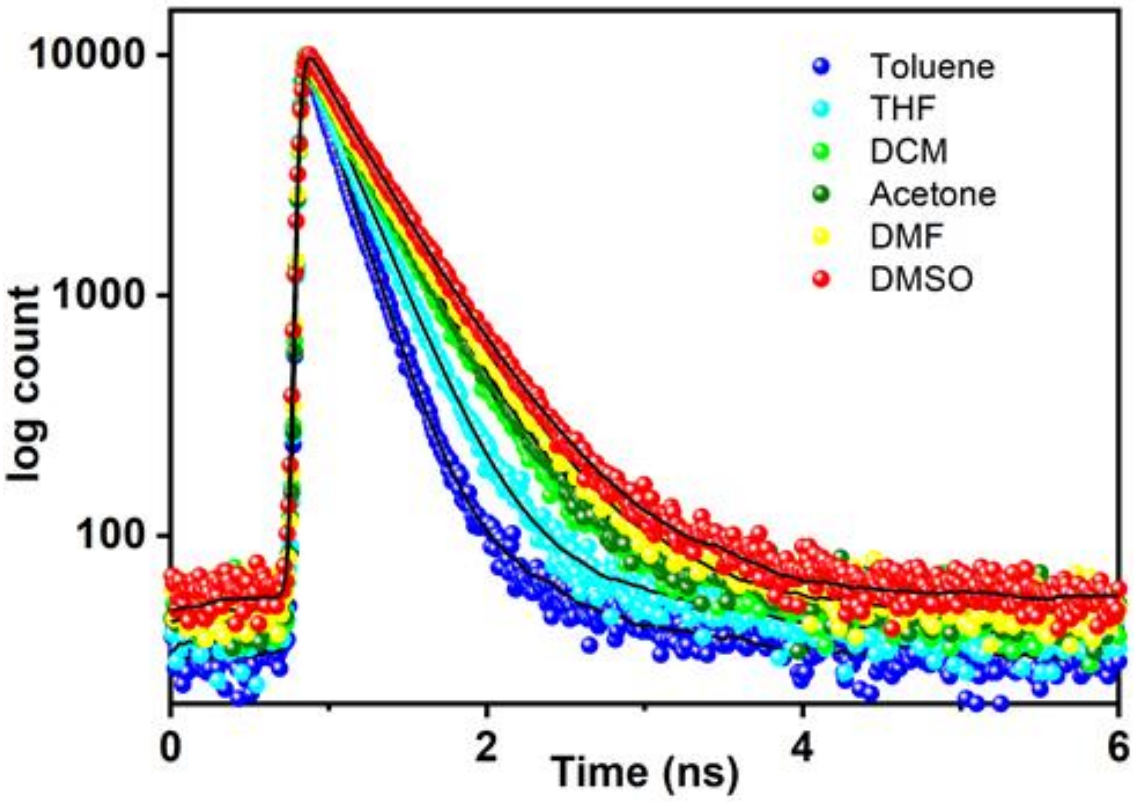

Figure 3.15 Fluorescence lifetime decay profile of **CS-3.1** in different solvents.

Further, fluorescence lifetime studies were carried out to evaluate the solvent-induced change in the lifetime of the fluorescence properties, especially the ICT band of the **CS-3.1**. The lifetime of **CS-3.1** in different solvents was collected at λmax of the fluorescence, which is used for recording the fluorescence spectra (Figure 3.15). The compound **CS-3.1** in various solvents showed biexponential decay, and the average lifetimes are shown in Table 3.1. Not surprisingly, the average lifetime was enhanced by approximately two times with an increase in the polarity of the solvent. In particular, the relative amplitude of the longer lifetime component increases substantiates the existence of CT in the excited state.[43] The transient decay of compound **CS-3.1** in different solvents showed an increment in the average lifetime (see Table 3.1) with an increase in solvent polarity in **CS-3.1**, representing the effect of the ICT state driven by solvent polarity. On comparing the steady state and transient spectral data, the formation of an excited CT state is possible, which is stabilized by increasing the polarity of the solvent. Further, we recorded the absolute quantum yield for the molecule **CS-3.1** in different solvents. The quantum yield for the compound showed a decrease with an increase in solvent polarity (see Table 3.1). The polarity dependence of the quantum yield can be explained

on the basis of quenching of fluorescence through ICT, where the polar solvents stabilize the charge separated state.[44] Similar to that of quantum yield values, the k_r values decreased with increased solvent polarity which manifest the ICT in **CS-3.1**, while the k_{nr} values showed comparable values irrespective of the solvent nature (see Table 3.1).[45,46]

Table 3.1. Fluorescence wavelength maximum, fluorescence quantum yield and average lifetime of **CS-3.1** in different solvents emitting states. Radiative and non-radiative rates (k_r, k_{nr}) were using equation $k_r = \Phi_F/\tau_F$ and $\tau_F = (k_r+k_{nr})^{-1}$ respectively.

Solvents	λ_{em} (nm)	Φ_F	τ_F (ns)	k_r (ns^{-1})	k_{nr} (ns^{-1})
Toluene	470	0.79	2.27	0.35	0.09
THF	481	0.77	2.97	0.26	0.08
DCM	496	0.80	3.64	0.22	0.06
Acetone	500	0.63	3.79	0.17	0.10
DMF	515	0.70	3.91	0.18	0.08
DMSO	525	0.67	4.09	0.16	0.08

3.5.4 Solid state emission of CS-3.1

The emission spectrum in the solid state was recorded on crystalline sample **CS-3.1** by exciting at 370 nm and presented in Figure 3.16. The fluorescence spectrum of the **CS-3.1** in the solid state showed a single band centred around 500 nm with red shifted of 30 nm compared to the solution spectrum recorded in toluene. We further compared the fluorescence lifetime in solution and solid states. Figure 3.17 shows the transient decay of fluorescence of compound **CS-3.1** (blue curve) recorded from the single crystalline sample by exciting at 370 nm. The compound **CS-3.1** showed biexponential decay in both in solution and solid state with an average lifetime of 2.27 ns and 2.65 ns, respectively. To compare the emission characteristics of the molecule in the solid and solution state the quantum yield of **CS-3.1** is recorded. Interestingly, the solution state quantum yield of the **CS-3.1** in various solvents showed higher quantum yield values with an average of 0.73. The comparatively lower quantum yield of 0.43 in the solid state to the dilute solution of **CS-3.1** can be due to the quenching mechanisms operating in the solid state. The increased quantum yield of **CS-3.1** in the solution state,

compared to that of previously reported[50] unsubstituted cyanostilbene derivatives, can be attributed to the intramolecular charge transfer in the molecule.

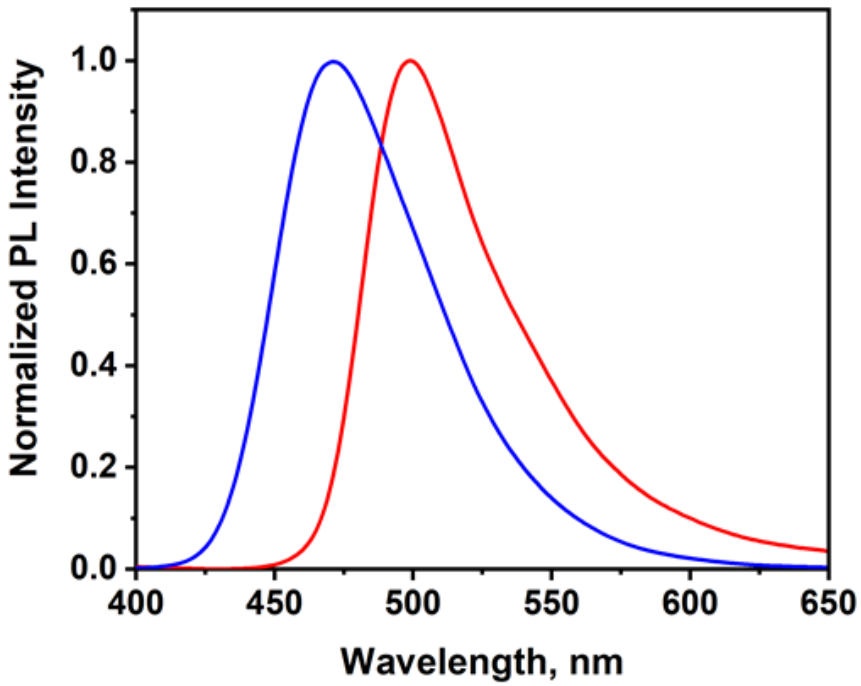

Figure 3.16 Emission spectra recorded from toluene solution (blue curve) and crystalline sample of **CS-3.1** (red curve).

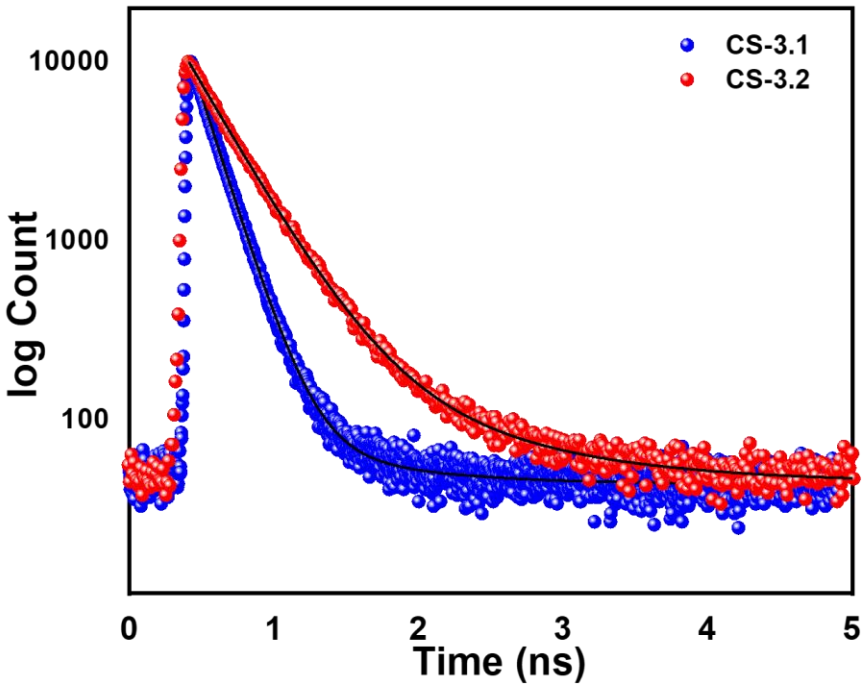

Figure 3.17 Transient decay of fluorescence of compound **CS-3.1** (blue curve) and **CS-3.2** (red curve) recorded from the single crystalline sample by exciting at 370 nm.

3.5.5 Aggregation Induced Emission in CS-3.1

The origin of sustained fluorescence emission in the solid state could be attributed to aggregate formation.[48,49] To prove the aggregation induced emission in **CS-3.1** we conducted an aggregation study by varying the water fraction (v/v, 10 to 90 %) in the THF solution of **CS-3.1** (see Figure 3.18 a). From the figure it is clear that the fluorescence intensity showed a considerable decrease up to a water fraction of 60 %. A further increase in water fraction showed increased fluorescence intensity with a shift in emission maximum (λ_{em}= 476 nm) compared to the crystalline sample with switching of emission colour from cyan to blue (see inset of Figure 3.18 b). Unlike the emission from the crystalline sample (500 nm) the blue shifted emission in the THF/water mixture could be attributed to the formation of different types of aggregates in THF/water mixture. The UV-Visible absorption spectra for the **CS-3.1** in THF/water mixture did not show any significant shift in wavelength maxima, however, an enhancement in absorption intensity on increasing water fraction above 50 % (see Figure 3.19). The aggregation of **CS-3.1** in THF/water mixture is further explored using the powder X-ray diffractograms recorded from the drop casted films of **CS-3.1** in different THF/water mixtures (see Figure 3.20). It is noteworthy that the powder X-ray diffractograms for samples with increased water fraction in the THF showed a substantial increase in crystallinity owing to the formation of well-ordered aggregates. To further establish the formation of aggregates in THF/water mixture we analyzed the particle size distribution using dynamic light scattering (DLS) method. The DLS data showed a consistent increase in particle size from 240 nm 350 nm on increasing water fraction from 50 % to 90 % (see Figure 3.21). To understand the mechanism of aggregation induced emission in **CS-3.1**, we conducted the fluorescence measurements in solutions of increased viscosity by varying the fraction of ethylene glycol in THF. The fluorescence spectra showed the signature of restricted intramolecular motion in the viscous environment on increasing the ethylene glycol fraction above 75% (see Figure 3.22).[50]

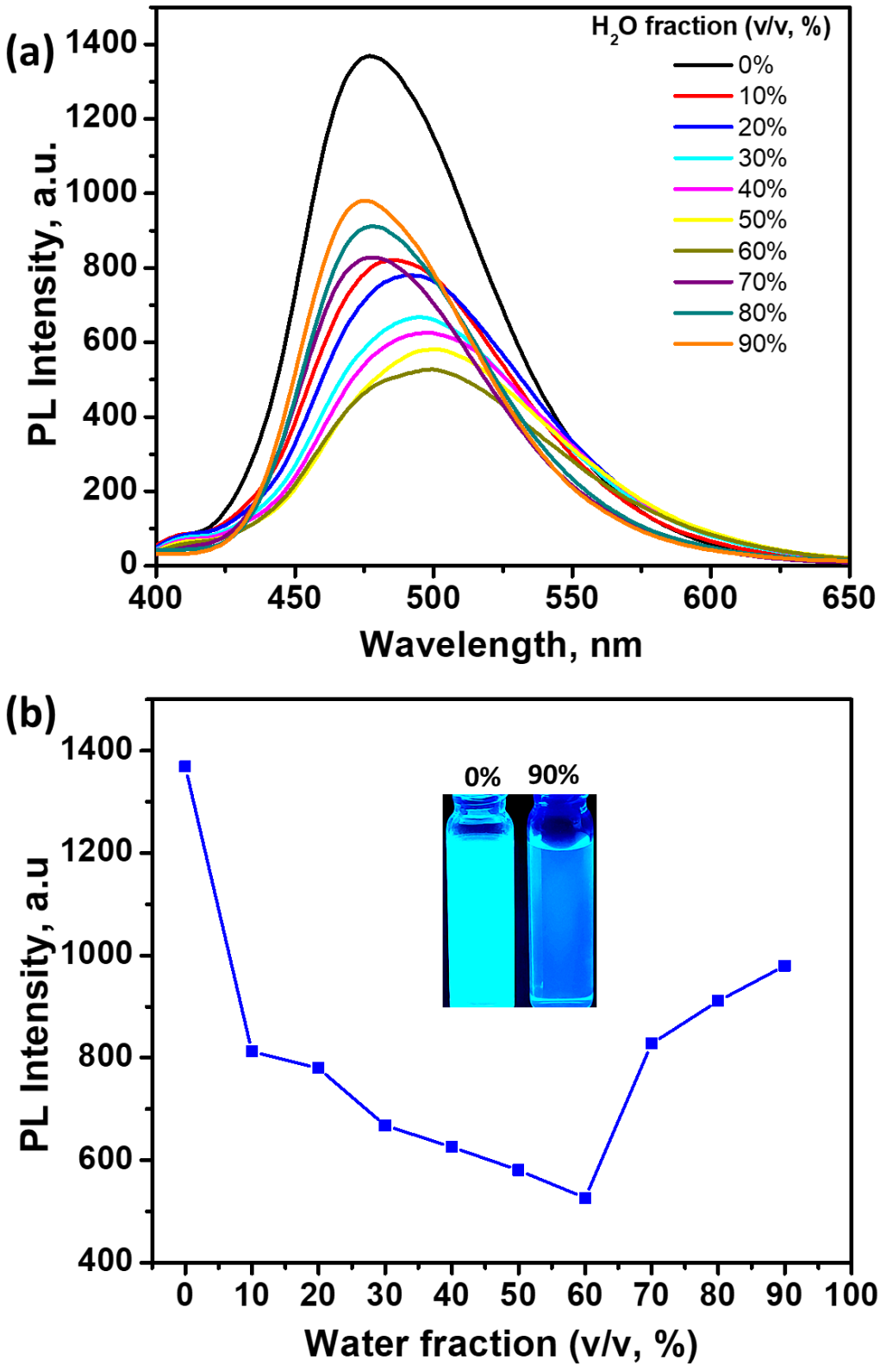

Figure 3.18 (a) Fluorescence spectra of **CS-3.1** in THF–H_2O mixtures with different water fractions; (b) fluorescent intensity respond to the changes of water fractions in THF–H_2O mixtures. Concentration: $30x10^{-6}$ M; λex: 370 nm; Inset: the photograph of the solutions (f_w 0% and 90%) under 365 nm irradiation ($30x10^{-6}$ M).

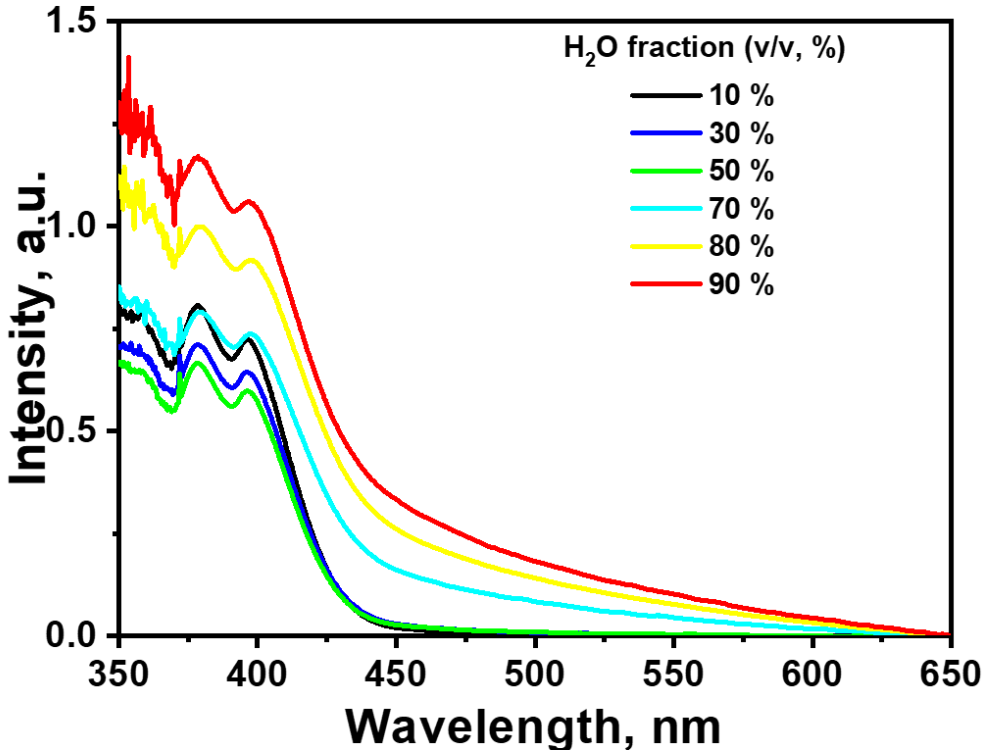

Figure 3.19 Change in UV-visible absorption spectra of **CS-3.1** in THF–H_2O mixtures with different water fractions ($30x10^{-6}$M).

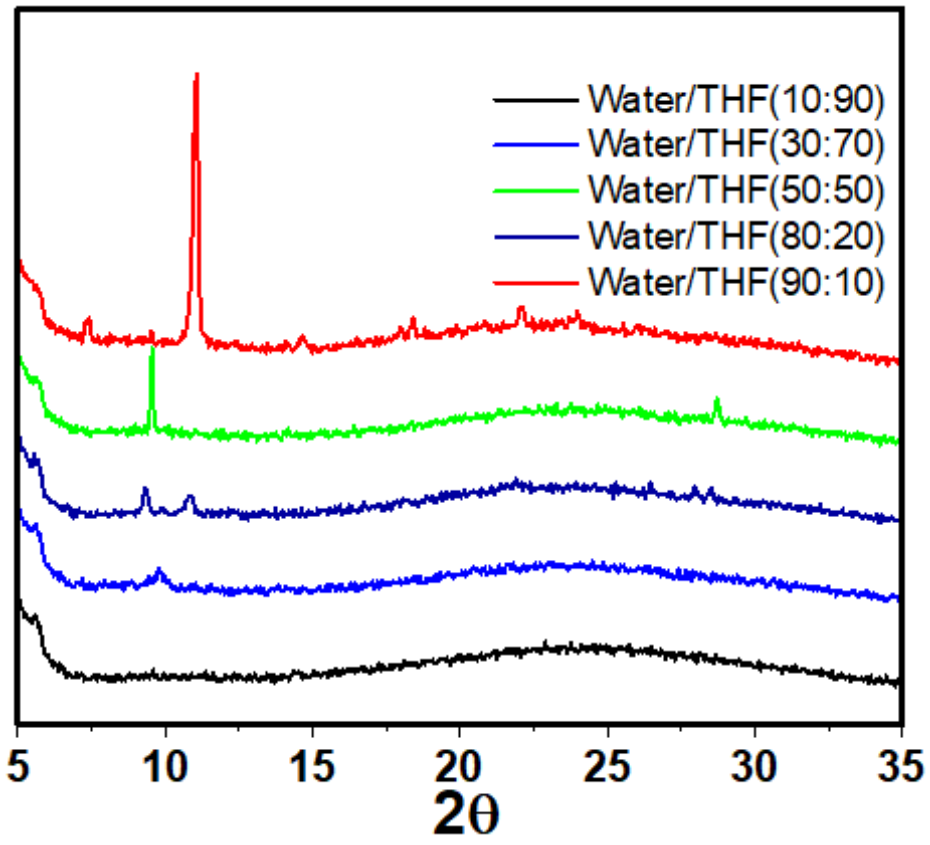

Figure 3.20 Change in powder X-ray diffractograms recorded for drop casted samples of **CS-3.1** respond to the changes of water fractions in THF–H_2O mixtures.

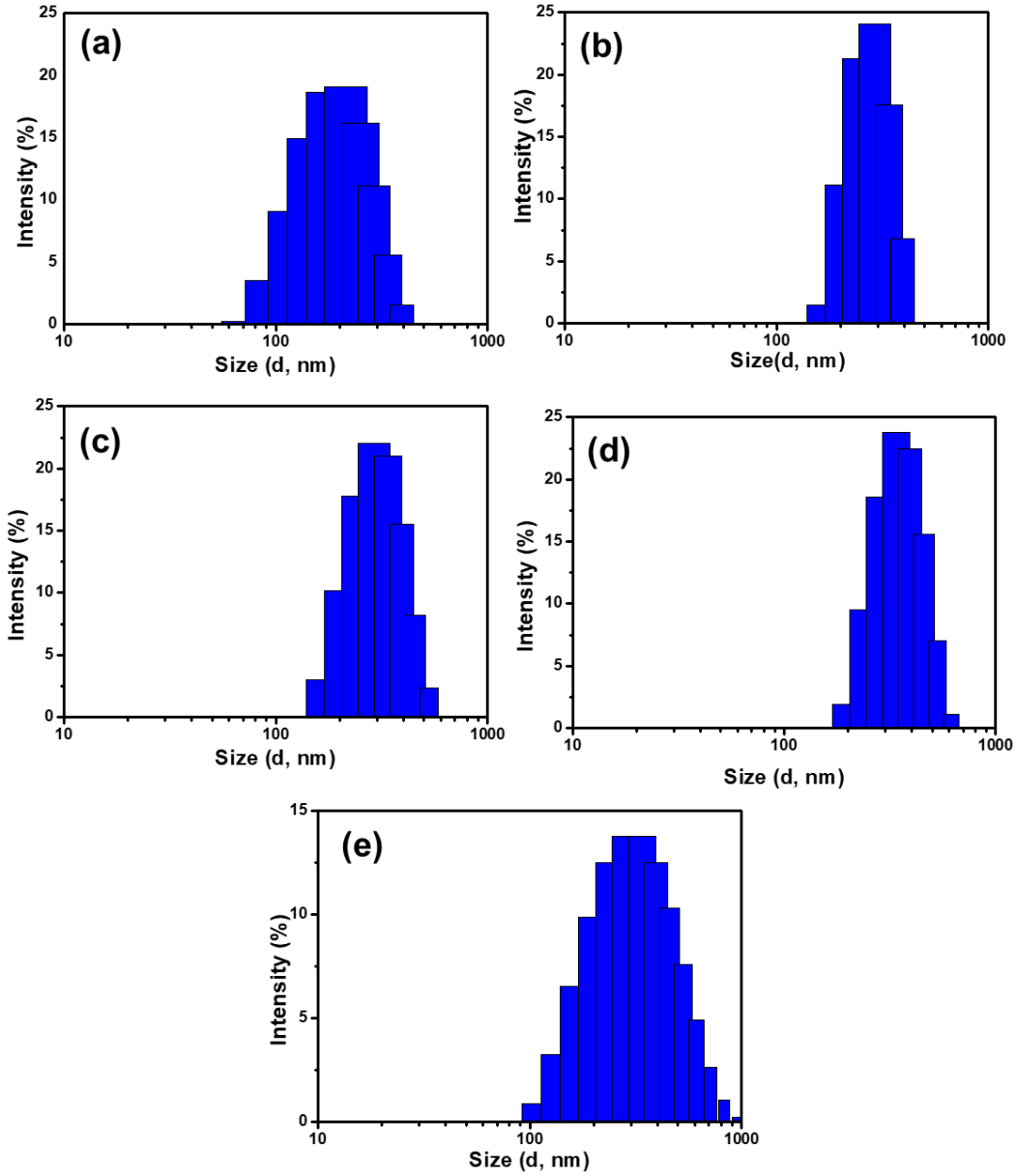

Figure 3.21 Dynamic light Scattering data showing the particle diameter on increasing the water fraction (a) 50 %, (b) 60 %, (c) 70 %, (d) 80 % and (e) 90 %.

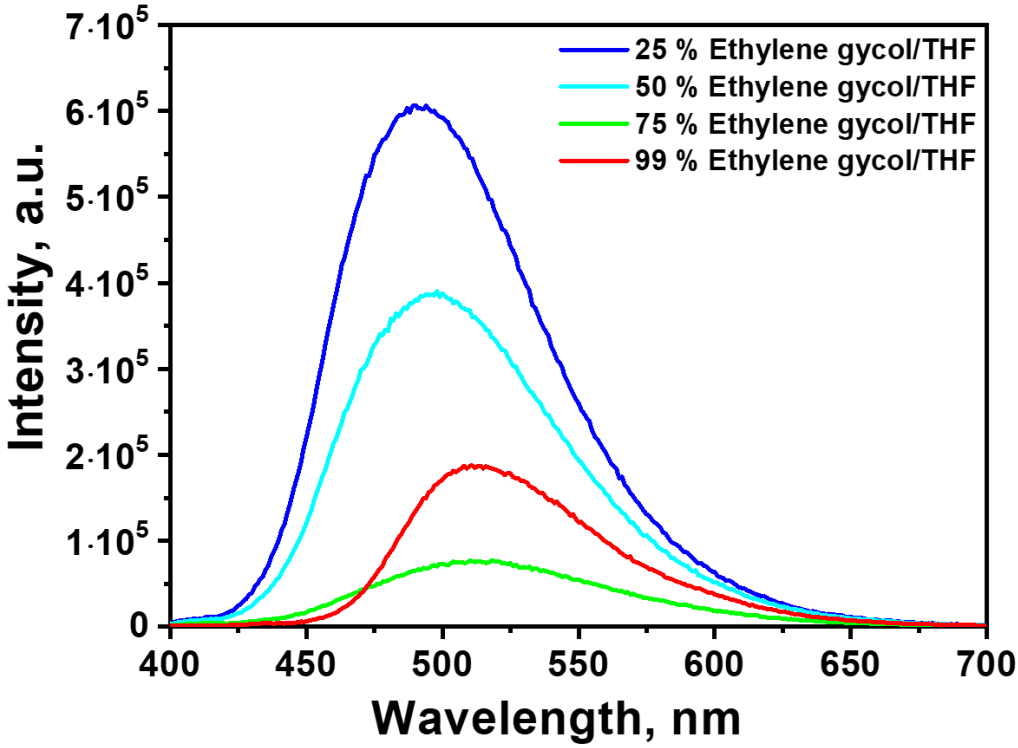

Figure 3.22 Photoluminescence spectra recorded for **CS-3.1** in different fractions of Ethylene glycol in THF.

3.5.6 Stimuli responsive emission in CS-3.1 and CS-3.2

The cyanostilbene class of molecules is well known for their stimuli responsive fluorescence emission in the solid state. To explore the effect of various stimuli on the solid state emission of **CS-3.1** and **CS-3.2** we examined the fluorescence in response to shear stress and annealing with solvent vapours. It is noteworthy that the emission spectrum of the sheared crystal of **CS-3.1** showed a blue shifted broader emission (λ_{em}=485 nm) compared to that obtained from its pristine samples (λ_{em}=500 nm) (see Figure 3.23). The ground sample of **CS-3.1** showed a reversible fluorescence switching upon fuming with ethyl acetate vapours. On applied shear stress the molecule **CS-3.2** showed a negligible change in emission maximum (λ_{em}=492 nm) compared to the pristine sample (λ_{em}=498 nm) (see Figure 3.24). Unlike the ground form of **CS-3.1**, ground **CS-3.2** was insensitive to solvent vapours.

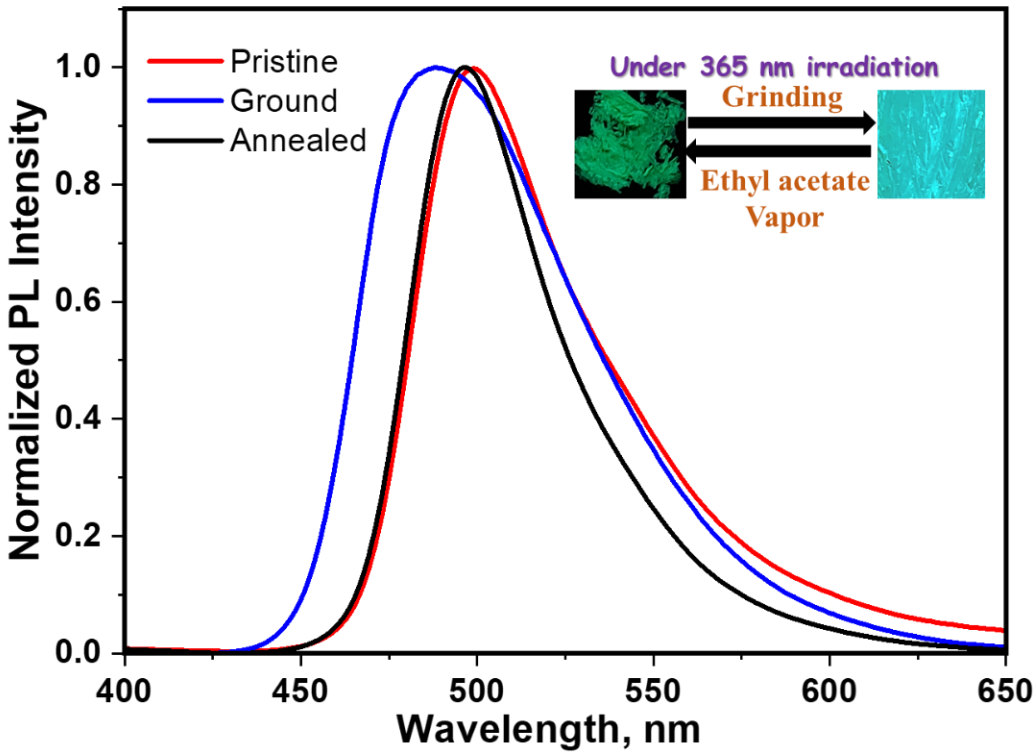

Figure 3.23 Normalized photoluminescence spectra of **CS-3.1** (red curve), ground **CS-3.1** (blue curve) and solvent vapour annealed **CS-3.1** (black curve). Fluorescence images of **CS-3.1** and its ground form under 365 nm irradiation (inset).

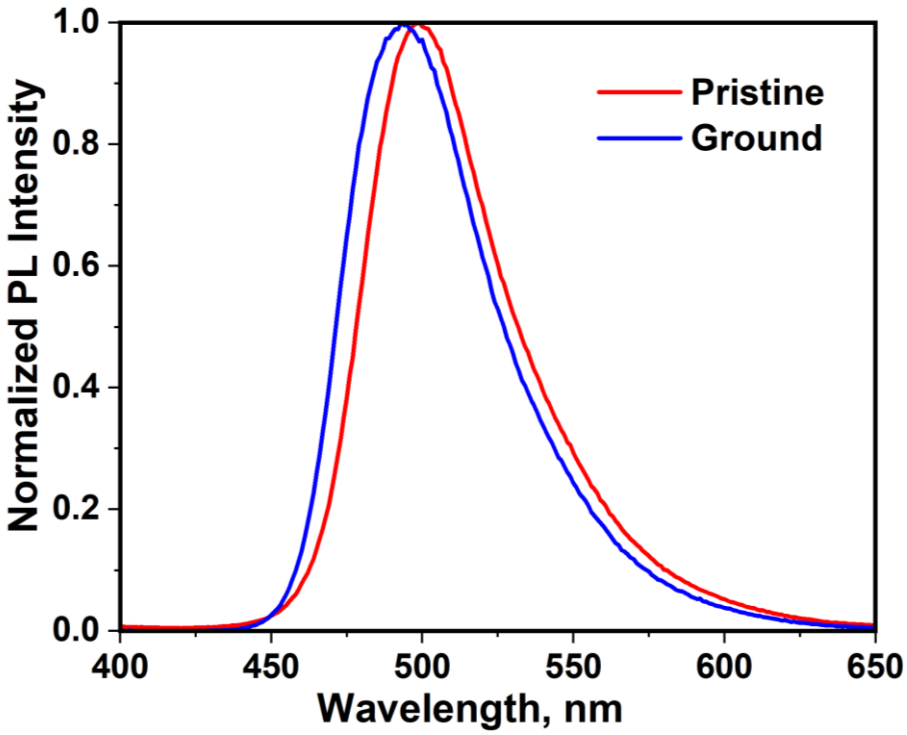

Figure 3.24 Normalized photoluminescence spectra of **CS-3.2** (red curve), **CS-3.2**G (blue curve).

In order to understand the structural origin of photophysical properties of **CS-3.1** and **CS-3.2**, we have recorded the powder x-ray diffractograms of pristine form, and other forms obtained by applying various stimuli (see Figure 3.25). The powder X-ray diffraction pattern clearly indicates that, despite of the applied stimuli the core of **CS-3.1** crystals maintains its crystallinity however with slightly broadened peaks. The blue shifted emission switching upon shearing stress compared to pristine sample can be attributed to the formation of amorphous outer layers where the molecules are aggregated differently. The reversible emission switching upon annealing with ethyl acetate vapours may be attributed to the regaining of crystallinity close to the pristine sample. The powder X-ray diffractograms of pristine and ground forms of **CS-3.2** showed comparable patterns with well separated peaks indicating that the applied stress could not create any substantial change in crystalline morphology.

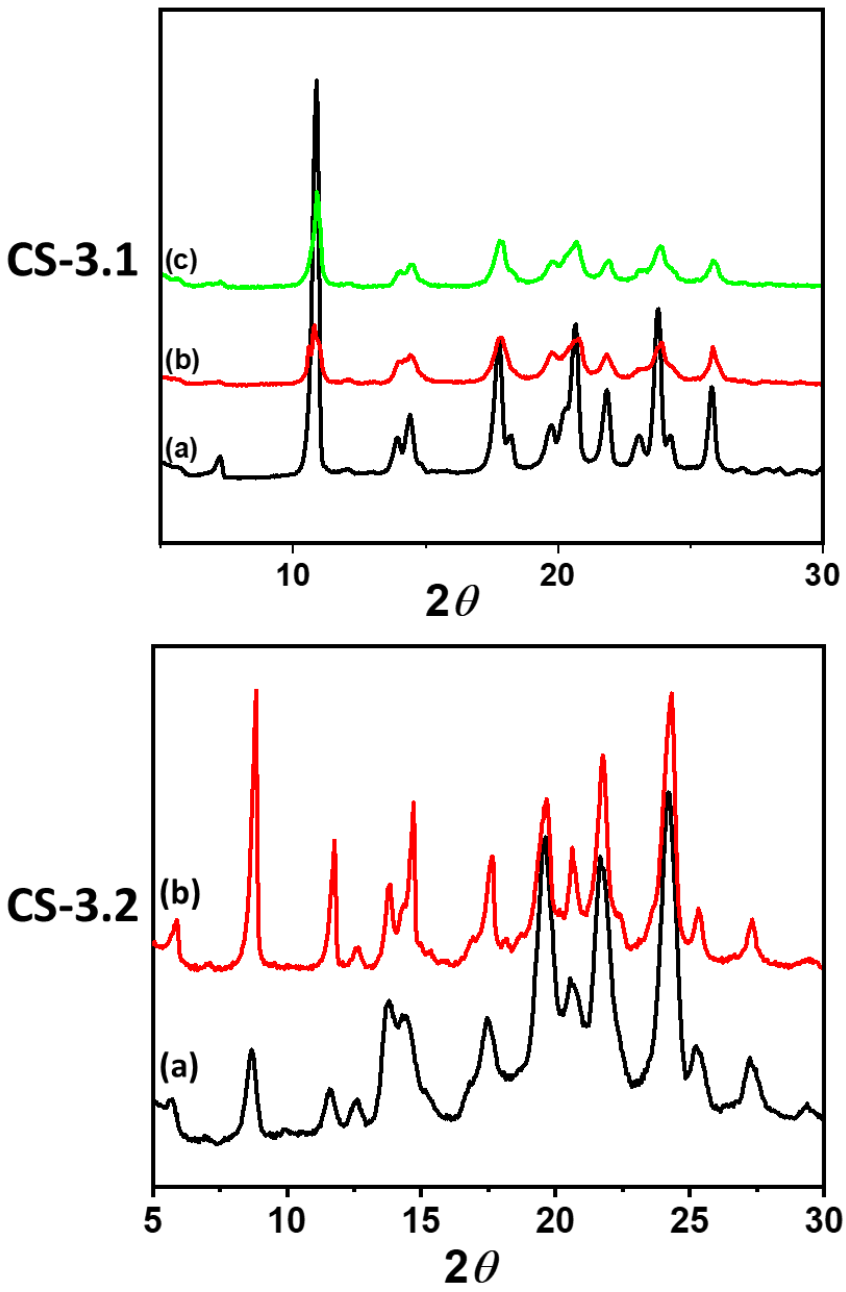

Figure 3.25 Powder X-ray diffractograms of compound **CS-3.1** (a) pristine sample (b) after grinding (c) after treatment with ethyl acetate vapours and **CS-3.2** (a) pristine sample and (b) after grinding.

3.5.7 Single-crystal analysis of CS-3.1

For further assessing the structural origin of the red-shifted emission in the solid state, the structure of **CS-3.1** obtained from the single crystal X-ray diffraction was investigated in detail. The single crystal data for **CS-3.1** were carried out on good quality single crystals grown from a dilute ethyl acetate solution by slow evaporation. Figure 3.26 shows the ORTEP plot of the compound at 50 % probability. The molecule crystallized in a triclinic P-1 space group with

half molecule in the asymmetric unit (see Table 3.2) with twisted geometry in the crystalline state having an interplanar angle of 70º between the anthracene and cyanostilbene moiety.

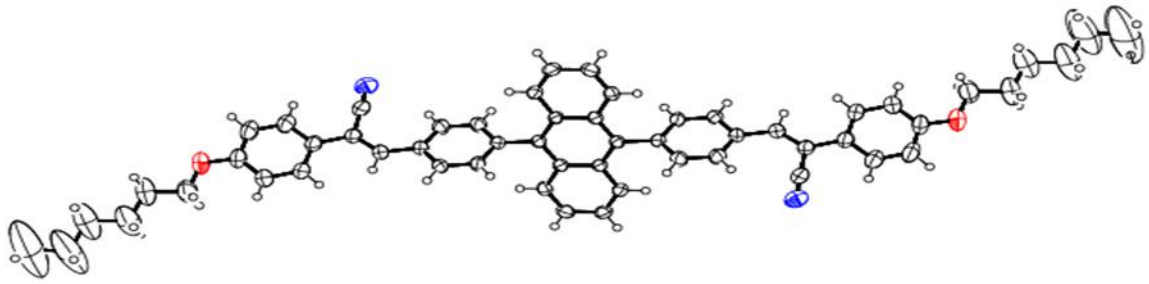

Figure 3.26 ORTEP plot of compound **CS-3.1** (ellipsoids are drawn at 50% probability).

Table 3.2 Summary of the Crystal data and structure refinement for **CS-3.1**

Empirical formula	$C_{56}H_{52}N_2O_2$	
Formula weight	784.99	
Temperature	296(2) K	
Wavelength	0.71073 Å	
Crystal system	Triclinic	
Space group	P -1	
Unit cell dimensions	a = 6.3607(3) Å	α= 83.237(2)°
	b = 7.3751(3) Å	β= 89.608(2)°
	c = 24.3886(13) Å	γ = 82.976(2)°
Volume	1127.57(9) Å3	
Z	1	
Density (calculated)	1.156 Mg/m^3	
Absorption coefficient	0.069 mm^{-1}	
F(000)	418	
Crystal size	0.600 x 0.250 x 0.060 mm^3	
Theta range for data collection	2.829 to 25.496°.	
Index ranges	-7<=h<=7, -8<=k<=8, -29<=l<=29	
Reflections collected	42195	
Independent reflections	4190 [R(int) = 0.0555]	
Completeness to theta = 25.242°	99.8 %	
Absorption correction	Semi-empirical from equivalents	
Max. and min. transmission	0.7457 and 0.4557	
Refinement method	Full-matrix least-squares on F2	
Data / restraints / parameters	4190 / 135 / 273	

Goodness-of-fit on F2	1.065
Final R indices [I>2sigma(I)]	R1 = 0.0586, wR2 = 0.1649
R indices (all data)	R1 = 0.0690, wR2 = 0.1801
Extinction coefficient	0.038(8)
Largest diff. peak and hole	0.346 and -0.239 e.Å-3
CCDC No.	2208185

Figure 3.27 shows the molecular packing in the solid state where the molecules adopt a slanting layered arrangement along the (001) plane through a pair of intermolecular interactions. Figure 3.28a shows the weak intermolecular and intramolecular interactions present in the crystals of **CS-3.1**. The molecules in the crystalline state showed various intermolecular interactions including C–H···N, C-H···π, π···π stacking interactions (see Table 3.3)· The H···N distance and C-H···N angle ranges from 2.667 Å to 2.896 Å and 141.2º to 149.9º respectively. In addition, the molecule showed a pair of intermolecular C–H···π interactions formed between the aromatic C-H and π system of anthracene and benzene units with H···π distance of 2.517 Å and 2.890 Å. It is noteworthy that the **CS-3.1** molecules form symmetric π···π stacking interactions at a distance of 3.606 Å, where these interaction results in molecular slip stack (see Figure 3.28 b).

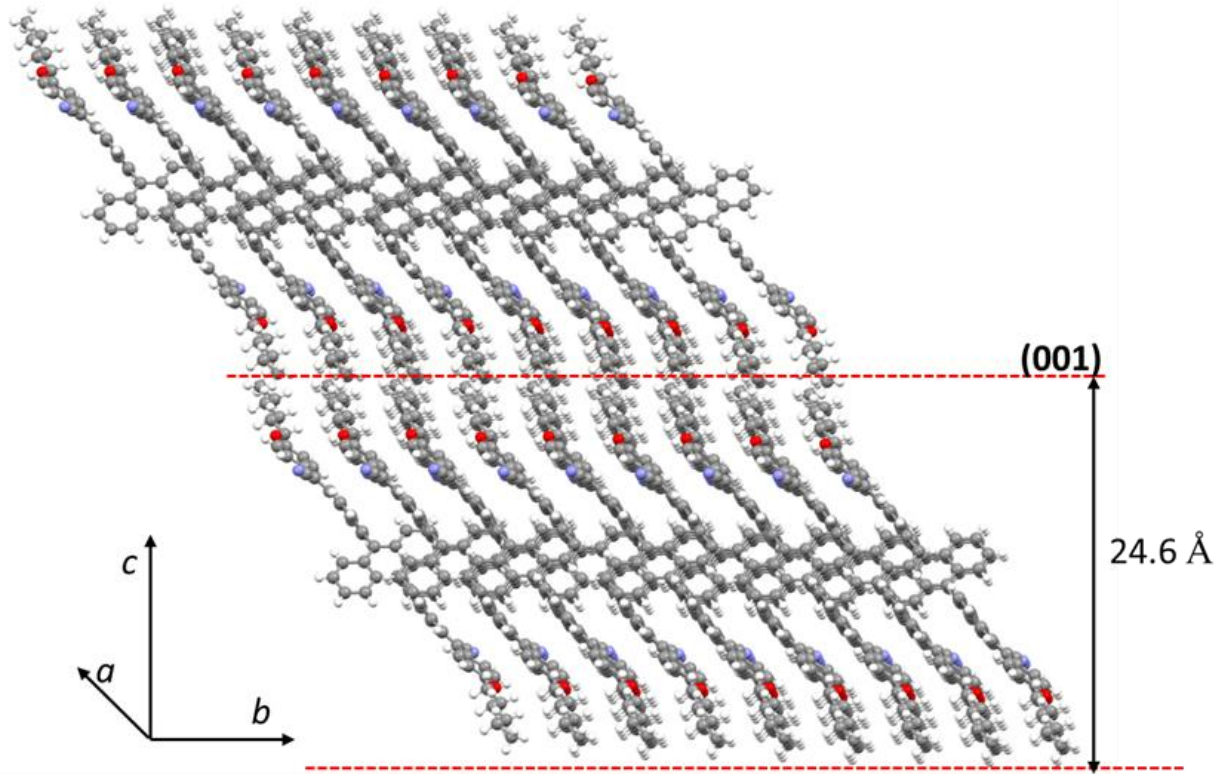

Figure 3.27 Molecular packing of **CS-3.1** in the crystals.

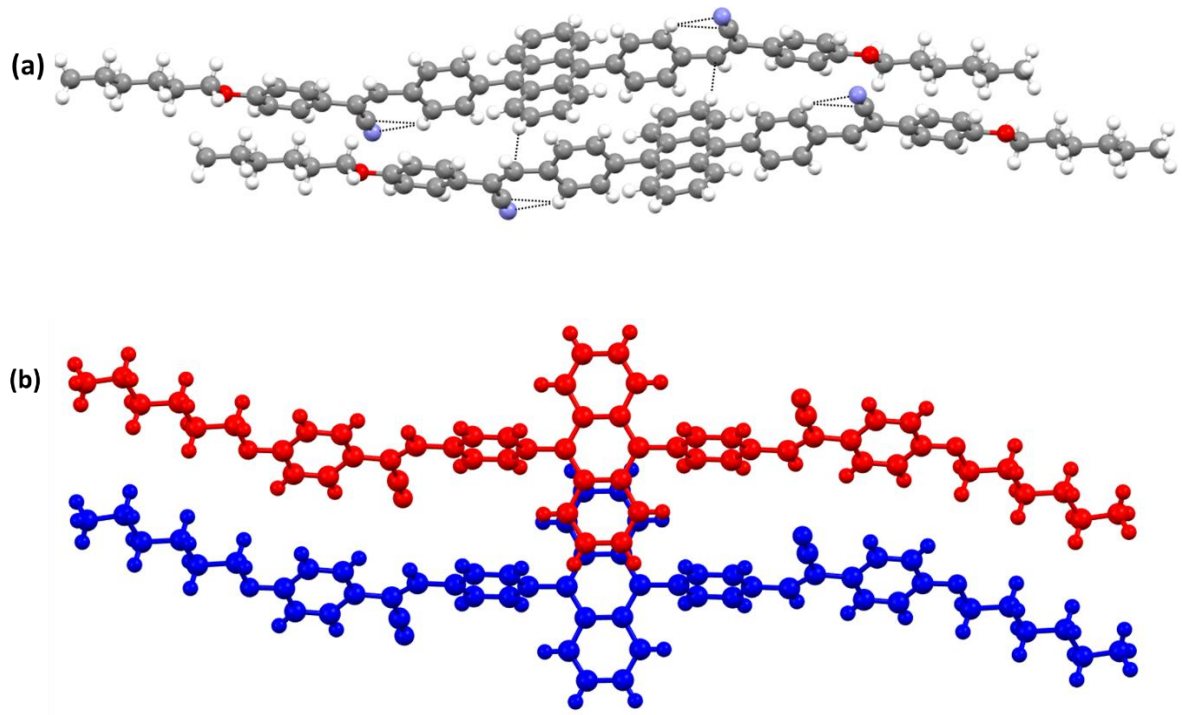

Figure 3.28 (a) Weak intermolecular and intramolecular interactions present in the crystals of **CS-3.1** and (b) J-aggregate pair in the crystal structure of **CS-3.1**.

Table 3.3 Weak intermolecular interactions in **CS-3.1**.

Bond Type	H···A(Å)	D···A(Å)	D–H···A (°)
C12–H1···N1	2.667(2)	3.449(3)	142.1(1)
C17–H17···N1	2.896(2)	3.671(3)	141.7(1)
C23–H23A···N1	2.866(2)	3.737(4)	149.9(2)
C7–H7··· Cg(4)*	2.890 (1)	3.693(2)	145
C10–H10···Cg(1)*	2.661 (2)	3.474(2)	147
Cg1...Cg(1)	3.606(9)		
Cg1...Cg(3)*	3.606(9)		

*Cg(4) = C8 –C9– C10– C11–C12–C13; *Cg(3) = C5–C6–C7a– C1a –C2a–C3a
*Cg(1) =C1–C2–C3–C5_a–C6_a–C7

To understand the origin of the aggregation induced emission in the solid samples of **CS-3.1**, we examined the aggregate pairs in the crystalline state of the molecule. It is noteworthy that the molecules are arranged along the molecular short axis stacking the anthracene rings as shown in Figure 3.28b, resulting in J-aggregate pair, and correspondingly a redshifted emission in the solid state.[51] From the analysis of single crystal X-ray diffraction data of compound **CS-3.1**, it is clear that the alkyl chain plays a pivotal role in the layered molecular arrangement in the (001) plane.

3.5.8 Comparison of structural and fluorescence properties of CS-3.1 and CS-3.2

To compare the influence of the alkyl chain on the photophysical characteristics, we analyzed the absorption and emission spectra of **CS-3.1** and its homologue **CS-3.2** in the solution state. The absorption and emission properties of both **CS-3.1** and **CS-3.2** in solution showed comparable spectral features (see Figure 3.29). It is noteworthy that, in spite of the relatively longer alkyl chain, **CS-3.2**, showed comparable solid state emission as similar to **CS-3.1** (see Figure 3.30). From the fluorescence data, it is clear that both **CS-3.1** and **CS-3.2** adopt similar arrangements of molecules in the solid state. To understand the origin of similar spectral features of both **CS-3.1** and **CS-3.2** we have compared their powder X-ray diffractograms with diffractogram of **CS-3.1** simulated from single crystal X-ray diffraction data (Figure 3.31). From the diffractogram it is clear that the 2θ value corresponding to (*h00*) and (*0k0*) planes are the same in both molecular arrangement along the molecular short axis determines the emission in the solid state while the interlayer distance, i.e., the arrangement of molecules in the molecular long axis does not play any decisive role in the solid state emission properties of these molecules.

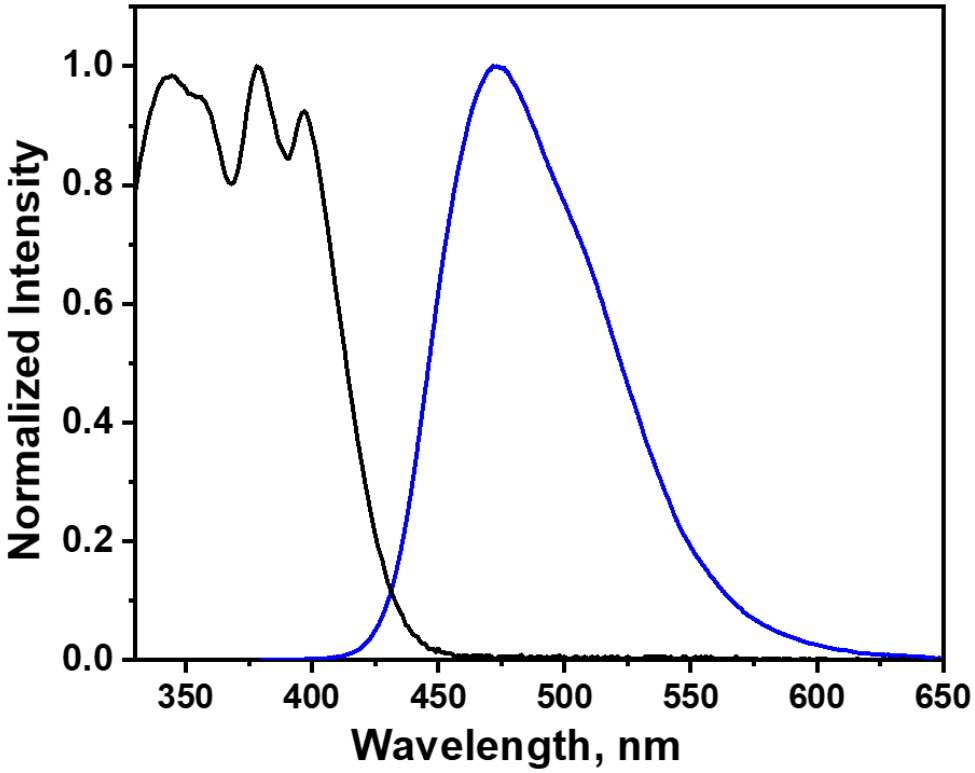

Figure 3.29 UV-Visible absorption (black) and emission spectra (blue) of **CS-3.2** in toluene.

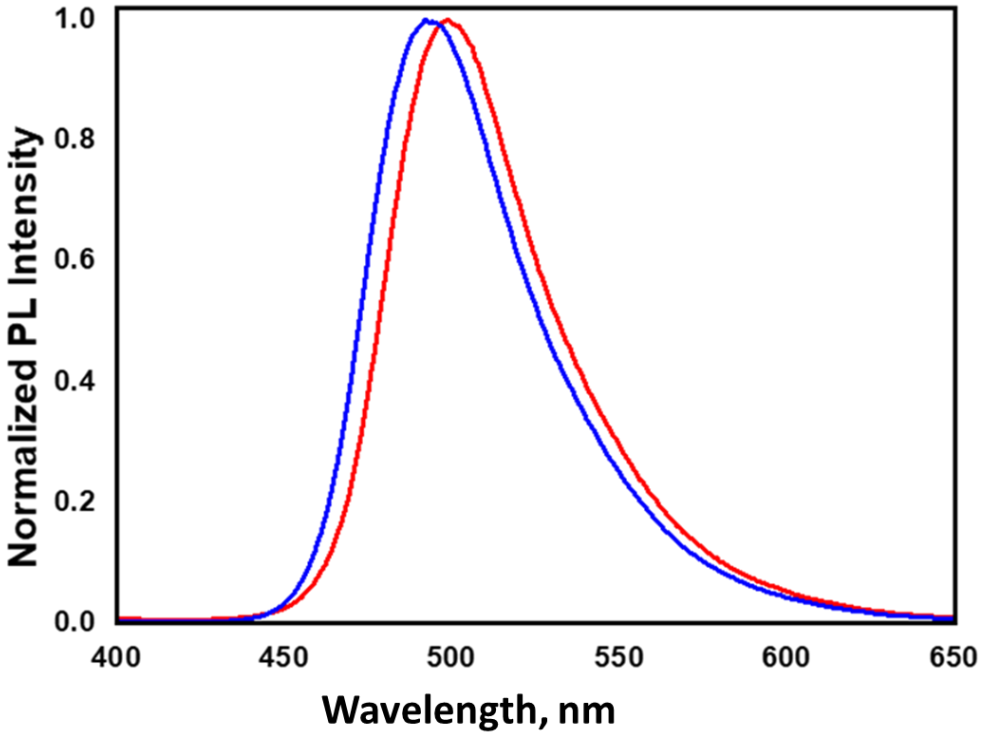

Figure 3.30 Solid state emission spectra recorded for the compounds **CS-3.1**(red curve) and **CS-3.2** (blue curve).

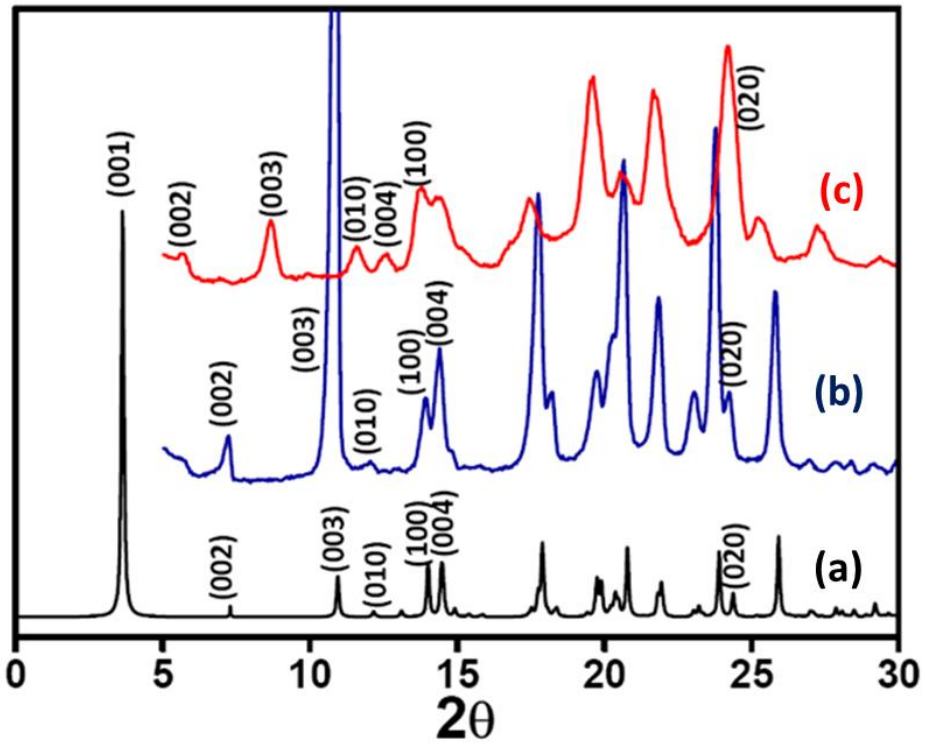

Figure 3.31 Comparison of powder X-ray diffractograms of compound **CS-3.1** (a) simulated from single crystal X-ray diffraction data (b) PXRD recorded for crystalline sample of **CS-3.1** and (c) **CS-3.2**.

3.5.9 Analysis of fluorescence properties of CS-3.1 and CS-3.2

The ground forms of **CS-3.1** showed a slight decrease in quantum yield (Φ_F=0.38) compared to the pristine sample (Φ_F=0.43) (Table 3.4). Similar trend was observed in the case of **CS-3.1** and **CS-3.2** while the peaks corresponding to (*00l*) in **CS-3.2** are shifted to lower 2θ values indicating the higher interplanar distances attributed to the increased chain length. From the crystallographic study, it can be summarized that the fluorescence lifetime before and after grinding with τ_F values 2.65 ns and 2.12 ns respectively (see Figure 3.32). The k_r values for the ground and pristine samples were comparable, however the ground **CS-3.1** showed considerable increment in k_{nr} value (k_{nr}=0.29 ns^{-1}) which is suggestive of the decreased quantum yield on grinding. A similar trend was observed in the case of pristine and ground from of **CS-3.2** (see Table 3.4). We then compared the emission characteristics of **CS-3.1** and **CS-3.2** in the solid state. In spite of comparable molecular packing in the solid state, the **CS-3.2** showed decreased quantum yield (Φ_F=0.37) in comparison to **CS-3.1** (Φ_F=0.43). The decrease in the quantum yield of **CS-3.2** in the solid state can be attributed to the decreased crystallinity and poor structural rigidity in the solid state.[52] The lifetime follows a reverse trend of quantum yield, where the **CS-3.2** showed a slight increase in lifetime, which may be caused by the defects in the polycrystalline sample.[48] The crystalline nature of the compound is reflected both in k_r and k_{nr} values were the polycrystallinity will induce the quenching of excitons at the grain boundaries.[53] The compound **CS-3.1** with better crystallinity showed increased k_r (0.16 ns^{-1}) value in comparison to **CS-3.2**. It is noteworthy that the non-radiative decay constant is higher in both **CS-3.1** and **CS-3.2**, indicating that the π-overlap between anthracene moieties opens up non-radiative decay pathways. Hence, in spite of the π···π stacking induced quenching in **CS-3.1** and **CS-3.2**, the aggregation induced emission competes to retain the solid state emission.

Table 3.4 Fluorescence wavelength maximum, fluorescence quantum yield and average lifetime of **CS-3.1** and **CS-3.2** emitting states. Radiative and non-radiative rates (k_r, k_{nr}) were calculated using equation $k_r = \Phi_F/\tau_F$ and $\tau_F = (k_r+k_{nr})^{-1}$ respectively.

Compound	State	λ_{em} (nm)	Φ_F	τ_F (ns)	k_r (ns^{-1})	k_{nr} (ns^{-1})
CS-3.1	Pristine	500	0.43	2.65	0.16	0.21
	Ground	485	0.38	2.12	0.18	0.29
CS-3.2	Pristine	498	0.37	3.72	0.10	0.17
	Ground	492	0.35	2.99	0.12	0.22

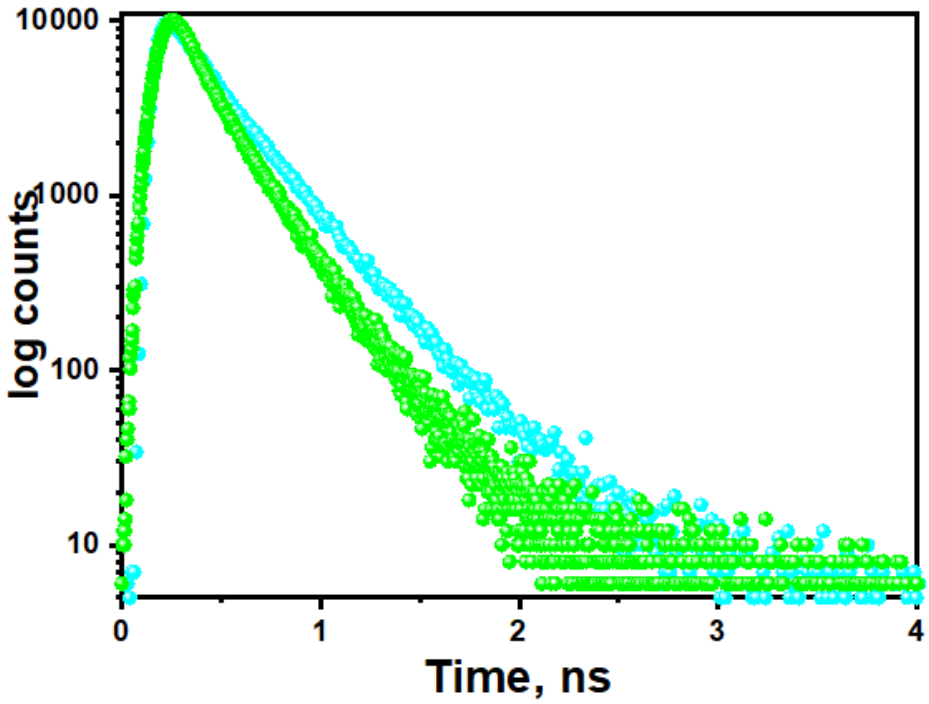

Figure 3.32 Fluorescence decay profile of (a) **CS-3.1** (green decay) and its ground for **CS-3.1** (cyan decay).

In summary, the new molecular design with charge transfer phenomena exhibits high quantum yield in both solution and solid state with multistimuli-responsive emission in **CS-3.1**.

3.6 Conclusion

In summary, the synthesis and photophysical property studies of anthracene and cyanostilbene-based donor-acceptor systems were carried out. A detailed analysis of fluorescence properties of **CS-3.1** with hexyloxy substitution in both solution and solid states was conducted and compared with that of **CS-3.2**. Both the molecules showed strong emission in the solution state attributed to the intramolecular charge transfer (ICT). The ICT band in **CS-3.1** showed a solvatochromic redshift with increase in dielectric constant of the solvents. Irrespective of the alkyloxy chain length, both the **CS-3.1** and **CS-3.2** showed comparable emission in the solid state attributed to the molecular aggregation. Interestingly, the molecule **CS-3.1** showed a stimuli responsive dual mode luminescence switching under applied stress and ethyl acetate vapours. Unlike **CS-3.1** the molecule **CS-3.2** was less sensitive to various stimuli. Owing to the rigid molecular packing, **CS-3.1** showed higher quantum yield (Φ=0.43) in the solid state in comparison to **CS-3.2** (Φ=0.37), where the latter showed poor crystallinity. In the solid state, two neighbouring molecules comprises a J-aggregate pair with molecular arrangement along molecular short axis. In both **CS-3.1** and **CS-3.2** the luminophores adopt similar arrangement,

hence, the identical emission properties in the solid state. The present work provides two novel compounds with the potential for various optoelectronic applications.

3.7 References

(1) Yuan, L.; Lin, W.; Zheng, K.; He, L.; Huang, W. Far-Red to near Infrared Analyte-Responsive Fluorescent Probes Based on Organic Fluorophore Platforms for Fluorescence Imaging. *Chem. Soc. Rev.* **2013**, *42* (2), 622–661.

(2) Park, S. K.; Varghese, S.; Kim, J. H.; Yoon, S.-J.; Kwon, O. K.; An, B.-K.; Gierschner, J.; Park, S. Y. Tailor-Made Highly Luminescent and Ambipolar Transporting Organic Mixed Stacked Charge-Transfer Crystals: An Isometric Donor–Acceptor Approach. *J. Am. Chem. Soc.* **2013**, *135* (12), 4757–4764.

(3) Garg, S.; Goel, N. Optoelectronic Applications of Conjugated Organic Polymers: Influence of Donor/Acceptor Groups through Density Functional Studies. *J. Phys. Chem. C* **2022**, *126* (22), 9313–9323.

(4) Fukaminato, T.; Doi, T.; Tamaoki, N.; Okuno, K.; Ishibashi, Y.; Miyasaka, H.; Irie, M. Single-Molecule Fluorescence Photoswitching of a Diarylethene−Perylenebisimide Dyad: Non-Destructive Fluorescence Readout. *J. Am. Chem. Soc.* **2011**, *133* (13), 4984–4990.

(5) He, Y.; Zhang, S.; Bisoyi, H. K.; Qiao, J.; Chen, H.; Gao, J.; Guo, J.; Li, Q. Irradiation-Wavelength Directing Circularly Polarized Luminescence in Self-Organized Helical Superstructures Enabled by Hydrogen-Bonded Chiral Fluorescent Molecular Switches. *Angew. Chemie Int. Ed.* **2021**, *60* (52), 27158–27163.

(6) Wang, B.; Wei, C. Stimuli-Responsive Fluorescence Switching of Cyanostilbene Derivatives: Ultrasensitive Water, Acidochromism and Mechanochromism. *RSC Adv.* **2018**, *8* (40), 22806–22812.

(7) Li, J.; Ji, D.; Hu, Y.; Chen, M.; Liu, J.; Qin, Z.; Sun, Y.; Dang, Y.; Zhen, Y.; Dong, H.; Li, L.; Hu, W. Substitution Site Effect of Naphthyl Substituted Anthracene Derivatives and Their Applications in Organic Optoelectronics. *J. Mater. Chem. C* **2020**, *8* (44), 15597–15602.

(8) Babu, S. S.; Hollamby, M. J.; Aimi, J.; Ozawa, H.; Saeki, A.; Seki, S.; Kobayashi, K.; Hagiwara, K.; Yoshizawa, M.; Möhwald, H.; Nakanishi, T. Nonvolatile Liquid Anthracenes for Facile Full-Colour Luminescence Tuning at Single Blue-Light Excitation. *Nat. Commun.* **2013**, *4* (1), 1969.

(9) Chen, M.; Yan, L.; Zhao, Y.; Murtaza, I.; Meng, H.; Huang, W. Anthracene-Based Semiconductors for Organic Field-Effect Transistors. *J. Mater. Chem. C* **2018**, *6* (28), 7416–7444.

(10) Zhang, C.; Chen, P.; Hu, W. Organic Light-Emitting Transistors: Materials, Device Configurations, and Operations. *Small* **2016**, *12* (10), 1252–1294.

(11) Yu, Y.; Jiao, B.; Wu, Z.; Li, Z.; Ma, L.; Zhou, G.; Yu, W.; So, S. K.; Hou, X. Fluorinated 9,9′-Bianthracene Derivatives with Twisted Intramolecular Charge-Transfer Excited States as Blue Host Materials for High-Performance Fluorescent Electroluminescence.

J. Mater. Chem. C **2014**, *2* (44), 9375–9384.

(12) Ghosh, T.; Kalita, K. J.; Ashtaman Pillai Syamaladevi, N.; Vijayaraghavan, R. K. Aromatic Ring Overlap Pedals the Nature of Exciton Coupling and Carrier Transport in a Series of Electron-Deficient Anthracenes. *J. Phys. Chem. C* **2022**, *126* (38), 16253–16261.

(13) Tonga, M. Effect of Π–conjugation on Aggregation–Induced Emission of α–Cyanostilbene Incorporated Polycyclic Aromatic Hydrocarbons. *J. Photochem. Photobiol. A Chem.* **2021**, *412*, 113247.

(14) Sundar, V. C.; Zaumseil, J.; Podzorov, V.; Menard, E.; Willett, R. L.; Someya, T.; Gershenson, M. E.; Rogers, J. A. Elastomeric Transistor Stamps: Reversible Probing of Charge Transport in Organic Crystals. *Science* **2004**, *303* (5664), 1644–1646.

(15) Dong, Y.; Guo, Y.; Zhang, H.; Shi, Y.; Zhang, J.; Li, H.; Liu, J.; Lu, X.; Yi, Y.; Li, T.; Hu, W.; Jiang, L. Cyclohexyl-Substituted Anthracene Derivatives for High Thermal Stability Organic Semiconductors. *Front. Chem.* **2019**, *7*.

(16) Santra, D. C.; Bera, M. K.; Sukul, P. K.; Malik, S. Charge-Transfer-Induced Fluorescence Quenching of Anthracene Derivatives and Selective Detection of Picric Acid. *Chem. – A Eur. J.* **2016**, *22* (6), 2012–2019.

(17) Islam, M. M.; Hu, Z.; Wang, Q.; Redshaw, C.; Feng, X. Pyrene-Based Aggregation-Induced Emission Luminogens and Their Applications. *Mater. Chem. Front.* **2019**, *3* (5), 762–781.

(18) Hong, Y.; Lam, J. W. Y.; Tang, B. Z. Aggregation-Induced Emission: Phenomenon, Mechanism and Applications. *Chem. Commun.* **2009**, No. 29, 4332–4353.

(19) Ni, Y.; Yang, L.; Kong, L.; Wang, C.; Zhang, Q.; Yang, J. Highly Efficient Dual-State Emission and Two-Photon Absorption of Novel Naphthalimide Functionalized Cyanostilbene Derivatives with Finely Tuned Terminal Alkoxyl Groups. *Mater. Chem. Front.* **2022**, *6* (23), 3522–3530.

(20) Mphahlele, M. J.; Paumo, H. K.; El-Nahas, A. M.; El-Hendawy, M. M. Synthesis and Photophysical Property Studies of the 2,6,8-Triaryl-4-(Phenylethynyl)Quinazolines. *Molecules* **2014**, *19* (1), 795–818.

(21) Sasaki, S.; Drummen, G. P. C.; Konishi, G. -i. Recent Advances in Twisted Intramolecular Charge Transfer (TICT) Fluorescence and Related Phenomena in Materials Chemistry. *J. Mater. Chem. C* **2016**, *4*, 2731.

(22) Zhao, Z.; Lu, P.; Lam, J. W. Y.; Wang, Z.; Chan, C. Y. K.; Sung, H. H. Y.; Williams, I. D.; Ma, Y.; Tang, B. Z. Molecular Anchors in the Solid State: Restriction of Intramolecular Rotation Boosts Emission Efficiency of Luminogen Aggregates to Unity. *Chem. Sci.* **2011**, *2* (4), 672–675.

(23) Matsumoto, H.; Nishimura, Y.; Arai, T. Fluorescence Sensor with A New ON1–OFF–ON2 Switching Mechanism Using the Excited State Intermolecular Proton Transfer Reaction of An Anthracene-Diurea Compound. *Photochem. Photobiol.* **2017**, *93* (5), 1187–1192.

(24) Ramya, N. K.; Femina, C.; Suresh, S.; Mohanakumari, D. S.; Krishnan, R.; Thomas, R. Dicyanodistyrylbenzene Based Positional Isomers: A Comparative Study of AIEE and Stimuli Responsive Multicolour Fluorescence Switching. *New J. Chem.* **2022**, *46* (3), 1339–1346.

(25) Wang, X.; Wang, L.; Mao, X.; Wang, Q.; Mu, Z.; An, L.; Zhang, W.; Feng, X.; Redshaw, C.; Cao, C.; Qin, A.; Tang, B. Z. Pyrene-Based Aggregation-Induced Emission Luminogens (AIEgens) with Less Colour Migration for Anti-Counterfeiting Applications. *J. Mater. Chem. C* **2021**, *9* (37), 12828–12838.

(26) Khalid Baig, M. Z.; Prusti, B.; Kondipati, S.; Chakravarty, M. Di-Styrylanthracenes as Established AIEgens: Can Di-Anthracylethenes Be AIE-Active? *J. Lumin.* **2019**, *209*, 188–196.

(27) Feng, X.; Zhang, J.; Hu, Z.; Wang, Q.; Islam, M. M.; Ni, J.-S.; Elsegood, M. R. J.; Lam, J. W. Y.; Zhou, E.; Tang, B. Z. Pyrene-Based Aggregation-Induced Emission Luminogens (AIEgen): Structure Correlated with Particle Size Distribution and Mechanochromism. *J. Mater. Chem. C* **2019**, *7* (23), 6932–6940.

(28) Xue, P.; Yao, B.; Liu, X.; Sun, J.; Gong, P.; Zhang, Z.; Qian, C.; Zhang, Y.; Lu, R. Reversible Mechanochromic Luminescence of Phenothiazine-Based 10,10′-Bianthracene Derivatives with Different Lengths of Alkyl Chains. *J. Mater. Chem. C* **2015**, *3* (5), 1018–1025.

(29) Würthner, F. Aggregation-Induced Emission (AIE): A Historical Perspective. *Angew. Chemie Int. Ed.* **2020**, *59* (34), 14192–14196.

(30) Yoon, S.-J.; Kim, J. H.; Kim, K. S.; Chung, J. W.; Heinrich, B.; Mathevet, F.; Kim, P.; Donnio, B.; Attias, A.-J.; Kim, D.; Park, S. Y. Mesomorphic Organization and Thermochromic Luminescence of Dicyanodistyrylbenzene-Based Phasmidic Molecular Disks: Uniaxially Aligned Hexagonal Columnar Liquid Crystals at Room Temperature with Enhanced Fluorescence Emission and Semiconductivity. *Adv. Funct. Mater.* **2012**, *22* (1), 61–69.

(31) Anandhan, K.; Cerón, M.; Perumal, V.; Ceballos, P.; Gordillo-Guerra, P.; Pérez-Gutiérrez, E.; Castillo, A. E.; Thamotharan, S.; Percino, M. J. Solvatochromism and PH Effect on the Emission of a Triphenylimidazole-Phenylacrylonitrile Derivative: Experimental and DFT Studies. *RSC Adv.* **2019**, *9* (21), 12085–12096.

(32) Noh, S. B.; Kim, R. H.; Kim, W. J.; Kim, S.; Lee, K.-S.; Cho, N. S.; Shim, H.-K.; Pudavar, H. E.; Prasad, P. N. Aggregation-Enhanced Two-Photon Absorption and up-Converted Fluorescence of Quadrupolar 1,4-Bis(Cyanostyryl)Benzene Derivatives Showing Solvatochromic Fluorescence. *J. Mater. Chem.* **2010**, *20* (35), 7422–7429.

(33) Yokoyama, S.; Nishiwaki, N. Fluorescence Behavior of Bis(Cyanostyryl)Pyrrole Derivatives Depending on the Substituent Position of Cyano Groups in Solution and in Solid State. *J. Org. Chem.* **2019**, *84* (3), 1192–1200.

(34) Zhang, Y.; Liang, C.; Jiang, S. A Solvatochromic Cyanostilbene Derivative as an Intensity and Wavelength-Based Fluorescent Sensor for Water in Organic Solvents. *New J. Chem.* **2017**, *41* (16), 8644–8649.

(35) Katla, J.; Nair, A. J. M.; Ojha, A.; Kanvah, S. Organogels Composed of Trifluoromethyl Anthryl Cyanostyrenes: Enhanced Emission and Self-Assembly. *Photochem. Photobiol. Sci.* **2018**, *17* (4), 395–403.

(36) Wang, Y.; Qian, Z.; Li, X.; Qin, A.; Guo, Y.; Tang, B. Polymorphism and Light Conversion Properties of Anthracene-Based Isomers. *Dye. Pigment.* **2022**, *197*, 109888.

(37) Zhan, K.; Li, Z.; Chen, J.; Hou, Y.; Zhang, J.; Sun, R.; Bu, Z.; Wang, L.; Wang, M.; Chen, X.; Hou, X. Tannic Acid Modified Single Nanopore with Multivalent Metal Ions

Recognition and Ultra-Trace Level Detection. *Nano Today* **2020**, *33*, 100868.
(38) Adamo, C.; Barone, V. Toward Reliable Density Functional Methods without Adjustable Parameters: The PBE0 Model. *J. Chem. Phys.* **1999**, *110* (13), 6158–6170.
(39) Guidon, M.; Hutter, J.; VandeVondele, J. Robust Periodic Hartree−Fock Exchange for Large-Scale Simulations Using Gaussian Basis Sets. *J. Chem. Theory Comput.* **2009**, *5* (11), 3010–3021.
(40) Skyner, R. E.; McDonagh, J. L.; Groom, C. R.; van Mourik, T.; Mitchell, J. B. O. A Review of Methods for the Calculation of Solution Free Energies and the Modelling of Systems in Solution. *Phys. Chem. Chem. Phys.* **2015**, *17* (9), 6174–6191.
(41) Nayyar, I. H.; Masunov, A. E.; Tretiak, S. Comparison of TD-DFT Methods for the Calculation of Two-Photon Absorption Spectra of Oligophenylvinylenes. *J. Phys. Chem. C* **2013**, *117* (35), 18170–18189.
(42) T. A. Keith, T. K. Gristmill Software, Overland Park KS, Aima. (Version 11. 05. 16. No Title. 2011.
(43) Zgorzelak, M.; Grajewski, J.; Gawroński, J.; Kwit, M. Solvent-Assisted Synthesis of a Shape-Persistent Chiral Polyaza Gigantocycle Characterized by a Very Large Internal Cavity and Extraordinarily High Amplitude of the ECD Exciton Couplet. *Chem. Commun.* **2019**, *55* (16), 2301–2304.
(44) Wen, L.; Sun, J.; Li, C.; Zhu, C.; Zhang, X.; Wang, Z.; Song, Q.; Lv, C.; Zhang, Y. Rich-Colour Mechanochromism of a Cyanostilbene Derivative with Chiral Self-Assembly. *New J. Chem.* **2021**, *45* (26), 11530–11535.
(45) Zhang, B.; Xiao, Y.; Fang, H.; Gao, H.; Wang, F.; Cheng, X. Mesogenic D–A Fluorophores Based on Cyanovinyl and Benzothiadiazole. *New J. Chem.* **2018**, *42* (20), 16709–16716.
(46) Kim, H.-J.; Gierschner, J.; Park, S. Y. Tricolor Fluorescence Switching in a Single Component Mechanochromic Molecular Material. *J. Mater. Chem. C* **2020**, *8* (22), 7417–7421.
(47) Ravi, M.; Soujanya, T.; Samanta, A.; Radhakrishnan, T. P. Excited-State Dipole Moments of Some Coumarin Dyes from a Solvatochromic Method Using the Solvent Polarity Parameter, E. *J. Chem. Soc. Faraday Trans.* **1995**, *91* (17), 2739–2742.
(48) Thomas, A.; Kirilova, E. M.; Nagesh, B. V; Krishna Chaitanya, G.; Philip, R.; Manohara, S. R.; Sudeeksha, H. C.; Siddlingeshwar, B. Influence of Nitro Group on Solvatochromism, Nonlinear Optical Properties of 3-Morpholinobenzanthrone: Experimental and Theoretical Study. *J. Photochem. Photobiol. A Chem.* **2023**, *437*, 114434.
(49) Zhao, Y. H.; Abraham, M. H.; Zissimos, A. M. Fast Calculation of van Der Waals Volume as a Sum of Atomic and Bond Contributions and Its Application to Drug Compounds. *J. Org. Chem.* **2003**, *68* (19), 7368–7373.
(50) Mahalingavelar, P.; Kanvah, S. α-Cyanostilbene: A Multifunctional Spectral Engineering Motif. *Phys. Chem. Chem. Phys.* **2022**, *24* (38), 23049–23075.

Chapter 4

Photophysical Divergence Driven by π-Spacer Variations in Anthracene-Cyanostilbene Architecture

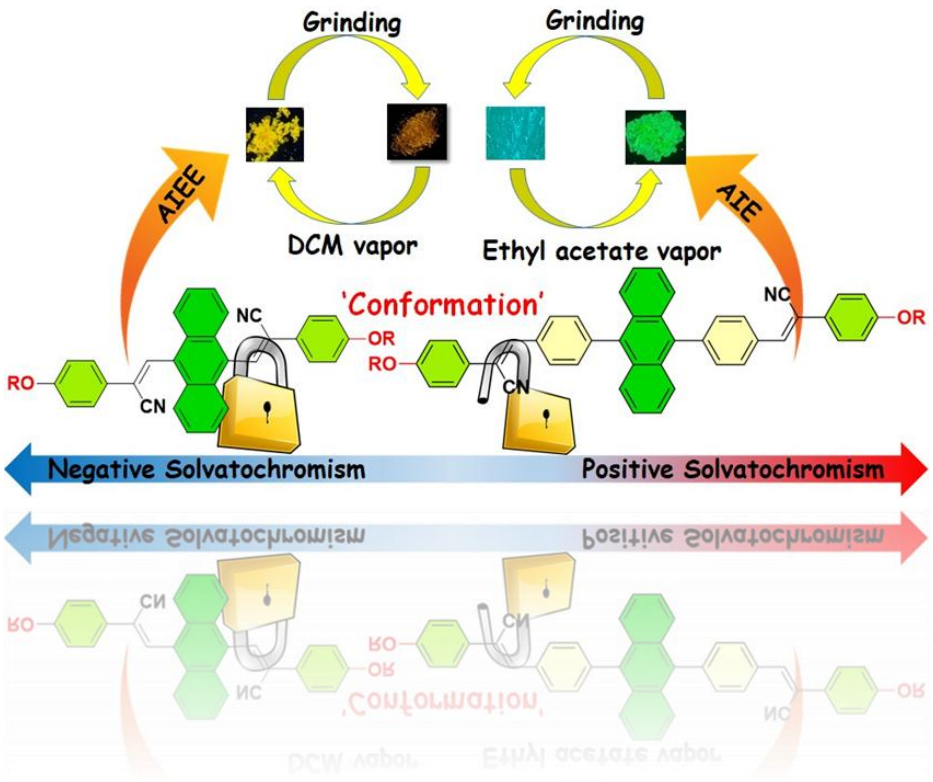

4.1 Abstract

A series of four anthracene-incorporated cyanostilbene derivatives with donor–π–acceptor (D–π–A) architectures was synthesized to investigate the effect of a phenyl π-spacer. Compounds without the spacer (**CS-4.1a**, **CS-4.1b**) showed low quantum yields (Φ_F = 0.05 – 0.25) in various solvents, negative solvatochromism, aggregation-induced enhanced emission (AIEE), and red-shifted mechanofluorochromism. In contrast, those with the spacer (**CS-4.2a**, **CS-4.2b**) exhibited high quantum yields (Φ_F = 0.75 – 0.85), positive solvatochromism, aggregation-induced emission (AIE), and blue-shifted mechanofluorochromism, highlighting the key role of the spacer in modulating photophysical properties. Quantum chemical calculations reveal that the compounds incorporating a phenyl π-spacer exhibit conformational flexibility between *syn*- and *anti*-conformers in both ground and excited states, due to an energetically more accessible transition state relative to analogues lacking the spacer. The findings in this study underscore the importance of strategic structural engineering in anthracene-based cyanostilbene systems, which profoundly influences their photophysical properties, paving the way for their potential use in future optoelectronic applications.

***Publication based on this chapter**

Femina, C.; Yamamoto, N.; Ramya, N. K.; Sajith, P. K.; Thomas, R. Photophysical Divergence Driven by π-Spacer Variations in the Anthracene–Cyanostilbene Architecture. *Phys. Chem. Chem. Phys.* **2025**, *27* (45), 24641–24654.

4.2 Introduction

Tuning of photophysical characteristics of organic luminescent materials under ambient conditions is an area of fundamental research and is extensively applied in the field of optoelectronics.[1–5] The conventional π-conjugated compounds without any functional modifications have simple photophysical properties with respect to their structural and functional moieties. Taking into account this, it is necessary to acquire more specific optoelectronic performances, which can be achieved by designing and constructing smart molecules in which the photophysical properties can be tuned in a controlled manner.[6] Therefore, novel molecular designs with tunable photophysical properties can serve as promising candidates for the development of versatile optoelectronic devices.[7–11] The construction and design of such smart molecular structures possessing stimuli-responsive fluorescence switching such as mechanochromism, thermochromism, vaprochromism etc. has received unprecedented attention.[12–16]

Organic luminogens, which are made up of molecules containing electron donor (D) and electron acceptor (A) units, have drawn considerable recognition due to their effectiveness in obtaining emissive compounds owing to their push-pull intramolecular electronic behaviour. Such systems have a wide range of applications in the fields of sensors, fluorescent probes, organic solar cells, and hybrid materials, etc.[17–22] The donor (D) and the acceptor (A) units are linked through π-conjugated spacers, creating an efficient path for the transport of charge carriers from the donor to the acceptor by intramolecular charge transfer (ICT) mechanism. ICT systems based on cyanostilbenes as acceptor units have been widely explored over the past decades and employed as fluorescent probes to indicate the micro-environmental changes.[23–25,26] Most of the studies in these classes of molecules focused on the proper management and utilization of the phenomena for achieving bioimaging, energy harvesting and display applications. The π-conjugated structures endow ample aggregation modes in the solid state, leading to enhanced solid-state emission, while the ICT phenomenon enhances the emission properties of these molecules in solution. Therefore, the design and synthesis of donor-acceptor-based molecules opens great promise to afford bright emissive materials with tunability in solution and solid states.[25]

Among various π-conjugated materials, cyanostilbene-based organic fluorophores have drawn interest due to their extraordinary emissive properties resulting from their rigid and twisted geometry along with tendency to form emissive aggregates in the solid state. Recent reports have shown that the cyanostilbene derivatives with alkyl chains provide flexible solid-state structure

with precise control on molecular packing and aggregation, wherein various external stimuli such as heat, light, pressure, etc. have resulted in tunable optoelectronic properties.[27–30] Various attempts have been made by supramolecular chemists to design and synthesis molecular systems with multi-stimuli responsive emission switching.[31,32] In this regard, some of the researchers have focused on constructing molecular systems capable of mechanofluorochromism (MFC) property, which has significant importance in the development of smart devices with potential in the field of sensing and imaging.[33,34] There are several notable examples of cyanostyryl-based donor-acceptor systems with triphenylamine,[35] carbazole,[33] fluorene[36] and perylene as donors showing multistimuli responsive photoluminescence properties. However, cyanostyryl systems incorporating anthracene,[37,38] a well-known chromophore with excellent photophysical properties, as the donor moiety remain relatively scarce in the literature.

4.3 Scope of the present investigation

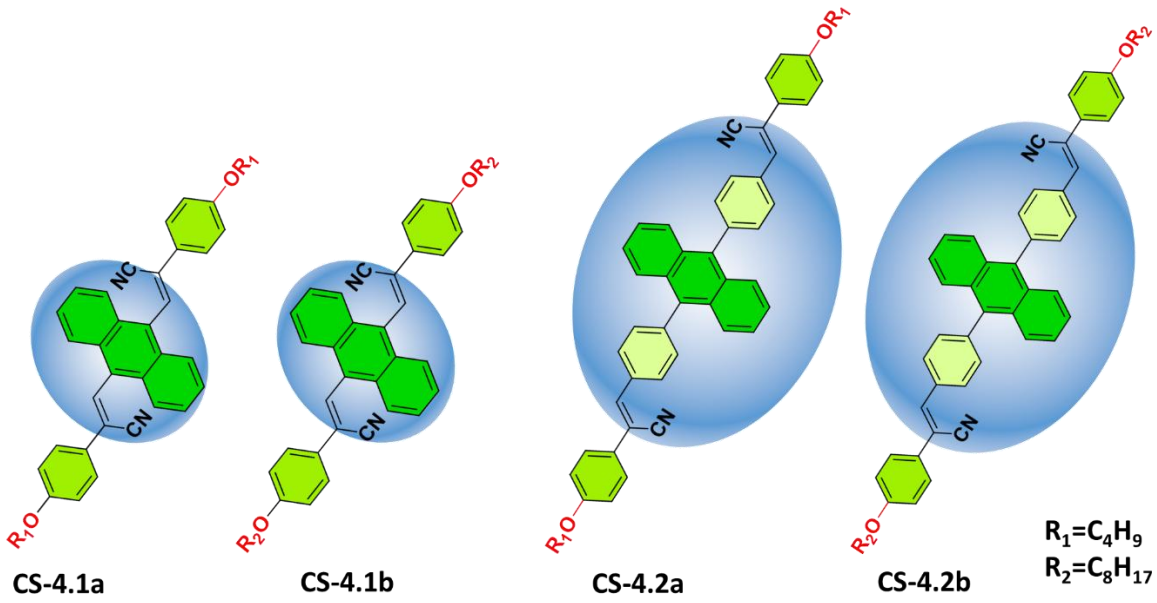

Figure 4.1 Chemical structure of compounds **CS-4.1a-b** and **CS-4.2a-b**.

Several cyanostyryl-based donor–acceptor systems with diverse donor groups have been reported, highlighting their multistimuli-responsive photoluminescence properties. Nevertheless, examples employing anthracene as the donor unit remain relatively rare in the literature. In the chapter 3, the ICT and multi-stimuli responsive emission behavior of alkyl chain variants in a symmetrically modified anthracene-dicyanostyryl D-π-A system is explored.[23] Building on these

findings, the content of this chapter is the investigation of the impact of inserting a phenyl ring between the anthracene donor and the cyanostyryl acceptor moiety. In pursuit of this objective, two series of compounds with proper alkyl variation: one featuring a direct linkage between anthracene and the cyanostyryl unit (**CS-4.1a** and **CS-4.1b**), and another incorporating a phenyl spacer between them (**CS-4.2a** and **CS-4.2b**), as depicted in Figure 4.1 were synthesized. The intrinsic properties of the core chromophore, independent of alkyl chain variations, are represented by compound **CS-4.1** (comprising **CS-4.1a** and **CS-4.1b**) and compound **CS-4.2** (comprising **CS-4.2a** and **CS-4.2b**). This chapter of the thesis tries to systematically compare the photophysical properties of the compounds in the light structural data obtained from spectroscopic and diffractions experiments.

4.4 Experimental section

All the chemicals and reagents required for the synthesis of anthracene-cyanostilbene derivatives (**CS-4.1a** to **CS-4.2b**) were purchased from commercial supplies and used without further purification. All the compounds were synthesized by following the reported procedures with modifications and the synthesized compounds were characterized using ^{1}H NMR and ^{13}C NMR spectroscopy in $CDCl_3$ with TMS as internal standard (see Figure 4.2 to 4.7). The mass spectral data were obtained from Electron Spray Ionization Mass Spectroscopy (ESI-MS), Model-Micromass QTof MicroTM and a Maxis Impact. UV-visible spectroscopic studies were carried out on Cary 5000 is a high-performance UV-Vis-NIR spectrophotometer with superb photometric performance in the 175-3300 nm range. The fluorescence lifetime and the steady state fluorescence studies were conducted on FLS1000-xS-t fluorescence lifetime spectrometer and on Edinburg FLS-1000 photoluminescence spectrometer attached with an integrating sphere. All the fluorescence spectra were recorded with a quartz cuvette of path length 1 cm at a slit width of 1 nm. Absolute fluorescence quantum yield of the compounds in both solid and solution states was recorded on LQE-100 LED Photo-Luminescence Quantum Yield Measurement system. The single crystal X-ray diffraction data were measured on a Bruker AXS Kappa Apex2 diffractometers. The powder X-ray diffraction intensities were measured on a Panalytical Aeris Research diffractometer.

4.4.1 Synthesis and characterization

Two series of anthracene-cyanostyrene based (D-π-A) compounds featuring variation in π-spacer and non-conjugating alkyl chains were synthesized. The synthetic routes to the target compounds are depicted in scheme 4.1. All the compounds presented in this report were synthesized following the protocols reported in the literature with necessary modifications. The compound **CS-4.1** with butyloxy and octyloxy substitution were synthesized by Knoevenagel condensation of 2-(4-alkyloxyphenyl)acetonitrile with anthracene-9,10-dicarbaldehyde, while the alkyl chain homologues in compound **CS-4.2** were prepared by condensation of 4,4′-(anthracene-9,10-diyl)dibenzaldehyde with 2-(4-alkyloxyphenyl)acetonitrile.

All the compounds were characterized using ^{1}H and ^{13}C NMR, and HRMS spectroscopic techniques (see Figure 4.2-4.13). Compounds **CS-4.1b** and **CS-4.2b** were further characterized using single-crystal X-ray diffraction. The single crystals of compounds **CS-4.1b** (orange-yellow crystal) and **CS-4.2b** (green crystal) were grown by slow evaporation at room temperature from respective dichloromethane and ethyl acetate solutions. Figure 4.14 shows the ORTEP of compounds **CS-4.1b** and **CS-4.2b** drawn at at 50 % probability.

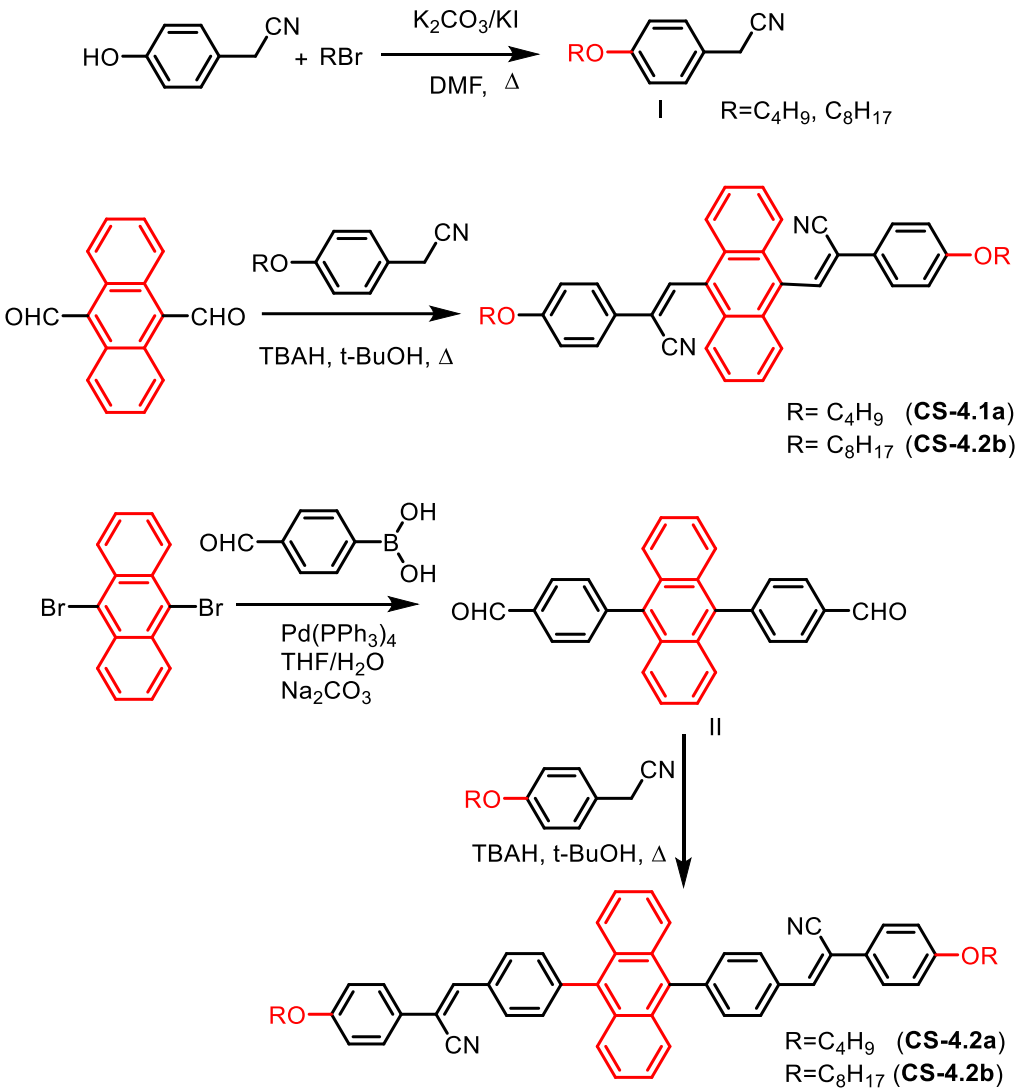

Scheme 4.1. Synthetic route of the target compounds.

1. General method for the synthesis of 2-(4-alkyloxyphenyl)acetonitrile, (1a and 1b)

4-alkyloxy substituted phenylacetonitriles were prepared by adopting the previously reported procedure.[23,39,40] A suspension of K_2CO_3 (4.05 g, 29.2 mmol) in dimethylformamide (15mL) was purged with argon for 15 minutes and heated to 80 ºC, and 2-(4-hydroxyphenyl)acetonitrile (1.47 g, 11.0 mmol) was added. 1-bromoalkane (14.2 mmol) was slowly added over 10 minutes and stirred at 80 ºC for 4 hours. The reaction mixture was evaporated and the organic phase was extracted with ethyl acetate and washed with water (3 x 50). The organic phase was evaporated and column chromatographed over silica gel using ethyl acetate/hexane (0.5:9.5) to obtain the target compound. The products

were characterized using **^{1}H NMR** and **^{13}C NMR** spectroscopy (see Figure 4.2 and Figure 4.5).

2-(4-(butyloxy)phenyl)acetonitrile, 1a: Colorless liquid, Yield: 81 %, **^{1}H NMR** (400 MHz, $CDCl_3$: δ 7.24 (d, 2H, *J* = 6.7 Hz), 6.91 (d, 2H, *J* = 8.7 Hz), 3.98 (t, 2H, *J* = 6.5 Hz), 3.70 (s, z2H), 1.83 – 1.74 (m, 2H), 1.50 (dd, 2H, *J* = 14.7, 7.5 Hz), 1.00 (t, 3H, *J* = 7.4 Hz). **^{13}C NMR** (400 MHz, $CDCl_3$): δ 158.94, 129.05, 121.53, 118.27, 115.09, 67.83, 31.25, 22.83, 19.23, 13.84.

2-(4-(octyloxy)phenyl)acetonitrile, 1b: Colorless solid, Yield: 84 %, **^{1}H NMR** (400 MHz, $CDCl_3$): δ (ppm) δ 7.21 (d, 2H, *J* = 8.8 Hz), 6.88 (d, 2H, *J* = 8.7 Hz), 3.94 (t, 2H, *J* = 6.6 Hz), 3.67 (s, 2H), 1.80 – 1.74 (m, 2H), 1.48 – 1.40 (m, 2H), 1.30 (dd, 8H, *J* = 14.4, 5.6 Hz), 0.89 (t, 3H, *J* = 7.0 Hz). **^{13}C NMR** (400 MHz, $CDCl_3$): δ 159.00, 129.12, 121.57, 118.34, 115.16, 68.23, 31.89, 29.4, 29.3, 29.2, 26.10, 22.83, 22.73, 14.19.

2. Synthesis of compounds CS-4.1a and CS-4.1b

A mixture of anthracene-9,10-dicarbaldehyde (0.8 g, 3.44 mmol) and 2-(4-(alkyloxy)phenyl)acetonitrile (6.9 mmol) in tert-butyl alcohol (20 mL) was stirred at 50 °C. Tetrabutylammonium hydroxide (TBAH, 1 M solution in methanol, 0.69 mL) was slowly dropped into the mixture and stirred for 2 hours.[41] The resulting precipitate was filtered and purified by column chromatography using dichloromethane as eluent. The structures of **CS-4.1a** and **CS-4.1b** were confirmed by ^{1}H and^{13}C NMR, and mass spectrometry (see Figure 4.6 and Figure 4.9). Further, the compound **CS-4.1b** was characterized using single-crystal X-ray diffraction.

Compound **CS-4.1a**: Yield: 69%, **^{1}H NMR** (400 MHz, $CDCl_3$): δ (ppm) 8.30 (s, 2H), 8.13 (dd, 4H, *J* = 6.7, 3.3 Hz), 7.82 (d, 4H, *J* = 8.8 Hz), 7.56 (dd, 4H, *J* = 6.8, 3.2 Hz), 7.05 (d, 4H, *J* = 8.8 Hz), 4.07 (t, 4H, *J* = 6.5 Hz,), 1.87 – 1.78 (m, 4H), 1.52 (d, 4H, *J* = 7.4 Hz), 1.01 (t, 6H, *J* = 7.4 Hz).**^{13}C NMR** (400 MHz, $CDCl_3$): δ 160.75, 137.26, 130.40, 129.30, 127.63, 126.63, 126.05, 125.44, 121.37, 116.68, 115.26, 68.12, 31.31, 19.33, 13.96. **HRMS (ESI)** calculated m/z for $C_{40}H_{36}N_2O_2$: 576.28 $[M]^+$. Found: 577.29 $[M+H]^+$

Compound **CS-4.1b**: Yield: 65%, **^{1}H NMR** (400 MHz, $CDCl_3$): δ 8.30 (s, 2H), 8.13 (dd, 4H, *J* = 6.7, 3.1 Hz), 7.82 (d, 4H, *J* = 8.5 Hz), 7.56 (dd, 4H, *J* = 6.8, 3.1 Hz), 7.05 (d, 4H, *J* = 8.5 Hz), 4.06 (t, 4H, *J* = 6.5 Hz), 1.84 (p, 4H, *J* = 6.7 Hz), 1.57 – 1.46 (m, 8H), 1.43 – 1.31 (m, 12H), 0.90 (t, *J* = 6.6 Hz, 6H). **^{13}C NMR** (400 MHz, $CDCl_3$): δ 160.75, 137.26, 130.40, 129.30, 127.63, 126.63, 126.05, 125.44, 121.37, 116.68, 115.26, 68.12, 31.31,

29.45, 29.34, 29.27, 26.11, 22.76, 14.21. **HRMS (ESI)** calculated m/z for $C_{48}H_{52}N_2O_2$: 688.40 $[M]^+$. Found: 689.41 $[M+H]^+$

3. Synthesis of compounds CS-4.2a and CS-4.2b

A mixture of (Compound **II**[23]) 4,4'-(anthracene-9,10-diyl)dibenzaldehyde (1.3 g, 3.44 mmol) and 2-(4-(alkyloxy)phenyl)acetonitrile (6.9 mmol) in tert-butyl alcohol (20 mL) was stirred at 50 °C. Tetrabutylammonium hydroxide (TBAH, 1 M solution in methanol, 0.69 mL) was slowly dropped into the mixture and stirred for 2 hours.[41] The resulting precipitate was filtered and purified by column chromatography using dichloromethane as eluent. The structures of **CS-4.2a** and **CS-4.2b** were confirmed by ^1H and ^{13}C NMR, and mass spectrometry (see Figure 4.10 and Figure 4.13). Further, the compound **CS-4.2b** was characterized using single-crystal X-ray diffraction.

Compound **CS-4.2a**: Yield: 75%, **^{1}H NMR** (400 MHz, $CDCl_3$): δ 8.12 (d, 4H, J = 8.1 Hz), 7.70 (m, 8H), 7.60 (d, 4H, J = 4.6 Hz), 7.58 (s, 2H), 7.37 (dd, 4H, J = 6.9, 3.2 Hz), 7.00 (d, 4H, J = 8.9 Hz), 4.04 (t, 4H, J = 6.5 Hz), 1.80 (dd, 4H, J = 13.7, 7.8 Hz), 1.51 (dd, 4H, J = 13.8, 8.5 Hz), 1.00 (t, 6H, J = 7.4 Hz).**^{13}C NMR** (400 MHz, $CDCl_3$): δ 160.12, 141.87, 141.12, 139.60, 136.73, 133.98, 132.41, 130.20, 129.49, 127.74, 126.85, 125.70, 118.31, 115.43, 111.62, 68.21, 31.50, 19.23, 14.03. **HRMS (ESI)** calculated m/z for $C_{52}H_{44}N_2O_2$: 728.34 $[M]^+$. Found: 729.41 $[M+H]^+$

Compound **CS-4.2b**: Yield: 78%, **^{1}H NMR** (400 MHz, $CDCl_3$): δ 8.12 (d,4H, J = 8.1 Hz), 7.72 (dd, 4H, J = 6.8, 3.2 Hz), 7.69 (d, 4H, J = 8.6 Hz), 7.60, (d, 6H, J = 6.9 Hz), 7.38 (dd, 4H, J = 6.8, 3.1 Hz), 7.01 (d, 4H, J = 8.7 Hz), 4.03 (t, 4H, J = 6.5 Hz), 1.83 (p, 4H, J = 6.7 Hz), 1.48 (q, 4H, J = 7.4 Hz), 1.31 (m, 16H), 0.90 (t, 6H, J = 6.7 Hz). **^{13}C NMR** (400 MHz, $CDCl_3$): δ 160.27, 141.38, 139.72, 136.44, 133.44, 132.06, 129.68, 129.26, 127.47, 126.85, 125.53, 118.44, 115.14, 111.63, 68.38, 31.91, 29.45, 29.34, 29.29, 26.12, 22.76, 14.21. **HRMS (ESI)** calculated m/z for $C_{60}H_{60}N_2O_2$: 840.47 $[M]^+$. Found: 841.41 $[M+H]^+$

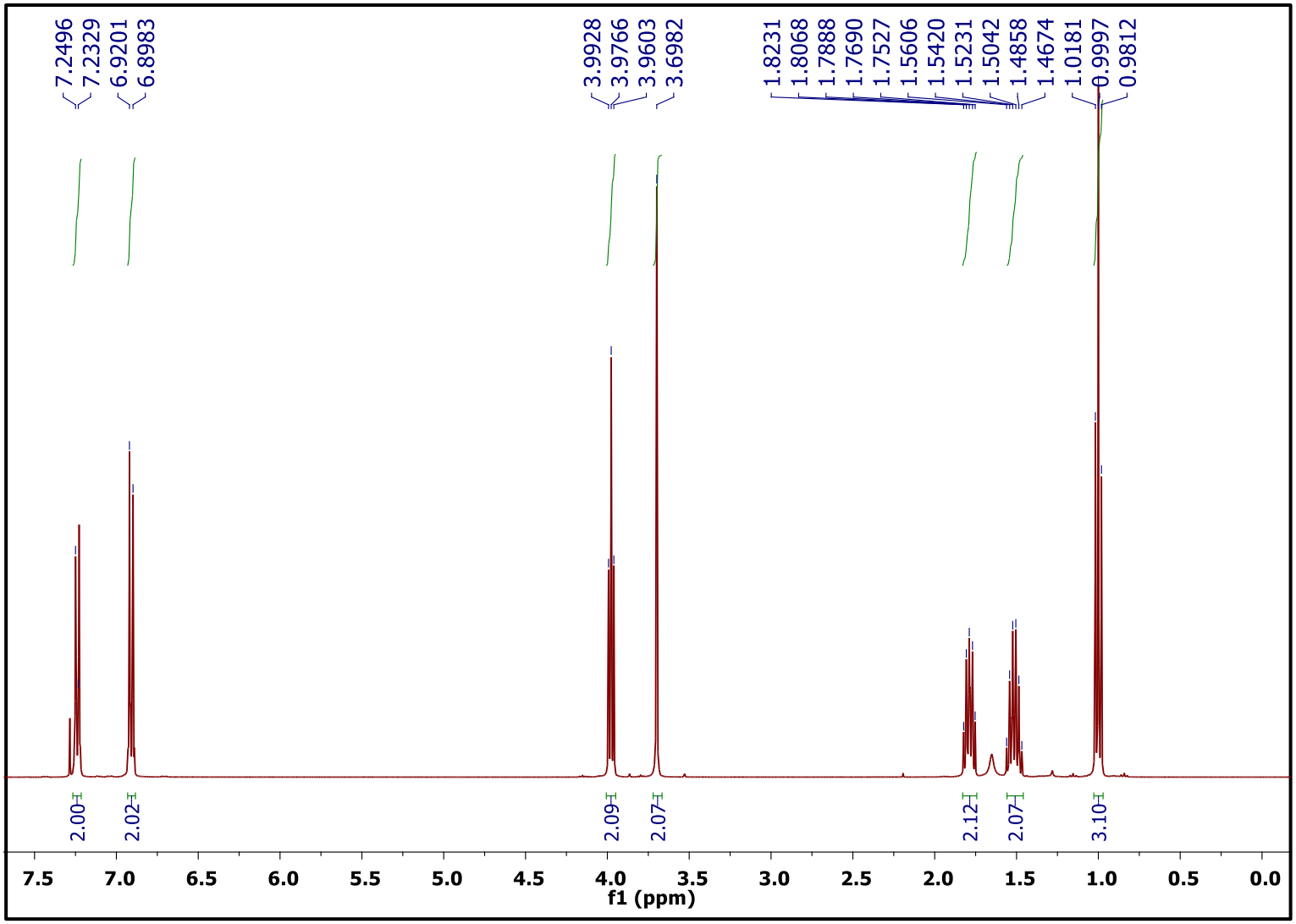

Figure 4.2 ^{1}H NMR spectra of the compound **1a** (400 MHz, $CDCl_3$).

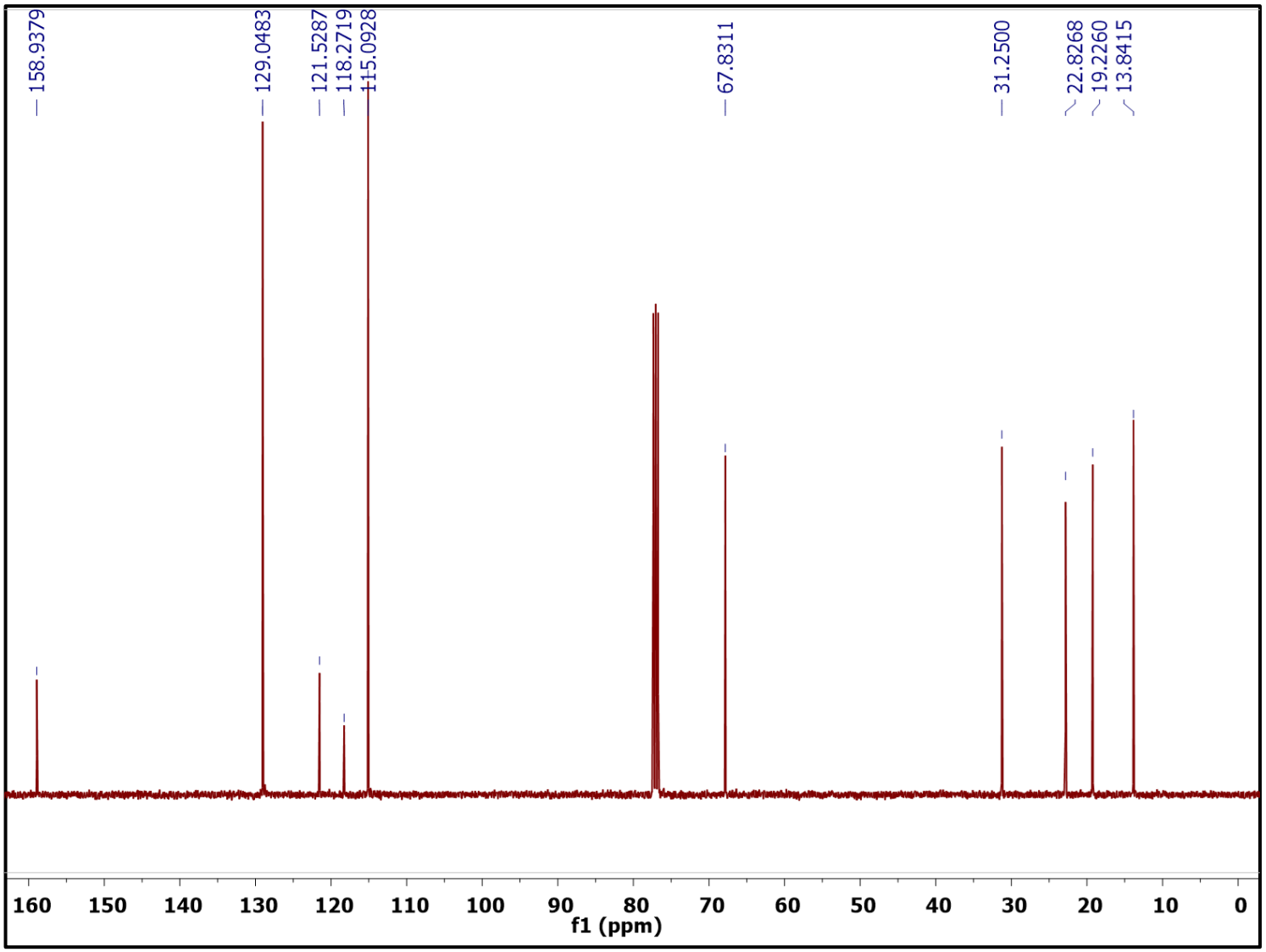

Figure 4.3 ^{13}C NMR spectra of the compound **1a** (400 MHz, $CDCl_3$).

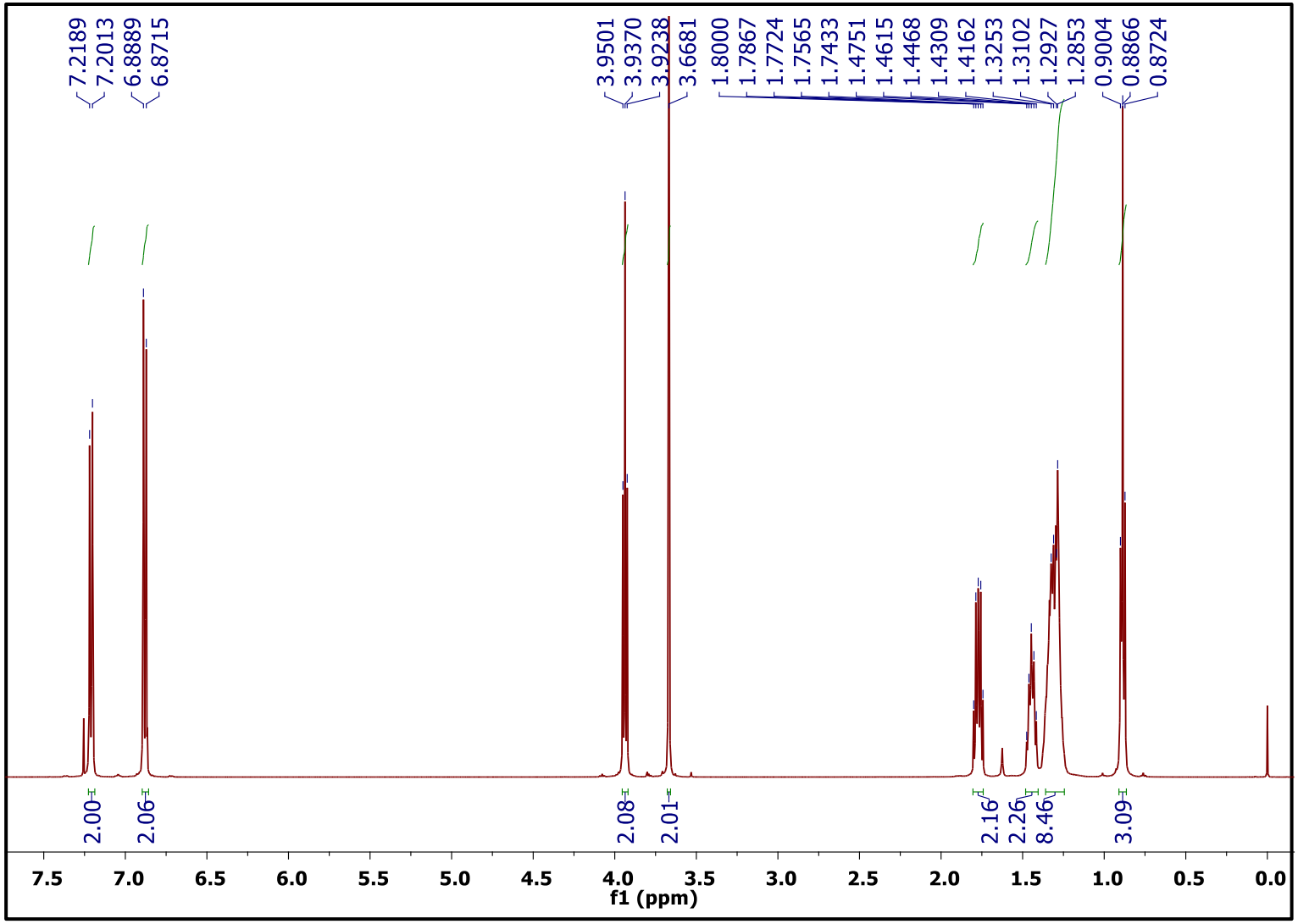

Figure 4.4 ^{1}H NMR spectra of the compound **1b** (400 MHz, $CDCl_3$).

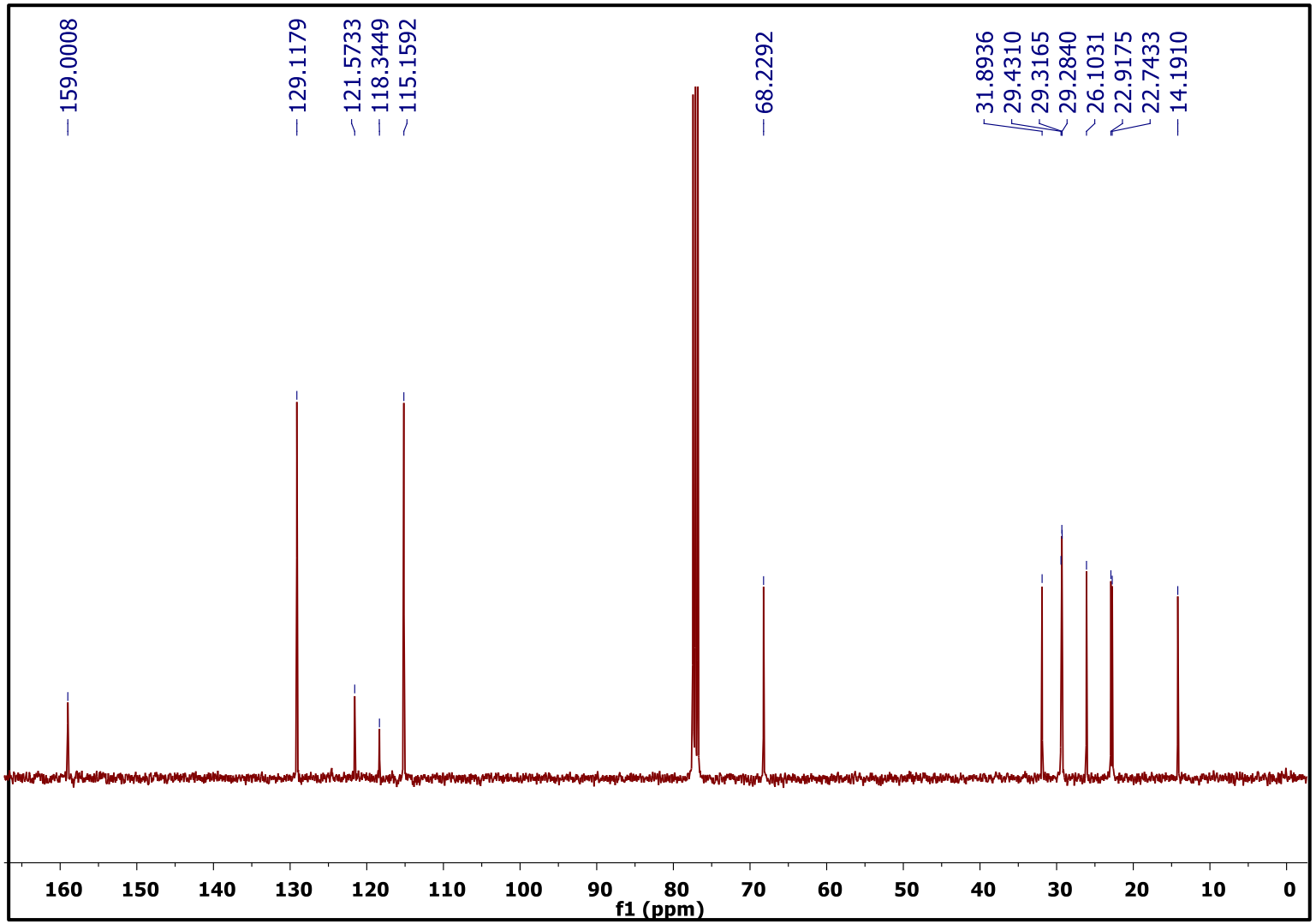

Figure 4.5 ^{13}C NMR spectra of the compound **1b** (400 MHz, $CDCl_3$).

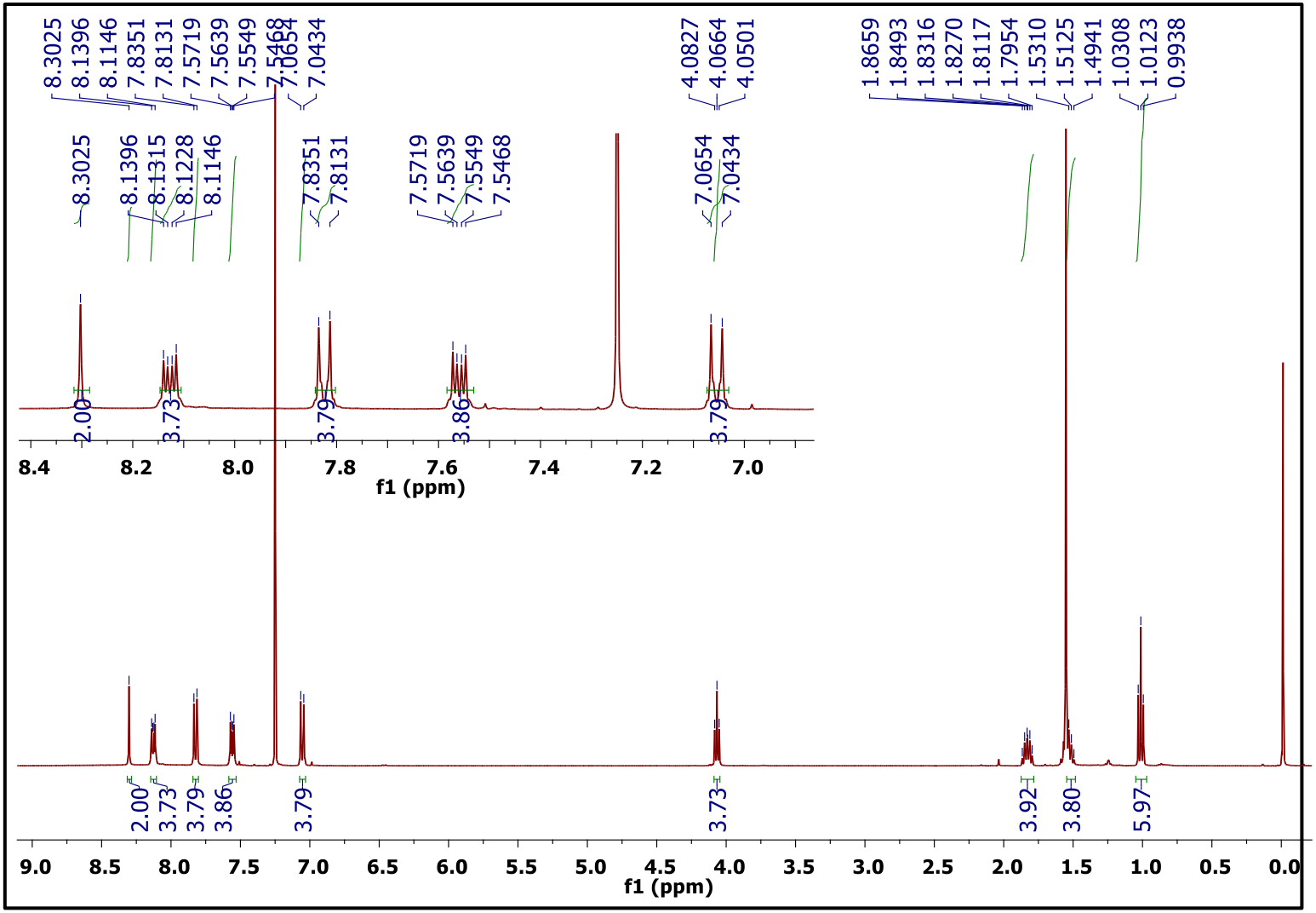

Figure 4.6 ^{1}H NMR spectra of the compound **CS-4.1a** (400 MHz, $CDCl_3$).

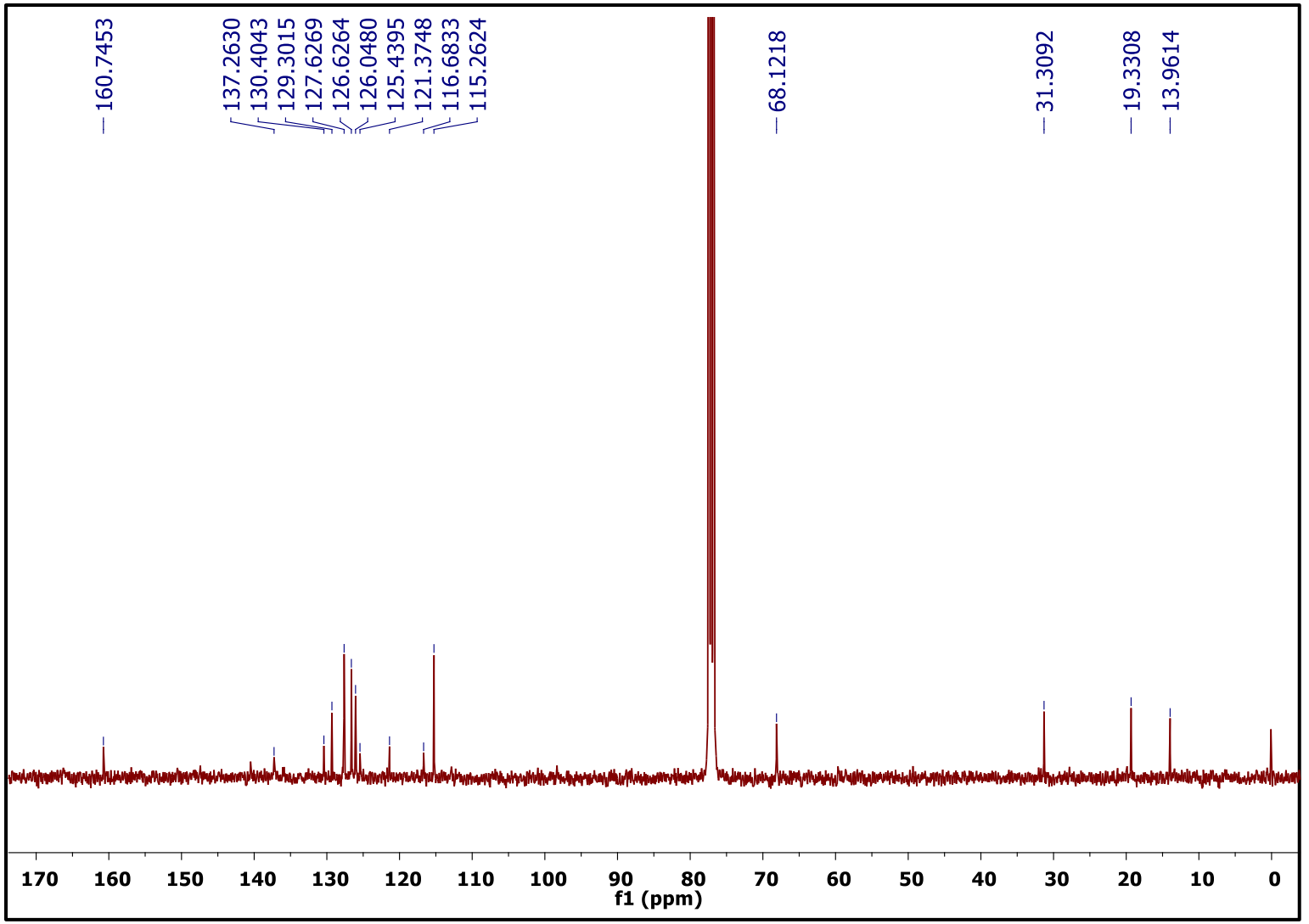

Figure 4.7 ^{13}C NMR spectra of the compound **CS-4.1a** (400 MHz, $CDCl_3$).

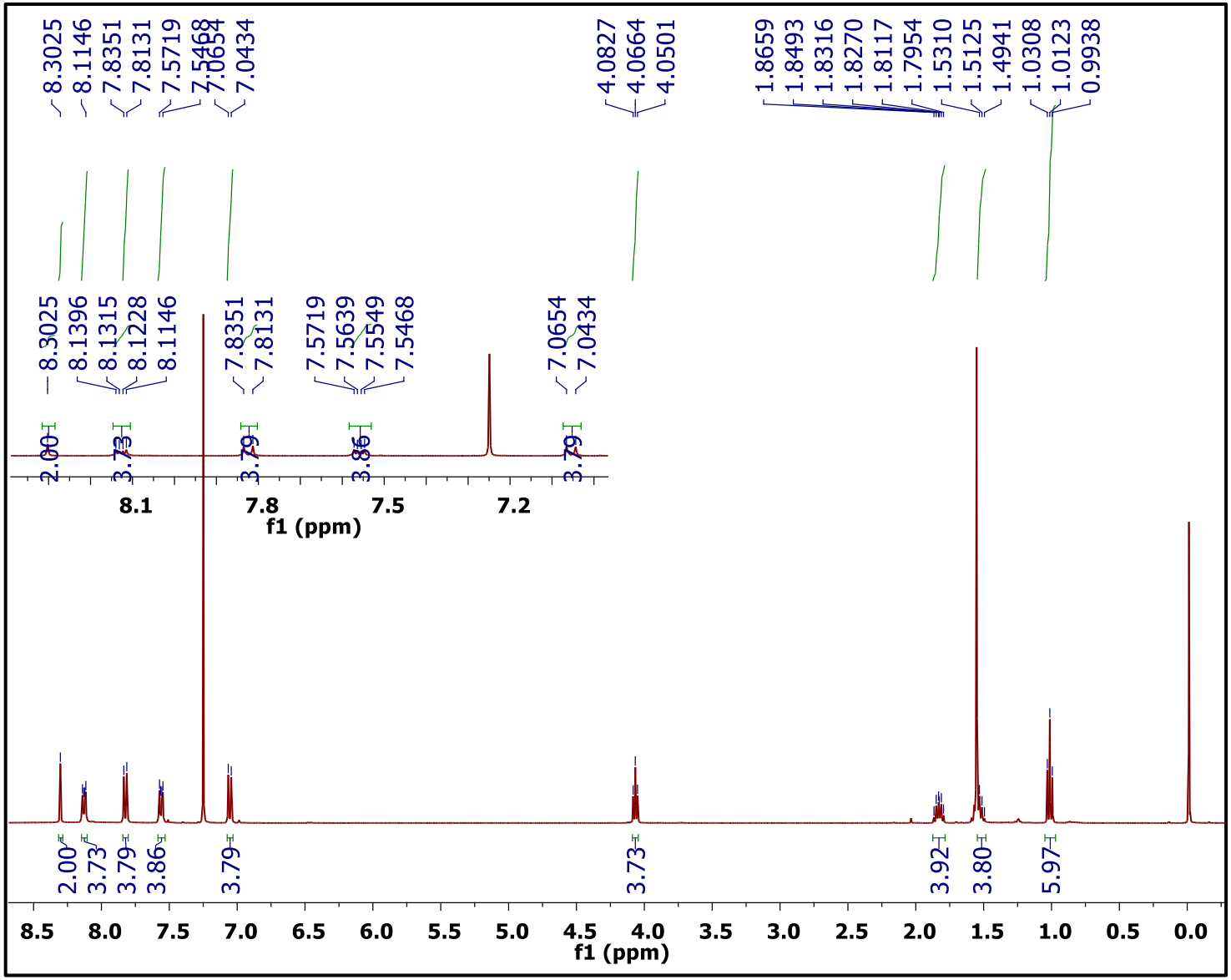

Figure 4.8 ^{1}H NMR spectra of the compound **CS-4.1b** (400 MHz, $CDCl_3$).

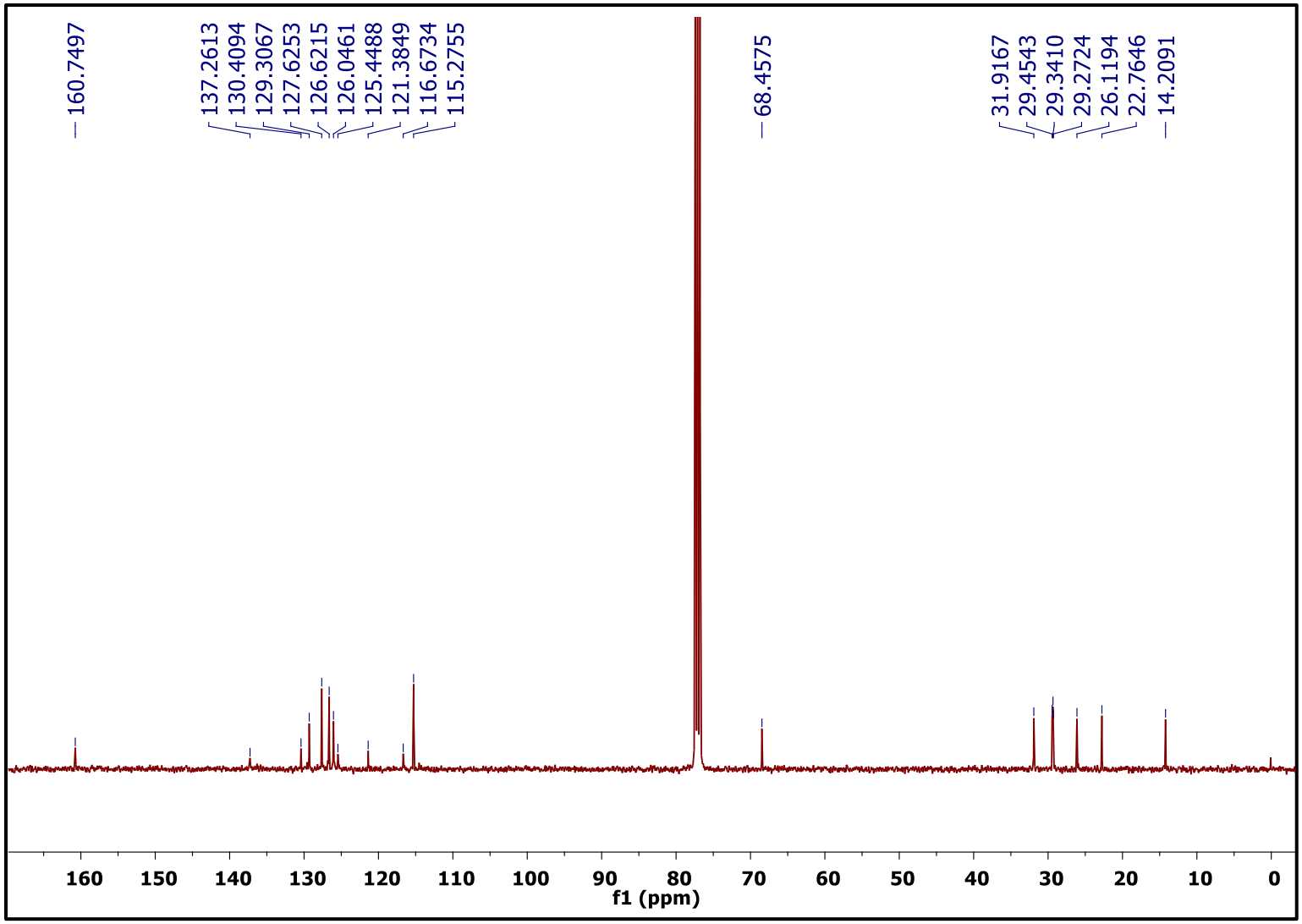

Figure 4.9 ^{13}C NMR spectra of the compound **CS-4.1b** (400 MHz, $CDCl_3$).

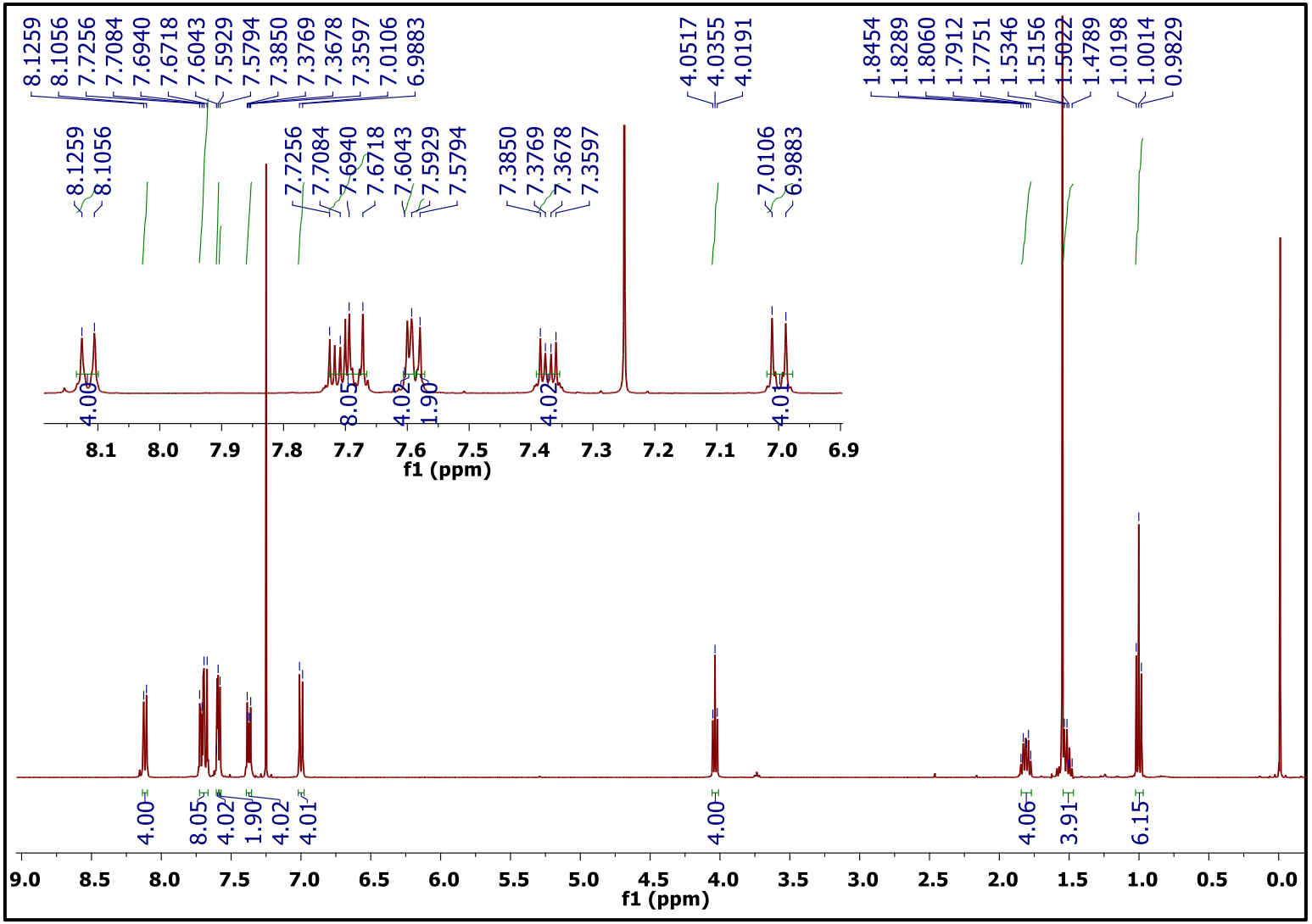

Figure 4.10 ^{1}H NMR spectra of the compound **CS-4.2a** (400 MHz, $CDCl_3$).

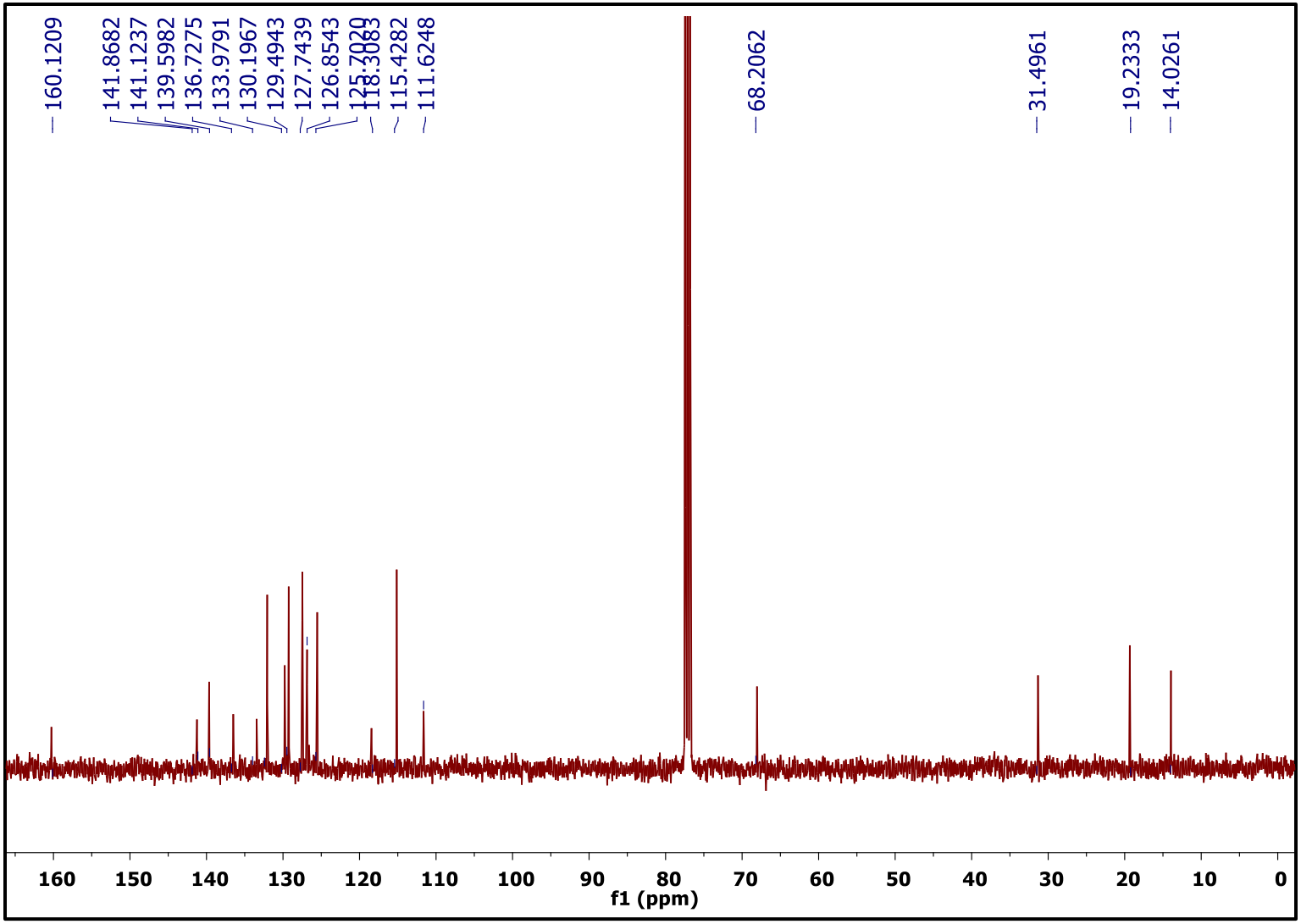

Figure 4.11 ^{13}C NMR spectra of the compound **CS-4.2a** (400 MHz, $CDCl_3$).

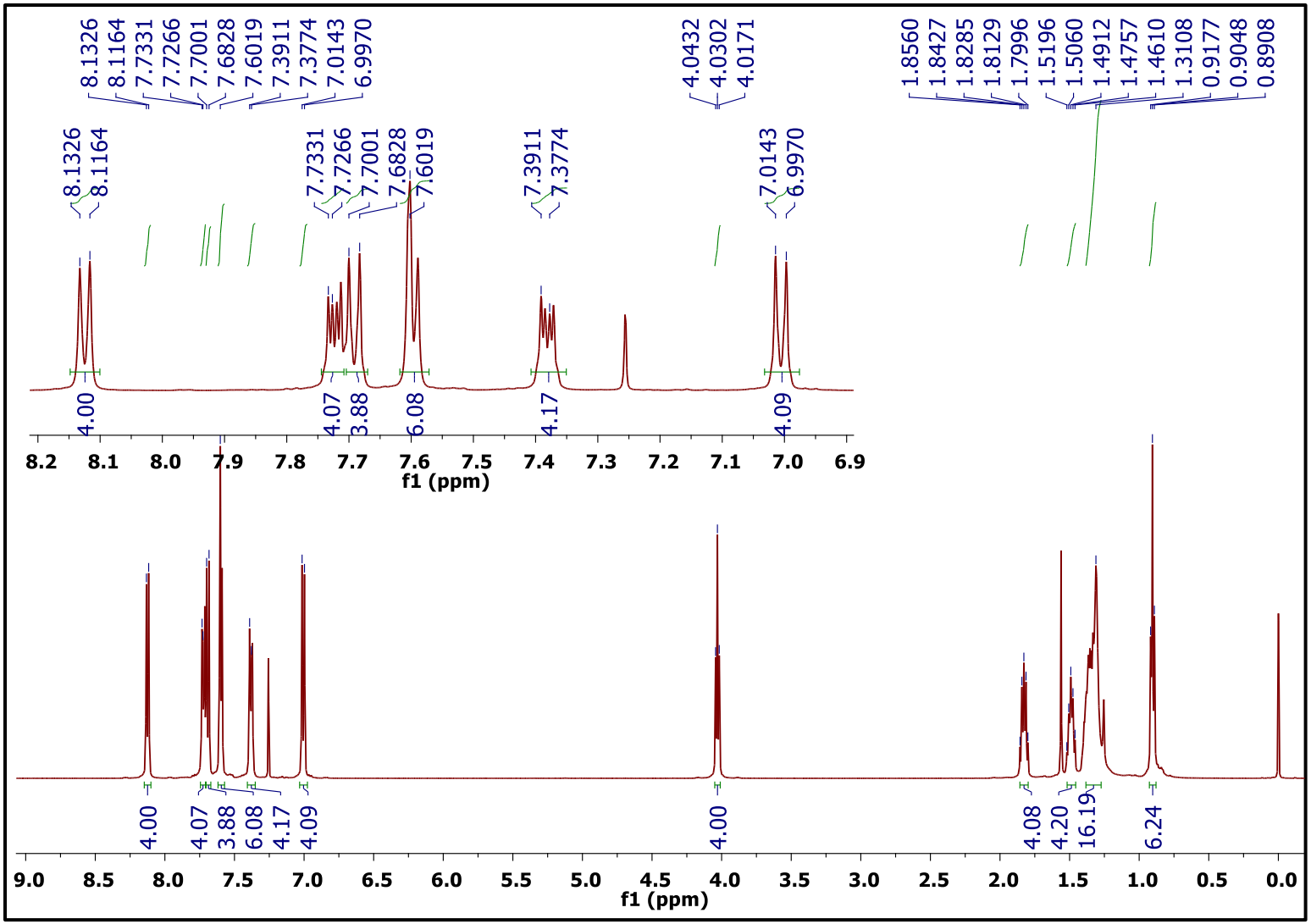

Figure 4.12 ^{1}H NMR spectra of the compound **CS-4.2b** (400 MHz, $CDCl_3$).

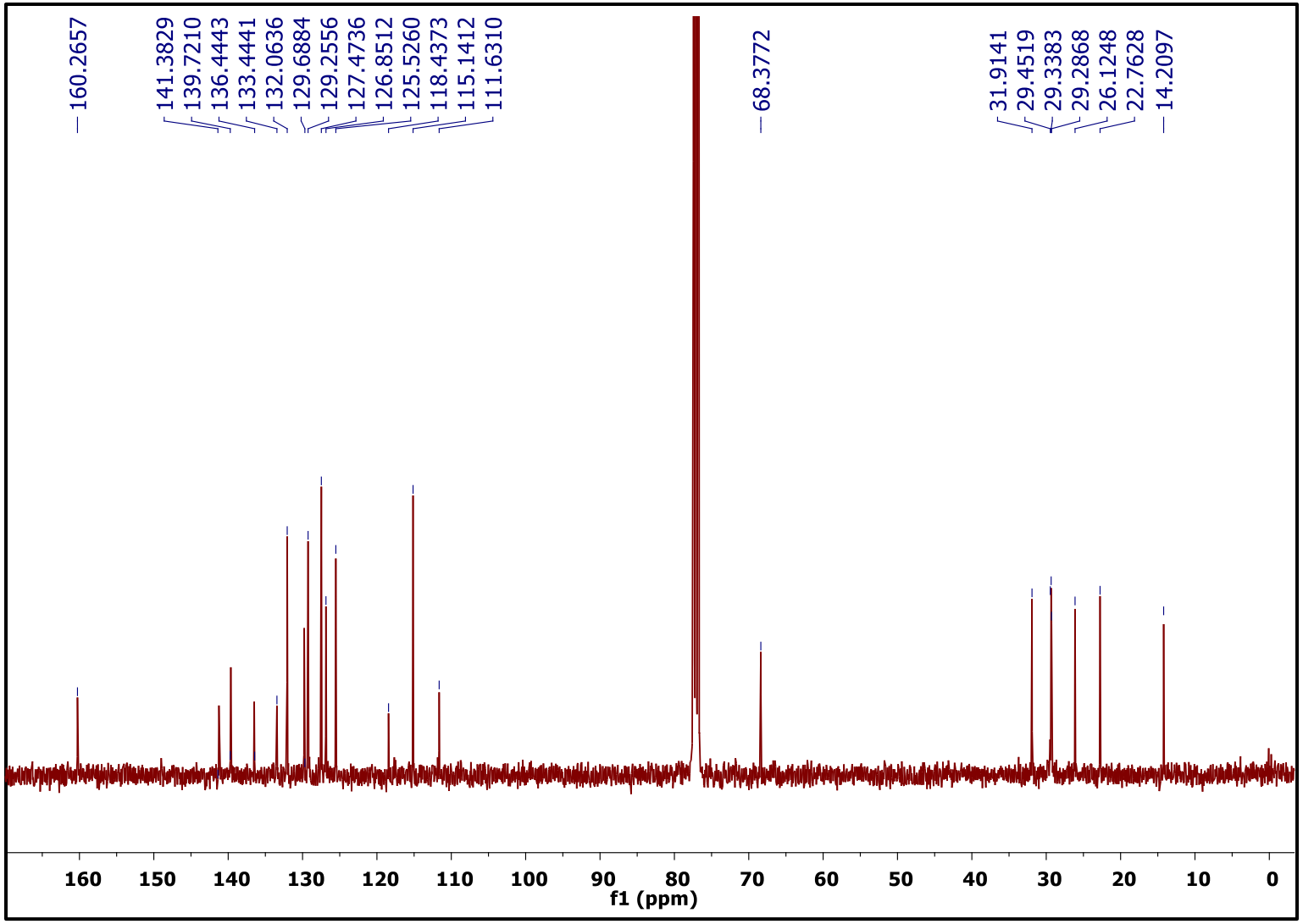

Figure 4.13 ^{13}C NMR spectra of the compound **CS-4.2b** (400 MHz, $CDCl_3$).

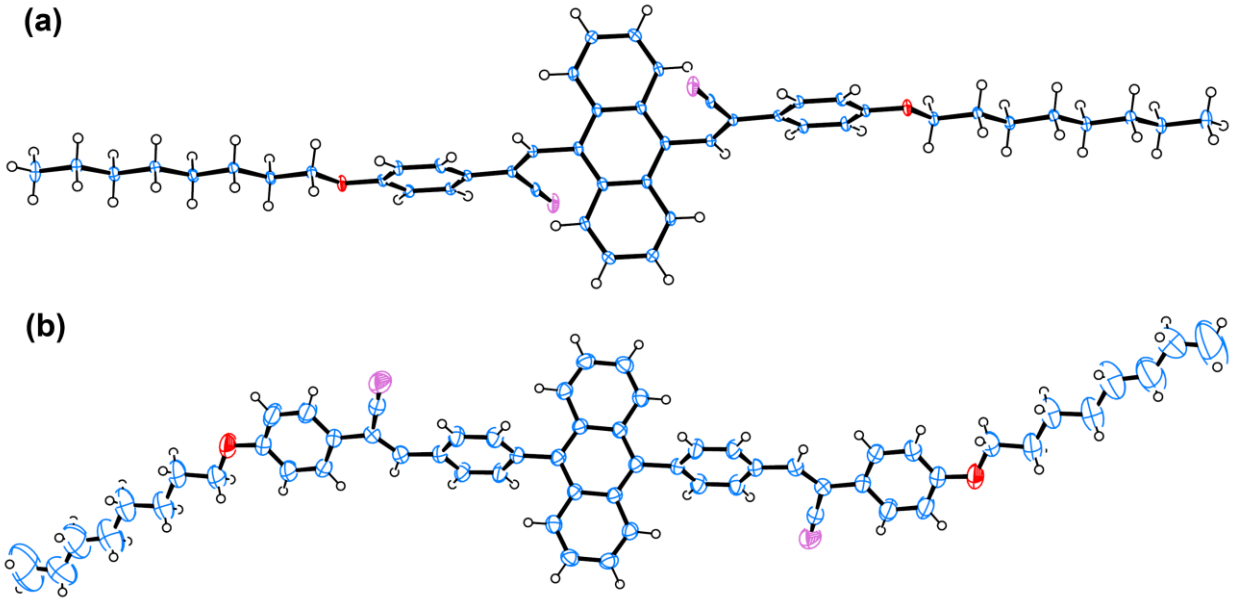

Figure 4.14 ORTEP plots of compounds **CS-4.1b** and **CS-4.2b** were drawn at 50 % probability.

4.5 Results and discussion

4.5.1 Solution state photophysical properties

In order to explore the role of extended conjugation and alkyl chain variation on solution state photophysical properties of newly synthesized anthracene-cyanostyrene derivatives **CS-4.1** and **CS-4.2**, we investigated the photophysical properties of these compounds from their dilute solutions in THF (1 μM) (Figure 4.15). The UV-visible absorption spectra of compounds **CS-4.2a** and **CS-4.2b** showed comparable absorption spectra with maxima centered at 396 nm with shoulder bands centered on 378 nm and 342 nm, respectively. The compounds **CS-4.1a** and **CS-4.1b** also exhibited similar absorption spectra with maxima centered on 409 nm (see Table 4.1). The emission spectra were recorded from respective THF solution at room temperature and upon 370 nm excitation, **CS-4.1a** and **CS-4.1b** exhibited emission bands at 415, 431 and a major charge transfer (CT) band at 545 nm. In homologues **CS-4.2**, the emission spectra showed a single band at 485 nm with high quantum yield values (Φ_F) of 0.87 and 0.82, respectively. Conversely, compound **CS-4.1** showed moderate Φ_F of around 0.05. This enhancement in Φ_F and life-time values (Table 4.1) is ascribed to the incorporation of the spacer group phenyl ring, which facilitates enhanced ICT compared to **CS-4.1a** and **CS-4.1b**.

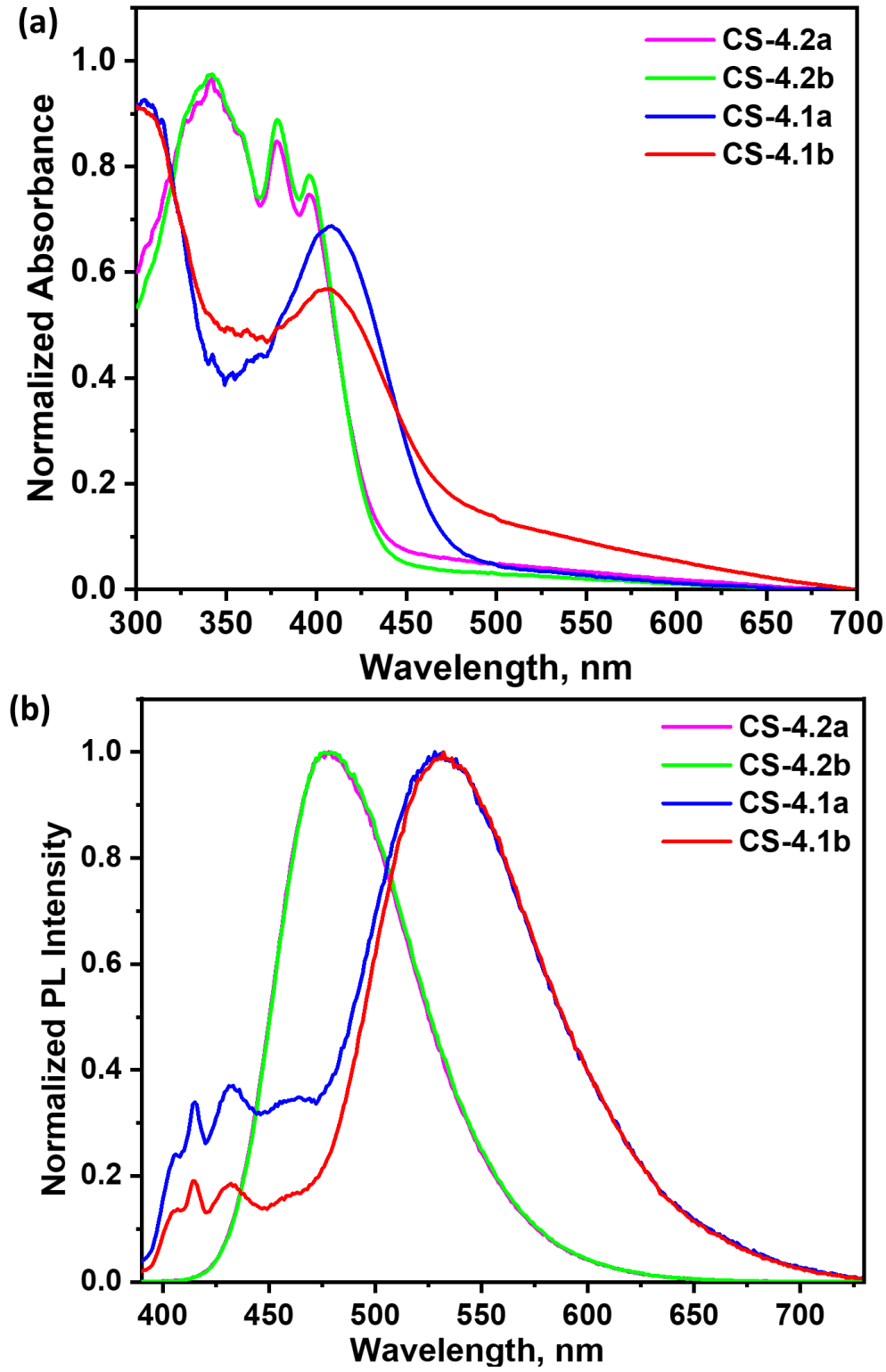

Figure 4.15 Normalized (a) UV-visible absorption and (b) emission spectra of the compounds **CS-4.1a–CS-4.2b** recorded from THF solutions (1μM), λ_{ex}= 370 nm.

Table 4.1 Absorption maximum, photoluminescence maximum, and fluorescence quantum yield of the compounds recorded in THF solvent.

Compounds	λ_{abs} (nm)	λ_{em} (nm)	τ (ns)	Φ_F
CS-4.1a	408	545	1.22	0.05
CS-4.1b	409	553	0.75	0.06
CS-4.2a	342, 379, 397	485	2.72	0.87
CS-4.2b	343, 378, 398	485	2.68	0.82

4.5.2 Solvatochromism

To examine how D-π-A features and solvent polarity influence on photoluminescence, we recorded the emission spectra of compounds **CS-4.1** and **CS-4.2** in solvents ranging from hexane to DMF. Figure 4.16 a and b show the photoluminescence spectra recorded for the compounds **CS-4.1a** and **CS-4.1b** in solvents with varying polarity from hexane to DMF. The photoluminescence spectra of these compounds in all the solvents showed three distinct emission bands. Irrespective of the nature of solvents, the high-energy bands in all the spectra were located at 415, and 431 nm, where these bands are assigned to the emission from the local excited state (LE). Conversely, the band corresponds to CT state showed a blue shift (584 nm to 524 nm) on increasing solvent polarity from hexane to DMF. The observed negative solvatochromic shift in **CS-4.1** implies that the dipole moment in the excited state is lower compared to the corresponding ground state. In contrast, the emission spectra recorded for the compound **CS-4.2** (see Figure 4.16c and d) for solvents of varying polarity showed a single band corresponding to ICT. The single emission band ranging from 460 nm (in hexane) to 535 nm (in DMF), along with reduced intensity on increasing solvent polarity, clearly indicates that the emissions are exclusively from the CT state. Further, we compared the solvent dependent intensity variation in both the series of compounds by taking **CS-4.1b** and **CS-4.2b** as representatives (see Figure 4.17). Despite the contrasting solvatochromic photoluminescence behaviour, the spectra of the compounds showed a gradual decrease in the emission intensity in response to increased solvent polarity attributed to the stabilization of the CT state. A detailed comparison of quantum yield in these molecules showed significant differences among the series.

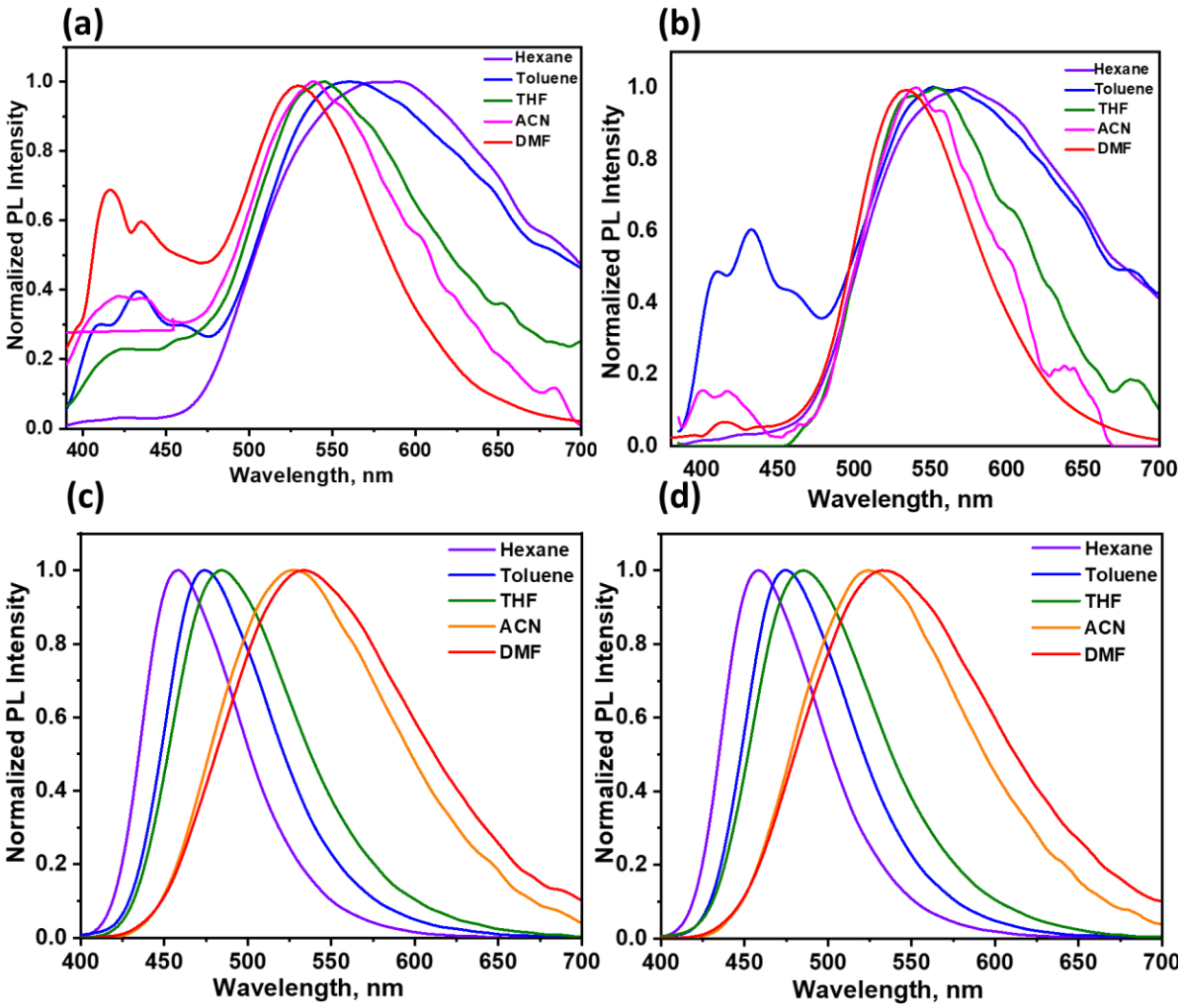

Figure 4.16 Normalized emission spectra of (a) **CS-4.1a**, (b) **CS-4.1b**, (c) **CS-4.2a**, and (d) **CS-4.2b** in solvents with different polarities.

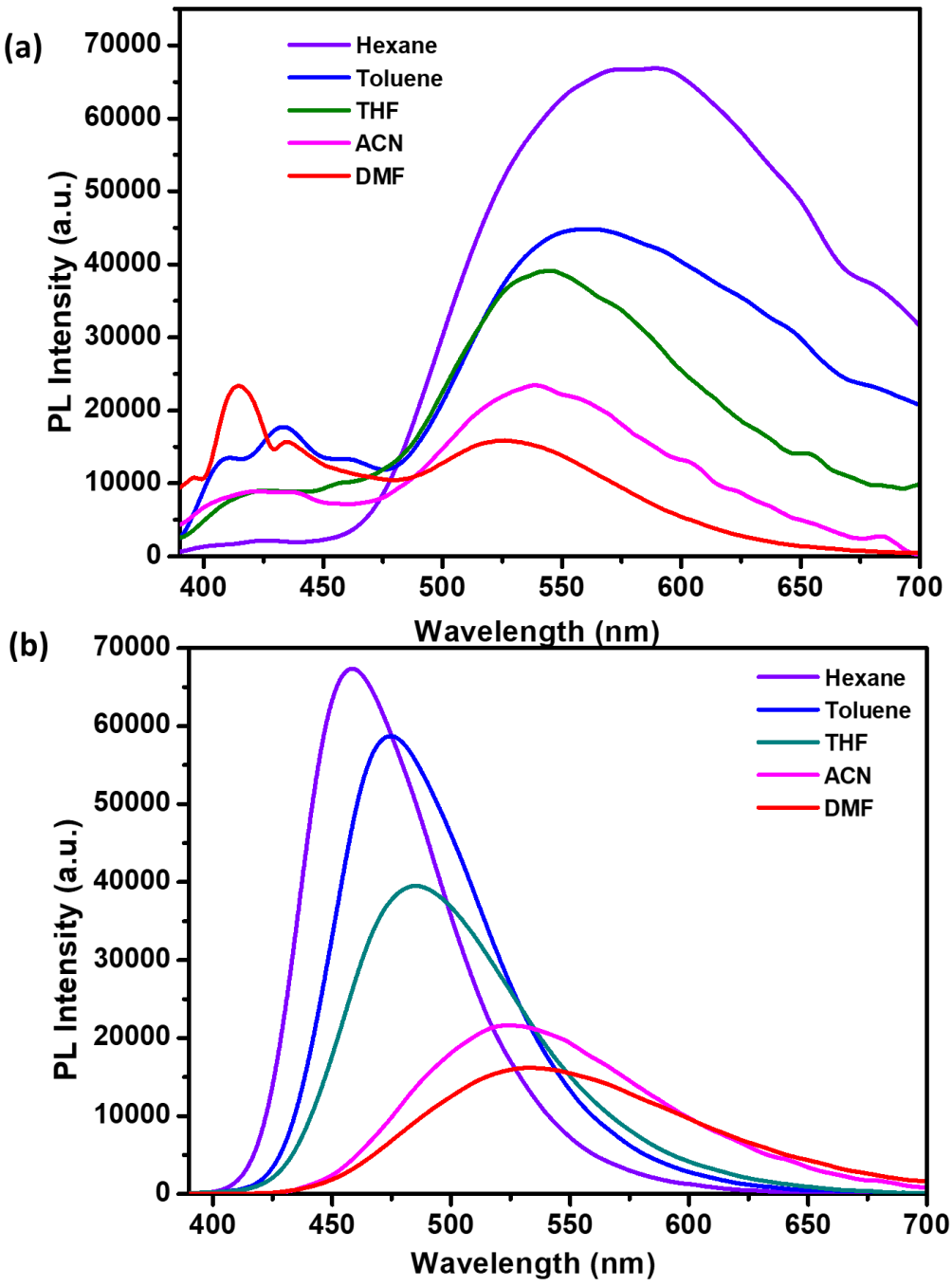

Figure 4.17 Emission spectra of (a) **CS-4.1b** and (b) **CS-4.2b** in solvents with different polarities.

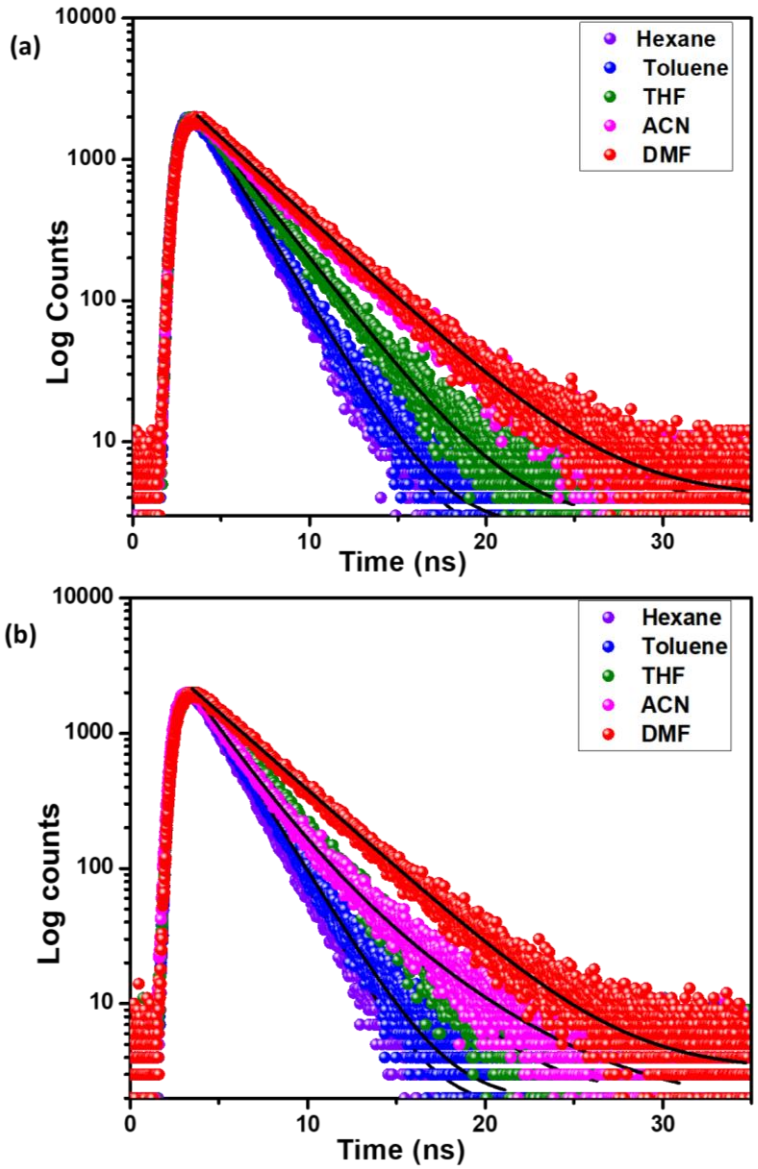

Figure 4.18 Time-resolved fluorescent decay curves of (a) **CS-4.2a** and (b) **CS-4.2b** in different solvents.

Interestingly, the compound **CS-4.2** showed approximately 3 to 10 times enhancement in the quantum yield in different solvents in comparison to compound **CS-4.1** (see Table 4.2). The molecules **CS-4.1a** and **CS-4.1b** showed reasonable quantum yield in nonpolar solvents hexane (0.24 and 0.25) and toluene (0.17 and 0.18), respectively, while in polar solvents the compounds showed negligible quantum yield values indicating the stabilization of CT states. The quantum yield enhancement in molecules **CS-4.2a** and **CS-4.2b** in comparison to molecule **CS-4.1a** and **CS-4.1b** indicates the influence of ICT in determining the photoluminescence of these molecules.

The compounds **CS-4.1a** and **CS-4.1b** in polar solvents like acetonitrile and DMF showed poor emission and therefore the lifetime was not recorded with reliability. It is noteworthy that the molecules **CS-4.1a** and **CS-4.1b** showed a decrease in lifetime and quantum yield on increasing the solvent polarity, while molecules **CS-4.2a** and **CS-4.2b** showed constant increase in lifetime (see Figure 4.18) moving from nonpolar to polar solvents (see Table 4.2). In general, the radiative decay constants for all the compounds showed a diminishing trend on increasing the solvent polarity indicating the stabilization of CT states in polar solvents.

Table 4.2 Photophysical parameters of compounds **CS-4.1** and **CS-4.2** in different solvents of varying polarity.

Compound	Solvent	λ_{abs} (nm)	λ_{em} (nm)	τ (ns)	Φ_F	k_r	k_{nr}
CS-4.1a	Hexane	407	584	2.57	0.24	0.09	0.296
	Toluene	408	560	1.53	0.17	0.11	0.542
	THF	408	545	1.22	0.05	0.04	0.779
	Acetonitrile	406	539	-	0.01	-	-
	DMF	410	524	-	0.05	-	-
CS-4.1b	Hexane	407	572	1.90	0.25	0.13	0.395
	Toluene	410	564	1.60	0.18	0.11	0.513
	THF	408	553	0.75	0.06	0.08	1.253
	Acetonitrile	406	541	-	0.01	-	-
	DMF	411	535	-	0.05	-	-
CS-4.2a	Hexane	376, 395	458	1.99	0.80	0.40	0.100
	Toluene	379, 400	474	2.14	0.79	0.37	0.098
	THF	379, 397	485	2.72	0.87	0.32	0.048
	Acetonitrile	378, 396	525	3.70	0.80	0.22	0.054
	DMF	380, 400	533	3.78	0.77	0.20	0.061
CS-4.2b	Hexane	375, 395	460	1.97	0.75	0.38	0.127
	Toluene	377, 397	475	2.09	0.80	0.38	0.096
	THF	378, 398	485	2.68	0.82	0.31	0.067
	Acetonitrile	378, 397	523	2.83	0.81	0.29	0.067
	DMF	380, 400	535	3.74	0.78	0.21	0.059

4.5.3 Solid state photoluminescence

Following the distinct solution state properties of the newly synthesized compounds, the investigation focused on evaluating the solid-state luminescent behaviour by analysing their photoluminescence spectra recorded from crystalline samples. The combined spectra are presented in Figure 4.19 with corresponding photoluminescence data summarized in Table 4.2. The photoluminescence spectra of both compounds **CS-4.1** and **CS-4.2** showed significant difference in the photoluminescence maxima in response to the molecular packing and difference in conjugation. Despite of the presence of phenyl π-spacer in **CS-4.2a** and **CS-4.2b**, the molecules **CS-4.1a** and **CS-4.1b** showed maximum red shifted emission from their crystalline samples. The red-shifted emission in **CS-4.1a** and **CS-4.1b** can be due to the molecular aggregation in the solid state.[42]

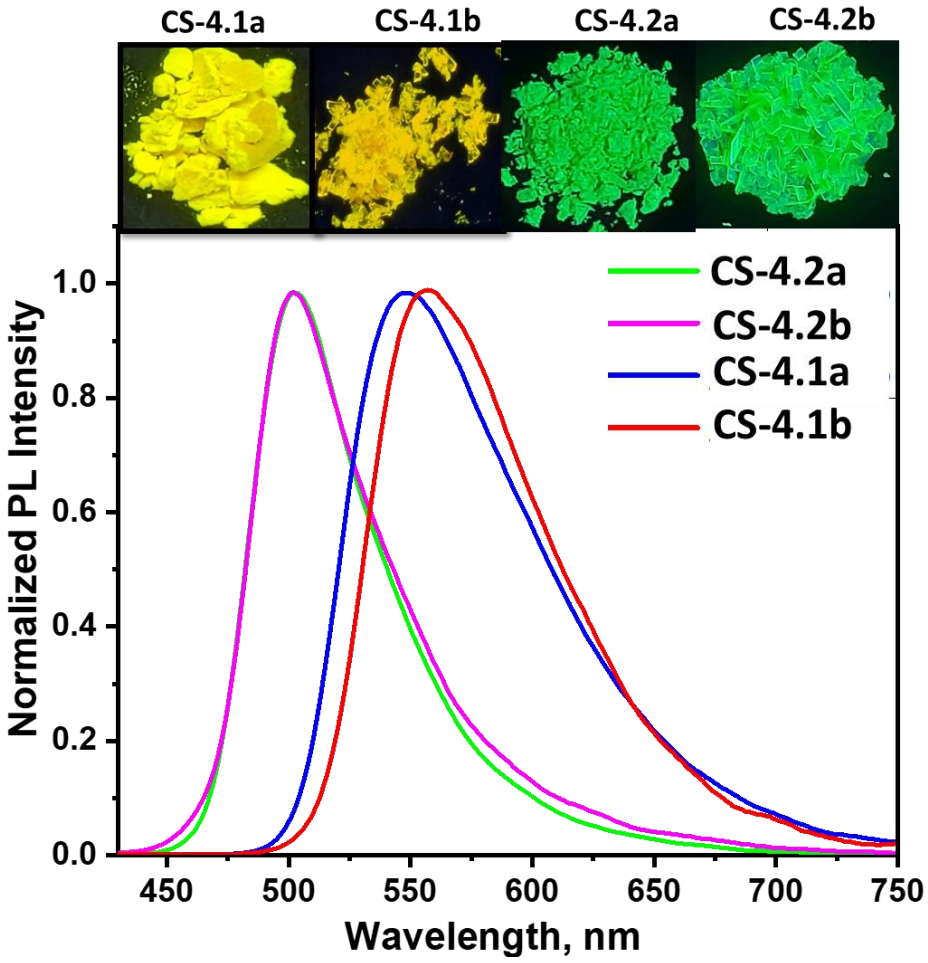

Figure 4.19 Normalized Solid-state emission spectra of compounds (**CS-4.1a**, **CS-4.1b**, **CS-4.2a,** and **CS-4.2b**), (λ_{ex} = 370 nm).

A detailed analysis using single-crystal X-ray diffraction studies revealed the molecular arrangements in the crystals of compounds **CS-4.1b** and **CS-4.2b** (see Table 4.3 and Figure 4.20). Both **CS-4.1b** and **CS-4.2b** showed different levels of twist in the molecular geometry with twist angles of 81 ° and 69 °, respectively. As seen in Figure 4.21 molecule **CS-4.1b** showed C-H…N and C-H…O interaction (H…N, 2.549 Å and H…O, 2.472 Å) and π…π stacking interaction involving the edges of the anthracene with a distance of 3.686 Å. The intermolecular interactions in **CS-4.2b** includes a C-H…π (2.873 Å) interaction along with π…π (3.593 Å) stacking involving the terminal phenyl rings. In comparison, molecule **CS-4.1b** showed a slipped molecular arrangement comprising a J-aggregate along the molecular long axis, while molecule **CS-4.2b** resulted in a pair of aggregates slipped along the molecular short axis (Figure 4.20). The molecule **CS-4.2b** with strong non-cofacial π-π stacking gives rise to strong orbital overlap between the aromatic rings, leading to red shifted emission compared to the spectra recorded from THF solution. The red-shifted absorption in the solid state compared to solutions confirms J-aggregate formation (Figure 4.22).

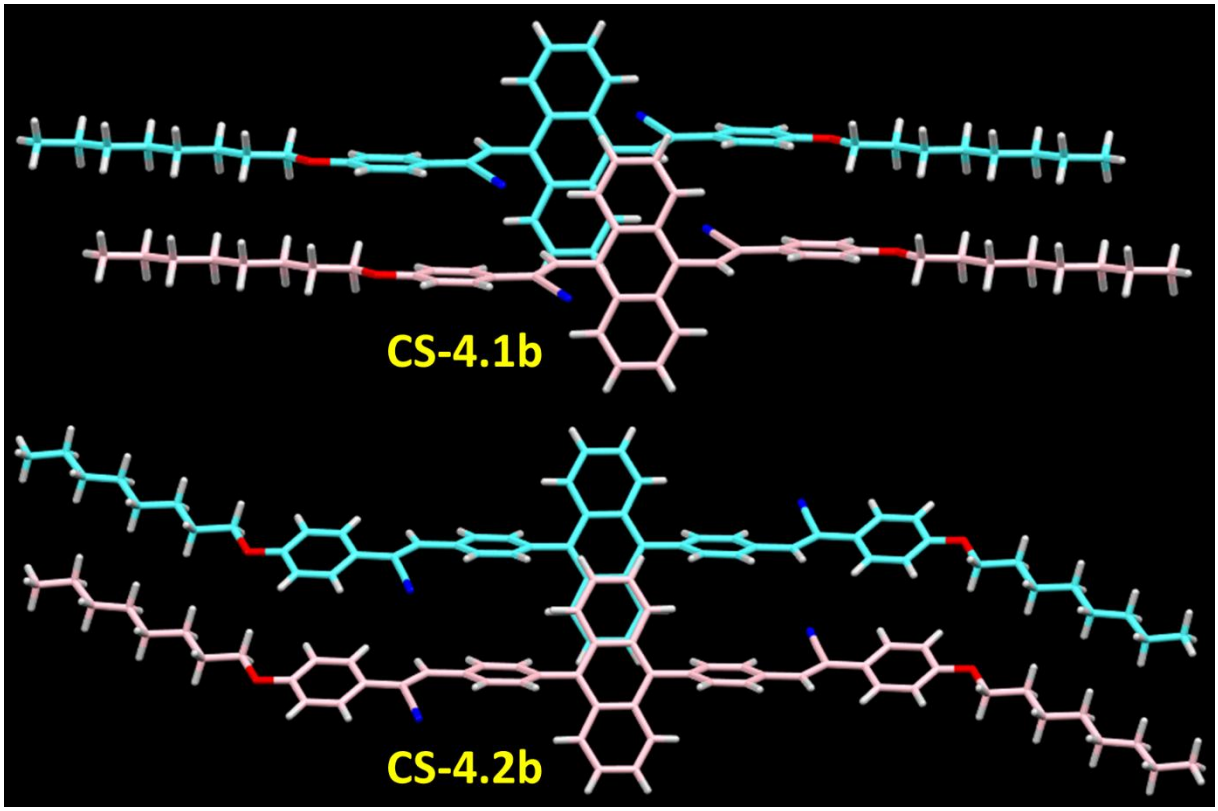

Figure 4.20 Depiction of the π-interaction in crystal structure of **CS-4.1b** and **CS-4.2b**.

Table 4.3 Summary of the crystal data structure and structure refinement for **CS-4.1b and CS-4.2b**.

Compound	CS-4.1b	CS-4.2b
Molecular formula	C_{48} H_{52} N_2O_2	C_{60} $H_{60}N_2O_2$
Formula weight	688.91	841.10
Cell setting	Triclinic	Triclinic
Space group	P -1	P -1
A (Å)	6.1036(3)	6.388(2)
B (Å)	8.6157(5)	7.282(2)
C (Å)	18.5115(10)	26.451(9)
α (°)	80.960(2)	91.253(8)
β (°)	81.390(2)	95.768(8)
γ (°)	85.005(2)	96.982(8)
Cell volume (Å^3)	948.52(9)	1214.4(7)
Z	1	1
F	370	450
ρ (Mg/m^3)	1.206	1.150
Crystal size (mm^3)	0.275 x 0.145 x 0.083	0.110 x 0.095 x 0.040
Data collection temperature	100(2) K	296(2) K
Index ranges	-7<=h<=7 -10<=k<=10 -22<=l<=22	-7<=h<=7 -8<=k<=8 -31<=l<=31
Reflections collected	32707	25783
Number of independent Reflections	3738 [R(int) = 0.0572]	4286 [R(int) = 0.0858]
R_1	0.0526	0.1245
wR_2 (all)	0.1321	0.1679
S	1.053	1.016
No. parameters refined	235	318
Max. eÅ^{-3}	0.322	0.169
CCDC Number	2417412	2417413

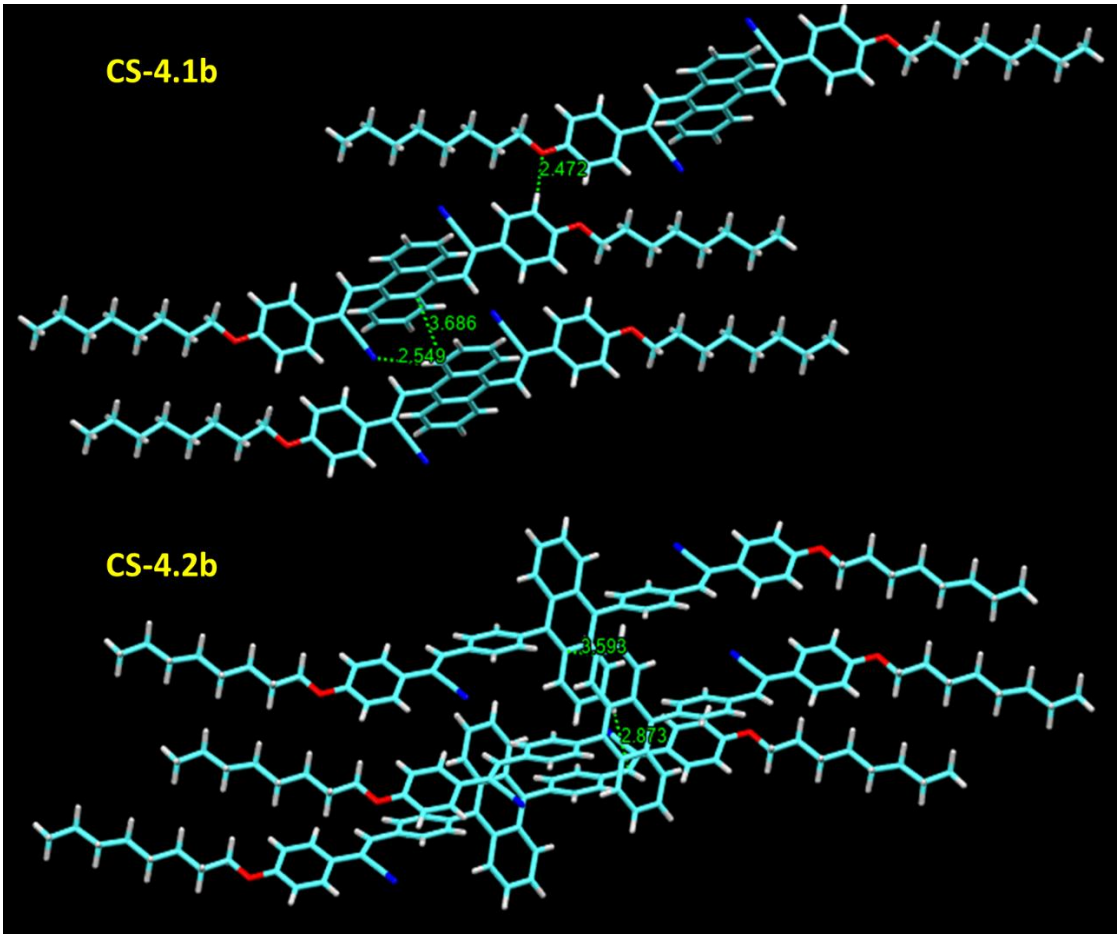

Figure 4.21 C-H…N and C-H…O interaction as well as π…π stacking interaction involving the edges of the anthracene in compounds **CS-4.1b** and **CS-4.2b**.

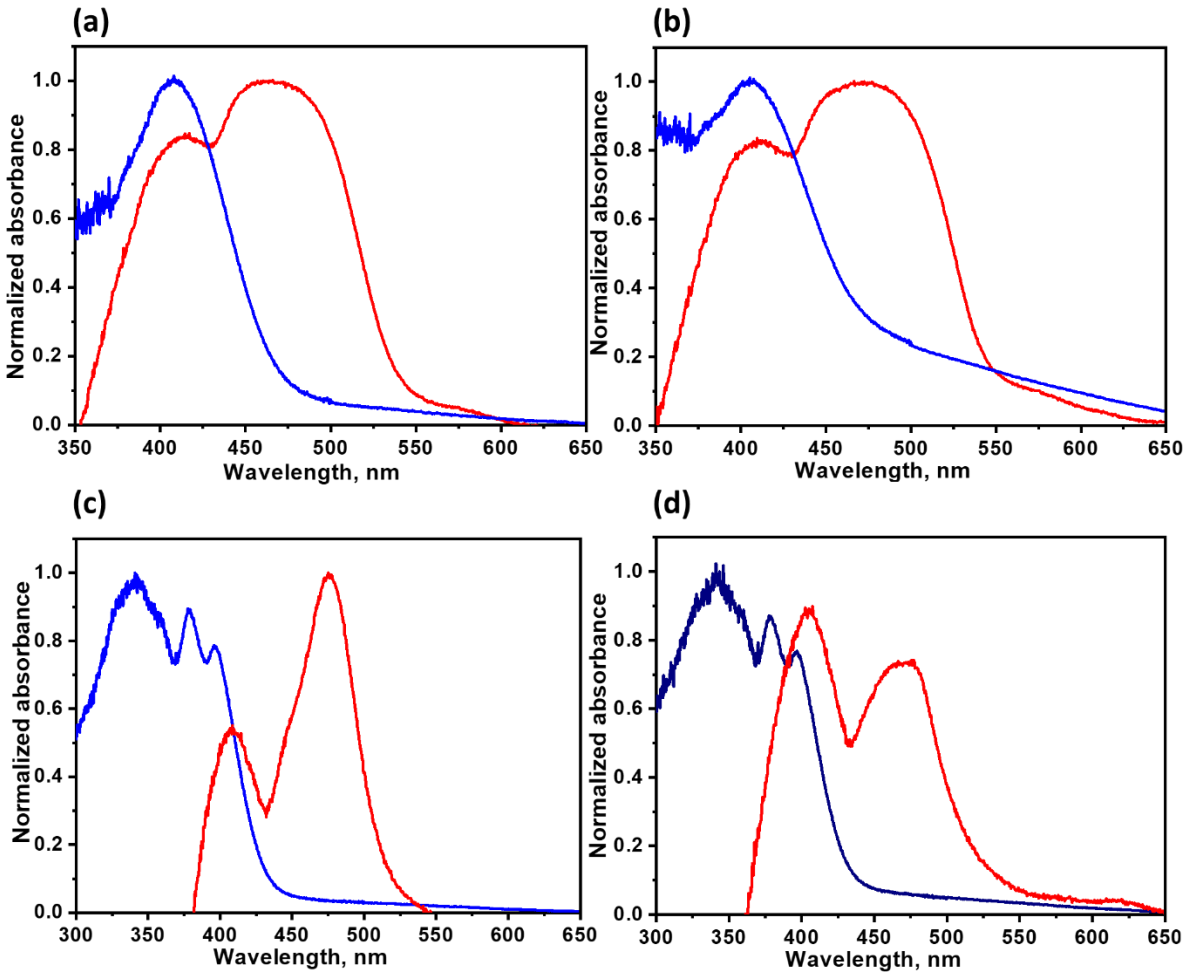

Figure 4.22 UV-visible absorption spectra of all the compounds (a) **CS-4.1a** (b) **CS-4.1b** (c) **CS-4.2a** and (d) **CS-4.2b** were recorded from THF solution (blue curve) (concentration: 1μM) and pristine solid sample (red curve).

4.5.4 Aggregation induced emission (AIE)

The study further explored the aggregation-induced emission (AIE) in both the class of compounds, taking **CS-4.1b** and **CS-4.2b** as representative molecules. The aggregation properties of the compounds were investigated by comparing the emission spectra recorded from respective THF solutions containing different water fractions. Figure 4.23a shows the emission spectra recorded for **CS-4.1b** from the THF-water mixtures. Up to 40 % of water fraction, the compound **CS-4.1b** showed a sharp decrease in spectral intensity of the CT band. The decreased emission intensity along with blue shift on increasing the water fraction can be attributed to the stabilization of the HOMO on increasing the polarity. Increasing the water fraction above 40 % showed an increase in emission intensity with a slight blue shift compared to the emission spectrum recorded

from THF solution, where this is clear evidence of aggregation-induced emission enhancement (AIEE) in compound **CS-4.1b** (see Figure 4.23b).

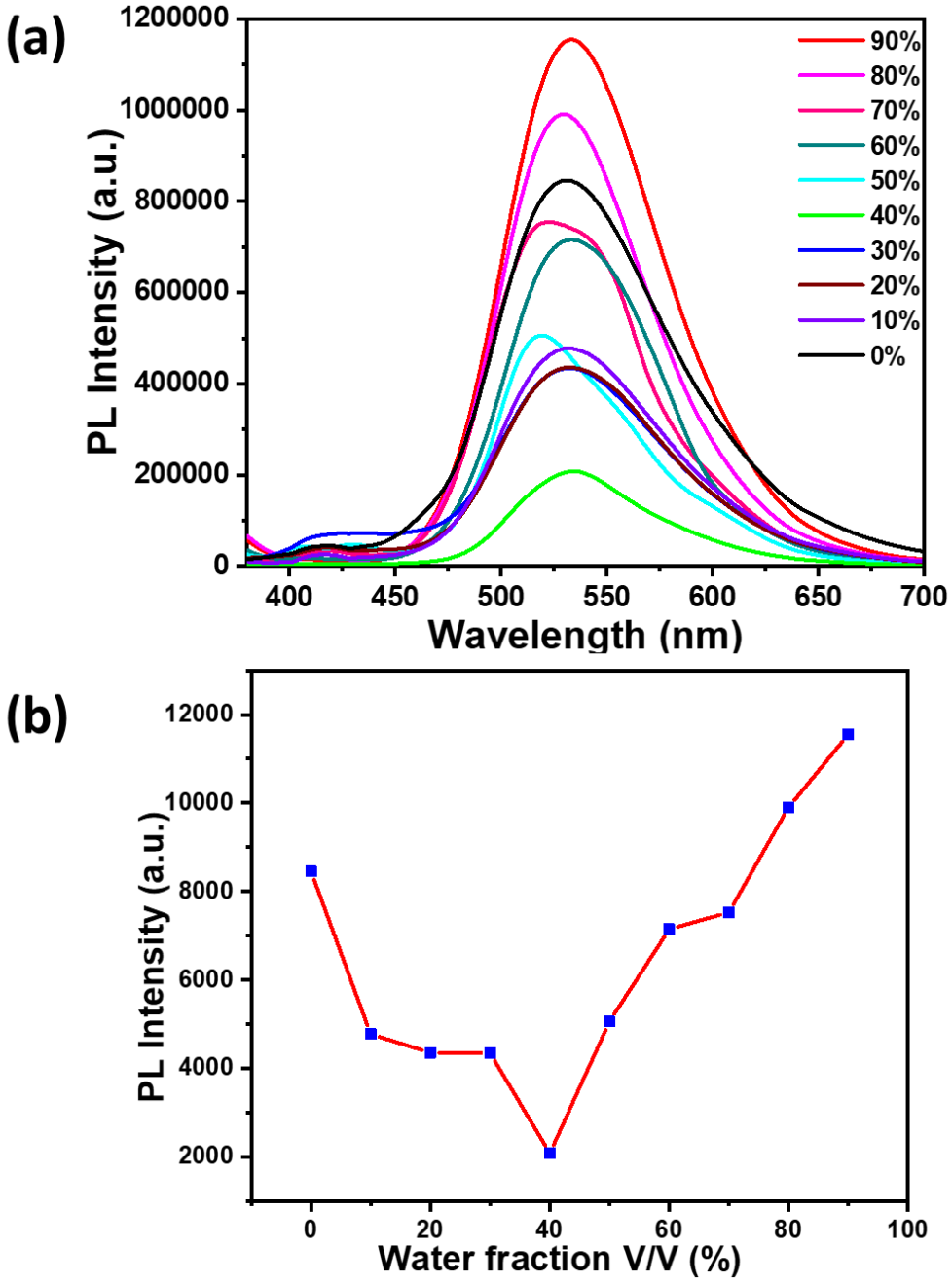

Figure 4.23 Fluorescence emission spectra of the compounds (a) **CS-4.1b** recorded by varying the water fraction in the THF-water mixtures with increase in concentration of water from 0 to 90%, (b) changes in the fluorescence intensity in response to the difference in the water fraction in the THF−water mixtures (λ_{ex} = 370 nm).

The compound **CS-4.2b** on increasing water fraction showed a gradual decrease in emission intensity with red shift as represented in solvent-dependent studies. A further increase of water fraction above 60 % resulted in blue-shifted emission with enhanced emission intensity (see Figure 4.24a and b), where this observation can be ascribed to aggregation induced emission (AIE) in these molecules.

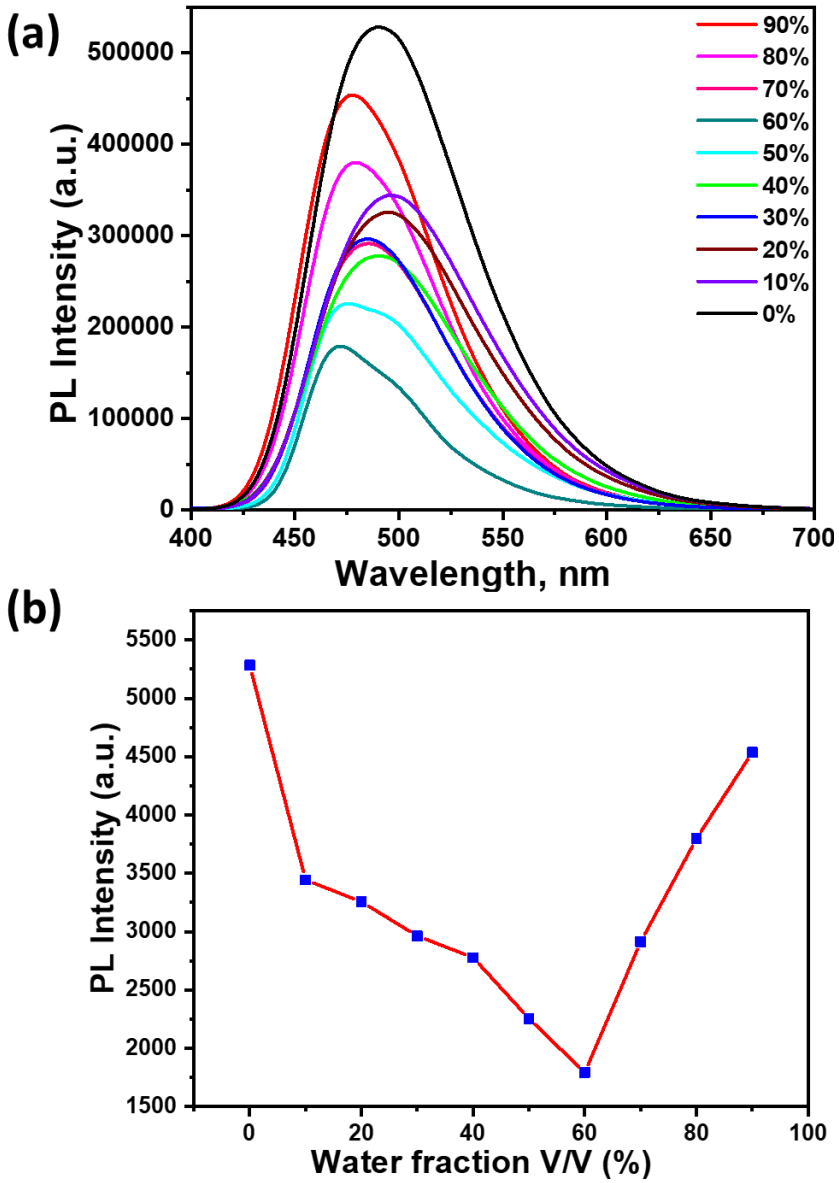

Figure 4.24 Fluorescence emission spectra of the compounds (a) **CS-4.2b** recorded by varying the water fraction in the THF-water mixtures with increase in concentration of water from 0 to 90%, (b) changes in the fluorescence intensity in response to the difference in the water fraction in the THF−water mixtures (λ_{ex} = 370 nm).

4.5.5 Stimuli responsive emission

The newly synthesized compounds were explored for multi-stimuli responsive photoluminescence properties. All the compounds showed mechanofluorochromism (MFC) in response to applied stress. To test the possible mechanofluorochromic properties of **CS-4.1a** and **CS-4.1b**, the solid-state photoluminescence changes of the compounds were examined before and after grinding. The emission spectrum of **CS-4.1a** exhibited a red shifted emission ($\Delta\lambda_{em}$ = 20 nm) along with an emission colour change of yellow to orange indicating an obvious MFC (see Figure 4.25a). A subsequent fuming of the grind sample with dichloromethane vapours converted the ground sample from orange to yellow emission (see Figure 4.25b). In contrast, the MFC studies of compounds **CS-4.2a** and **CS-4.2b** showed blue-shifted emission ($\Delta\lambda_{em}$ = 12 nm) compared to pristine samples accompanied by a change in emission colour from green to cyan. The ground samples on fuming with ethyl acetate vapours resulted in recovery of emission analogous to the emission of pristine sample (Figure 4.25c and d).

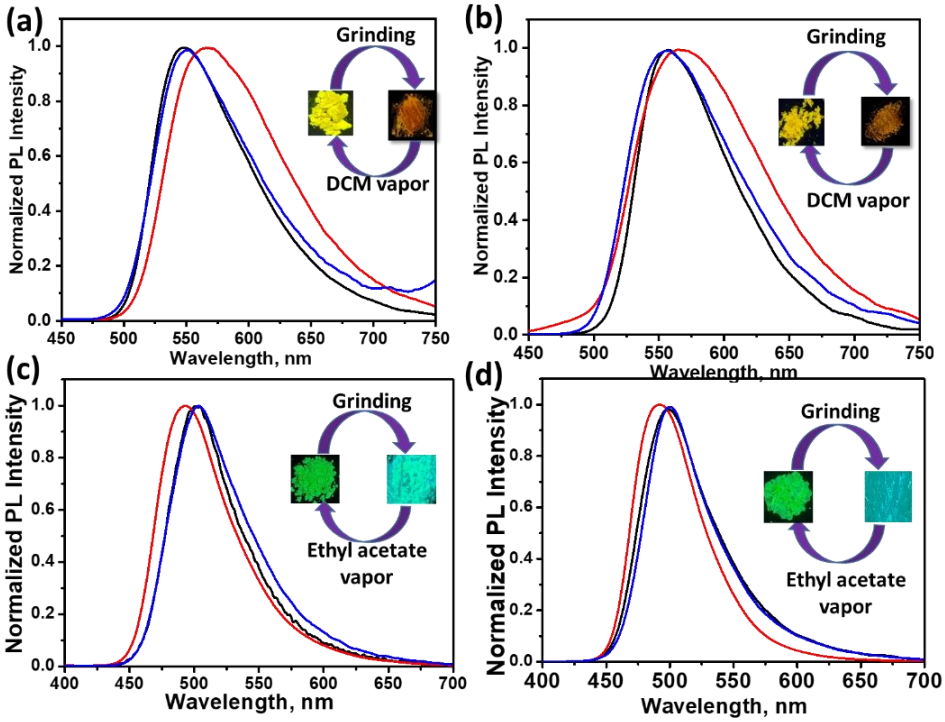

Figure 4.25 Mechanochromic fluorescence spectra of (a) **CS-4.1a**, (b) **CS-4.1b**, (c) **CS-4.2a** and (d) **CS-4.2b** (λ_{ex}= 370 nm), pristine sample (black curve), ground sample (red curve), and fumed with solvent vapours (blue curve). Images taken under a UV lamp at 365 nm are shown in the inset.

In order to explore the structural origin of stimuli-responsive emission of all the compounds, the powder X-ray diffraction studies were carried out on different phases. Figure 4.26a and b shows the powder X-ray diffractograms recorded from different phases of **CS-4.1a** and **CS-4.1b**. The pristine sample of both the compounds were crystalline in nature as indicated by the sharp peaks in the diffractogram. The compounds on grinding resulted in crystal to amorphous transition as represented by broad featureless diffractograms in Figure 4.26a and b. The diffractogram recorded from the DCM fumed sample in both cases showed peaks corresponding to solvent-induced crystallisation similar to pristine sample. Similarly, the diffractograms of **CS-4.2a** and **CS-4.2b** also indicate the crystalline nature of their pristine samples. The ground samples showed the formation of amorphous phase under applied stress. Interestingly, the ground samples on fuming with ethyl acetate showed recovery of the pristine phase as indicated by the sharp peaks resembling that of pristine samples. The study demonstrates the distinct multiple stimuli-responsive nature two series of compounds, especially with sensitivity towards vapours of dichloromethane and ethyl acetate.

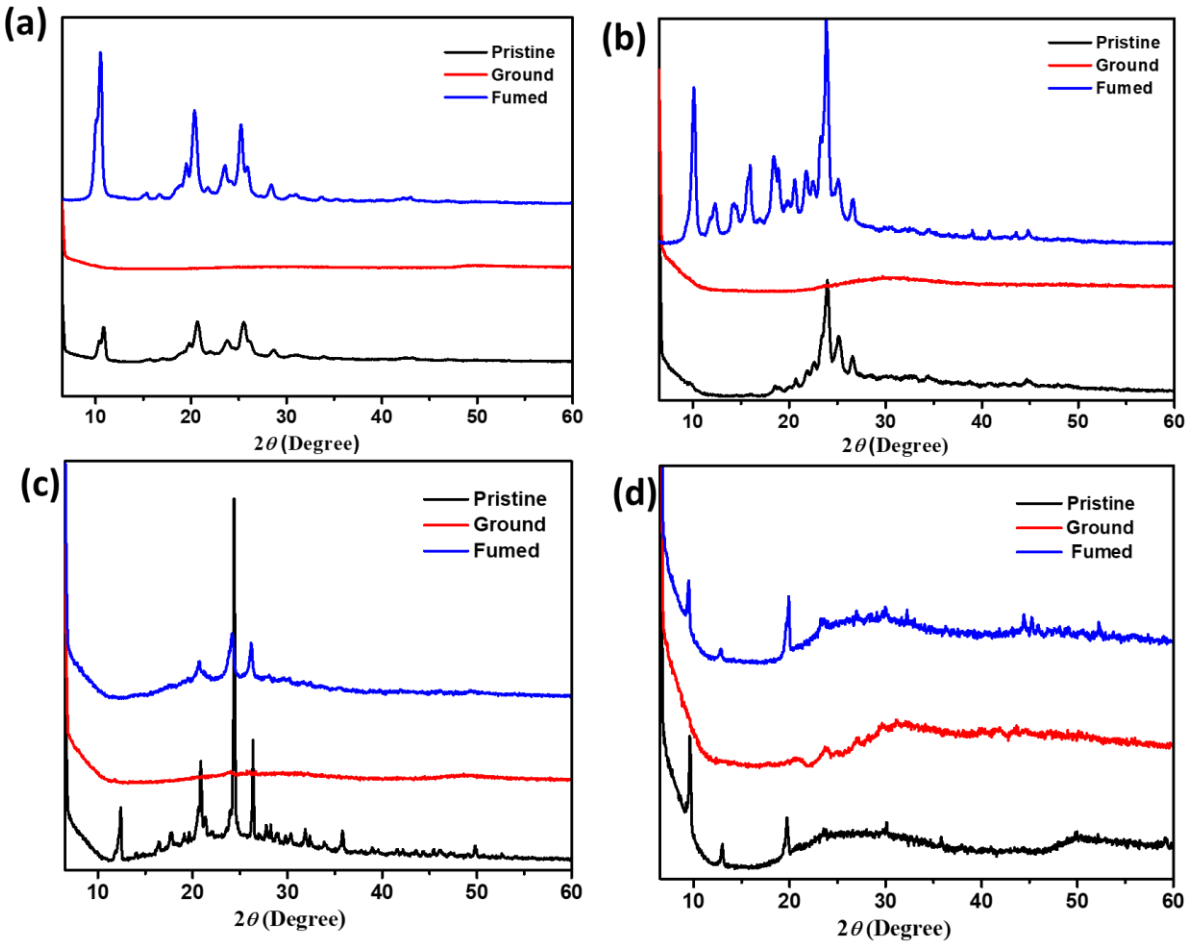

Figure 4.26 PXRD patterns of compounds (a) **CS-4.1a** (b) **CS-4.1b** (c) **CS-4.2a** (d) **CS-4.2b.**

The contrasting stimuli responsive behaviour of compounds **CS-4.1** and **CS-4.2** are further evidenced by their distinct photophysical properties. Table 4.4 shows the quantum yield, fluorescence lifetime (see Figure 4.27) and corresponding radiative and nonradiative decay constants for the different phases of each compound. From the tabulated data, it is evident that on grinding the photoluminescence lifetime and quantum yield decrease as a result of the introduction of new decay pathways. In all the pristine samples, the nonradiative decay is prominent as indicated by nonradiative decay constants (k_{nr}). On applying mechanical stress, the radiative decay constants for compounds **CS-4.1a** and **CS-4.1b** showed a substantial decrease may be due to a more disordered arrangement of molecules in the amorphous state. In contrast, the pristine and ground phases of **CS-4.2a** and **CS-4.2b** showed comparable radiative and nonradiative decay constants indicating the similar molecular arrangement in the pristine and ground phases.

Table 4.4 Fluorescence wavelength maximum, fluorescence quantum yield and average lifetime of **CS-4.1a−CS-4.2b** emitting states. Radiative and non-radiative rates (k_r, k_{nr}) were calculated using equation $k_r = \phi_F/\tau_F$ and $\tau_F = (k_r + k_{nr})^{-1}$ respectively.

Compounds		**λ_{em} (nm)**	**ϕ_F**	**τ_F (ns)**	**k_r (ns^{-1})**	**k_{nr} (ns^{-1})**
CS-4.1a	Pristine	548	0.24	3.1	0.077	0.25
	Ground	568	0.13	3.9	0.033	0.22
CS-4.1b	Pristine	555	0.10	3.3	0.030	0.27
	Ground	568	0.07	3.7	0.019	0.25
CS-4.2a	Pristine	503	0.31	3.9	0.079	0.18
	Ground	492	0.26	3.0	0.087	0.25
CS-4.2b	Pristine	501	0.36	4.2	0.085	0.15
	Ground	490	0.31	3.7	0.087	0.19

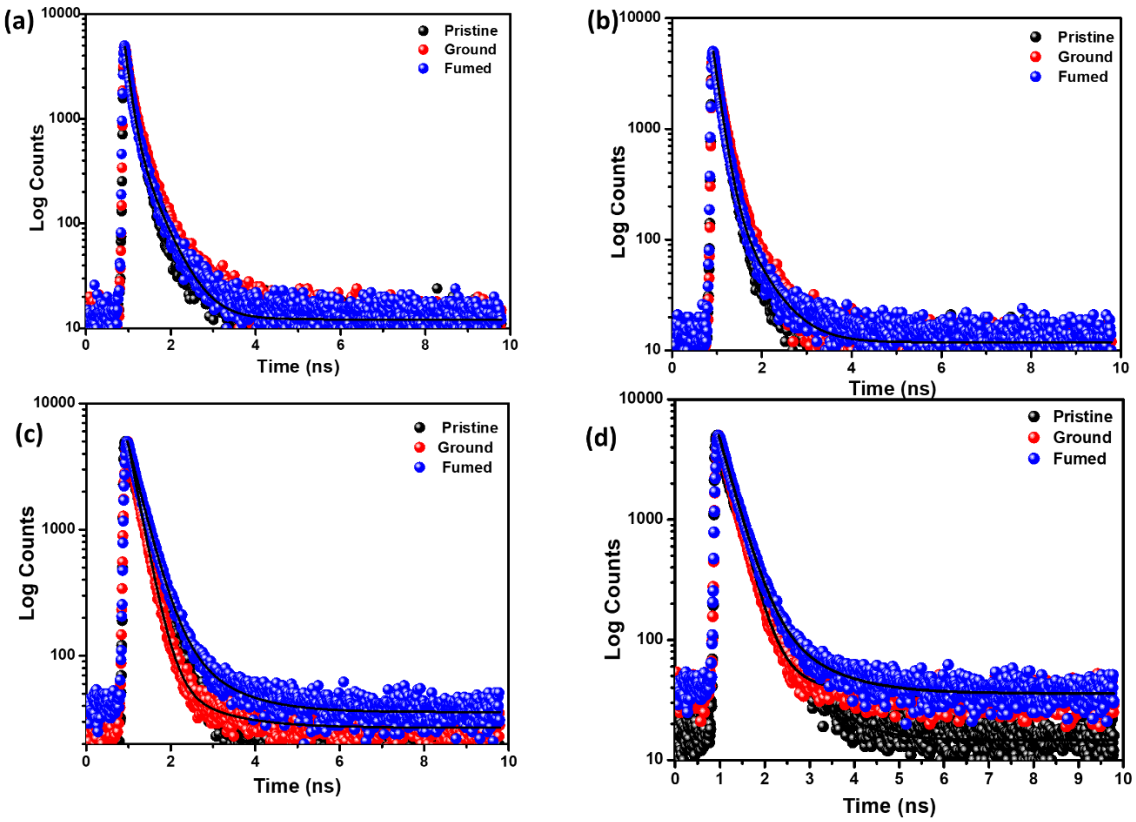

Figure 4.27 Time-resolved fluorescent decay curves of (a) **CS-4.1a** and (b) **CS-4.1b** (c) **CS-4.2a** (d) **CS-4.2b** in different phases.

4.6 Conclusion

In summary, this chapter demonstrates the markedly distinct photophysical properties of anthracene–cyanostilbene derivatives, strongly affected by the nature of the π-spacer. The newly synthesized compounds, **CS-4.1** (lacking a phenyl spacer) and **CS-4.2** (containing a phenyl spacer), showed pronounced differences in their fluorescence emission, lifetime, quantum yield, and external stimuli response. Notably, variation in alkyl chain length exerted minimal influence on the photophysical properties, underscoring the dominant effect of π-conjugation tuning via spacer modification. Crystallographic analysis revealed distinct molecular packing and intermolecular interactions that correlate with their emissive characteristics, while theoretical calculations provided insight into the electronic structures and excited-state dynamics. DFT/TD-DFT calculations were employed to investigate the electronic structures and conformational landscapes of compounds **CS-4.1** and **CS-4.2** in their S_0 and S_1 states. The remarkable

photoluminescence properties of these compounds offer promising opportunities for further investigation towards sensing and optoelectronic applications.

4.7 References

(1) Ostroverkhova, O. Organic Optoelectronic Materials: Mechanisms and Applications. *Chem. Rev.* **2016**, *116* (22), 13279–13412.

(2) Grimsdale, A. C.; Leok Chan, K.; Martin, R. E.; Jokisz, P. G.; Holmes, A. B. Synthesis of Light-Emitting Conjugated Polymers for Applications in Electroluminescent Devices. *Chem. Rev.* **2009**, *109* (3), 897–1091.

(3) Pope, M.; Swenberg, C. E. Electronic Processes in Organic Crystals and Polymers. Oxford University Press December 2, **1999**.

(4) An, B.-K.; Gierschner, J.; Park, S. Y. π-Conjugated Cyanostilbene Derivatives: A Unique Self-Assembly Motif for Molecular Nanostructures with Enhanced Emission and Transport. *Acc. Chem. Res.* **2012**, *45*, 544.

(5) Chen, X.; Tan, D.; Yang, D.-T. Multiple-Boron–Nitrogen (Multi-BN) Doped π-Conjugated Systems for Optoelectronics. *J. Mater. Chem. C* **2022**, *10* (37), 13499–13532.

(6) Femina, C.; Yamagami, T.; Yamamoto, N.; Thomas, R.; Sajith, P. K. Theoretical Insights into Aggregation-Induced Emission of Bis(Cyanostyryl)Pyrrole Derivatives. *Phys. Chem. Chem. Phys.* **2025**,*27,* 8478-8487.

(7) Qin, W.; Yang, Z.; Jiang, Y.; Lam, J. W. Y.; Liang, G.; Kwok, H. S.; Tang, B. Z. Construction of Efficient Deep Blue Aggregation-Induced Emission Luminogen from Triphenylethene for Nondoped Organic Light-Emitting Diodes. *Chem. Mater.* **2015**, *27* (11), 3892–3901.

(8) Chen, S.-Y.; Chiu, Y.-W.; Liou, G.-S. Substituent Effects of AIE-Active α-Cyanostilbene-Containing Triphenylamine Derivatives on Electrofluorochromic Behavior. *Nanoscale* **2019**, *11* (17), 8597–8603.

(9) Sagara, Y.; Karman, M.; Verde-Sesto, E.; Matsuo, K.; Kim, Y.; Tamaoki, N.; Weder, C. Rotaxanes as Mechanochromic Fluorescent Force Transducers in Polymers. *J. Am. Chem. Soc.* **2018**, *140* (5), 1584–1587.

(10) Wang, Y.; Tan, X.; Zhang, Y.-M.; Zhu, S.; Zhang, I.; Yu, B.; Wang, K.; Yang, B.; Li, M.; Zou, B.; Zhang, S. X.-A. Dynamic Behavior of Molecular Switches in Crystal under Pressure and Its Reflection on Tactile Sensing. *J. Am. Chem. Soc.* **2015**, *137* (2), 931–939.

(11) Femina, C.; Sajith, P. K.; Remya, K.; Thomas, R.; Solomon, R. V. Theoretical Insights into the Structural and Optical Properties of D−π–A-Based Cyanostilbene Systems of α and β Variants. *ACS Omega* **2024**, *9* (21), 22764–22776.

(12) Gouthaman, S.; Jayaraj, A.; Sugunalakshmi, M.; Sivaraman, G.; P, C. A. S. Supramolecular Self-Assembly Mediated Aggregation-Induced Emission of Fluorene-Derived Cyanostilbenes: Multifunctional Probes for Live Cell-Imaging. *J. Mater. Chem. B* **2022**, *10* (13), 2238–2250.

(13) Huang, G.; Chang, X.; Jiang, Y.; Lin, B.; Li, B. S.; Tang, B. Z. Multi-Stimuli Responsive

Cyanostilbene Derivatives: PH, Amine Vapor Sensing and Mechanoluminescence. *Mater. Chem. Front.* **2020**, *4* (6), 1720–1728.

(14) Zhang, Y.; Li, H.; Zhang, G.; Xu, X.; Kong, L.; Tao, X.; Tian, Y.; Yang, J. Aggregation-Induced Emission Enhancement and Mechanofluorochromic Properties of α-Cyanostilbene Functionalized Tetraphenyl Imidazole Derivatives. *J. Mater. Chem. C* **2016**, *4* (14), 2971–2978.

(15) Wang, B.; Wei, C. Stimuli-Responsive Fluorescence Switching of Cyanostilbene Derivatives: Ultrasensitive Water, Acidochromism and Mechanochromism. *RSC Adv.* **2018**, *8* (40), 22806–22812.

(16) Fan, G.; Yan, D. Positional Isomers of Cyanostilbene: Two-Component Molecular Assembly and Multiple-Stimuli Responsive Luminescence. *Sci. Rep.* **2014**, *4* (1), 4933.

(17) Wang, X.; Ding, Z.; Ma, Y.; Zhang, Y.; Shang, H.; Jiang, S. Multi-Stimuli Responsive Supramolecular Gels Based on a D–π–A Structural Cyanostilbene Derivative with Aggregation Induced Emission Properties. *Soft Matter* **2019**, *15* (7), 1658–1665.

(18) Dou, C.; Han, L.; Zhao, S.; Zhang, H.; Wang, Y. Multi-Stimuli-Responsive Fluorescence Switching of a Donor−Acceptor π-Conjugated Compound. *J. Phys. Chem. Lett.* **2011**, *2* (6), 666–670.

(19) Rana, S.; Vaidyanathan, S.; Patel, S. Aggregation Induced Emission (AIE) Based Donor–π–Acceptor Fluorophores: An Approach to Fabricate Acidochromic Sensors and White Light Emitting Diodes. *J. Mater. Chem. C* **2024**, *12* (35), 14148–14164.

(20) Qian, G.; Dai, B.; Luo, M.; Yu, D.; Zhan, J.; Zhang, Z.; Ma, D.; Wang, Z. Y. Band Gap Tunable, Donor−Acceptor−Donor Charge-Transfer Heteroquinoid-Based Chromophores: Near Infrared Photoluminescence and Electroluminescence. *Chem. Mater.* **2008**, *20* (19), 6208–6216.

(21) B. M., S.; Barkale, H. V; Devadiga, D.; Dey, N.; T. N., A. Donor-Acceptor-Based Conjugated Fluorescent Probes for Volatile Acid Detection. *ChemistrySelect* **2024**, *9* (31), e202401790.

(22) Zhao, J.; Yao, C.; Ali, M. U.; Miao, J.; Meng, H. Recent Advances in High-Performance Organic Solar Cells Enabled by Acceptor–Donor–Acceptor–Donor–Acceptor (A–DA′D–A) Type Acceptors. *Mater. Chem. Front.* **2020**, *4* (12), 3487–3504.

(23) Femina, C.; Shanthil, M.; Sajith, P. K.; Thomas, R. Anthracene-Incorporated Cyanostilbene Based Donor–Acceptor Systems: Intramolecular Charge Transfer and Aggregation Induced Emission. *New J. Chem.* **2023**, *47* (29), 13810–13819.

(24) Jiang, Z.; Zhao, H.; Wu, W.; Chen, K.; Yu, H.; Wang, T.; Huang, X.; Wang, N.; Zhou, L.; Hao, H. Multi-Stimuli Responsive Organic Polymorphic Crystals: Anisotropic Elasticity and Plasticity, Mechanochromism and Photomechanical Motions. *J. Mater. Chem. C* **2023**, *11* (13), 4375–4383.

(25) Huang, Z.; Tang, F.; He, F.; Kong, L.; Huang, J.; Yang, J.; Ding, A. Pyrene and Triphenylamine Substituted Cyanostyrene and Cyanostilbene Derivatives with Dual-State Emission for High-Contrast Mechanofluorochromism and Cell Imaging. *Org. Chem. Front.*

2022, *9* (19), 5118–5124.

(26) Athira, P.; Nelliyulla Kappumchalil, R.; Sachin, A. R.; Yoosuf, M.; Thomas, R.; Gopakumar, G. Intramolecular Charge Transfer and Stimuli-Responsive Emission in Cholesterol-Appended Phenothiazine–Cyanostyryl-Based Donor–Acceptor Systems. *J. Phys. Chem. A* **2024**, *128* (20), 3935–3946.

(27) Chen, S.-Y.; Pai, M.-H.; Liou, G.-S. Effects of Alkyl Chain Length and Anion on the Optical and Electrochemical Properties of AIE-Active α-Cyanostilbene-Containing Triphenylamine Derivatives. *J. Mater. Chem. C* **2020**, *8* (22), 7454–7462.

(28) Kumar, N.; Maity, D.; Som, S.; Banerjee, S. Multi-Stimuli Responsive Cyanostilbene Assemblies in Aqueous Media: Temporal Luminescence Modulation Through PH-Feedback Network. *Small* **2025**, *n/a* (n/a), 2503123.

(29) Zhu, L.; Zhao, Y. Cyanostilbene-Based Intelligent Organic Optoelectronic Materials. *J. Mater. Chem. C* **2013**, *1* (6), 1059–1065.

(30) Hang, C.; Wu, H.-W.; Zhu, L.-L. π-Conjugated Cyanostilbene-Based Optoelectric Functional Materials. *Chinese Chem. Lett.* **2016**, *27* (8), 1155–1165.

(31) Yu, H.; Wu, W.; Zhao, H.; Chen, K.; Li, S.; Tan, M.; Wang, T.; Huang, X.; Wang, N.; Hao, H. Cyanostyrene Derivative with Multi-Stimuli Responsive Properties: Multicolor- and High-Color-Contrast Switching in Response to Force, Heat and Light. *Dye. Pigment.* **2023**, *220*, 111727.

(32) Xiong, J.; Wang, K.; Yao, Z.; Zou, B.; Xu, J.; Bu, X.-H. Multi-Stimuli-Responsive Fluorescence Switching from a Pyridine-Functionalized Tetraphenylethene AIEgen. *ACS Appl. Mater. Interfaces* **2018**, *10* (6), 5819–5827.

(33) Afrin, A.; Chinna Ayya Swamy, P. Symphony of Light: AIE and MFC in Carbazole-Based Cyanostilbenes. *J. Mater. Chem. C* **2024**, *12* (6), 1923–1944.

(34) Sun, M.; Liu, J.; Jiang, T.; Lin, J.; Xu, M.; Zhao, Y.; Liu, Q.; Chen, K.; Zeng, C. A Thiophene-Substituted Cyanostilbene Derivative: Understanding the Mechanism of Its Aggregation-Induced Emission, Acidochromism and Mechanochromism from the Molecular Level. *J. Mol. Struct.* **2025**, *1337*, 142262.

(35) Shabashini, A.; Ramar, V.; Karthikeyan, B.; Panda, M. K.; Nandi, G. C. Design and Synthesis of Triphenylamine Based Cyano Stilbenes for Picric Acid Sensing and Two Photon Absorption Applications. *ChemistrySelect* **2021**, *6* (44), 12300–12308.

(36) Zhang, D.; Liu, Y.; Gao, H.; Chang, Q.; Cheng, X. α-Cyanostilbene and Fluorene Based Bolaamphiphiles: Synthesis, Self-Assembly, and AIEE Properties with Potential as White-Light Emissive Materials and Light-Emitting Liquid Crystal Displays. *J. Mater. Chem. C* **2020**, *8* (48), 17474–17481.

(37) Zhang, H. C.; Guo, E. Q.; Zhang, Y. L.; Ren, P. H.; Yang, W. J. Donor−Acceptor-Substituted Anthracene-Centered Cruciforms: Synthesis, Enhanced Two-Photon Absorptions, and Spatially Separated Frontier Molecular Orbitals. *Chem. Mater.* **2009**, *21* (21), 5125–5135.

(38) He, J.; Xu, B.; Chen, F.; Xia, H.; Li, K.; Ye, L.; Tian, W. Aggregation-Induced Emission in

the Crystals of 9,10-Distyrylanthracene Derivatives: The Essential Role of Restricted Intramolecular Torsion. *J. Phys. Chem. C* **2009**, *113*, 9892.

(39) Wen, L.; Sun, J.; Li, C.; Zhu, C.; Zhang, X.; Wang, Z.; Song, Q.; Lv, C.; Zhang, Y. Rich-Colour Mechanochromism of a Cyanostilbene Derivative with Chiral Self-Assembly. *New J. Chem.* **2021**, *45* (26), 11530–11535.

(40) Zhang, B.; Xiao, Y.; Fang, H.; Gao, H.; Wang, F.; Cheng, X. Mesogenic D–A Fluorophores Based on Cyanovinyl and Benzothiadiazole. *New J. Chem.* **2018**, *42* (20), 16709–16716.

(41) Kim, H.-J.; Gierschner, J.; Park, S. Y. Tricolor Fluorescence Switching in a Single Component Mechanochromic Molecular Material. *J. Mater. Chem. C* **2020**, *8* (22), 7417–7421.

(42) Ma, S.; Du, S.; Pan, G.; Dai, S.; Xu, B.; Tian, W. Organic Molecular Aggregates: From Aggregation Structure to Emission Property. *Aggregate* **2021**, *2* (4), e96.

Chapter 5

A Computational Study on Anthracene-Cyanostilbene Derivatives

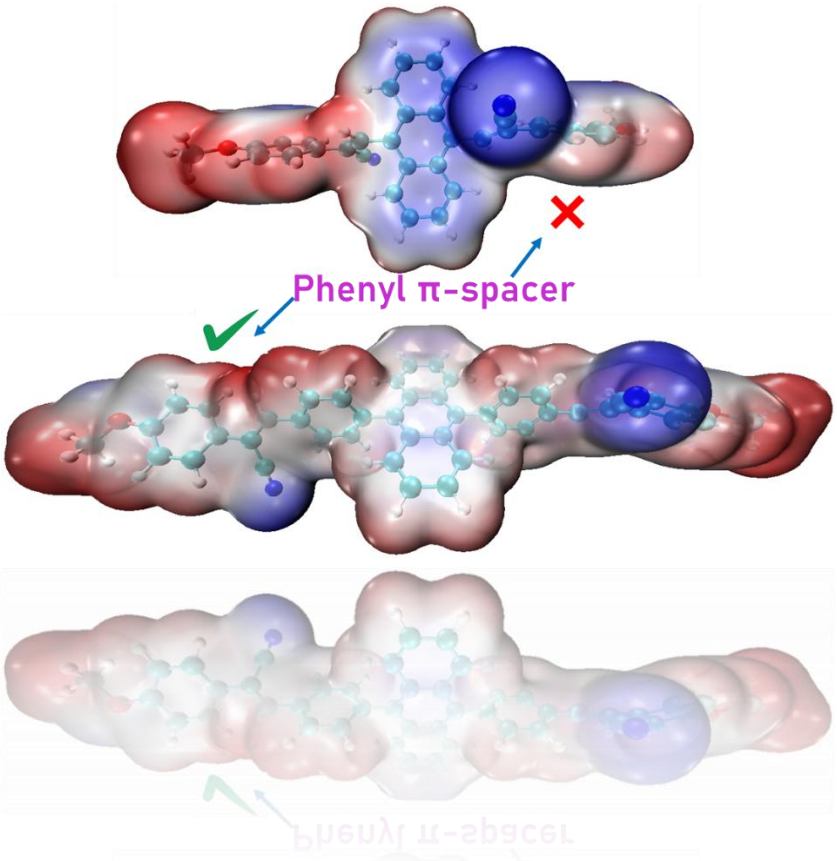

5.1 Abstract

Intermolecular interactions contributing to supramolecular aggregation of anthracene-cyanostilbene compounds reported in the previous chapters 3 and 4 were systematically analyzed using Hirshfeld surface and noncovalent interaction (NCI) analysis. The compound lacking a phenyl π-spacer (**CS-5.1**) exhibits weaker C–H···π and π···π interactions compared to its phenyl substituted analogue (**CS-5.2**), highlighting the role of phenyl groups in enhancing supramolecular stabilization. Further, quantum chemical calculations reveal the presence of two distinct conformers- *syn* and *anti*- for compounds **CS-5.1** and **CS-5.2**, which are energetically comparable in both the ground and excited states. The blue-shifted absorption observed for compound **CS-5.1** is supported by frontier molecular orbital analysis and is further corroborated by molecular electrostatic potential calculations. Compound **CS-5.2** exhibits conformational flexibility between *syn* and *anti* conformers in both the ground and excited states, attributed to a more energetically accessible transition state compared to analog **CS-5.1**. The presence of the *anti* conformer in the first excited state for both compounds **CS-5.1** and **CS-5.2** is confirmed by the close agreement between quantum chemically predicted emission wavelengths and experimental data, whereas emission from the *syn* form is absent in compound **CS-5.1** but remains possible in compound **CS-5.2**. Thus, the quantum chemical studies presented in this chapter offer valuable insights into the structure–activity relationships of compounds **CS-5.1** and **CS-5.2**, demonstrating how conformational preferences, electronic properties, and intermolecular interactions influence their photophysical behavior and supramolecular aggregation.

*__Publication based on this chapter__

Femina, C.; Yamamoto, N.; Ramya, N. K.; Sajith, P. K.; Thomas, R. Photophysical Divergence Driven by π-Spacer Variations in the Anthracene–Cyanostilbene Architecture. *Phys. Chem. Chem. Phys.* **2025**, *27* (45), 24641–24654.

5.2 Introduction

Controlling the photophysical behavior of organic π-conjugated systems through molecular design is essential for developing novel materials with enhanced photophysical properties.[1,2]Quantum chemical calculations, especially DFT and TD-DFT, provide powerful tools to guide and accelerate this process.[3–6] The influence of π-donor groups on photophysical properties and their roles in applications such as nonlinear optics (NLO) and dye-sensitized solar cells (DSSC) have been extensively investigated.[7] For instance, Jaccob and coworkers designed a series of triphenylamine (TPA)-benzothiadiazole based organic sensitizers, in which systematic variation of the TPA π-spacers was employed to tune their optoelectronic properties.[8] Using DFT and TD-DFT calculations, they demonstrated that the incorporation of heteroatom linkers plays a decisive role in governing molecular planarity, absorption-emission properties and HOMO-LUMO energy levels.[9,10] The designed systems are predicted to be promising candidates for DSSC and NLO applications. Another DFT/TDDFT study demonstrated that cyan-acrylic acid systems incorporating a series of π-spacers exhibited enhanced performance for DSSC applications.[8,11] Collectively, these findings underscore the importance of π-linker engineering for the fine-tuning of photophysical properties.[12–14] The literature review revealed that quantum chemical studies on cyanostilbene systems are surprisingly limited.[15,16] In this context, Yamamoto and coworkers have conducted notable research on cyanostilbene systems, which includes elucidating the E/Z isomerism and aggregation-related properties of these systems.[17,18] In one of the studies, Yamamoto explored the E-Z isomerization of cyanostilbene systems by employing DFT and TD-DFT methods. The study revealed that light induced Z to E isomerization and thermally activated E to Z transition plays the pivotal role in the emission outcomes of the derivatives. In the second study the free energy profile of the AIE process of cyanostilbene systems with E and Z forms were explored using the free energy perturbation approach at the molecular mechanics level.[17,18]

5.3 Scope of the present investigation

This chapter provides a comprehensive theoretical analysis of the experimentally observed optoelectronic properties of the D-π-A systems **CS-5.1** and **CS-5.2** (Scheme 5.1), which correspond to anthracene-cyanostilbene derivatives with and without a phenyl π-spacer, respectively, regardless of the alkoxy substituent, discussed in Chapters 3 and 4. With the help of DFT and TD-DFT calculations, the structural and electronic properties of these systems were thoroughly examined. First of all, Hirshfeld surface and noncovalent interaction (NCI) analyses

were performed on the crystal structures of these compounds, as reported in the previous chapters.[19–21] These analyzes provide an insight into the strength of noncovalent interactions that lead to aggregate formation in compounds **CS-5.1** and **CS-5.2** compounds. The conformational analysis and absorption features of the compounds are then explored with the help of electronic structure calculations.

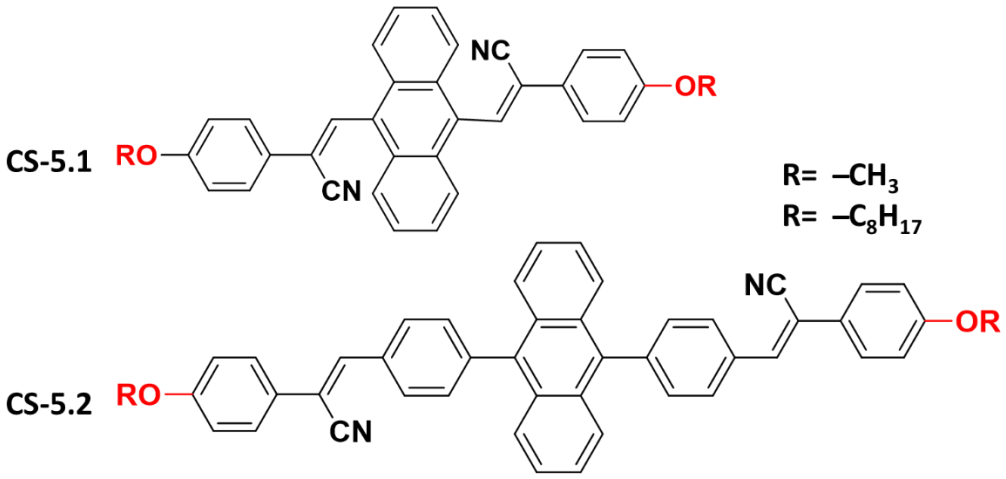

Scheme 5.1 The ChemDraw images of the studied compounds.

5.4 Computational details

5.4.1 Crystallographic studies

5.4.1.1 Hirshfeld Studies.

Intermolecular interactions and molecular packing in **CS-5.1** and **CS-5.2**, where R= octyl, were examined using the computational software Crystal Explorer version 17.5.[22] Hirshfeld surfaces were generated to visualize molecular packing and surface characteristics.[19] In addition, the corresponding fingerprint plots for the crystal structures of compounds **CS-5.1** and **CS-5.2** were analyzed to further investigate their intermolecular interactions.

5.4.1.2 NCI Analysis

Noncovalent interaction (NCI) analysis[23]was carried out using the Multiwfn software package[23] to gain deeper insight into the noncovalent interactions present in the crystal structures of compounds **CS-5.1** and **CS-5.2** both featuring an octyloxy group as the R substituent. Wave functions for the NCI analysis were generated from single-point calculations at the ωB97X-D/6-311+G(d) level of theory with Gaussian 16 software packages,[24] using geometries extracted from the crystal structures. Visualization of the reduced density gradient (RDG) isosurfaces obtained from the NCI analysis was performed using the VMD software package.[25]

5.4.2 Electronic structure calculations at the molecular level

All electronic structure calculations were performed using the Gaussian 16, Revision C.02 program package.[24] The geometries of the ground state (S_0) and the first singlet excited state (S_1) were fully optimized for compounds **CS-5.1** and **CS-5.2** (featuring a methyl group as the R substituent) in the gas phase using density functional theory (DFT) and its time-dependent extension (TD-DFT), respectively. The long-range corrected ωB97-XD functional was employed in conjunction with the 6-311+G(d) basis set for all atoms.[26] Frequency calculations were subsequently carried out at the same level of theory to verify that each optimized structure was a true energy minimum, characterized by the absence of imaginary frequencies. The Gibbs free energies (ΔG) of these conformers were computed at 298.15 K and 1 atm based on the results of the frequency analyses under the harmonic oscillator approximation. The transition state (TS) structures connecting the *syn* and *anti*-conformers were also located and were confirmed to be first-order saddle points by the presence of a single imaginary frequency corresponding to the isomerization coordinate. Vertical absorption energies ($S_0 \rightarrow S_1$) and their corresponding wavelengths were calculated by performing TD-DFT calculations on the S_0-Min geometries. To simulate the fluorescence process, the geometries of the first singlet excited state (S_1) were optimized for all conformers. Emission wavelengths ($S_1 \rightarrow S_0$) were then determined by computing the vertical transition energies from these S_1 optimized structures.

The percentage contribution of fragment molecular orbitals (FMOs) was analyzed using the QMForge program.[21] QMForge reads the output files and decomposes the molecular orbitals into contributions from atomic orbitals. This decomposition provides a quantitative measure of how much each atom or fragment of the molecule contributes to the HOMO or LUMO. Such information is especially valuable because the character of HOMO and LUMO determines many molecular properties, including reactivity, charge transfer pathways, electronic transitions, and interaction sites**.** For example, if the HOMO has a high percentage contribution from a donor group, and the LUMO is localized on an acceptor group, the molecule may exhibit strong charge-transfer behavior in excited states. By offering this breakdown, QMForge helps to interpret electronic structures more clearly, linking computational results to chemical intuition and experimental observations.

5.5 Results and Discussion

5.5.1 Hirshfeld Surface Analysis

To gain a deeper understanding of the differences in noncovalent interactions contributing to the formation of supramolecular aggregates in compounds **CS-5.1** and **CS-5.2**, their crystal structures were further examined using Hirshfeld surface analysis.[19] Compounds **CS-5.1** and **CS-5.2** bearing an octyl substituent were used for this analysis. This method facilitated the identification and evaluation of key intermolecular interactions through a color-coded scheme, offering detailed insight into the nature and strength of forces such as hydrogen bonding, π–π interactions, and van der Waals (vdW) contacts that influence molecular organization within the crystal lattice. The red regions highlight intermolecular contacts that are shorter than the sum of the vdW radii of the interacting atoms, typically indicating strong and significant interactions such as hydrogen bonds. The blue regions correspond to contacts that are longer than the sum of the vdW radii, representing weaker, non-bonded interactions and the white regions denote contacts that are approximately equal to the sum of the vdW radii, suggesting neutral or vdW-type interactions. The mapped Hirshfeld surface (d_{norm}) is illustrated in Figure 5.1 (a) and (b), where the molecular structure is displayed in a ball-and-stick model for clarity and transparency. Distinct red spots on the d_{norm} surfaces confirm the presence of close intermolecular interactions and hydrogen bonding. In compounds **CS-5.1** and **CS-5.2**, these are predominantly observed around electronegative oxygen and nitrogen atoms, consistent with their role as hydrogen bond acceptors.

In addition to Hirshfeld surfaces, the molecular electrostatic potential (MESP)[27] surface mapping was generated to further understand the charge distribution over the molecular framework (see Figure 5.1 (c) and (d)). The MESP maps reveal regions of electron density (coloured red), corresponding to electronegative centers such as oxygen and nitrogen atoms, and electron-deficient regions (coloured blue), typically localized around hydrogen atoms bound to electronegative atoms. This complementary analysis provides a clear visualization of potential donor–acceptor sites within the molecule and strongly supports the hydrogen-bonding interactions identified in the Hirshfeld surface study.

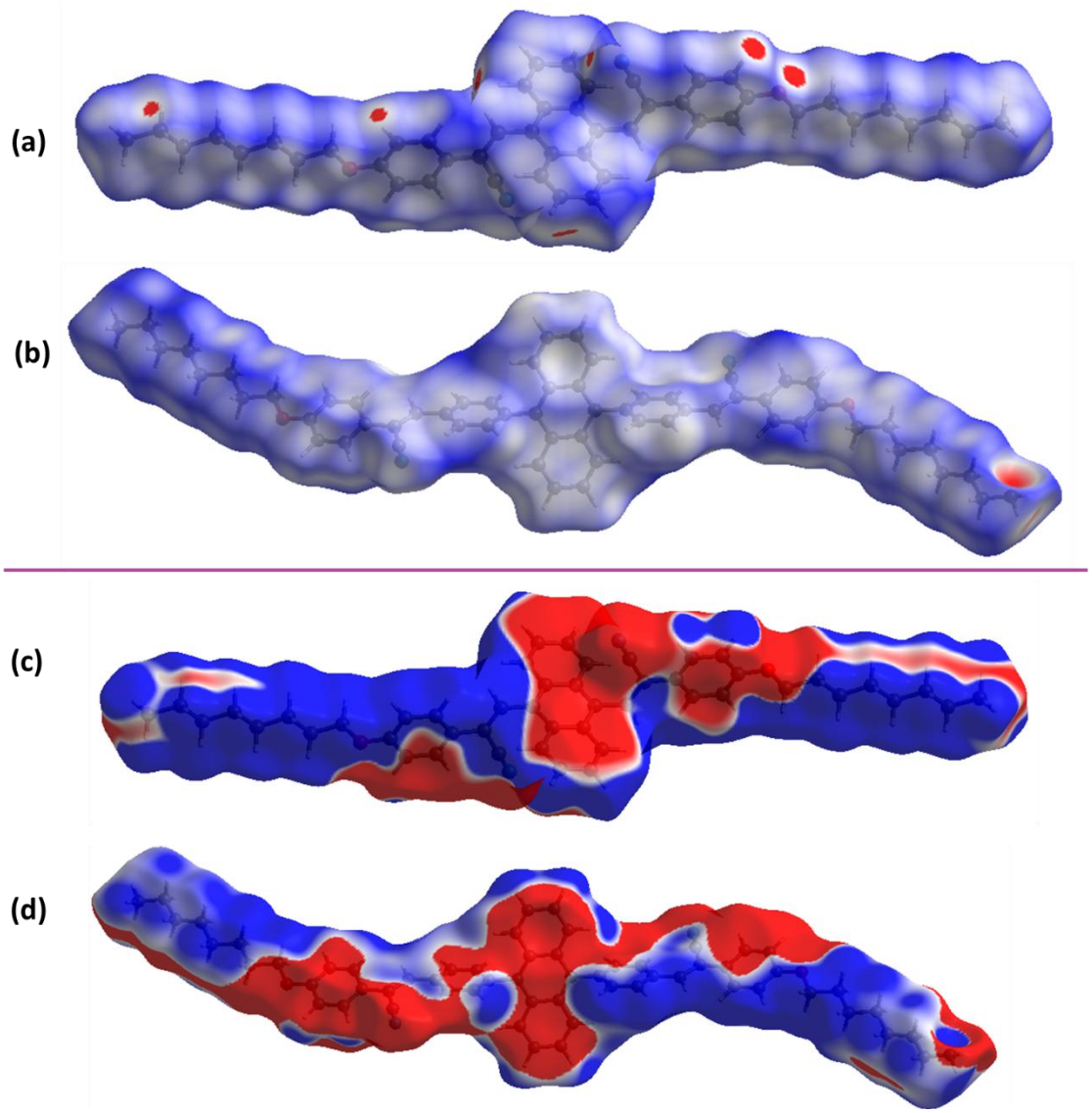

Figure 5.1 Hirshfeld analysis of Compound: (a) d_{norm} surface of **CS-5.1**, (b) d_{norm} surface of **CS-5.2**, (c) electrostatic potential map of **CS-5.1**, (d) electrostatic potential map of **CS-5.2**. **CS-5.1** and **CS-5.2** with octyl substituent is used for this analyses**.**

The two-dimensional fingerprint plots derived from Hirshfeld surface analysis provide a quantitative measure of the various intermolecular interactions that contribute to crystal packing. Characteristic sharp spikes and distinct features in the plots correspond to specific types of contacts, including O···H, N···H, C···C, C···H, and H···H interactions. The quantitative analysis reveals the percentage contributions of these non-covalent interactions, highlighting their relative importance in the stabilization of the crystal lattice. In both compounds, the H···H contacts make the maximum contribution, accounting for nearly 60% of the total interactions. This indicates that vdW-type contacts arising from hydrogen atoms

dominate the packing arrangement. In contrast, the O···H contacts contribute the least, consistent with their more localized role as specific hydrogen-bonding interactions. The fingerprint plots and the detailed percentage contributions are illustrated in Figure 5.2. A comparative examination of the two compounds shows notable differences. In compound **CS-5.1**, the contribution from C···C contacts (associated with π···π stacking) is minimal, around 1%, whereas in compound **CS-5.2,** this value increases to 3%, suggesting a greater degree of π···π interactions in the latter. Similarly, C···H contacts, which often correspond to C–H···π interactions, account for only 14% in compound **CS-5.1**, but increase substantially to 26% in compound **CS-5.2**. This enhanced contribution indicates that compound **CS-5.2**exhibits a higher prevalence of both C–H···π and π···π interactions, which play a significant role in stabilizing its crystal packing compared to compound **CS-5.1**.

Importantly, the intense O···H and N···H contributions observed in the fingerprint plots directly correlate with the red regions on the MESP surface, confirming that these interactions originate from electron-rich heteroatoms acting as acceptors and electron-deficient hydrogen atoms functioning as donors. Collectively, the Hirshfeld surface analysis, fingerprint plots, and MESP surface mapping provide a comprehensive understanding of the interplay between strong directional hydrogen bonds and weaker vdW interactions in compounds **CS-5.1**and **CS-5.2**, emphasizing the critical role of charge distribution in guiding crystal packing.

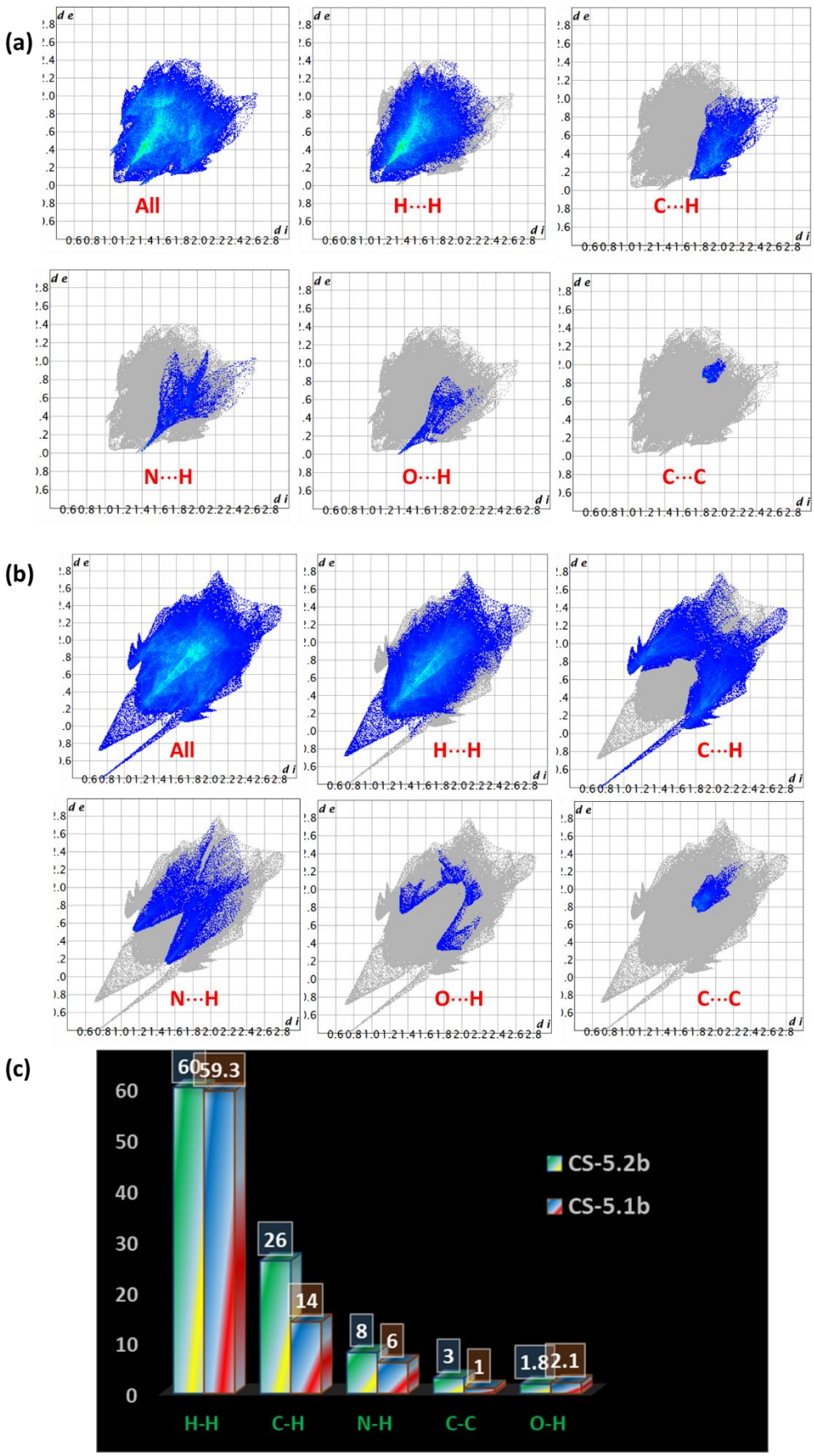

Figure 5.2 Hirshfeld surface fingerprint plots of (a) compound **CS-5.1** (b) compound **CS-5.2** and (c) fingerprint analysis of **Cs-5.1** and **CS-5.2**, plotted as a bar chart.

5.5.2 Noncovalent interaction (NCI) analysis

Reduced isodensity (RDG) calculations were carried out to obtain deeper insights into the noncovalent interactions governing the aggregated structures of compounds **CS-5.1**and **CS-5.2**. The analysis involved generating three-dimensional (3D) isodensity surface plots together with two-dimensional (2D) reduced density gradient (RDG) scatter plots (see Figure 5.3). In the 3D isodensity surfaces of the monomer units, the green isosurfaces observed between the monomeric units are indicative of stabilizing π–π interactions.[23] As illustrated in Figure 5.3, compound **CS-5.2**displays a more pronounced green isosurface between the phenyl rings of the anthracene unit compared to compound **CS-5.1**, signifying stronger and more extended π–π stacking interactions. In compound **CS-5.2**, improved π–π interactions facilitate the formation of well-ordered J-aggregates, which likely contribute to the enhanced quantum yield observed in comparison to compound **CS-5.1**.[28]

The 2D RDG scatter plots further support this interpretation. In these plots, the sign(λ_2)ρ values are plotted against RDG, where negative values correspond to attractive interactions and positive values indicate repulsive interactions. The scatter plots of both compounds reveal green spikes, characteristic of weak vdW or π–π interactions; however, compound **CS-5.2** exhibits sharper and more negative green spikes, confirming the presence of stronger attractive π–π interactions relative to compound **CS-5.1**. Additionally, minor blue spikes, corresponding to hydrogen bonding, are also observed but are less prominent than the π–π contributions. Taken together, the 3D isosurface maps and 2D RDG scatter plots consistently indicate that the anthracene units in compound **CS-5.2** engage in more efficient J-aggregate formation compared to those in compound **CS-5.1**.

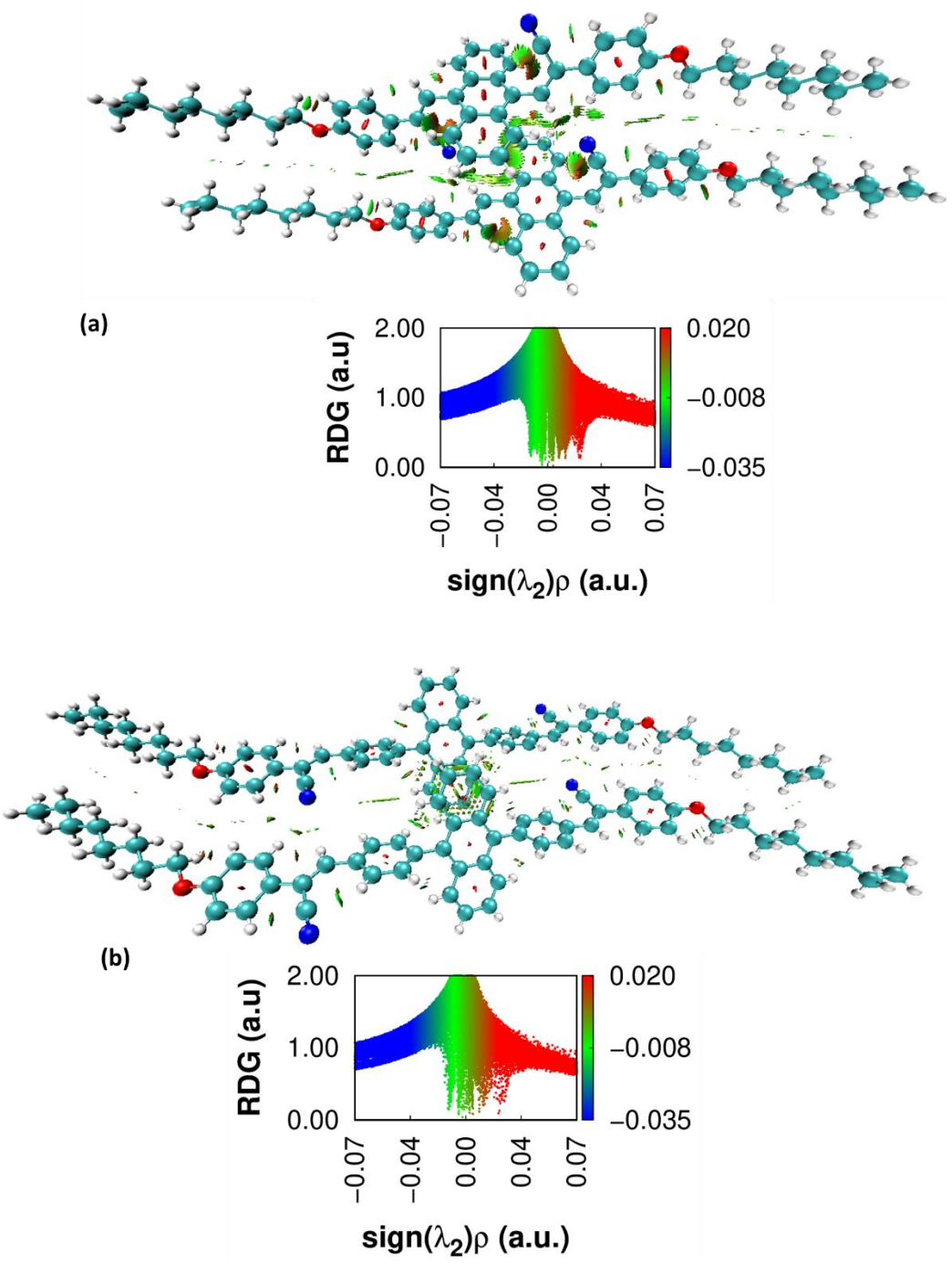

Figure 5.3 NCI-RDG isodensity surface plot and scatter plot (isovalue = 0.50 a.u.) of dimers of (a) **CS-5.1** and (b) **CS-5.2** under study. **CS-5.1** and **CS-5.2** with octyl substituent is used for NCI analysis.

5.5.3 Gas phase optimization of the compounds CS-5.1 and CS-5.2

To gain additional insights into the structural and photophysical properties of the synthesized compounds, DFT and TD-DFT calculations were carried out at the ωB97-XD /6-311+G(d)

level of theory. To reduce computational cost, the calculations were performed on simplified model structures by using methoxy groups for alkyl chains. The calculations showed that both compounds **CS-5.1**and **CS-5.2** can exist as two primary conformers, *syn* and *anti*, based on the orientation of their terminal cyano groups. The optimized ground state geometries are referred to as S_0-Min. The *syn* and *anti* conformers of compounds **CS-5.1** and **CS-5.2** are denoted as *syn*-**CS-5.1**, *anti*-**CS-5.1**, and *syn*-**CS-5.2**, *anti*-**CS-5.2**, respectively. The optimized geometries show good agreement with the corresponding crystal structures of **CS-5.1** and **CS-5.2**, as illustrated in Figure 5.4. In compound **CS-5.2**, the phenyl ring adopts an almost perpendicular orientation relative to the linked anthracene moiety. Relative energetics of *syn* and *anti* conformers showed a clear preference for the *anti* conformer in compound **CS-5.1** (ΔE = 1.2 kcal/mol), whereas compound **CS-5.2** displayed no significant energy difference between the two forms.

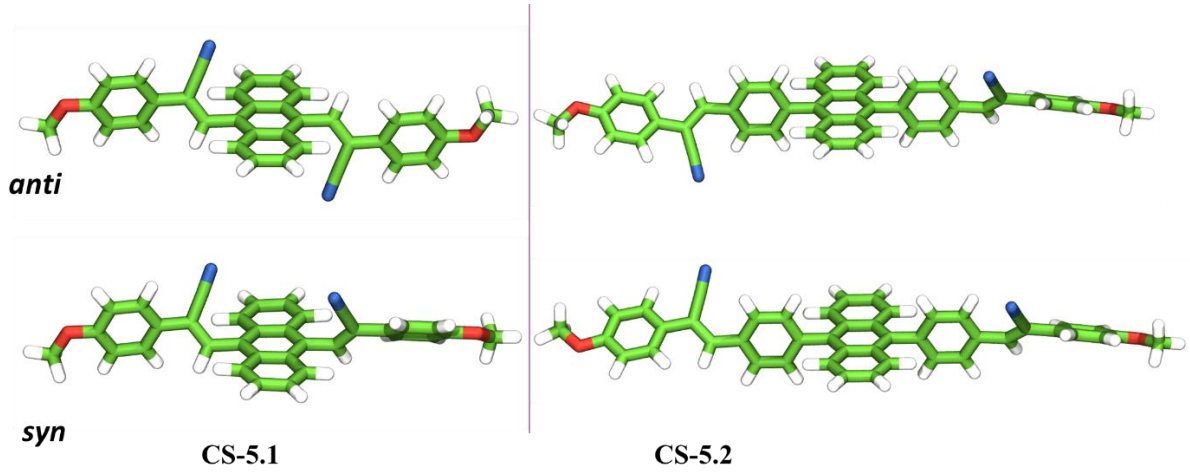

Figure 5.4 Optimized geometries (ωB97-XD/6-311+G(d)) of the ground-state minima for the *syn* and *anti*-conformers of Compounds **CS-5.1** and **CS-5.2**.

5.5.3.1 Frontier Molecular Orbital (FMO) Analysis

The Frontier Molecular Orbitals, specifically the HOMO and LUMO, are fundamental in understanding the chemical behavior and stability of a molecule. The energy gap between the HOMO and LUMO (ΔE_{HL}) is a key factor in determining the reactivity and kinetic stability of **CS-5.1** and **CS-5.2**. The HOMO, LUMO, HOMO-1, and LUMO+1 energies along with ΔE_{HL} values of the compounds **CS-5.1** and **CS-5.2** are presented in Figure 5.5. The ΔE_{HL} of compounds **CS-5.1** and **CS-5.2** indicate that the *syn* and *anti* conformers in both cases exhibit nearly identical values, suggesting that their conformational isomers have comparable

electronic properties and similar levels of reactivity and stability. However, the ΔE_{HL} of compound **CS-5.2** is approximately 0.28 eV higher than that of compound **CS-5.1**. Therefore, compound **CS-5.2** can be considered slightly more chemically inert and thermodynamically stable than compound **CS-5.1**. This electronic effect is also reflected in the photophysical behavior: the increased energy gap corresponds to a shift of the absorption band toward shorter wavelengths (a hypsochromic or blue shift) in the UV–Vis spectrum of compound **CS-5.2** relative to compound **CS-5.1**. The molecular isosurfaces of the HOMO, LUMO, as well as adjacent orbitals such as HOMO–1 and LUMO+1, of compounds **CS-5.1** and **CS-5.2** are shown in Figures 5.6 and 5.7. From the figure, it is obvious that the HOMO and LUMO distributions of compound **CS-5.2** are localized predominantly on the central anthracene unit and cyanostilbene moieties. Instead, the HOMO of compound **CS-5.2** is largely confined to the anthracene moiety, while the LUMO extends over the cyanostilbene groups, indicating the presence of intramolecular charge transfer (ICT).

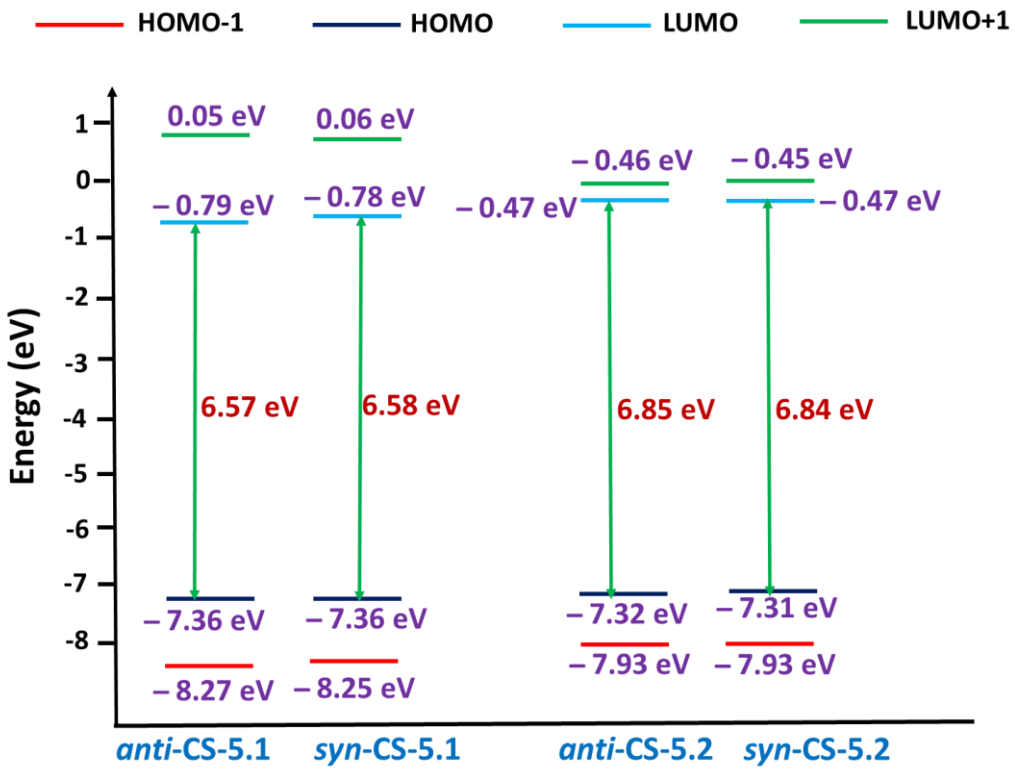

Figure 5.5 The FMO energies and ΔE_{HL} values of *syn* and *anti* conformers of **CS-5.1** and **CS-5.2**.

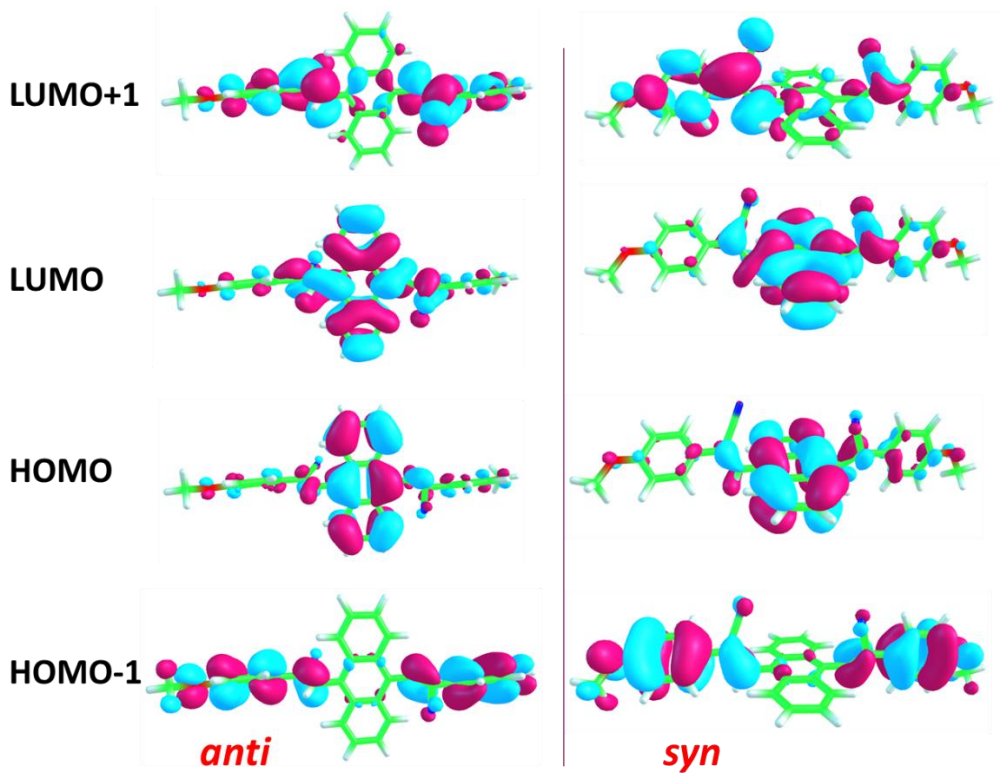

Figure 5.6 Frontier molecular orbitals of *syn* and *anti* conformers of compound **CS-5**.1

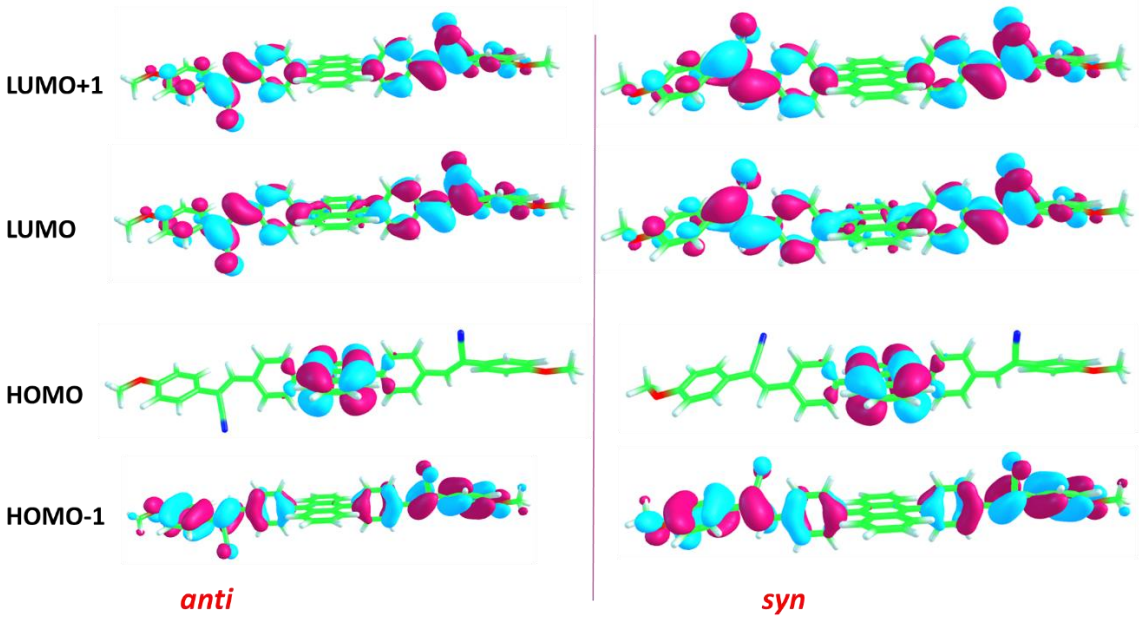

Figure 5.7 Frontier molecular orbitals of *syn* and *anti* conformers of compound **CS-5.2**.

To analyze the percentage contributions of different molecular fragments to the FMOs, the molecule was divided into three parts, Ant, CN-1 and CN-2. The fragmentations of both *syn* and *anti* forms of **CS-5.1** and **CS-5.2** are illustrated in Scheme 5.2. This approach enables the determination of the percentage contribution of the anthracene (Ant) moiety to the HOMO and LUMO. Figure 5.8 illustrates the percentage contributions of the fragments to the FMOs in a visual format. The general trend observed in the diagram indicates that the anthracene moiety contributes the major share towards the HOMO in both the *syn* and *anti* isomers of compounds **CS-5.1** and **CS-5.2**. In both the *syn* and *anti* conformers of compound **CS-5.1**, the anthracene moiety contributes approximately 66% to the HOMO. For compound **CS-5.2**, the contribution from the anthracene unit is comparatively higher in both conformers, accounting for around 77%. Another noteworthy observation is that the anthracene moiety contributes approximately 40% to the LUMO in both the *syn* and *anti* conformers of compound **CS-5.1**. In contrast, its contribution is significantly lower in compound **CS-5.2**, accounting for only about 8% in both conformers.

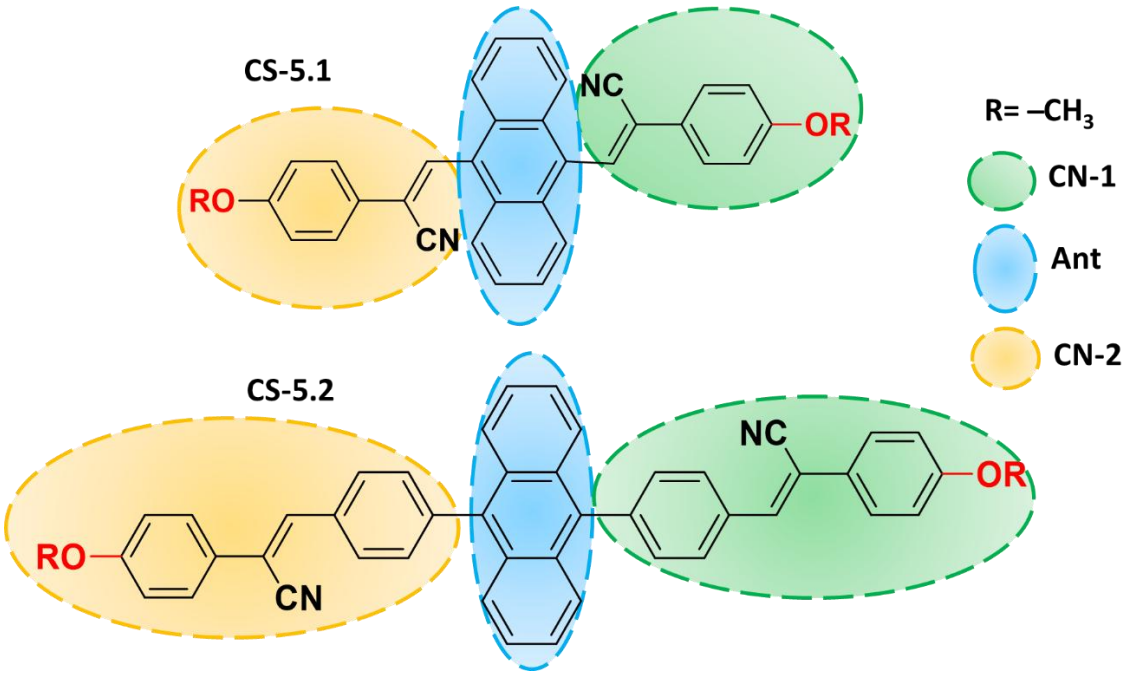

Scheme 5.2. Fragments considered to study their contributions to FMOs.

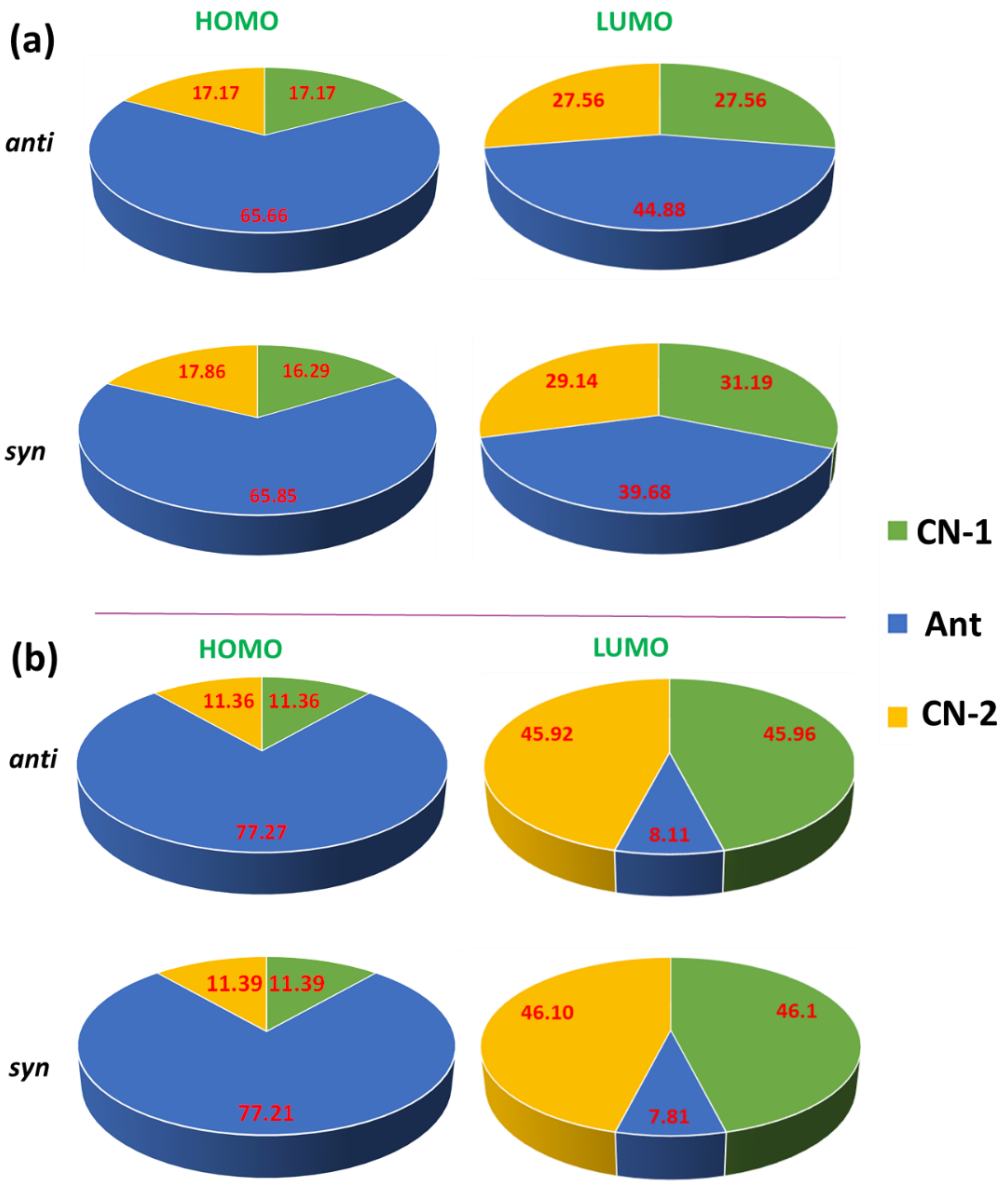

Figure 5.8 Percentage contributions of different molecular fragments to the HOMO and LUMO of the *syn* and *anti* conformers of compounds (a) **CS-5.1** and (b) **CS-5.2**.

5.5.3.2 Energetics of *syn*–*anti* Conversion

The conformational landscapes in the ground (S_0) of **CS-5.1** and **CS-5.2** (Figure 12) were further investigated. The optimized ground state geometries are shown in Figure 12. A critical difference between the two compounds emerges from the rotational barrier between these conformers in the ground state. For Compound **CS-5.2**, the calculated activation barrier for the *anti* → *syn* isomerization is merely 2.92 kcal/mol. This low barrier allows for rapid interconversion at room temperature, meaning the *syn* and *anti*-conformers, which are nearly

isoenergetic (ΔG = −0.02 kcal/mol), exist as a dynamic equilibrium mixture. In stark contrast, the corresponding barrier for compound **CS-5.1** is 18.44 kcal/mol. This substantial barrier effectively prevents rotation at room temperature, indicating that the *syn* and *anti*-conformers of compound **CS-5.1** are configurationally locked isomers. Given that the ***anti*-CS-5.1** conformer is thermodynamically more stable by 1.17 kcal/mol, it is the predominant species, and photoexcitation will occur from this ground-state population.

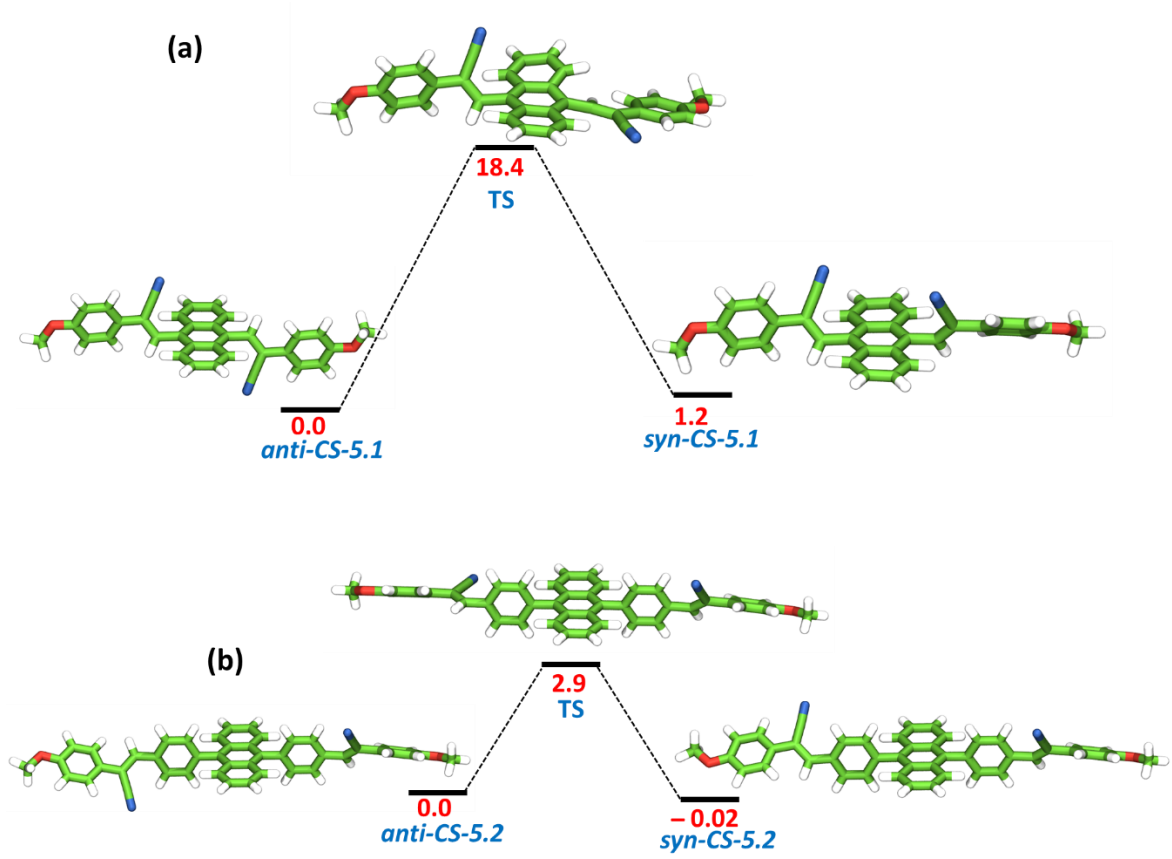

Figure 5.9 Energy profile diagram for the *syn-anti* conversion of compounds (a) **CS-5.1** and (b) **CS-5.2**. Relative energy values are in kcal/mol.

Conformational analysis reveals that the *anti* forms of compounds **CS-5.1** and **CS-5.2** (*anti*-**CS-5.1** and *anti*-**CS-5.2**) are the predominant conformers in the ground state (S_0), and were thus selected for subsequent investigations of ground-state properties. While the *syn* conformer of compound **CS-5.2** is nearly isoenergetic and could also be considered, the *anti* form was chosen to maintain consistency across both compounds.

5.5.3.3 Simulated Absorption Spectra

To assign the orbital transitions corresponding to the experimental absorption maxima, vertical singlet excitation energies were computed using time-dependent DFT (TD-ωB97X-D) with the 6-31+G(d,p) basis set. TD-DFT calculations for compound **CS-5.1** indicate that the most intense absorption band at 391 nm arises predominantly from the HOMO → LUMO transition, closely matching the experimental absorption maximum near 410 nm. For compound **CS-5.2**, the principal computed transition occurs at 315 nm, in reasonable agreement with the experimental value of approximately 340 nm. The calculated wavelength of absorption, oscillator strength, and significant orbital transitions (in %) for compound **CS-5.1** and **CS-5.2** are presented in Table 5.1.

Table 5.1. The electronic vertical excitation energies, oscillator strength, and assignment of various peaks of **CS-5.1** and **CS-5.2** in the anti-form in calculated at the TD/ωB97-XD/6-311+G(d) levels of theory.

Serial No.	Compound	Absorption Wavelength (λ in nm)	Oscillator strength (f)	Transition
1	*anti*-**CS-5.1**	391	0.5900	HOMO → LUMO (95%)
2	*anti*- **CS-5.2**	315	1.8361	HOMO-2 → LUMO (40%) HOMO-1 → LUMO+1 (43%)

5.5.3.4 Molecular electrostatic potential (MESP) analysis

The MESP topology[27] analysis offers a visual representation of the π-electron cloud and lone pair regions in a molecule. The minimum electrostatic potential values (V_{min}) serve as a useful quantitative descriptor for assessing the electron density in these regions. The longer wave length for absorption corresponding to the lowest energy transition ($S_0 \rightarrow S_1$) observed for **CS-5.1**, compared to **CS-5.2**, can be rationalized based on MESP analysis. The MESP plot depicted in Figure 5.10(a) showed that the V_{min} for the -CN region in compound **CS-5.1** is more negative (−53.2 kcal/mol) than that observed in compounds **CS-5.2** (−51.0 kcal/mol). In addition, the V_{min} value around the central anthracene segment in compound **CS-5.2** is slightly more negative than that in compound **CS-5.1**, indicating a reduced delocalization of electron density in

compound **CS-5.2** relative to **CS-5.1**, which in turn influences the FMO energy levels. This [29,30]influences the $S_0 \rightarrow S_1$ transition, resulting in a red-shifted absorption for compound **CS-5.1** relative to compound **CS-5.2**. The calculated MESP of **CS-5.1** and **CS-5.2** are shown in Figure 5.10b. The electron densities are localized (shown in blue) around the cyanide and anthracene moieties. The alkyl groups in the vicinity of the oxygen atom exhibit a more electron-deficient (red color) character. The green colour reflects an intermediate potential shown by most of the molecular regions.

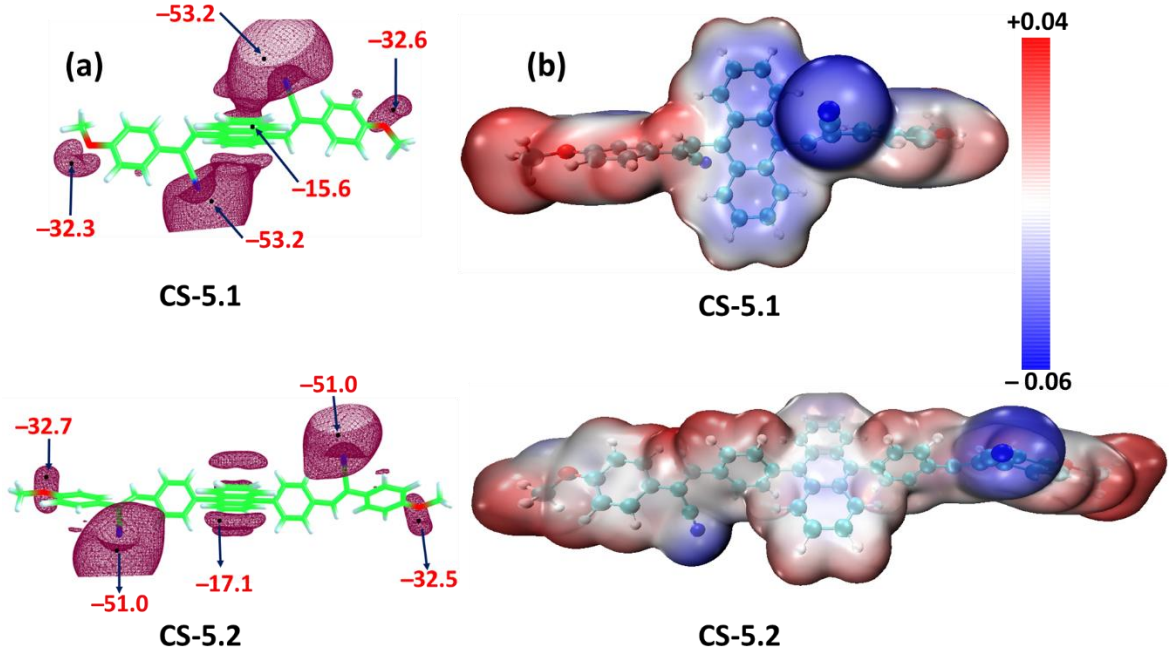

Figure 5.10. (a) V_{min} values at relevant molecular fragments of compounds **CS-5.1** and **CS-5.2** **(b)** MESP surfaces ((isovalue = 0.001 a.u.) of compound **CS-5.1**and **CS-5.2**.

5.5.4 Excited-State Dynamics of *syn* and *anti* Conformers

In the S_1 state, the potential energy surface reveals a complex landscape. While Compound **CS-5.2** shows minimal geometric changes upon excitation, Compound **CS-5.1** exhibits a dramatic transformation. The optimized geometries of all conformers in the S_1 state, denoted with an asterisk (*), are shown in Figure 5.11. The *syn*-**CS-5.1*** conformer, in particular, undergoes a profound structural change, adopting a significantly bent and non-planar geometry where the central anthracene core is distorted out of its plane. This distorted structure is the thermodynamic global minimum on the S_1 potential energy surface for compound **CS-5.1**.

For Compound **CS-5.2**, which exists as a rapidly equilibrating mixture, the calculated properties of the *anti*-conformer (absorption at 357 nm, emission at 459 nm) are in good

agreement with the experimental data. The small Stokes shift is consistent with its rigid, largely planar structure in both the S_0 and S_1 states.

For Compound **CS-5.1**, the calculated absorption for the dominant *anti*-**CS-5.1** conformer (384 nm) matches the experimental spectrum well. Our calculations predict that emission from the bent, thermodynamically stable *syn*-**CS-5.1*** structure would appear at 674 nm. However, this long-wavelength emission is absent in the experimental spectrum. This absence strongly implies that the excited-state isomerization from *anti*-**CS-5.1*** to *syn*-**CS-5.1*** is kinetically hindered, likely by a high activation barrier on the S_1 surface (11.3 kcal/mol), and thus does not occur.

Therefore, the major emission band observed for Compound **CS-5.1** at ~530 nm must be assigned to emission from the locally excited state of the *anti*- **CS-5.1** conformer. The calculated emission wavelength for *anti*-**CS-5.1*** is 537 nm, which closely matches the experimental result. The large Stokes shift observed for **CS-5.1** can thus be attributed to the significant geometric relaxation of the *anti*-**CS-5.1*** conformer itself within its own S_1 potential well, without undergoing isomerization. Finally, a minor shoulder is observed in the experimental emission of **CS-5.1** around 400-450 nm. This higher-energy emission is not assigned to the fully relaxed S_1 state. We postulate that it could be emission from the initially populated, unrelaxed state of *anti*-**CS-5.1*** before complete geometric relaxation occurs (i.e., hot luminescence).

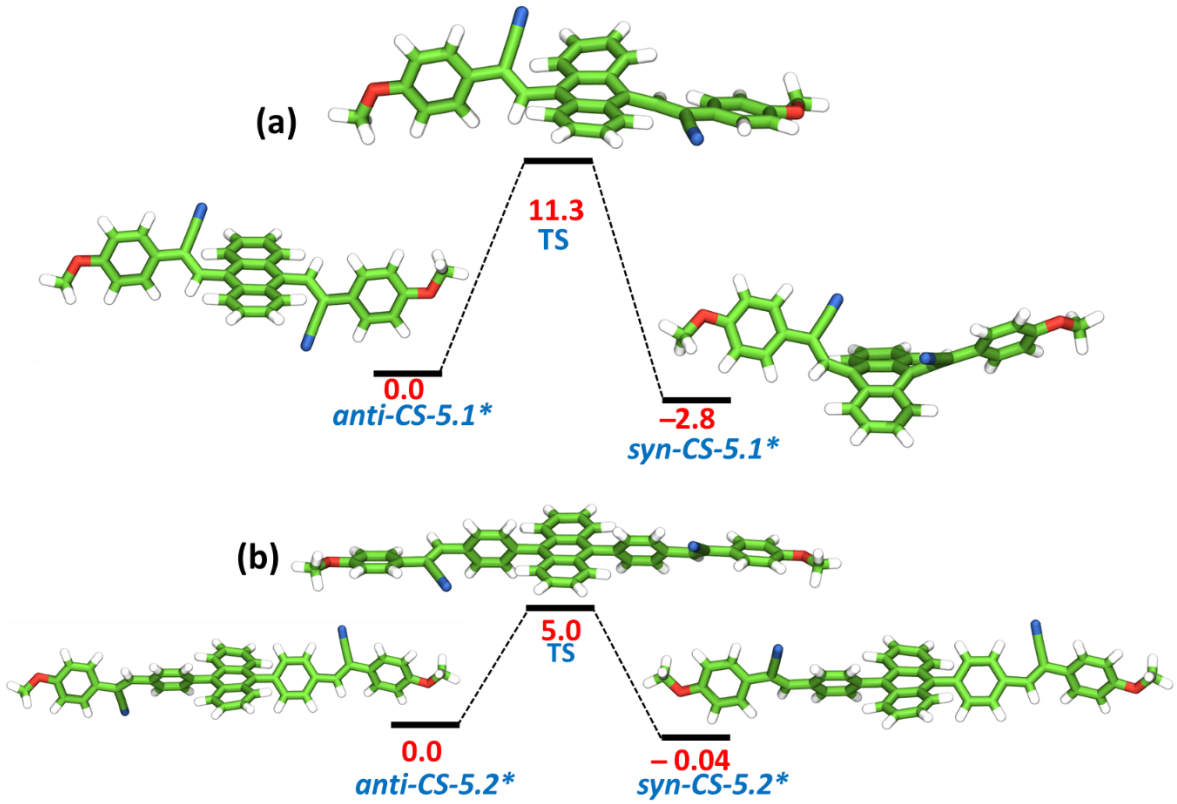

Figure 5.11. Energy profile diagram of the *syn-anti* conversion of (a) **CS-5.1** and (b) **CS-5.2** in the first excited state (S_1). The relative energies are in kcal/mol.

5.6 Conclusion

In conclusion, the newly synthesized anthracene-cyanostilbene D–π–A systems **CS-5.1** and **CS-5.2** have been theoretically analyzed, with their structural and electronic properties thoroughly examined using DFT and TD-DFT calculations. Hirshfeld surface and NCI analyses of the crystal structures revealed that **CS-5.2** exhibits stronger C–H···π and π···π interactions than **CS-5.1**, owing to the presence of the phenyl substituent. Furthermore, NCI analysis predicted a more efficient J-aggregate formation in compound **CS-5.2** compared to compound **CS-5.1**.

Theoretical calculations at the ωB97-XD/6-311+G(d) level of theory provided insight into the electronic structures and excited-state dynamics of **CS-5.1** and **CS-5.2** . FMO analysis revealed that the HOMO–LUMO gap in **CS-5.2** is slightly larger than that in **CS-5.1**, which can be attributed to the perpendicular orientation of the phenyl moieties in **CS-5.2**, leading to

reduced conjugation and consequently a slightly wider energy gap. The analysis of the percentage contribution of the anthracene moiety to the FMOs reveals that the HOMO is primarily derived from this moiety. In contrast, the anthracene contributes approximately 40% to the LUMO in **CS-5.1** , whereas its contribution drops to below 10% in **CS-5.2**.

The TDDFT calculations successfully reproduced the main absorption features of both compounds. The calculated absorption maximum for compound **CS-5.1** appears at approximately 384 nm, while for compound **CS-5.2,** it is observed at around 357 nm. The predicted blue shift in **CS-5.2** relative to **CS-5.1** is in excellent agreement with the experimental results. This blue shift can be rationalized by using deepest minimum MESP value located at the anthracene core.

In the S_0 state, the *anti*-to-*syn* conversion requires a free energy barrier of 18.4 kcal/mol for compound **CS-5.1**, whereas for compound **CS-5.2**, the barrier is significantly lower value of 2.9 kcal/mol, indicating that the conversion is energetically more favourable for **CS-5.2** and considerably hindered for **CS-5.1**. In the S_1 state, this trend persists: the activation barrier for compound **CS-5.2** is only 5.0 kcal/mol, compared to 11.3 kcal/mol for compound **CS-5.1**, suggesting that the *anti*-to-*syn* isomerisation is also kinetically more accessible in **CS-5.2** in the first excited state. The absence of the predicted 674 nm emission band for *syn*- **CS-5.1** in the experimental spectra supports the theoretical prediction.

5.7 References

(1) Mahalingavelar, P.; Kanvah, S. α-Cyanostilbene: A Multifunctional Spectral Engineering Motif. *Phys. Chem. Chem. Phys.* **2022**, *24* (38), 23049–23075.

(2) Zhao, J.; Zaheer, M.; You, J.; Owyong, T. C.; Giel, M.-C.; Praveen, P.; Li, W.; Hou, J.; Hogan, C. F.; Zhao, E.; Ding, S.; Hong, Y. Functionalized α-Cyanostilbene Derivatives for Detection of Hypoxia or Proteostasis Imbalance in Live Cells. *Chem. – A Eur. J.* **2024**, *30* (69), e202402630.

(3) Mariya Tedy, A.; Manna, A. K. Theoretical Understanding of Photoluminescence and Singlet Oxygen Quantum Yields in a Few Halogenated Fluorescein Dyes. *Chem. – An Asian J.* **2025**, *20* (5), e202401065.

(4) Tedy, A. M.; Manna, A. K. Nature and Energetics of Low-Lying Excited Singlets/Triplets and Intersystem Crossing Rates in Selone Analogs of Perylenediimide: A Theoretical Perspective. *J. Chem. Phys.* **2024**, *160* (11), 114306.

(5) Panthakkal Das, P.; Mazumder, A.; Rajeevan, M.; Swathi, R. S.; Hariharan, M. Energy

Landscape of Perylenediimide Chromophoric Aggregates. *Phys. Chem. Chem. Phys.* **2024**, *26* (3), 2007–2015.

(6) Krishna, P. E. S.; Baiju, H.; Hariharan, M. Thermally Activated Delayed Fluorescence in Aminoacene-Linked Phenanthroline. *Phys. Chem. Chem. Phys.* **2025**, *27* (31), 16301–16305.

(7) Solomon, R. V.; Veerapandian, P.; Vedha, S. A.; Venuvanalingam, P. Tuning Nonlinear Optical and Optoelectronic Properties of Vinyl Coupled Triazene Chromophores: A Density Functional Theory and Time-Dependent Density Functional Theory Investigation. *J. Phys. Chem. A* **2012**, *116* (18), 4667–4677.

(8) Panneerselvam, M.; Kathiravan, A.; Solomon, R. V.; Jaccob, M. The Role of π-Linkers in Tuning the Optoelectronic Properties of Triphenylamine Derivatives for Solar Cell Applications – A DFT/TDDFT Study. *Phys. Chem. Chem. Phys.* **2017**, *19* (8), 6153–6163.

(9) Lyu, R.; Huang, Z.; Deng, H.; Wei, Y.; Chen, J.; Zhong, K.; Wang, R.; Mou, C.; Wang, L. Exploration for the Optical Properties and Fluorescent Prediction of Nitrotriazole and Nitrofurazan: First-Principles and TD-DFT Calculations. *ACS Omega* **2022**, *7* (23), 19694–19705.

(10) Kulhánek, J.; Klikar, M.; Pytela, O.; Růžičková, Z.; Bureš, F. Ferrocene Donor Linked to Pyridine/Pyridinium Acceptor via a Systematically Enlarged π-Linker. *RSC Adv.* **2021**, *11* (61), 38804–38813.

(11) Solomon, R. V.; Jagadeesan, R.; Vedha, S. A.; Venuvanalingam, P. A DFT/TDDFT Modelling of Bithiophene Azo Chromophores for Optoelectronic Applications. *Dye. Pigment.* **2014**, *100*, 261–268.

(12) Leenaers, P. J.; Maufort, A. J. L. A.; Wienk, M. M.; Janssen, R. A. J. Impact of π-Conjugated Linkers on the Effective Exciton Binding Energy of Diketopyrrolopyrrole–Dithienopyrrole Copolymers. *J. Phys. Chem. C* **2020**, *124* (50), 27403–27412.

(13) Rani, A.; Zafar, F.; Hussain, R.; Adnan, M.; Iqbal, J.; Zafar, W.-U.-I.; Noureen Shahi, M.; Kousar, S. Impact of π-Linker Modifications on the Photovoltaic Performance of Organic Solar Cells: A Theoratical Perspective. *Comput. Theor. Chem.* **2023**, *1225*, 114137.

(14) Lyakurwa, M.; Numbury, S. B. DFT and TD-DFT Study of Optical and Electronic Properties of New Donor–Acceptor–Donor (D–A–D′) Monomers for Polymer Solar Cells. *Oxford Open Mater. Sci.* **2023**, *3* (1), itad003.

(15) Gierschner, J.; Shi, J.; Milián-Medina, B.; Roca-Sanjuán, D.; Varghese, S.; Park, S. Luminescence in Crystalline Organic Materials: From Molecules to Molecular Solids. *Adv. Opt. Mater.* **2021**, *9* (13), 2002251.

(16) Ghora, M.; Manna, R. K.; Park, S. K.; Oh, S.; Kim, S.-I.; Park, S. Y.; Gierschner, J.; Varghese, S. Molecular Packing Topology and Interactions to Decipher Mechanical

Compliances in Dicyano-Distyrylbenzene Derivatives. *Chem. – A Eur. J.* **2024**, *30* (45), e202401023.

(17) Yamamoto, N. Mechanisms of Aggregation-Induced Emission and Photo/Thermal E/Z Isomerization of a Cyanostilbene Derivative: Theoretical Insights. *J. Phys. Chem. C* **2018**, *122* (23), 12434–12440.

(18) Yamamoto, N. Free Energy Profile Analysis to Identify Factors Activating the Aggregation-Induced Emission of a Cyanostilbene Derivative. *Phys. Chem. Chem. Phys.* **2021**, *23* (2), 1317–1324.

(19) Spackman, M. A.; Jayatilaka, D. Hirshfeld Surface Analysis. *CrystEngComm* **2009**, *11* (1), 19–32.

(20) Peccati, F. NCIPLOT4 Guide for Biomolecules: An Analysis Tool for Noncovalent Interactions. *J. Chem. Inf. Model.* **2020**, *60* (1), 6–10.

(21) Femina, C.; Shanthil, M.; Sajith, P. K.; Thomas, R. Anthracene-Incorporated Cyanostilbene Based Donor–Acceptor Systems: Intramolecular Charge Transfer and Aggregation Induced Emission. *New J. Chem.* **2023**, *47* (29), 13810–13819.

(22) Femina, C.; Sajith, P. K.; Remya, K.; Thomas, R.; Solomon, R. V. Theoretical Insights into the Structural and Optical Properties of D−π–A-Based Cyanostilbene Systems of α and β Variants. *ACS Omega* **2024**, *9* (21), 22764–22776.

(23) Johnson, E. R.; Keinan, S.; Mori-Sánchez, P.; Contreras-García, J.; Cohen, A. J.; Yang, W. Revealing Noncovalent Interactions. *J. Am. Chem. Soc.* **2010**, *132* (18), 6498–6506.

(24) Ramya, N. K.; Femina, C.; Suresh, S.; Mohanakumari, D. S.; Krishnan, R.; Thomas, R. Dicyanodistyrylbenzene Based Positional Isomers: A Comparative Study of AIEE and Stimuli Responsive Multicolour Fluorescence Switching. *New J. Chem.* **2022**, *46* (3), 1339–1346.

(25) Humphrey, W.; Dalke, A.; Schulten, K. VMD: Visual Molecular Dynamics. *J. Mol. Graph.* **1996**, *14* (1), 33–38.

(26) Chai, J.-D.; Head-Gordon, M. Long-Range Corrected Hybrid Density Functionals with Damped Atom–Atom Dispersion Corrections. *Phys. Chem. Chem. Phys.* **2008**, *10* (44), 6615–6620.

(27) Politzer, P.; Landry, S. J.; Waernheim, T. Proposed Procedure for Using Electrostatic Potentials to Predict and Interpret Nucleophilic Processes. *J. Phys. Chem.* **1982**, *86* (24), 4767–4771.

(28) Dar, A. A.; Lone, S. H.; Ahmad, I.; Ahangar, A. A.; Ganie, A. A.; Femina, C. Engineering the Solid-State Luminescence of Organic Crystals and Cocrystals. *Mater. Adv.* **2024**, *5* (3), 1056–1064.

(29) Suresh, C. H.; Remya, G. S.; Anjalikrishna, P. K. Molecular Electrostatic Potential Analysis: A Powerful Tool to Interpret and Predict Chemical Reactivity. *WIREs*

Comput. Mol. Sci. **2022**, *12* (5), e1601.

(30) Gadre, S. R.; Suresh, C. H.; Mohan, N. Electrostatic Potential Topology for Probing Molecular Structure, Bonding and Reactivity. *Molecules*. 2021.

Chapter 6

Theoretical Insight into the Structural and Optical Properties of D-π-A Based Cyanostilbene Systems of α and β Variants

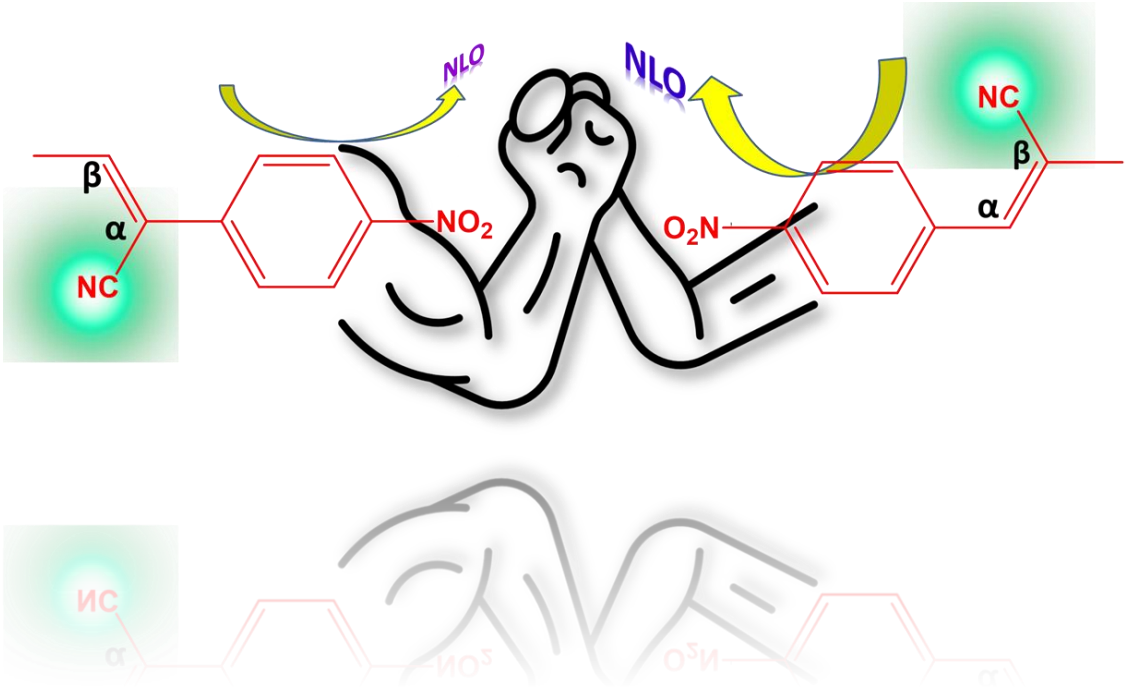

6.1 Abstract

The π-conjugated organic molecules containing cyanostilbene motifs have been extensively investigated due to their great potential applications in several optoelectronic and biological fields. Developing efficient molecules in this respect requires strategic structural engineering and a deep understanding of the structure-property relationship at the molecular level. In this context, understanding the impact of positional isomerism in cyanostilbene systems is a fundamental aspect of designing desired materials with improved photophysical properties. Herein, we designed ten donor-π-acceptor (D-π-A) type cyanostilbene derivatives (**P_1** – **P_{10}**) with different π linkers and compared their structural and optoelectronic properties arising from the positional variations of -CN group (α and β- variations) through the utilization of density functional theory (DFT) and time-dependent DFT (TDDFT) methods. The topological analyses of the electron density are used to explain the relatively high stability of α isomer compared to that of β. Frontier molecular orbital analysis reveals that seventeen molecules tend to show a reduced HOMO-LUMO gap, and most of them showed a greater nonlinear optical (NLO) character compared to the parent molecule. TDDFT calculations indicate that β isomers show higher absorption maxima compared to their α counterparts. Amongst all the scrutinized molecules, the absorption maximum extended up to 602 nm for **P_9** and it possesses the highest first-order hyperpolarizability. This study sheds light on positional isomers and their reactivity, absorption spectra, and NLO properties of D-π-A type architecture that can be suitably tuned by appropriating the π-bridge for practical applications.

*__Publication based on this chapter__

Femina, C.; Sajith, P. K.; Remya, K.; Thomas, R.; Solomon, R. V. Theoretical Insights into the Structural and Optical Properties of D−π–A-Based Cyanostilbene Systems of α and β Variants. *ACS Omega* **2024**, *9* (21), 22764–22776.

6.2 Introduction

The functional architecture of cyanostilbene features π-conjugated backbones covalently attached to a cyano group.[1-8] The linkage of the -CN group at various positions in the stilbene skeleton serves as an effective strategy to modulate the photochemical properties of these compounds.[9-12] The resulting positional isomers are classified based on the location of the -CN group relative to the ethylenic double bond.[13-21] Attachment of the -CN group at the α-position gives rise to α-cyanostilbene, while substitution at the β-position leads to the formation of β-cyanostilbene.[3] This positional variation affects molecular packing and, consequently, the optical properties, as demonstrated in the studies by Zhang et al.[17] Yoon and colleagues demonstrated how such positional variations influence the control of photophysical properties in both solution and solid states.[4] Existing literature reveals a limited number of experimental studies that directly correlate this kind of positional variations in cyanostilbenes, with the observed differences in optical properties.[1-21] Moreover, the structural, energetic, and optical properties of the α- and β isomers of cyanostilbene remain unexplored, including from a theoretical perspective. In this context, a molecular level understanding gained through appropriate theoretical methodologies can provide valuable insights into the properties that are derived from cyano positional variations and thus offer a new direction for designing efficient optoelectronic materials.

The importance of D-π-A skeleton, in which a cyano moiety acts as the acceptor (A), was thoroughly discussed in the previous chapters. This kind of architecture of cyanostilbene serves as a simple and efficient model for a comprehensive understanding of cyano positional variations, due to its inherent flexibility in molecular design.[6,22–24] In this regard, Singh et al. recently synthesized various cyanostilbene incorporated D-π-A systems incorporating the 9,9-dimethyl-9H-fluoren-2-amine core unit, which exhibited excellent NLO performance.[30–32] This provides a new design strategy for structurally tuning D-π-A systems to develop improved NLO candidates through the proper selection of organic heterocyclic luminophores.[33–40] More importantly, it can serve as an ideal model for investigating the impact of positional isomerism in cyanostilbene derivatives.[29,40]

6.3 Scope of the present investigation

In recent years, organic heterocyclic luminophores have attracted significant attention and achieved remarkable progress as emerging functional materials. These advances inspired us to

computationally design cyanostilbene-based NLO materials incorporating different heterocyclic rings as π-linkers. Furthermore, such systems provide an excellent platform for probing the influence of positional isomerism in cyanostilbene derivatives. Guided by these considerations, the present chapter discuss a systematic comparative investigation of the structural features, orbital distributions, and relative stabilities of the α- and β-isomeric forms (hereafter referred to as '**a'** and '**b'** analogs, respectively) of various cyanostilbene derivatives using density functional theory (DFT) calculations. For this purpose, a series of cyanostyryl-appended D-π-A systems with diverse π-linkers were designed. Their absorption behaviours were carefully analyzed through time-dependent DFT (TDDFT) calculations. In addition, the effect of different π-linkers on the NLO responses of the designed molecules was thoroughly examined. To gain deeper insights into structure–property relationships, Bader's quantum theory of atoms in molecules (QTAIM),[41,42] non-covalent interaction (NCI),[43] and molecular electrostatic potential (MESP)[44] analyses were also performed. This work aims to establish the structure–property relationships governing cyanostilbene derivatives, with particular emphasis on how π-linkers and positional isomerism affect their optical and electronic responses. The insights gained are intended to guide the rational design of stable and efficient NLO-active materials at the molecular level.

6.4 Theoretical calculations

All DFT and TDDFT calculations are performed using the Gaussian 16 suite of programs.[45] The geometry optimizations followed by frequency calculations of all molecules are done in the gaseous state at the B3LYP/6-31+G(d,p) level of theory.[46,47] Vibrational frequency calculations confirm that all the reported geometries correspond to true minima, ensuring the absence of imaginary frequencies.

The frontier molecular orbital (FMO) analysis is done with the optimized geometries of the designed molecules and FMOs are plotted using the Chemcraft software.[48] QMForge program[49] is used for the FMO percentage analysis to understand the role of the donor, acceptor, and the π-bridge towards the stabilization of HOMO and LUMO of these molecules.

From the optimized geometries, the topological analyses of the designed molecules are performed using the B3LYP/6-31+G(d,p) method. The wfn files generated from the Gaussian outputs are used for this purpose. Noncovalent interaction (NCI)[43] and quantum theory of atoms in molecules (QTAIM)[42] analyses are computed using the Multiwfn[50] and AIMAll[51] software, respectively. The reduced gradient density (RDG) isosurface plots resulting from

NCI analysis are further visualized using the VMD package.[52]

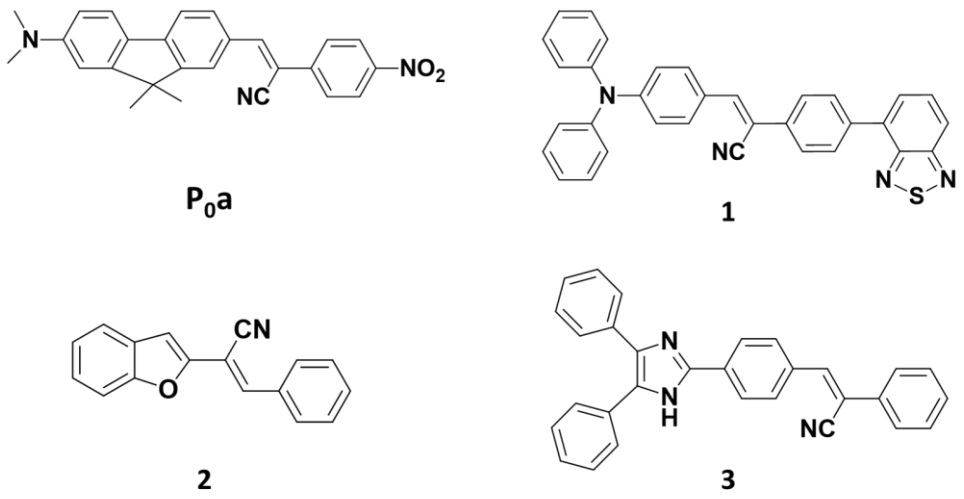

Figure 6.1 The molecules selected for the benchmark study.

The literature shows plenty of functionals capable of predicting the absorption maxima and therefore it is highly essential to identify and validate the correct functional that can reproduce the experimental results in cyanostilbene systems. In this context, to identify the suitable functional to simulate the experimental absorption maxima (λ_{max}) in the solution state of these cyanostilbene derivatives, all computations including geometry optimizations and subsequent time-dependent DFT (TD-DFT) calculations were performed with different functionals *viz*. B3LYP, CAM-B3LYP,[53] PBE0,[54] and BMK[55] coupled with the 6-31+G(d,p) basis set. The SMD solvation model[56] with the relevant solvent reported in the experimental work was adopted for these calculations. Figure 6.1 shows the selected molecules (**P$_0$a**[23], **1**[10], **2**[11], and **3**[14]) for the simulation of absorption spectra. The graphical comparison of the absorption maxima (λ_{max}) obtained using different functionals calculated at the TD/DFT/SMD/6-31+G(d,p) level is displayed in Figure 6.2. It is clear from Figure 6.2 that the BMK is the best functional for the simulation of absorption spectra since it gives λ_{max} values that are consistently in agreement with the experimental values. Indeed, the CAM-B3LYP results are closer to the experimental results of the three systems, but **P$_0$a** shows a significant deviation. This suggests that the BMK method is better suited to TDDFT calculations for the present study. In addition, there have been some previous reports suggesting the use of the BMK method for the study of absorption spectra in organic compounds.[57,58] In fact, Table 6.1 shows that the λ_{max} calculated at the TD-BMK/ SMD/6-31+G(d,p) level from the gas phase optimized geometries of B3LYP/6-31+G(d,p) agrees well with the experimentally observed

λ_{max}. Subsequently, this methodology was adopted herein for the computation of the vertical excitations and oscillator frequency. The simulated absorption spectral data are analyzed with the GaussSum software.[59]

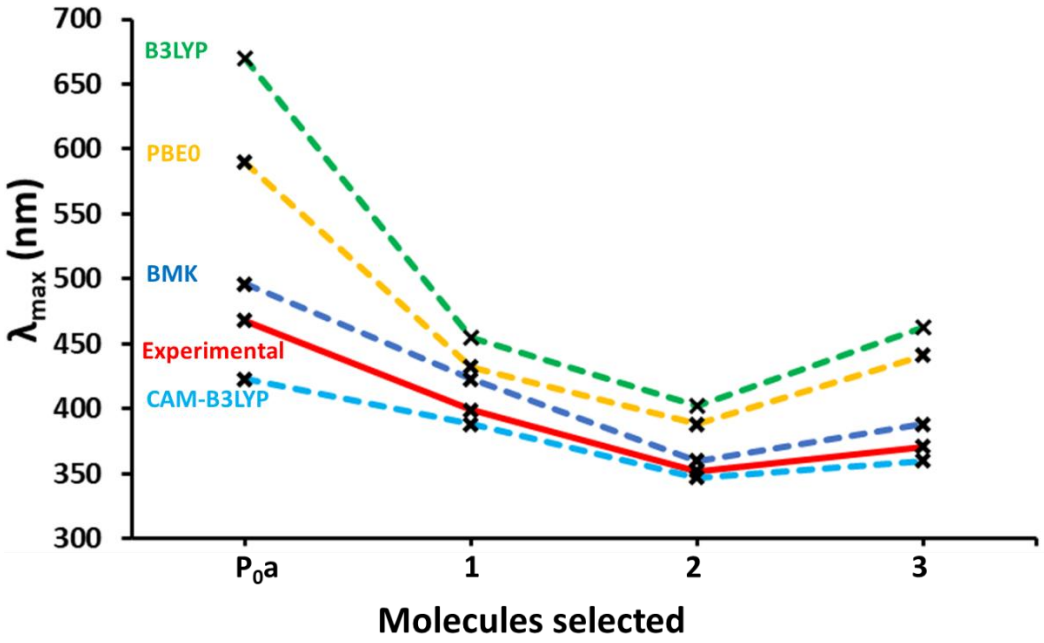

Figure 6.2 Graphical comparison of the experimentally reported absorption maxima of selected molecules with the corresponding simulated values. Solid curve corresponds to the experimentally reported values, and broken curves represent simulated values obtained using different functionals.

The optimized geometries at the B3LYP/6-31+G(d,p) level were used to compute first and second-order hyperpolarizabilities to characterize the NLO activity of the designed molecules. The first-order hyperpolarizability (β_0), described by a 3 × 3 × 3 matrix, is computed from the x, y, and z hyperpolarizability tensor components using the equation (1).[60]

$$\beta_0 = [(\beta_{xxx}+\beta_{xyy}+\beta_{xzz})^2 + (\beta_{yyy}+\beta_{yzz}+\beta_{yxx})^2 + (\beta_{zzz}+\beta_{zxx}+\beta_{zyy})^2]^{1/2} \quad \text{(Eq. 6.1)}$$

Second-order hyperpolarizability (γ) is calculated from its components using the equation (2).[60]

$$\gamma = 1/5\ [\gamma_{xxxx}+\gamma_{yyyy}+\gamma_{zzzz}+2(\gamma_{xxyy}+\gamma_{yyzz}+\gamma_{xxzz})] \quad \text{(Eq. 6.2)}$$

Table 6.1 The experimental and calculated absorption maxima (λ_{max}) of selected molecules. The gas phase optimized geometries at the B3LYP/6-31+G(d,p) level were used for the TDDFT calculations.

Molecule	Solvent used	Experimental λ_{max} (nm)	TD/BMK/SMD /6-31+G(d,p) calculated λ_{max} (nm)
P_0a	Dichloromethane	468[23]	486
1	Tetrahydrofuran	399[10]	428
2	Trichloromethane	352[11]	365
3	Dichloromethane	371[14]	396

6.5 Results and discussion

Twenty different D-π-A systems derived from an experimentally reported structure **P_0a** (Figure 6.3(A))[30,31] are designed and considered for the present study. All the designed molecules are cyanostyryl-based structures with a dimethylamino group as the donor and a cyano-substituted nitrostyryl group as the acceptor part. The cyano group here functions as an additional electron-withdrawing group on the D-π-A structure. The initial geometry of the reference molecule **P_0a** is taken from the X-ray crystallographic data.[30] Molecules with ten different spacer groups (π bridges, designated as **L_n**), each having '**a**' and '**b**' forms with respect to the position of the -CN group, as shown in Figure 6.3 (B), have been included in the study. Hence, a total of twenty D-π-A architectures have been examined to understand the role of π-linkers as well as the positioning effect of the -CN group on their structural and optoelectronic properties. In addition, the reference compound **P_0a** and its positional isomer **P_0b** are also considered for comparison. The different spacer groups (L_0 – L_{10}) used in designing the D-π-A systems are shown in Figure 6.4. The selected spacer groups include aromatic π conjugated systems of phenyl-based and heterocyclic rings containing heteroatoms such as nitrogen, oxygen, and sulphur.[61,62]

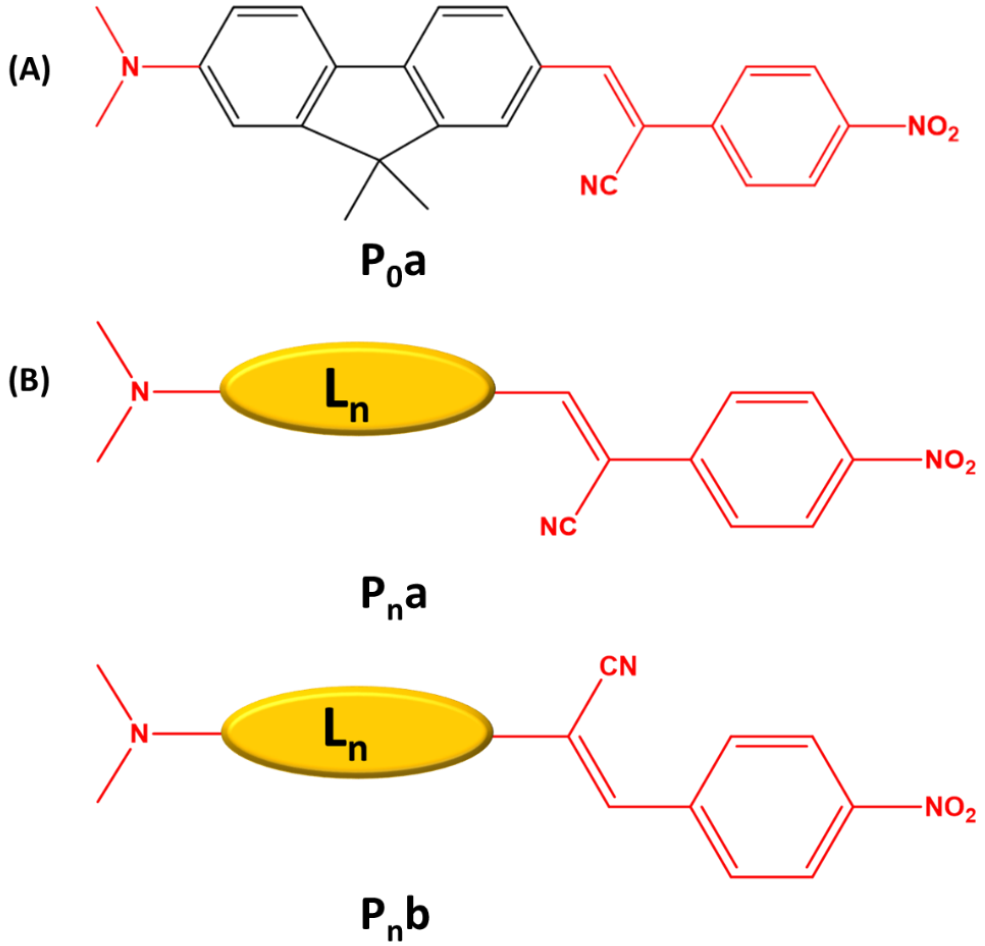

Figure 6.3 (A) Reference system considered (B) The isomers ('**a**' and '**b**' variants) investigated in this study.

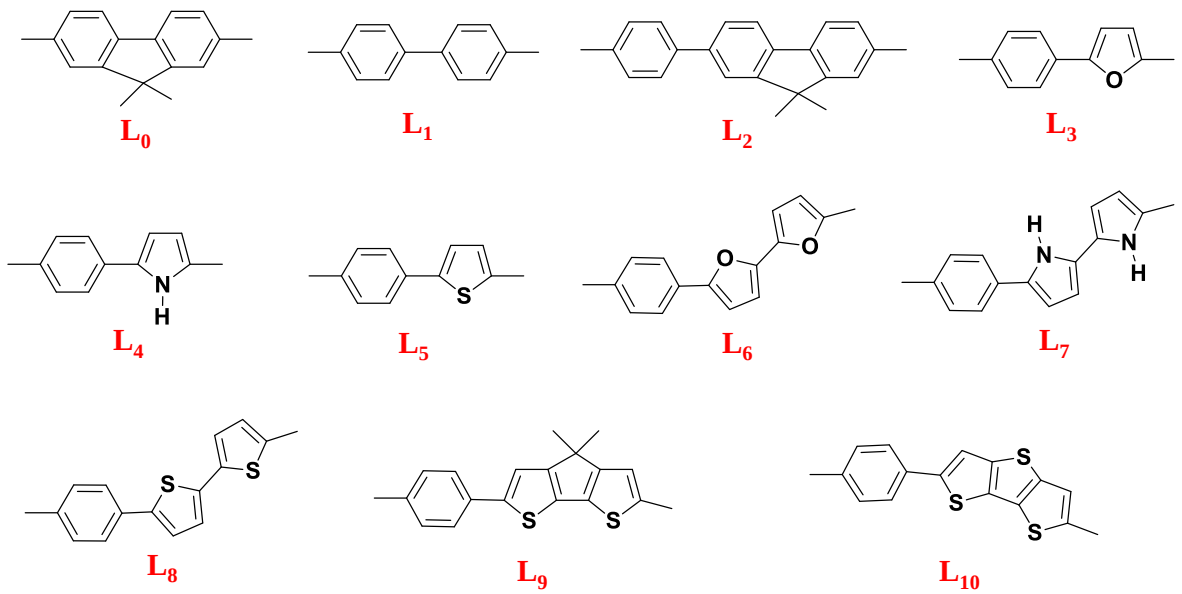

Figure 6.4 Sketches of the π-spacers used for the study.

6.5.1 Optimized molecular geometries

Optimized geometries of four representative molecules *viz*. **P_1a**, **P_1b** (with no heteroatom in the spacer group), **P_3a**, and **P_3b** (with oxygen as the heteroatom in the spacer group) are shown in Figure 6.5. As can be seen in the figure, **P_na** and **P_nb** possess the same D-π-A backbone, with only a difference in the position of the -CN group. The computed dihedral angles ϕ_1 and ϕ_2, as indicated in Figure 6.5, have been considered for analyzing the planarity of the systems under study. ϕ_1 is the $C\alpha C_\beta C_1 C_2$ dihedral angle (where C_α and C_β are the α and β carbon atoms and to which the -CN group is attached in the '**a**' and '**b**' isomers, respectively, and C_1 and C_2 are two carbon atoms of the phenyl ring of the styryl group) and ϕ_2 is a C–C–C–C/X (where 'X' is the hetero atom) dihedral angle inside the spacer group, as illustrated in Figure 6.5. The dihedral angle ϕ_2 is not significant for the two **P_0** molecules because the spacer group **L_0** does not contain a phenyl ring that is connected to the remaining part of the π-spacer through a single bond. The ϕ_1 and ϕ_2 values of all the D-π-A systems under study are listed in Table 6.2. All the scrutinized molecules are distorted from planarity to different extents. As can be observed from Table 6.2, there is a significant decrease in the value of ϕ_1 (~ 10 to 20 degrees) in the '**b**' series, as compared to the '**a**' series, indicating a remarkable increase in planarity as the position of the -CN group changes from '**a**' to '**b**' positions. The lower values ϕ_1 indicate less distortion of '**b**' forms and a slightly higher conjugation effect. Molecules such as **P_{10}b**, **P_9b**, **P_8b**, **and P_5b** having sulfur-containing heterocyclic rings possess very small ϕ_1 values (less than 1 degree) leading to more efficient π-delocalization in the backbone. The smaller values of dihedral angles for molecules with heteroatoms in their spacer groups indicate higher planarity in them compared to those without heteroatoms. As indicated by the small dihedral angles, **P_3b** and **P_6b**, both having furanoid rings in their spacer groups, possess the highest planarity. Among all the systems studied, **P_6** possesses the lowest ϕ_2. In all the designed molecules, the delocalization of π-electrons throughout the molecule is evident from the calculated geometrical parameters and dihedral angles.

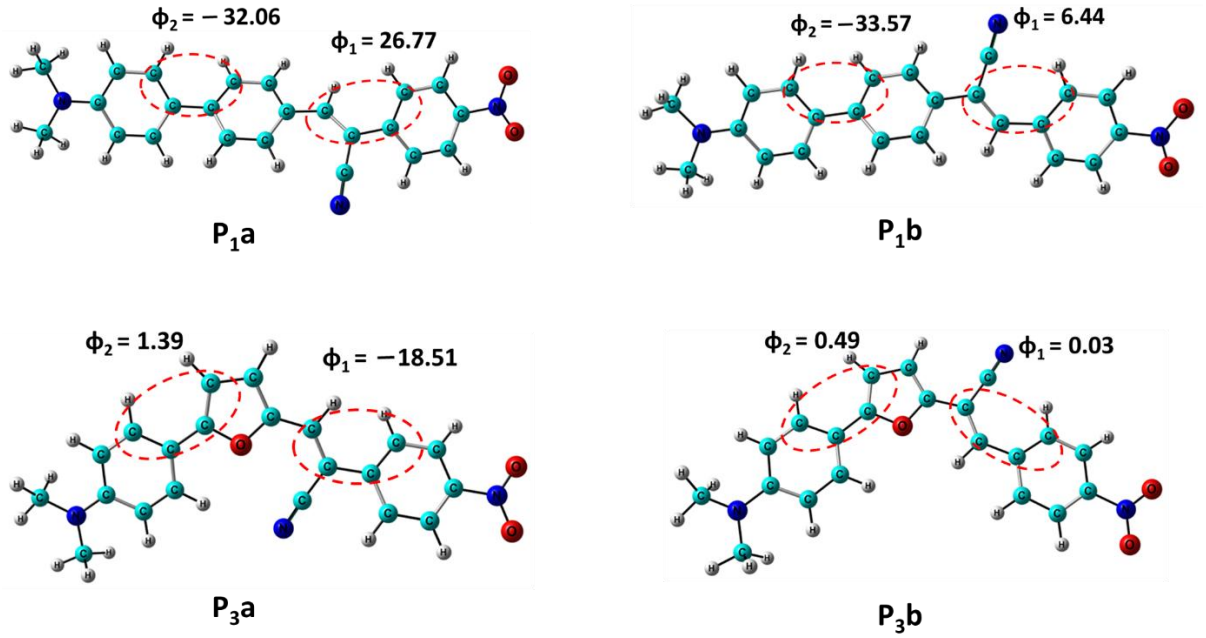

Figure 6.5 Optimized geometries of representative structures. The two dihedral angles ϕ_1 and ϕ_2 (in degrees) are also shown.

Analyzing the different bond lengths in the positional isomers has shown that in all the cases, the '**b**' isomer has a slightly shorter -C–N bond (Table 6.2). The increased planarity as indicated by dihedral angle and better π delocalization slightly increased the -C–N bond strengths in the '**b**' isomers.

The calculated dipole moments of all designed molecules are also presented in Table 6.2. From this table, it is clear that most of the molecules showed a higher dipole moment compared to the reference molecule **P0a** (12.51 D). Among all the scrutinized molecules, the highest dipole moment of 16.07 D is exhibited by **P9a**. The dipole moments of the isomers '**a**' and '**b**' are quite similar, indicating that the net molecular polarity is not much affected by positional changes.

Table 6.2 The dihedral angles, -C–N bond distance, and dipole moment of studied molecules along with ΔE_{ba} values.

Molecule	ϕ_1 (in degrees)	ϕ_2 (in degrees)	-C–N distance (Å)	Dipole moment (Debye)	ΔE_{ba} (kcal/mol)
P_0a	−25.61	……	1.166	12.51	2.1
P_0b	− 6.99	……	1.165	12.63	
P_1a	26.77	−32.06	1.165	12.10	1.2
P_1b	6.44	−33.57	1.165	11.69	
P_2a	−26.59	−36.02	1.166	11.87	1.7
P_2b	7.36	−36.46	1.165	12.31	
P_3a	−18.51	1.39	1.166	11.98	2.4
P_3b	0.03	0.49	1.164	12.94	
P_4a	12.30	7.08	1.168	12.43	7.4
P_4b	−2.96	23.91	1.164	13.49	
P_5a	20.71	18.09	1.166	13.13	2.2
P_5b	− 0.43	21.57	1.164	13.35	
P_6a	−18.67	− 0.10	1.166	14.12	2.0
P_6b	− 0.04	− 0.10	1.164	14.19	
P_7a	−12.29	−25.41	1.168	14.74	7.1
P_7b	−2.82	−25.85	1.164	14.65	
P_8a	−20.57	23.57	1.166	14.59	2.2
P_8b	0.10	−24.66	1.164	14.49	
P_9a	18.61	23.85	1.166	16.07	2.5
P_9b	− 0.25	24.59	1.164	15.43	
P_{10}a	21.17	25.12	1.166	14.33	2.0
P_{10}b	− 0.06	26.00	1.164	14.45	

6.5.2 Relative stabilities of ‘a’ and ‘b’ forms

Next, the energies of the isomeric structures '**a**' and '**b**' were examined to assess their relative stability. The difference in energy between the isomers ‘**b**’ and ‘**a**’ (denoted as ΔE_{ba}; given in Table 6.2) is noted. In all cases, ΔE_{ba} is positive, indicating that the isomer ‘**a**’ is more stable than ‘**b**’. This may be attributed to the possibility of additional intramolecular interactions in the ‘**a**’ isomer, which needs to be further confirmed by analyzing the electron density topology analyses. ΔE_{ba} values in all cases are compared with the help of bar diagrams provided in Figure 6.6. It is obvious that **P_4a** and **P_7a** exhibit more stability (ΔE_{ba} values of 7.4 kcal/mol and 7.1 kcal/mol, respectively) than the corresponding ‘**b**’ analog. The lowest ΔE_{ba} value of 1.2 kcal/mol is noted for **P_1** isomers.

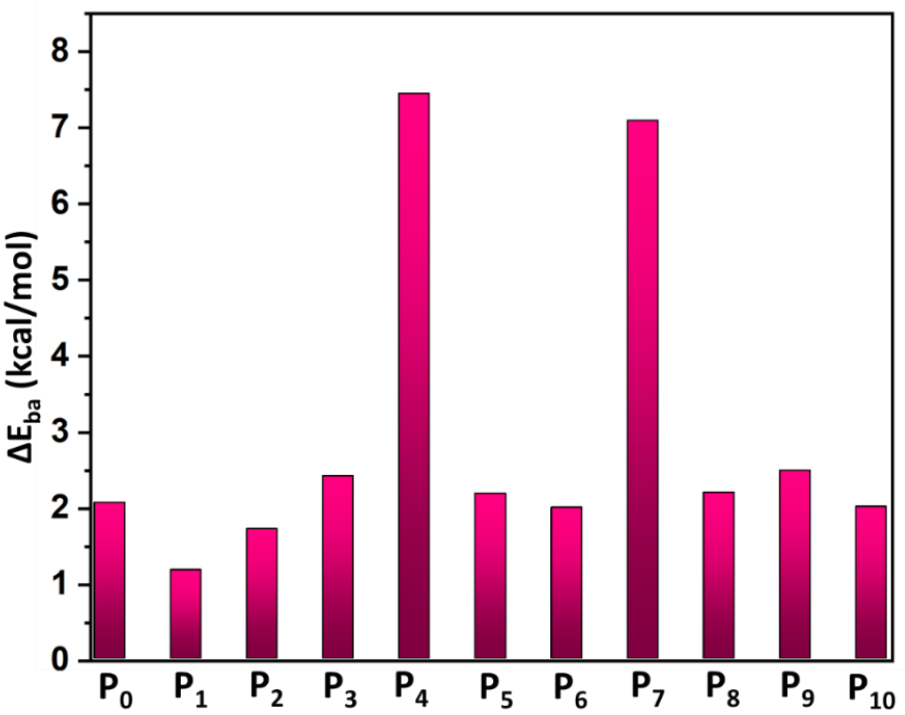

Figure 6.6 Bar chart representation of the calculated ΔE_{ba} values of the studied molecules.

6.5.3 NCI and QTAIM Analysis

NCI and QTAIM analyses serve as a valuable tool to identify, visualize, and quantify various inter and intramolecular chemical interactions present in molecular systems.[636–65] We further performed NCI and QTAIM analyses to unravel various noncovalent interactions present within the designed molecules. As seen in Figure 6.7, the reduced density gradient (RDG) isosurfaces resulting from the NCI analysis of the representative isomeric pairs **P4** and **P7** are shown. The color scheme and the area of the isosurface serve as a convenient means of understanding the nature of non-covalent interactions.[43] For instance, the red-coloured zones correspond to repulsive interaction, whereas the green-coloured zones are indicative of weak van der Waals interactions. In Figure 6.7, the appearance of green zones shows the attractive intramolecular interactions present in these systems. A close examination of the NCI isosurface indicates that the '**a**' isomers have a slightly larger area of green isosurfaces compared to their '**b**' counterparts, particularly around the -CN centers. This shows that the attractive intramolecular interactions present in the '**a**' isomer are greater compared to the '**b**' isomer.

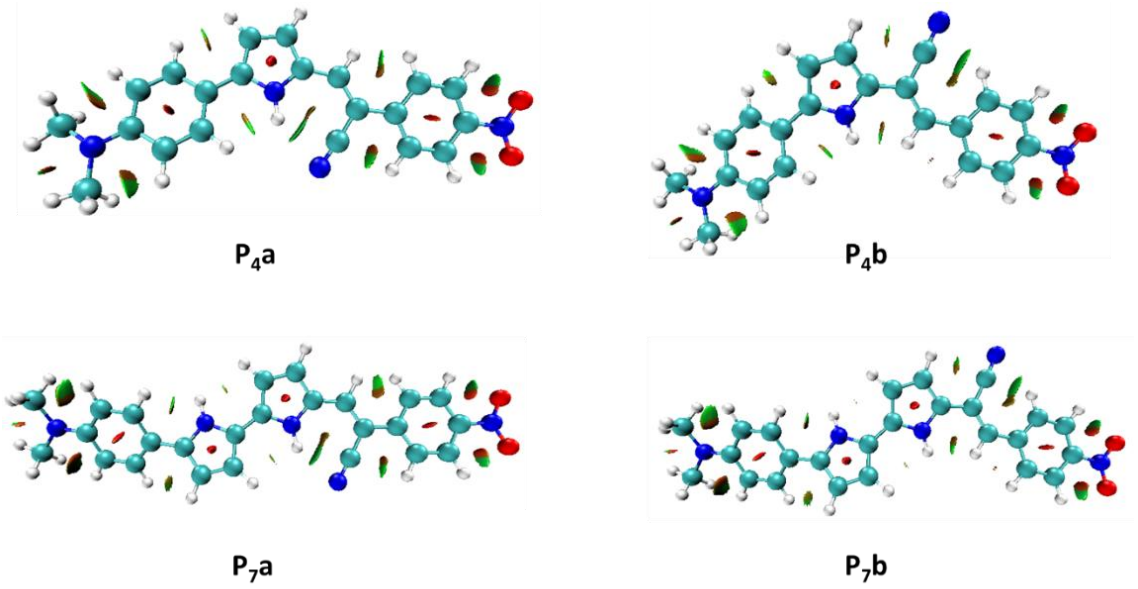

Figure 6.7 NCI- RDG isodensity surface plot (isovalue = 0.50 au) of **P4** and **P7** isomers.

On the other hand, the QTAIM analysis uncovers not only the occurrence of intramolecular noncovalent interactions but also the nature of such interactions through the appearance of (3,-1) bond critical points (BCPs).[66,67] These BCPs are characterized by the corresponding electron density (ρ) values. As representative systems, the QTAIM features of two pairs of isomers *viz*. **P4** (‘**a**’ and ‘**b**’) and **P7** (‘**a**’ and ‘**b**’) are displayed in Figure 6.8. **P4a** isomer possesses intramolecular interaction between the H (from the N–H group in the spacer group) and the -C–N group with a ρ at the BCP of 0.01482 au. The -CH(phenyl)…CN interaction (ρ = 0.01282 au) is evident in the QTAIM molecular graph of **P4b**. For ‘**a**’, ρ value is larger than that of the ‘**b**’ isomers indicating the stronger interaction present in ‘**a**’. In addition, the existence of another BCP corresponding to CH…HC contact is evident in the ‘**a**’ isomer for both **P4** and **P7**. Thus, in line with the NCI plots, the QTAIM analysis clearly suggests that stronger intermolecular interactions are present in ‘**a**’ compared to their ‘**b**’ counterparts; this corroborates the higher ΔE_{ba} values obtained for **P4** and **P7** and thus explains the relatively higher stabilities of ‘**a**’ isomers.

The increased intramolecular interactions of -C–N present in the ‘**a**’ isomer decrease the -C–N bond strength, and consequently the value of ρ at the BCP of -C–N of ‘**a**’ (ρ_{CN}(**a**)) is found to be smaller than their ‘**b**’ counterparts (ρ_{CN}(**b**)), in all cases. ρ_{CN}(**a**) and ρ_{CN}(**b**) values of **P4** and **P7** given in Figure 6.8 in green color. The difference in ρ values at the BCP of -C–N between ‘**b**’ and ‘**a**’ ($\Delta\rho = \rho_{CN}$(**b**) – ρ_{CN}(**a**)) roughly correlates with the ΔE_{ba} values (See Figure

6.9 and Table 6.3). This further confirms that the relatively high stability of the '**a**' isomer originates from intramolecular interactions.

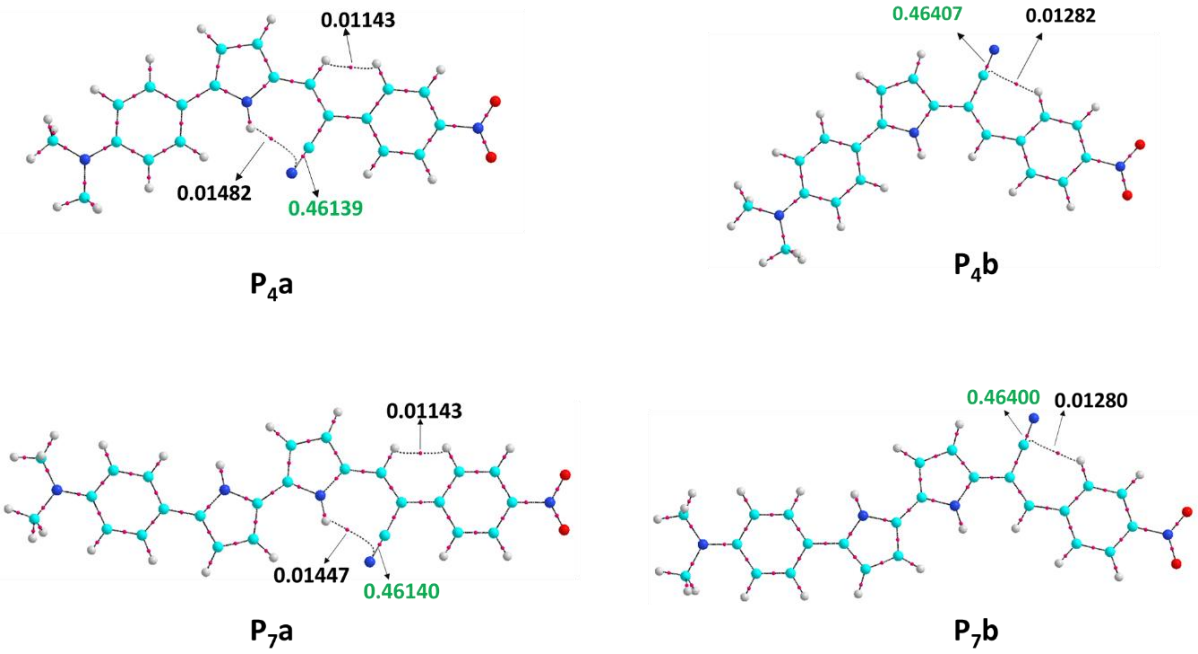

Figure 6.8 QTAIM features (ρ values in au) at the BCP of the relevant bond paths of both isomers of **P4** and **P7**. Small red circles represent the BCPs.

Table 6.3 The electron density (ρ) at the bond critical point (BCP) of -C–N bond and the corresponding Δρ.

Molecule	ρ(in au)		Δρ (au)
	a	**b**	
P0	0.46262	0.46361	0.00099
P1	0.46287	0.46360	0.00073
P2	0.46280	0.46360	0.00079
P3	0.46227	0.46395	0.00168
P4	0.46139	0.46407	0.00268
P5	0.46223	0.46380	0.00157
P6	0.46232	0.46393	0.00161
P7	0.46140	0.46400	0.00260
P8	0.46225	0.46380	0.00155
P9	0.46197	0.46377	0.00180
P10	0.46228	0.46380	0.00153

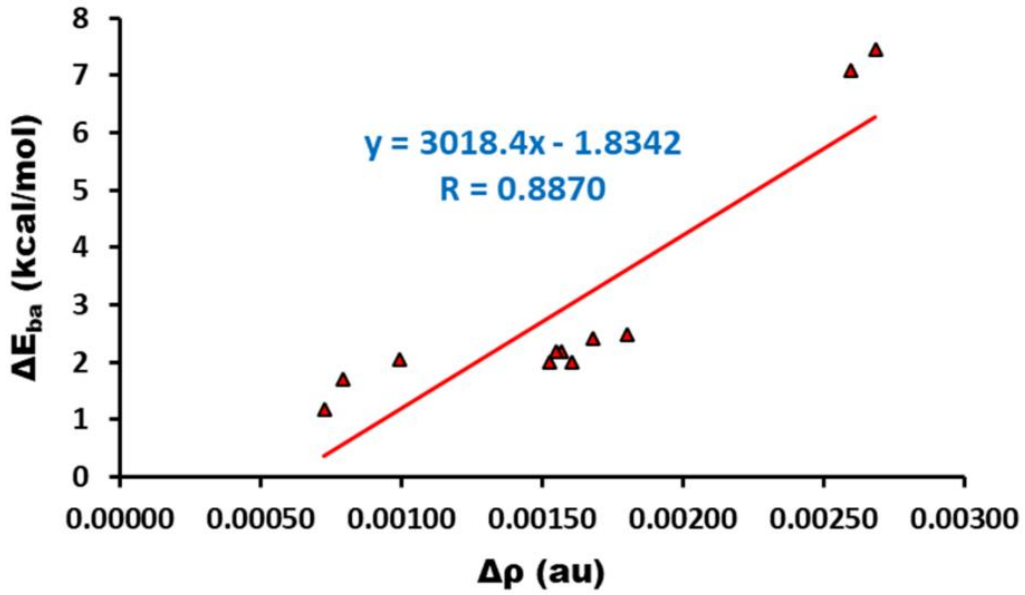

Figure 6.9 Correlation between Δρ and ΔE_{ba}.

6.5.4 Molecular electrostatic potential (MESP) surfaces

The MESP maps provide valuable information about the region around a molecule where an electrophilic and nucleophilic attack is possible.[68] It also gives an idea about the possible noncovalent interaction of molecules with their surroundings.[69,70] The MESP isosurfaces of the two isomers of representative systems (**P_4** and **P_7**) are shown in Figure 6.10. The highest negative potential (red region) is located mainly around oxygen atoms of -NO_2 and N of the -CN group. The MESP isosurfaces shown in Figure 6.10 indicate that the positive electrostatic potential regions (blue-colored regions) are dispersed around the H atoms present in the molecule. The possibility of intramolecular interaction between -CN and the nearby -NH region of pyrrole is evident from the negative and positive charge localization of the corresponding moieties of the '**a**' isomer (Figure 6.10).

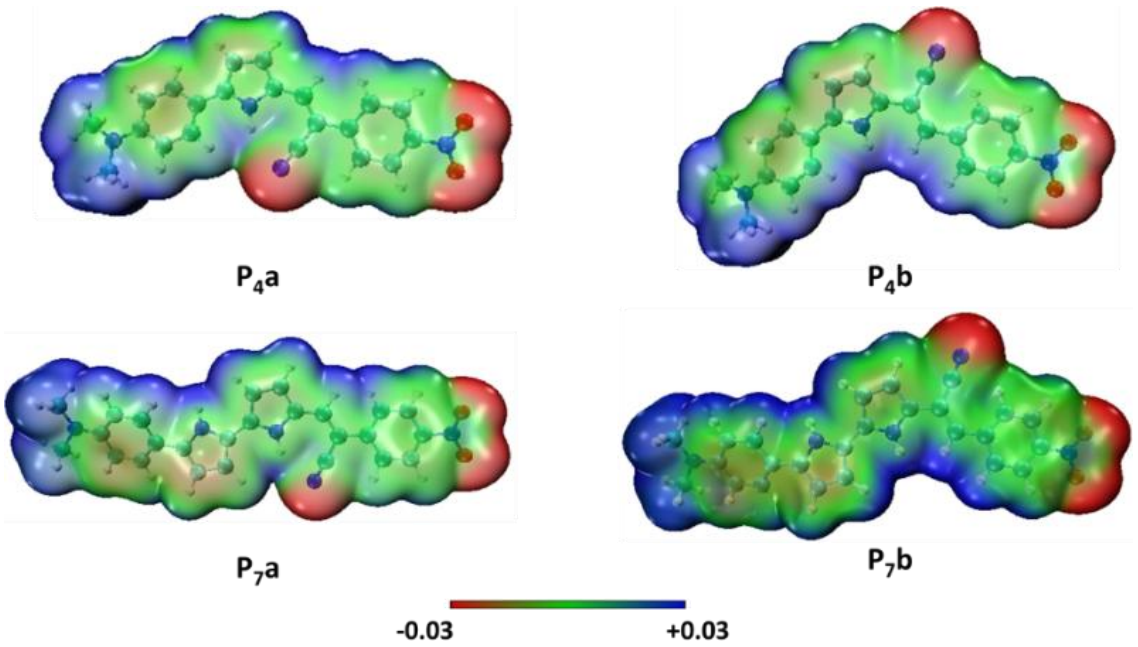

Figure 6.10 MESP distribution of **P4** and **P7** isomers represented on the 0.001 au electron density surface with color codes ranging from –0.03 (red) to 0.03 au (blue).

6.5.5 Frontier Molecular Orbitals

It is well known that the frontier molecular orbital (FMO) analysis sheds light on the chemical reactivity, which in turn helps to estimate the optoelectronic properties of D-π-A systems.[714,72] Therefore, the FMOs such as highest occupied molecular orbital (HOMO) and lowest unoccupied molecular orbital (LUMO) obtained from the optimized geometries are studied. The calculated energies of HOMO and LUMO together with the HOMO-LUMO energy gap (ΔE_{HL}) are collected in Table 6.4. The '**a**' isomers show a wider ΔE_{HL} compared to their '**b**' counterpart (see Figure 6.11 for **P0** – **P3**, and the remaining in Figure 6.12). Among the 22 molecules, **P1a** is found to be the most stable molecule with ΔE_{HL} of 2.489 eV, which is higher than that of the reference molecule by 0.054 eV. Three molecules (**P1a, P4a & P5a**) show more stability than the reference molecule, and all other molecules, irrespective of '**a**' or '**b**' isomers, tend to show higher reactivity with reduced ΔE_{HL} compared to that of the reference molecule. Molecules such as **P6b, P7b,** and **P9b** show higher reactivity with lower ΔE_{HL} values of 1.960, 1.963, and 1.974 eV, respectively. Among '**a**' series, **P6a**, and **P7a** are highly reactive with ΔE_{HL} values 2.151 and 2.188 eV respectively. The reactivity increases when two heteroatoms are introduced into the molecular framework (**P6 − P9**) which is observed from the computed ΔE_{HL}. On the other hand, the introduction of two heteroatoms does not alter the energy of HOMO a lot but does impact the LUMO energy level. It is observed that HOMO of **P6a** and

P_6b lie in −5.214 and −5.216 eV which clearly tells that HOMO is almost unaffected by the position of the –CN group. However, the LUMO energy (−3.062 eV) of **P_6a** is altered to −3.257 eV when the position of the -CN group changes in the '**b**' isomer. The decreasing order of ΔE_{HL} in '**a**' isomer is as follows **P_1a** > **P_5a** > **P_4a** > **P_0a** > **P_3a** > **P_2a** > **P_{10}a** > **P_8a** > **P_9a** > **P_7a** > **P_6a** while the same for '**b**' isomer is **P_5b** > **P_1b** > **P_4b** > **P_3b** > **P_0b** > **P_2b** > **P_{10}b** > **P_8b** > **P_9b** > **P_7b** >**P_6b**. This clearly shows that irrespective of the position of the -CN group, the **P_6**, **P_7**, and **P_9** are potential candidates with excellent chemical reactivity.

Table 6.4 E_{HOMO}, E_{LUMO}, and E_{HL} values of the studied molecules. All values are in eV.

Molecule	E_{HOMO}	E_{LUMO}	ΔE_{HL}
P_0a	−5.448	−3.013	2.435
P_0b	−5.414	−3.213	2.200
P_1a	−5.578	−3.089	2.489
P_1b	−5.530	−3.280	2.250
P_2a	−5.385	−3.107	2.278
P_2b	−5.370	−3.289	2.081
P_3a	−5.392	−2.999	2.393
P_3b	−5.423	−3.206	2.218
P_4a	−5.353	−2.916	2.437
P_4b	−5.382	−3.138	2.244
P_5a	−5.502	−3.046	2.456
P_5b	−5.501	−3.244	2.257
P_6a	−5.214	−3.062	2.151
P_6b	−5.216	−3.257	1.960
P_7a	−5.109	−2.921	2.188
P_7b	−5.1056	−3.144	1.963
P_8a	−5.342	−3.141	2.201
P_8b	−5.326	−3.312	2.014
P_9a	−5.228	−3.030	2.199
P_9b	−5.181	−3.206	1.974
P_{10}a	−5.401	−3.141	2.260
P_{10}b	−5.375	−3.321	2.053

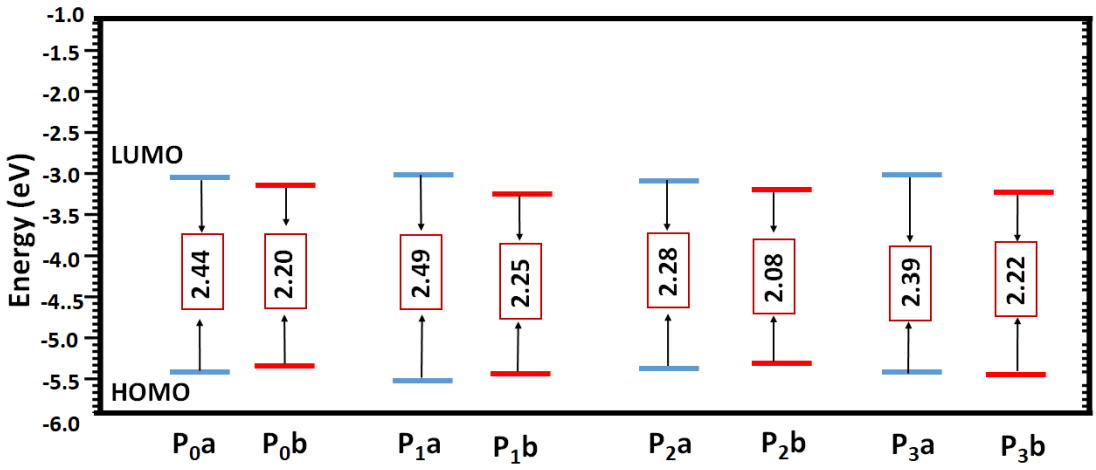

Figure 6.11 Frontier molecular orbital energy level diagram of '**a**' and '**b**' variants of **P0** - **P3**.

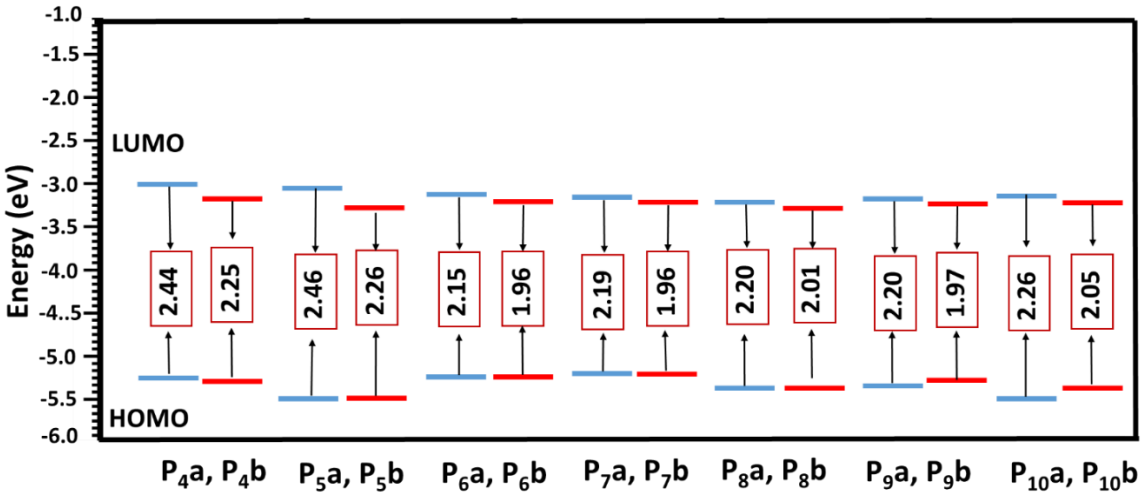

Figure 6.12 Frontier Molecular Orbital energy level diagram of designed molecules (**P4** to **P10**).

The frontier molecular orbitals such as HOMO and LUMO for both the isomers are collected in Figure 6.13. From the figure, it is clear that the HOMO occupies the donor and a part of the π-bridge (left-hand side) while LUMO spread through the acceptor unit and the other part of the π-bridge (right-hand side). It is interesting to note that in '**a**' isomers, the –CN group involves in the stabilization of both HOMO & LUMO while its role in the stabilization of HOMO in the '**b**' isomers is zero. Thus, the HOMO of the '**a**' isomers is very similar to that of the '**b**' isomer except for the contribution of the -CN group. However, the LUMO of '**b**' isomers is observed to be very similar to that of '**a**' isomers where -the CN group is involved in stabilization. Analyzing the HOMOs and LUMOs of these molecules indicates that there can be intramolecular charge transfer along with π- π* transitions. In some molecules, the π- π* transitions are expected to be predominant. For instance, the HOMO and LUMO of **P9a** are

lying on the most of the molecule compared to **P2a**. Thus, these molecules will tend to show both intramolecular charge transfer (ICT) and π- π* transitions in their absorption spectra.

Compound	a		b	
	HOMO	LUMO	HOMO	LUMO
P_0	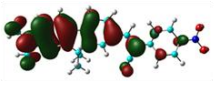	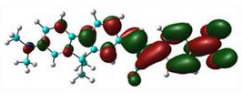	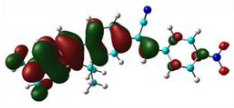	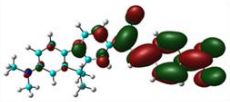
P_1	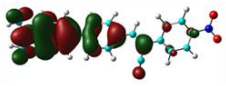	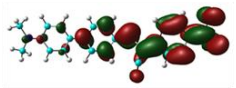	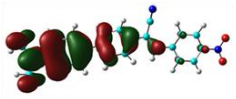	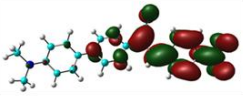
P_2	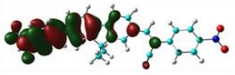	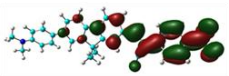	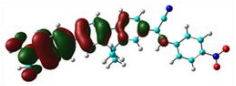	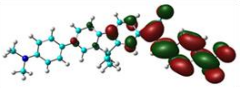
P_3	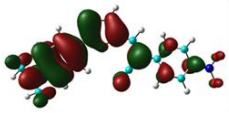	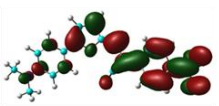	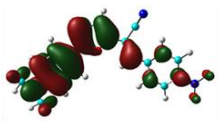	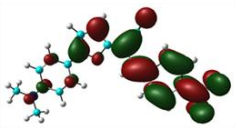
P_4	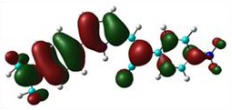	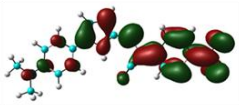	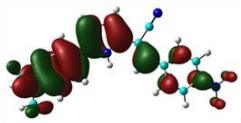	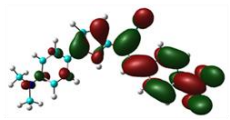
P_5	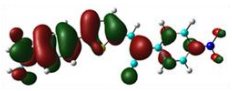	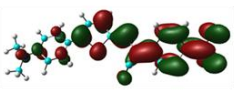	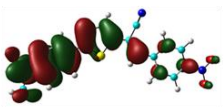	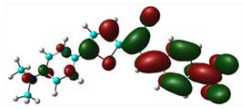
P_6	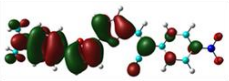	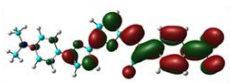	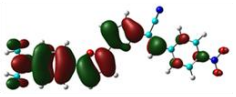	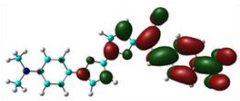
P_7	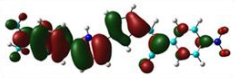	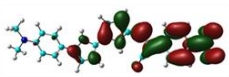	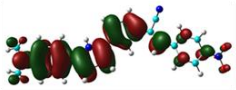	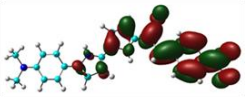
P_8		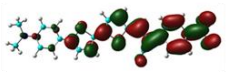	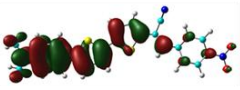	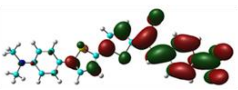
P_9		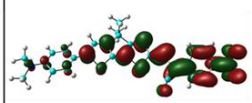		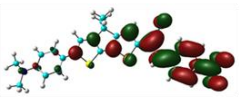
P_{10}				

Figure 6.13 Frontier molecular orbitals of the studied molecules.

To gain more insight into the frontier molecular orbitals, it is essential to understand how donor, acceptor, and π-bridge fragments contribute to the FMOs. The whole molecule is divided into three parts (donor, acceptor, and π-bridge), and their percentage contributions from these fragments towards HOMO and LUMO are calculated and summarized in Table 6.5 and Figure 6.14. In Figure 6.14, it is clear that the contribution of the donor unit to stabilising LUMO is very negligible (0.1–1%) while its contribution to HOMO varies from 2.5% to 23.4%. It is interesting to note that the donor's contribution to HOMO is higher in the '**b**' isomer compared to its '**a**' isomer except in **P$_{10}$b** where a slight edge (~0.1%) is observed. The results indicate that the LUMO gets much contributions from the acceptor unit and a poor contribution is rendered by the acceptor unit towards the stabilization of HOMO. For instance, the LUMO of **P$_6$b** is stabilized up to 83.5% by the acceptor unit while it gets only 9% towards HOMO. It is observed that the **P$_3$a**, **P$_5$a**, and **P$_6$a** molecules tend to get almost equal contributions from the acceptor unit for the stabilization of HOMO and LUMO. For example, the HOMO and LUMO of **P$_5$a** are stabilized by acceptor units almost equally (40.4 and 41.7%). Moving to the contribution of π-bridge, it can be inferred that HOMO is getting much contribution compared to LUMO. In particular, the HOMO of the '**b**' isomer largely benefited out of the π-bridge than the '**a**' isomer. In summary, this section portrays that the insertion of two heteroatoms tunes these molecules compared to those of one or none of the heteroatom-containing molecules.

Table 6.5 The percentage contributions of the fragments (donor, π-bridge, and acceptor) towards HOMO and LUMO (values given in %).

Molecule	Donor		π-bridge		Acceptor	
	HOMO	LUMO	HOMO	LUMO	HOMO	LUMO
P$_0$a	10.8	0.4	51.5	24.7	37.7	74.9
P$_0$b	16.8	0.2	70.7	38.4	12.5	61.4
P$_1$a	8.0	0.3	67.9	44.6	24.1	55.1
P$_1$b	12.3	0.1	80.1	66.0	7.6	33.9
P$_2$a	8.2	0.1	83.1	37.0	8.7	63.0
P$_2$b	10.1	0.0	81.8	44.2	8.1	55.7
P$_3$a	4.5	0.4	20.8	22.2	74.7	77.4
P$_3$b	23.4	1.0	62.3	13.8	14.4	85.2
P$_4$a	6.1	0.3	47.1	37.9	46.8	61.9
P$_4$b	12.5	0.2	69.1	71.2	18.4	28.6

P_5a	9.3	0.3	50.2	58.0	40.4	41.7
P_5b	10.6	0.4	68.9	54.2	20.5	45.4
P_6a	3.2	0.1	30.3	38.5	66.5	61.4
P_6b	17.5	0.4	73.5	16.2	9.0	83.5
P_7a	2.5	0.1	43.8	59.4	53.7	40.6
P_7b	8.0	0.1	85.1	58.7	7.0	41.2
P_8a	6.2	0.2	61.1	38.9	32.8	60.9
P_8b	7.1	0.3	88.5	28.0	4.3	71.7
P_9a	5.0	0.2	82.2	45.9	12.8	53.9
P_9b	5.3	0.3	90.3	60.8	4.4	39.0
P_{10}a	4.9	0.2	79.5	57.8	15.6	42.1
P_{10}b	4.8	0.2	74.8	68.8	20.4	31.1

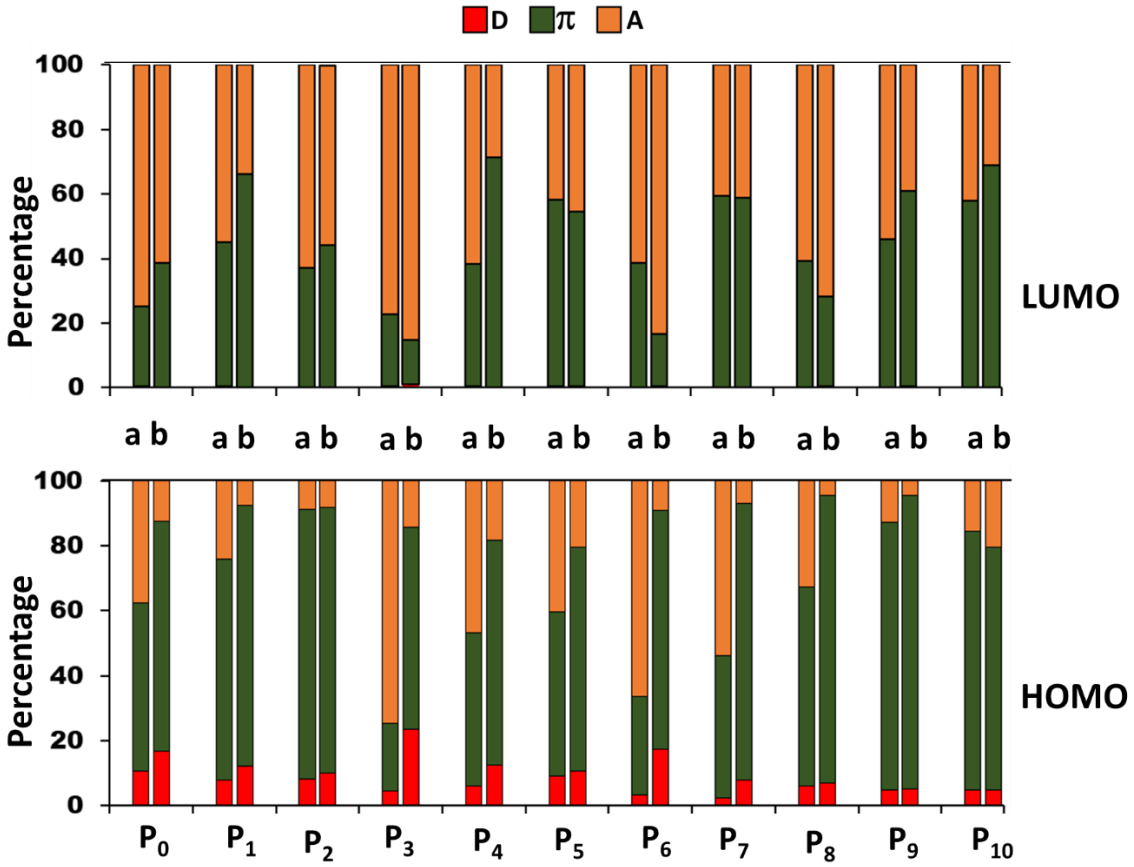

Figure 6.14 Percentage contributions of the fragments (donor, π-bridge, and acceptor) towards HOMO and LUMO of the studied molecules.

6.5.6 Absorption Spectra

It is important to note that the molecule's ability to exhibit a significant absorption maximum makes it a promising candidate for optoelectronic applications.[73,74] In this context, TDDFT calculations on the optimized geometries help us in forecasting a molecule's excited state

properties. Hence, TDDFT calculations have been conducted at the TD-BMK/SMD(dichloromethane)/6-31+G(d,p) level to compute the vertical singlet excitations to predict the absorption maxima with its oscillatory strength. This analysis further helps us to estimate the percentage contributions from FMOs towards various configurations of these excitations. The details of the absorption spectra of '**a**' and '**b**' isomers, obtained through TDDFT calculations, for all the systems under study, are compared in Table 6.6. The optical properties studied include the absorption maxima (λ_{max}), oscillator strength (f), and the percentage contribution of different transitions towards the absorption maxima. In the '**a**' isomer series, the calculated λ_{max} ranges from 459-565 nm while the same applies to the '**b**' isomers ranging from 476-602 nm, and all transitions are from $S_0 \rightarrow S_1$. In both cases, the **P**$_2$ molecule shows the lowest absorption maxima and **P**$_9$ is the one that shows the highest absorption maxima. As expected, the **P**$_6$**b**, **P**$_7$**b,** and **P**$_9$**b** molecules show exceptional λ_{max} values with more than 590 nm. In all the cases, the consistent red shift in the λ_{max} value in the '**b**' isomer compared to the '**a**' isomer shows an increased wavelength of absorption as the position of the -CN group changes from the '**a**' to the '**b**' position. The shift in λ_{max} value ranges from 15 nm (for the **P**$_1$**a** – **P**$_1$**b** isomer pair) to 52 nm (for the **P**$_7$**a** – **P**$_7$**b** isomer pair). This red shift in the absorption maximum can be attributed to the increase in planarity and the consequent increase in the effectiveness of π-delocalization. For instance, a 37 nm increase in λ_{max} is observed between the isomers '**a**' and '**b**' of **P**$_6$ and **P**$_9$. Another substantial increase in the λ_{max} is seen in **P**$_4$ and **P**$_3$ with 41 and 40 nm, respectively. It can be seen that the values of λ_{max} for all the cases lie in the visible range, making them advisable for solar cell applications. The oscillator strengths (f), a measure of the intensity of absorption, show higher values for '**a**' isomers in all the cases. The difference in f values ranges from 0.32 (for the **P**$_3$**a** – **P**$_3$**b** isomer pair) to 0.548 (for the **P**$_2$**a** – **P**$_2$**b** isomer pair). For example, one can witness the strong intense peak at 459 with an oscillatory strength of 1.315 for **P**$_2$**a** and the same in **P**$_2$**b** shows a less intense peak with an oscillatory strength of 0.767 for the 476 nm absorption. Hence, the intensity of absorption tends to be lower in the '**b**' isomer for all pairs of isomers under study though they tend to show longer λ_{max}. All these peaks are getting maximum contributions from HOMO→LUMO transitions for all these molecules and minor contributions (less than 10%) are from HOMO−1→LUMO. It is interesting to note that the HOMO→LUMO contributes to a higher percentage in the '**b**' isomer compared to that of the '**a**' isomer. For instance, an intense peak at 548 nm from **P**$_7$**a** arose due to 87% contribution from HOMO→LUMO while its percentage increased to 93% for the peak at 600 nm when the position –CN changes in **P**$_7$**b**. This trend is observed for all the molecules studied here. These HOMO→ LUMO transitions

can arise from the intramolecular charge transfer (ICT) coupled with π-π* transitions. For instance, **P_5a** tends to show a peak at 510 nm with 1.449 oscillator strength arising from HOMO→LUMO transition resulting from π-π* transitions and ICT. This trend is observed in almost all the molecules. The UV -absorption spectra of two pairs of '**a**' and '**b**' isomers *viz.* **P_5a** – **P_5b** pair and **P_6a** – **P_6b** pair in dichloromethane solvent are compared in Figure 6.15. The red shift in absorption maxima as well as the lowering of intensities in the '**b**' isomers can be clearly visualized in the figure.

Table 6.6 Maximum absorption wavelength (λ_{max}) along with oscillator strengths (f) and MO contribution of the studied molecules.

isomer '**a**'				isomer '**b**'			
Molecule	λ_{max} (nm)	f	MO contribution (in %)	Molecule	λ_{max} (nm)	f	MO contribution (in %)
P_0a	486	1.334	H→L (87) H→L+1 (8) H−1→L (4)	**P_0b**	515	0.834	H→L (93) H−1→L (3) H→L+1 (3)
P_1a	461	1.186	H→L (86) H−1→L (5) H→L+1 (8)	**P_1b**	481	0.728	H→L (92) H−1→L (4) H→L+1 (3)
P_2a	459	1.315	H→L (78) H→L (12) H→L+1 (7)	**P_2b**	476	0.767	H→L (86) H−1→L (10) H→L+1 (2)
P_3a	521	1.252	H→L (89) H−1→L (3) H→L+1 (7)	**P_3b**	561	0.932	H→L (95) H−1→L (2) H→L+1 (3)
P_4a	515	1.405	H→L (90) H−1→L (3) H→L+1 (6)	**P_4b**	556	1.034	H→L (95) H−1→L (3) H→L+1 (2)
P_5a	510	1.449	H→L (87) H−1→L (4) H→L+1 (8)	**P_5b**	540	1.086	H→L (93) H−1→L (3), H→L+1 (3)

P_6a	556	1.501	H→L (86) H−1→L (5) H→L+1 (7)	**P_6b**	593	1.088	H→L (92) H−1→L (5), H→L+1 (3)
P_7a	548	1.521	H→L (87) H−1→L (6) H→L+1 (6)	**P_7b**	600	1.098	H→L (93) H−1→L (4) H→L+1 (2)
P_8a	548	1.719	H→L (83) H−1→L (7) H→L+1 (8)	**P_8b**	567	1.327	H→L (87) H−1→L (7) H→L+1 (5)
P_9a	565	1.940	H→L (86) H−1→L (5) H→L+1 (7)	**P_9b**	602	1.501	H→L (90) H−1→L (5) H→L+1 (4)
P_{10}a	527	1.783	H→L (84) H−1→L (7) H→L+1 (7)	**P_{10}b**	552	1.336	H→L (88) H−1→L (7) H→L+1 (3)

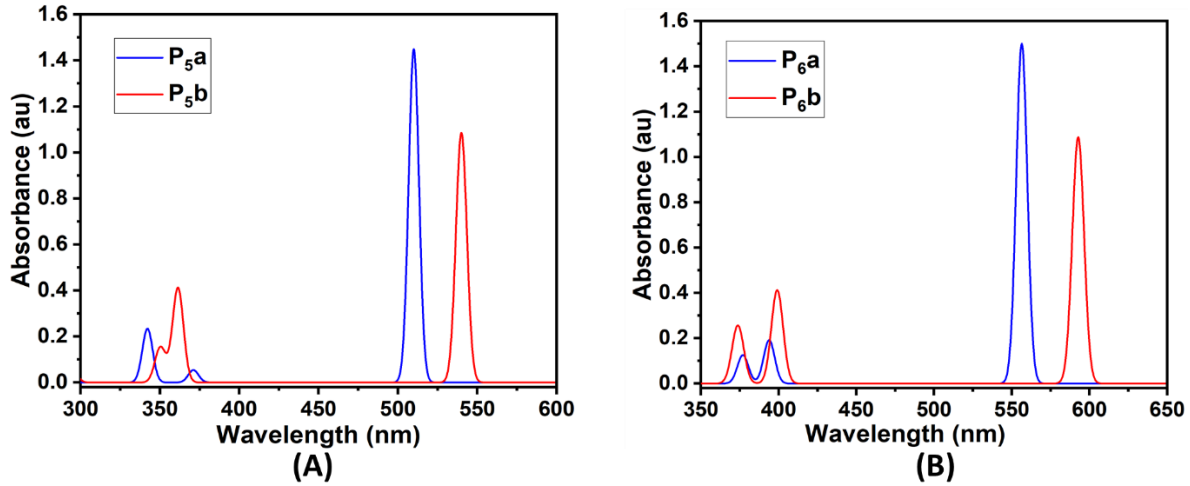

Figure 6.15 Comparison of simulated UV- absorption spectra of (A) **P_5a** & **P_5b** (B) **P_6a** & **P_6b**.

6.5.7 NLO Properties

The Nonlinear Optical (NLO) behavior of a molecule occurs due to the oscillation of molecular electrons when subjected to a fluctuating field, like electromagnetic radiation.[75–77]

Consequently, this induces polarization within the molecule and the effect becomes more prominent in D-π-A molecules, generating asymmetric polarization. It is well known that electrons tend to migrate more readily toward the electron acceptor group rather than the donor group, contributing to this asymmetry.[78] As these molecules also fall under D-π-A architecture with excellent absorption maxima, it is intriguing to study their NLO properties.[79] We calculated the first-order hyperpolarizability (β_0) and second-order hyperpolarizability (γ) obtained at 1064 nm for all these molecules and the results are depicted in Figures 6.16 and 6.17 respectively. The data pertaining to x, y, and z components of β_0 and γ are collected in Table 6.7. Our results show that the '**b**' isomers show better NLO activities compared to their '**a**' isomers. The computed first-order hyperpolarizabilities for **P9a** is 955.62 x 10^{-30} esu, while the same for **P9b** is estimated to be 1245.86 x 10^{-30} esu. A similar trend is observed for all the molecules. It is interesting to note that the molecules with lower ΔE_{HL} show higher β_0 values while molecules with wider ΔE_{HL} show lower β_0 values. For example, among all the molecules **P3a** shows the lowest β_0 value with 432.51 x 10^{-30} esu while **P9b** shows the highest β_0 value of 1245.86 x 10^{-30} esu. Among the 22 scrutinized molecules, the '**b**' isomers of **P6 – P10** show higher β_0 values. Moving from the '**a**' isomer to the '**b**' isomer, there is an increase in the β_0 values and the increase is significantly pronounced in **P9** where a shift of 290 x 10^{-30} esu, while this effect is minimum with only a small increment (35.45 x 10^{-30} esu) is observed in **P2** isomers. The calculated results reveal that six of the ten designed candidates were found to show higher β_0 values and thus better NLO activity compared to the reference molecule **P0**. In general, the higher the chemical reactivity (lower the ΔE_{HL}), the higher will be the first order hyperpolarizability.

Finally, we noted the γ values of the designed molecules, and the values are compared graphically in Figure 6.17. It can be inferred from Figure 6.17 that the isomers '**b**' show higher γ compared to the isomers '**a**'. This is very similar to what we observed for first-order hyperpolarizability. The increment is very minimal in the case of **P3**, **P4**, and **P5** while is maximum in **P8**. Especially **P8b** has the maximum γ value followed by **P2b** with 7147.22 x 10^{-36} esu and 6909.72 x 10^{-36} esu respectively. Among the ten designed molecules, six of them showed higher γ values suggesting the significance of modulating the π-bridge to tune the NLO properties of D-π-A type molecules.

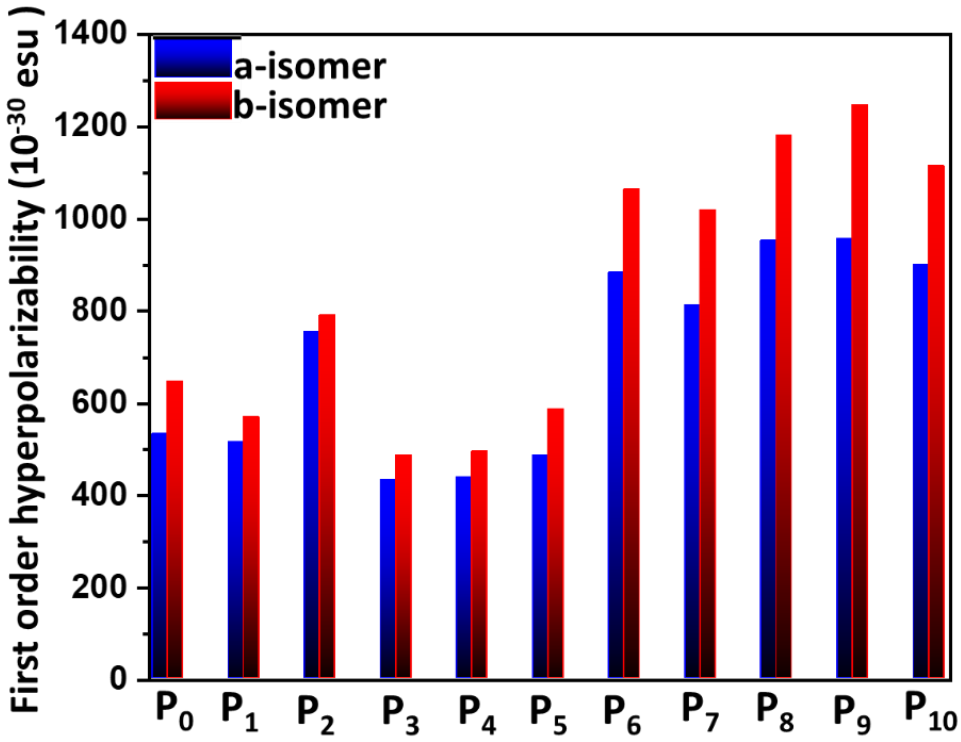

Figure 6.16 Comparison of β_0 values of the studied molecules.

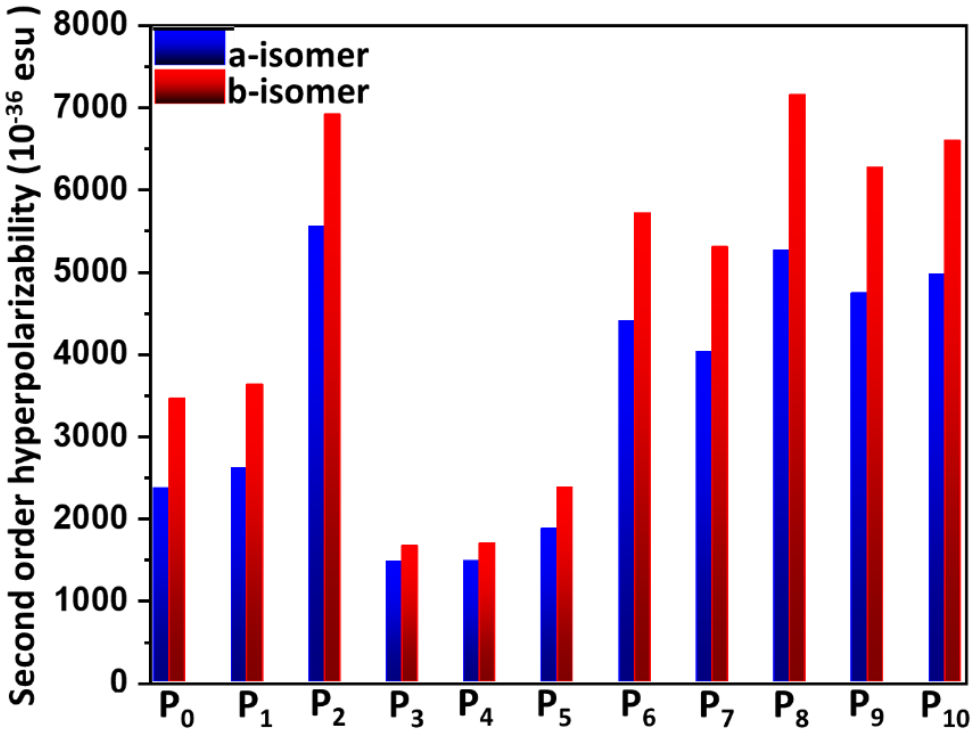

Figure 6.17 Comparison of γ values of the studied molecules.

Table 6.7 The computed first order (β_0) and second order (γ) hyperpolarizabilities.

Molecule	β (10^{-30} esu)	γ (10^{-36} esu)
P_0a	531.22	2356.45
P_0b	644.79	3448.65
P_1a	513.44	2600.63
P_1b	568.31	3619.53
P_2a	753.05	5549.33
P_2b	788.50	6909.72
P_3a	432.51	1463.35
P_3b	485.16	1653.81
P_4a	437.24	1469.94
P_4b	493.38	1687.99
P_5a	484.76	1861.68
P_5b	585.75	2368.12
P_6a	882.10	4391.06
P_6b	1062.81	5705.10
P_7a	811.54	4020.31
P_7b	1017.98	5296.69
P_8a	950.93	5252.98
P_8b	1180.10	7147.22
P_9a	955.62	4730.53
P_9b	1245.86	6263.49
P_{10}a	898.78	4956.47
P_{10}b	1113.69	6589.51

6.6 Conclusions

In summary, this study provides valuable theoretical insight into how α and β cyano positional variation (‘**a**’ and ‘**b**’ isomeric forms) influences the structure, electronic, and optical properties of D-π-A based cyanostilbene derivatives by means of DFT/TDDFT calculations. Ten distinct sets of D-π-A structures (**P_1** – **P_{10}**) and their positional isomers from a reference compound **P_0a** were designed by varying the π-linkers. The B3LYP/6-31+G(d,p) method was used to optimize the designed molecules and the solvation effect was included wherever necessary with the dichloromethane solution using the SMD model. The findings reveal that the ‘**b**’ isomers are less distorted from planarity compared to ‘**a**’ and molecules having furanoid rings in their spacer groups are found to have better planarity. Comparisons of ‘**a**’ and ‘**b**’ isomers showed that the ‘**a**’ isomer is more stable than ‘**b**’ due to strong intramolecular interactions, as evident

from the NCI and QTAIM analyses. The ΔE_{ba} values show the extent of stability of '**a**' and the highest (7.4 kcal/mol) and the lowest value (1.2 kcal/mol) are found for $\mathbf{P_4}$ and $\mathbf{P_1}$, respectively.

Further theoretical analyses reveal that the '**b**' isomers show higher chemical reactivity, higher absorption maxima, and higher hyperpolarizabilities compared to their '**a**' counterpart. Especially, the red shift in absorption maximum of '**b**' isomers arises from enhanced π-delocalization and planarity. Among all, $\mathbf{P_9b}$ tends to show the highest absorption maxima characterized by intramolecular charge transfer (ICT) coupled with π-π* transitions. NLO studies indicate that the molecules with reduced HOMO-LUMO gap show greater first and second-order hyperpolarizabilities. Overall, this study helps experimental scientists to design new molecules with D-π-A architecture with varying π-linkers and the interplay between the chemical reactivity and other optoelectronic properties can be envisaged prior to synthesis.

6.7 References

(1) Khasbaatar, A.; Xu, Z.; Lee, J.-H.; Campillo-Alvarado, G.; Hwang, C.; Onusaitis, B. N.; Diao, Y. From Solution to Thin Film: Molecular Assembly of π-Conjugated Systems and Impact on (Opto)Electronic Properties. *Chem. Rev.* **2023**, *123* (13), 8395–8487.

(2) Albano, G.; Pescitelli, G.; Di Bari, L. Chiroptical Properties in Thin Films of π-Conjugated Systems. *Chem. Rev.* **2020**, *120* (18), 10145–10243.

(3) Mahalingavelar, P.; Kanvah, S. α-Cyanostilbene: A Multifunctional Spectral Engineering Motif. *Phys. Chem. Chem. Phys.* **2022**, *24* (38), 23049–23075.

(4) Yoon, S.-J.; Varghese, S.; Park, S. K.; Wannemacher, R.; Gierschner, J.; Park, S. Y. Color-Tuned, Highly Emissive Dicyanodistyrylbenzene Single Crystals: Manipulating Intermolecular Stacking Interactions for Spontaneous and Stimulated Emission Characteristics. *Adv. Opt. Mater.* **2013**, *1* (3), 232–237.

(5) Femina, C.; Shanthil, M.; Sajith, P. K.; Thomas, R. Anthracene-Incorporated Cyanostilbene Based Donor–Acceptor Systems: Intramolecular Charge Transfer and Aggregation Induced Emission. *New J. Chem.* **2023**, *47* (29), 13810–13819.

(6) Martínez-Abadía, M.; Giménez, R.; Ros, M. B. Self-Assembled α-Cyanostilbenes for Advanced Functional Materials. *Adv. Mater.* **2018**, *30* (5), 1704161.

(7) König, N. F.; Mutruc, D.; Hecht, S. Accelerated Discovery of α-Cyanodiarylethene Photoswitches. *J. Am. Chem. Soc.* **2021**, *143* (24), 9162–9168.

(8) Jimenez, E. R.; Rodríguez, H. Aggregation-Induced Emission: A Review of Promising Cyano-Functionalized AIEgens. *J. Mater. Sci.* **2020**, *55* (4), 1366–1387.

(9) Martínez-Abadía, M.; Varghese, S.; Milián-Medina, B.; Gierschner, J.; Giménez, R.; Ros, M. B. Bent-Core Liquid Crystalline Cyanostilbenes: Fluorescence Switching and

Thermochromism. *Phys. Chem. Chem. Phys.* **2015**, *17* (17), 11715–11724.

(10) Zhu, X.; Feng, L.; Cao, S.; Wang, J.; Niu, G. Donor-Acceptor-Acceptor-Conjugated Dual-State Emissive Acrylonitriles: Investigating the Effect of Acceptor Unit Order and Biological Imaging. *Org. Lett.* **2022**, *24* (45), 8305–8309.

(11) Ibrahim, N.; Loumaigne, M.; Grolleau, J.; Allain, M.; Frère, P. Dual-State Emission versus No Emission by Manipulating the Molecular Structures of Cyanovinyl–Benzofuran Derivatives. *Mol. Syst. Des. Eng.* **2022**, *7* (9), 1119–1128.

(12) Hang, C.; Wu, H.-W.; Zhu, L.-L. π-Conjugated Cyanostilbene-Based Optoelectric Functional Materials. *Chinese Chem. Lett.* **2016**, *27* (8), 1155–1165.

(13) Zhu, L.; Zhao, Y. Cyanostilbene-Based Intelligent Organic Optoelectronic Materials. *J. Mater. Chem. C* **2013**, *1* (6), 1059–1065.

(14) Anandhan, K.; Cerón, M.; Perumal, V.; Ceballos, P.; Gordillo-Guerra, P.; Pérez-Gutiérrez, E.; Castillo, A. E.; Thamotharan, S.; Percino, M. J. Solvatochromism and PH Effect on the Emission of a Triphenylimidazole-Phenylacrylonitrile Derivative: Experimental and DFT Studies. *RSC Adv.* **2019**, *9* (21), 12085–12096.

(15) Huang, Z.; Tang, F.; He, F.; Kong, L.; Huang, J.; Yang, J.; Ding, A. Pyrene and Triphenylamine Substituted Cyanostyrene and Cyanostilbene Derivatives with Dual-State Emission for High-Contrast Mechanofluorochromism and Cell Imaging. *Org. Chem. Front.* **2022**, *9* (19), 5118–5124.

(16) Fan, G.; Yan, D. Positional Isomers of Cyanostilbene: Two-Component Molecular Assembly and Multiple-Stimuli Responsive Luminescence. *Sci. Rep.* **2014**, *4* (1), 4933.

(17) Zhang, Y.; Zhuang, G.; Ouyang, M.; Hu, B.; Song, Q.; Sun, J.; Zhang, C.; Gu, C.; Xu, Y.; Ma, Y. Mechanochromic and Thermochromic Fluorescent Properties of Cyanostilbene Derivatives. *Dye. Pigment.* **2013**, *98* (3), 486–492.

(18) Yokoyama, S.; Nishiwaki, N. Fluorescence Behavior of Bis(Cyanostyryl)Pyrrole Derivatives Depending on the Substituent Position of Cyano Groups in Solution and in Solid State. *J. Org. Chem.* **2019**, *84* (3), 1192–1200.

(19) Zeng, C.; Dai, J.; Yang, T.; Wang, Z.; Gao, Y.; Xia, J.; Chen, Y.; Sun, M. Multi-Stimuli Fluorescence Responsiveness of α-Cyanostilbene Derivative: AIEE, Stimuli Response to Polarity, Acid, Force and Light, Applications in Anti-Counterfeiting and Single Phosphor w-OLED. *Dye. Pigment.* **2024**, *222*, 111906.

(20) Udayakumar, M.; Cerón, M.; Ceballos, P.; Percino, M. J.; Thamotharan, S. Interplay of Weak Noncovalent Interactions in Two Conjugated Positional Isomers: A Combined X-Ray, Optical Properties and Theoretical Investigation. *J. Mol. Struct.* **2019**, *1195*, 32–42.

(21) Castillo, A.; Ceballos, P.; Santos, P.; Cerón, M.; Venkatesan, P.; Pérez-Gutiérrez, E.; Sosa-Rivadeneyra, M.; Thamotharan, S.; Siegler, M. A.; Percino, M. J. Solution and Solid-State Photophysical Properties of Positional Isomeric Acrylonitrile Derivatives

with Core Pyridine and Phenyl Moieties: Experimental and DFT Studies. *Molecules*. **2021**, *26*(6), 1500.

(22) Zeng, S.; Yin, L.; Ji, C.; Jiang, X.; Li, K.; Li, Y.; Wang, Y. D–π–A–π–D Type Benzothiadiazole–Triphenylamine Based Small Molecules Containing Cyano on the π-Bridge for Solution-Processed Organic Solar Cells with High Open-Circuit Voltage. *Chem. Commun.* **2012**, *48* (86), 10627–10629.

(23) Wang, X.; Ding, Z.; Ma, Y.; Zhang, Y.; Shang, H.; Jiang, S. Multi-Stimuli Responsive Supramolecular Gels Based on a D–π–A Structural Cyanostilbene Derivative with Aggregation Induced Emission Properties. *Soft Matter* **2019**, *15* (7), 1658–1665.

(24) El-Meligy, A. B.; Koga, N.; Iuchi, S.; Yoshida, K.; Hirao, K.; Mangood, A. H.; El-Nahas, A. M. DFT/TD-DFT Calculations of the Electronic and Optical Properties of Bis-N,N-Dimethylaniline-Based Dyes for Use in Dye-Sensitized Solar Cells. *J. Photochem. Photobiol. A Chem.* **2018**, *367*, 332–346.

(25) Majumder, R.; Dey, S.; Jana, D.; Ghorai, B. K. Donor-Acceptor Cyanostilbene Based Nano-AIEgens: Synthesis and Properties. *Results Chem.* **2023**, *5*, 100856.

(26) Lim, H. C.; Kim, J.-J.; Jang, J.; Hong, J.-I. Effect of the π-Linker on the Performance of Organic Photovoltaic Devices Based on Push–Pull D–π–A Molecules. *New J. Chem.* **2018**, *42* (14), 11458–11464.

(27) Sajid, H.; Ayub, K.; Gilani, M. A.; Mahmood, T. Donor-π-Acceptor N-Methyl-4,5-Diazacarbazole Based Ultra-High Performance Organic Solar Cells: A Density Functional Theory Study. *Energy Technol.* **2023**, *11* (1), 2201164.

(28) Bedoura, S.; Xi, H.-W.; Goh, H. W.; Lim, K. H. DFT/TDDFT Investigation on Donor-Acceptor Triazole-Based Copolymers for Organic Photovoltaics. *J. Mol. Struct.* **2022**, *1248*, 131406.

(29) Zaier, R.; Martel, A.; Antosiewicz, T. J. Effect of Benzothiadiazole-Based π-Spacers on Fine-Tuning of Optoelectronic Properties of Oligothiophene-Core Donor Materials for Efficient Organic Solar Cells: A DFT Study. *J. Phys. Chem. A* **2023**, *127* (50), 10555–10569.

(30) Shivani; Mishra, A.; Kaur, P.; Singh, K. Synthesis and Nonlinear Optical Behavior of Thermally Stable Chromophores Based on 9,9-Dimethyl-9H-Fluoren-2-Amine: Improving Intrinsic Hyperpolarizability through Modulation of "Push–Pull." *ACS Omega* **2022**, *7* (43), 39045–39060.

(31) Shivani; Mishra, A.; Kaur, P.; Singh, K. Perpetual Extension of Conjugation of Fluorene-Based Donor–Acceptor Dyads Yield Diminished Nonlinear Optical Response. *J. Phys. Chem. C* **2023**, *127* (2), 1260–1272.

(32) Gong, L.; Ma, C.; Liu, T.; Lv, J.; Xun, X. Theoretical Study on Functionalized Acrylonitrile Compounds with a Large Second-Order Nonlinear Optical Response. *New J. Chem.* **2020**, *44* (45), 19623–19629.

(33) Shivani; Mishra, A.; Kumar, V.; Kaur, P.; Singh, K. Synthesis, Linear and Non-Linear Optical Properties of "Push-Pull" Chromophores Based on 9,9-Dimethyl-9H-Fluoren-2-Amine. *Dye. Pigment.* **2022**, *200*, 110160.

(34) Kaur, P.; Singh, K. Second-Order Nonlinear Polarizability of "Push-Pull" Chromophores. A Decade of Progress in Donor-π-Acceptor Materials. *Chem. Rec.* **2022**, *22* (6), e202200024.

(35) Shivani; Kaur, I.; Chemmanghattu, K.; Kaur, P.; Singh, K. Non-Linear Optical Behavior of Benzothiazole Based Chromophores: Second Harmonic Generation. *Dye. Pigment.* **2020**, *183*, 108739.

(36) Khan, M. A.; Ayub, A. R.; Alrowaili, Z. A.; Ilyas, M.; Hui, L.; Abbas, S. Z. Self-Assembly of 2D Coordination Complex of Cytidine Monophosphate to Boost up the Optical Phenomena. *J. Mol. Struct.* **2022**, *1268*, 133655.

(37) Akram, S. J.; Hadia, N. M. A.; Iqbal, J.; Mehmood, R. F.; Iqbal, S.; Shawky, A. M.; Asif, A.; Somaily, H. H.; Raheel, M.; Khera, R. A. Impact of Various Heterocyclic π-Linkers and Their Substitution Position on the Opto-Electronic Attributes of the A–π–D–π–A Type IECIO-4F Molecule: A Comparative Analysis. *RSC Adv.* **2022**, *12* (32), 20792–20806.

(38) Sun, Z.-Z.; Long, R. Thia[5]Helicene-Based D−π–A-Type Molecular Semiconductors for Stable and Efficient Perovskite Solar Cells: A Theoretical Study. *J. Phys. Chem. C* **2023**, *127* (19), 8953–8962.

(39) Rehman, F. U.; Hameed, S.; Khera, R. A.; Shaban, M.; Essid, M.; Aloui, Z.; Al-Saeedi, S. I.; Ibrahim, M. A. A.; Waqas, M. High-Efficiency and Low-Energy-Loss Organic Solar Cells Enabled by Tuning the End Group Modification of the Terthiophene-Based Acceptor Molecules to Enhance Photovoltaic Properties. *ACS Omega* **2023**, *8* (45), 42492–42510.

(40) Zaier, R.; Ayachi, S. Designing Well-Organized Donor-Bridge-Acceptor Conjugated Systems Based on Cyclopentadithiophene as Donors in Bulk Heterojunction Organic Solar Cells: DFT-Based Modeling and Calculations; Elseman, A. M., Ed.; IntechOpen: Rijeka, 2021; p Ch. 5.

(41) Bader, R. F. W. A Quantum Theory of Molecular Structure and Its Applications. *Chem. Rev.* **1991**, *91* (5), 893–928.

(42) Bader, R. F. W. Atoms in Molecules. *Acc. Chem. Res.* **1985**, *18* (1), 9–15.

(43) Johnson, E. R.; Keinan, S.; Mori-Sánchez, P.; Contreras-García, J.; Cohen, A. J.; Yang, W. Revealing Noncovalent Interactions. *J. Am. Chem. Soc.* **2010**, *132* (18), 6498–6506.

(44) Politzer, P.; Landry, S. J.; Waernheim, T. Proposed Procedure for Using Electrostatic Potentials to Predict and Interpret Nucleophilic Processes. *J. Phys. Chem.* **1982**, *86* (24), 4767–4771.

(45) Frisch, M. J.; Trucks, G. W.; Schlegel, H. B.; Scuseria, G. E.; Robb, M. A.; Cheeseman,

J. R.; Scalmani, G.; Barone, V.; Petersson, G. A.; Nakatsuji, H..et al. *Gaussian 16*, Revision B.01; Gaussian, Inc.: Wallingford, CT, 2016.

(46) Becke, A. D. Density-functional Thermochemistry. III. The Role of Exact Exchange. *J. Chem. Phys.* **1993**, *98* (7), 5648–5652.

(47) Lee, C.; Yang, W.; Parr, R. G. Development of the Colle-Salvetti Correlation-Energy Formula into a Functional of the Electron Density. *Phys. Rev. B* **1988**, *37* (2), 785–789.

(48) Zhurko, G. *Chemcraft 1.8 program*. Ivanovo, Russia, 2005, https://chemcraftprog.com.

(49) Tenderholt, Adam L. "QMForge: A Program to Analyze Quantum Chemistry Calculations", Version 3.2, https://qmforge.net.

(50) Lu, T.; Chen, F. Multiwfn: A Multifunctional Wavefunction Analyzer. *J. Comput. Chem.* **2012**, *33* (5), 580–592.

(51) T. A. Keith, AIMAll program (version 17.11.14), TK Gristmill Software, Overland Park KS, USA, 2017, http://aim.tkgristmill.com.

(52) Humphrey, W.; Dalke, A.; Schulten, K. VMD: Visual Molecular Dynamics. *J. Mol. Graph.* **1996**, *14* (1), 33–38.

(53) Yanai, T.; Tew, D. P.; Handy, N. C. A New Hybrid Exchange–Correlation Functional Using the Coulomb-Attenuating Method (CAM-B3LYP). *Chem. Phys. Lett.* **2004**, *393* (1), 51–57.

(54) Adamo, C.; Barone, V. Toward Reliable Density Functional Methods without Adjustable Parameters: The PBE0 Model. *J. Chem. Phys.* **1999**, *110* (13), 6158–6170.

(55) Boese, A. D.; Martin, J. M. L. Development of Density Functionals for Thermochemical Kinetics. *J. Chem. Phys.* **2004**, *121* (8), 3405–3416.

(56) Marenich, A. V; Cramer, C. J.; Truhlar, D. G. Universal Solvation Model Based on Solute Electron Density and on a Continuum Model of the Solvent Defined by the Bulk Dielectric Constant and Atomic Surface Tensions. *J. Phys. Chem. B* **2009**, *113* (18), 6378–6396.

(57) Liang, J.; Feng, X.; Hait, D.; Head-Gordon, M. Revisiting the Performance of Time-Dependent Density Functional Theory for Electronic Excitations: Assessment of 43 Popular and Recently Developed Functionals from Rungs One to Four. *J. Chem. Theory Comput.* **2022**, *18* (6), 3460–3473.

(58) Zhang, T.; Zhu, G.; Lin, L.; Mu, J.; Ai, B.; Li, Y.; Zhuo, S. Cyano Substitution Effect on the Emission Quantum Efficiency in Stilbene Derivatives: A Computational Study. *Org. Electron.* **2019**, *68*, 264–270.

(59) O'Boyle, N. M.; Tenderholt, A. L.; Langner, K. M. Cclib: A Library for Package-Independent Computational Chemistry Algorithms. *J. Comput. Chem.* **2008**, *29* (5), 839–845.

(60) Kurtz, H. A.; Stewart, J. J. P.; Dieter, K. M. Calculation of the Nonlinear Optical Properties of Molecules. *J. Comput. Chem.* **1990**, *11* (1), 82–87.

(61) Bella, A. P.; Solomon, R. V.; Vedha, S. A.; Merlin, J. P. Enhanced Luminescence Efficiency of Structurally Tailored New Coumarin-Based Heterocyclic Organic Materials: A DFT/TD-DFT Study. *Theor. Chem. Acc.* **2019**, *138* (4), 53.

(62) Panneerselvam, M.; Kathiravan, A.; Solomon, R. V.; Jaccob, M. The Role of π-Linkers in Tuning the Optoelectronic Properties of Triphenylamine Derivatives for Solar Cell Applications – A DFT/TDDFT Study. *Phys. Chem. Chem. Phys.* **2017**, *19* (8), 6153–6163.

(63) Zhao, C.; Lu, Y.; Zhu, Z.; Liu, H. Theoretical Exploration of Halogen Bonding Interactions in the Complexes of Novel Nitroxide Radical Probes and Comparison with Hydrogen Bonds. *J. Phys. Chem. A* **2018**, *122* (22), 5058–5068.

(64) Ganie, A. A.; Rashid, S.; Ahangar, A. A.; Ismail, T. M.; Sajith, P. K.; Dar, A. A. Expanding the Scope of Hydroxyl-Pyridine Supramolecular Synthon to Design Molecular Solids. *Cryst. Growth Des.* **2022**, *22* (3), 1972–1983.

(65) Abdulla, H. M.; Gangwar, P.; Sajith, P. K.; Ramachandran, C. N. Probing the Interaction of NO with C60: Comparison between Endohedral and Exohedral Complexes. *J. Phys. Chem. A* **2023**, *127* (16), 3598–3607.

(66) Sajith, P. K.; Suresh, C. H. Mechanisms of Reductive Eliminations in Square Planar Pd(II) Complexes: Nature of Eliminated Bonds and Role of Trans Influence. *Inorg. Chem.* **2011**, *50* (17), 8085–8093.

(67) Ganie, A. A.; Ismail, T. M.; Sajith, P. K.; Dar, A. A. Validation of the Supramolecular Synthon Preference through DFT and Physicochemical Property Investigations of Pyridyl Salts of Organo-Sulfonates. *New J. Chem.* **2021**, *45* (10), 4780–4790.

(68) Murray, J. S.; Politzer, P. The Electrostatic Potential: An Overview. *WIREs Comput. Mol. Sci.* **2011**, *1* (2), 153–163.

(69) Ismail, T. M.; Mohan, N.; Sajith, P. K. Theoretical Study of Hydrogen Bonding Interactions in Substituted Nitroxide Radicals. *New J. Chem.* **2021**, *45* (8), 3866–3875.

(70) Sajith, P. K.; Suresh, C. H. Quantification of the Trans Influence in Hypervalent Iodine Complexes. *Inorg. Chem.* **2012**, *51* (2), 967–977.

(71) Woodward, R. B.; Hoffmann, R. The Conservation of Orbital Symmetry. *Angew. Chemie Int. Ed. English* **1969**, *8* (11), 781–853.

(72) El-Demerdash, S. H.; Halim, S. A.; El-Nahas, A. M.; El-Meligy, A. B. A Density Functional Theory Study of the Molecular Structure, Reactivity, and Spectroscopic Properties of 2-(2-Mercaptophenyl)-1-Azaazulene Tautomers and Rotamers. *Sci. Rep.* **2023**, *13* (1), 15626.

(73) Samuvel Michael, D.; Serangolam Krishnasami, S.; Vijay Solomon, R. A Two-Step MM and QM/MM Approach to Model AIEE of Aryloxy Benzothiadiazole Derivatives for Optoelectronic Applications. *Phys. Chem. Chem. Phys.* **2022**, *24* (6), 4051–4064.

(74) Francis, R. R.; Ebenezer, C.; Vijay Solomon, R.; Wilson, P. Computational Assessment of Amino Acid-Coupled Benzanthrone 2-Aminoacetamides as Molecular Probes for Insulin Amyloid Fibril Visualization. *New J. Chem.* **2023**, *47* (28), 13247–13259.

(75) Noudem, P.; Fouejio, D.; Mveme, C. D. D.; Nya, F. T.; Zekeng, S. S. Electronic, Nonlinear Optical, UV–Vis and NBO Analysis of Methyl Methacrylate for Optoelectronic and Optical Applications: DFT Study and Impact of Conformation. *Spectrochim. Acta Part A Mol. Biomol. Spectrosc.* **2023**, *303*, 123267.

(76) Hannachi, D.; Khelfaoui, N.; Zaidi, M.; Yahiaoui, D.; Lakehal, S.; Morell, C.; Chermette, H. The Effect of Resonance-Assisted Hydrogen Bond on the Second-Order Nonlinear Optical Properties of Pyridine Hydrazone Photoswitches: A Quantum Chemistry Investigation. *New J. Chem.* **2023**, *47* (39), 18359–18373.

(77) Kamli, D.; Hannachi, D.; Samsar, D.; Chermette, H. Bis-TTF-Ge Derivatives: Promising Linear and Nonlinear Optical Properties, a Theoretical Investigation. *New J. Chem.* **2023**, *47* (3), 1234–1246.

(78) Khalid, M.; Zafar, M.; Hussain, S.; Asghar, M. A.; Khera, R. A.; Imran, M.; Abookleesh, F. L.; Akram, M. Y.; Ullah, A. Influence of End-Capped Modifications in the Nonlinear Optical Amplitude of Nonfullerene-Based Chromophores with a D−π–A Architecture: A DFT/TDDFT Study. *ACS Omega* **2022**, *7* (27), 23532–23548.

(79) Khalid, M.; Naz, S.; Mahmood, K.; Hussain, S.; Carmo Braga, A. A.; Hussain, R.; Ragab, A. H.; Al-Mhyawi, S. R. First Theoretical Probe for Efficient Enhancement of Optical Nonlinearity via Structural Modifications into Phenylene Based D–π–A Configured Molecules. *RSC Adv.* **2022**, *12* (48), 31192–31204.

Chapter 7

Conclusions

7.1 General Conclusions

The thesis discuss the design, synthesis and photophysical properties of some donor-acceptor systems based on cyanostyryl derivatives. The systematic structural and quantum chemical calculations offer valuable insights into the structure-activity relationships of the newly synthesized compounds. The structural versatility of the cyanostilbene-based system allows for facile molecular engineering making it a hot area of research in the field of optoelectronics. In the experimental part of the thesis the cyanostyrene-anthracene donor-acceptor system are functionalized with various alkyl chains to explore the aggregation induced emission and stimuli-responsive emission behaviour in the solid and the solution state. In addition, one of the chapters presented the comparative study of positional variations of the cyanostilbene-based D-π-A systems using density functional theory (DFT), which offers an excellent platform for experimental researchers to design new molecules with D-π-A architecture incorporating various π-linkers to explore the interplay between the molecular structure and nonlinear optical properties

The role of intramolecular charge transfer (ICT) and aggregation induced emission (AIE) in the anthracene-cyanostilbene based donor-acceptor systems with varying alkyl chains are systematically explored in *Chapter 3*. After synthesizing the hexyloxy (**CS-3.1**) and dodecyloxy (**CS-3.2**) substituted compound, conducted a detailed analysis of fluorescence properties in both solution and solid states and compared their luminescent behaviour. Both the molecules showed strong emission in the solution state attributed to the intramolecular charge transfer (ICT). The ICT band in **CS-3.1** showed a solvatochromic redshift with increase in dielectric constant of the solvents. Irrespective of the alkyloxy chain length, both the **CS-3.1** and **CS-3.2** showed comparable emission in the solid state attributed to the molecular aggregation. Interestingly, the molecule **CS-3.1** showed a dual mode stimuli responsive luminescence switching under applied stress and ethyl acetate vapours. Unlike **CS-3.1** the molecule **CS-3.2** was less sensitive to various stimuli. Owing to the rigid molecular packing, **CS-3.1** showed higher quantum yield (Φ_F=0.43) in the solid state in comparison to **CS-3.2** (Φ_F=0.37), where the latter showed poor crystallinity. In the solid state, two neighbouring molecules comprises a J-aggregate pair with molecular arrangement along molecular short axis. In both **CS-3.1** and **CS-3.2** the luminophores adopt similar arrangement, hence, the identical emission properties in the solid state. The present work provides two novel compounds with highly emissive behaviour both in solid and solution state.

In *chapter 4* the study explores the comparative study of the series of compounds with and without the π-spacer groups. The present study demonstrates the markedly distinct photophysical properties of anthracene-cyanostilbene derivatives, strongly affected by the nature of the π-spacer. The newly synthesized compounds, **CS-4.1** (lacking a phenyl spacer) and **CS-4.2** (containing a phenyl spacer), showed pronounced differences in their fluorescence emission, lifetime, quantum yield, and external stimuli response. Notably, variation in alkyl chain length exerted minimal influence on the photophysical properties, underscoring the dominant effect of π-conjugation tuning via spacer modification. Crystallographic analysis revealed distinct molecular packing and intermolecular interactions that correlate with their emissive characteristics. The present study demonstrates the effect of the π-spacer in the donor-acceptor system to enhance the emissive behaviour of the organic luminogens.

The newly synthesized anthracene-cyanostilbene D-π-A systems of previous chapter by replacing the alkyl groups as methoxy group, for all the theoretical studies to reduce the computational cost and named the compounds as **CS-4.1** and **CS-4.2**, have been theoretically analysed in *chapter 5* with their structural and electronic properties thoroughly examined using DFT and TD-DFT calculations. Hirshfeld surface and NCI analyses of the crystal structures of the compounds revealed that **CS-4.2** exhibits stronger C–H···π and π···π interactions than **CS-4.1**, owing to the presence of the phenyl substituent. Furthermore, NCI analysis predicted a more efficient J-aggregate formation in compound **CS-4.2** compared to compound **CS-4.1**. FMO analysis revealed that the HOMO–LUMO gap in **CS-4.2** is slightly larger than that in **CS-4.**, which can be attributed to the perpendicular orientation of the phenyl moieties in **CS-4.2**, leading to reduced conjugation and consequently a slightly wider energy gap. The TDDFT calculations successfully reproduced the main absorption features of both compounds. The predicted blue shift in **CS-4.2** relative to **CS-4.1** is in excellent agreement with the experimental results. This blue shift can be rationalized by using deepest minimum MESP value located at the anthracene core. The study also gives the idea about the two conformers of the compounds, namely *syn* and *anti* forms. In the S_0 state, the *anti*-to-*syn* conversion requires a free energy barrier of 18.4 kcal/mol for compound **CS-4.1**, whereas for compound **CS-4.2**, the barrier is significantly lower value of 2.9 kcal/mol, indicating that the conversion is energetically more favourable for **CS-4.2** and considerably hindered for **CS-4.1**. In the S_1 state, this similar trend persists. This chapter sheds insight to the structure-activity relationships of compounds **CS-4.1** and **CS-4.2**, highlighting how conformational preferences, electronic properties, and intermolecular interactions influence their photophysical behaviour.

The *Chapter 6* discusses the theoretical design of ten different sets of D-π-A structures (**P_1** – **P_{10}**) and their positional isomers from a reference compound **P_0a** by varying the π-linkers. The findings reveal that the '**b**' isomers are less distorted from planarity compared to '**a**' and molecules having furanoid rings in their spacer groups are found to have better planarity. Comparisons of '**a**' and '**b**' isomers showed that the '**a**' isomer is more stable than '**b**' due to strong intramolecular interactions, as evident from the NCI and QTAIM analyses. The ΔE_{ba} values show the extent of stability of '**a**' and the highest (7.4 kcal/mol) and the lowest value (1.2 kcal/mol) are found for **P_4** and **P_1**, respectively. Further theoretical analyses reveal that the '**b**' isomers show higher chemical reactivity, higher absorption maxima, and higher hyperpolarizabilities compared to their '**a**' counterpart. Especially, the red shift in absorption maximum of '**b**' isomers arises from enhanced π-delocalization and planarity. Among all, **P_9b** tends to show the highest absorption maxima characterized by intramolecular charge transfer (ICT) coupled with π-π* transitions. NLO studies indicate that the molecules with reduced HOMO-LUMO gap show greater first and second-order hyperpolarizabilities. Overall, this study helps experimental scientists to design new molecules with D-π-A architecture with varying π-linkers and the interplay between the chemical reactivity and other optoelectronic properties can be envisaged prior to synthesis.

In summary the works in the thesis investigates the experimental and theoretical exploration of photophysical studies of the cyanostilbene based D-π-A architecture. The compounds synthesized in this thesis are designed to demonstrate the role of molecular structure, Intramolecular charge transfer and packing of the molecules in the solid state on observed photophysical properties especially the aggregation induced emission and its stimuli responsive switching. The study also explores how the introduction of π-spacer group brings significant changes in the luminescent properties of the system. In addition, the study investigates the quantum chemical behaviour of the compounds and thoroughly examined through a combination of density functional theory (DFT) and time-dependent density functional theory (TD-DFT) calculations. Furthermore, a systematic comparative theoretical study was undertaken to evaluate the structural properties, orbital analysis, and relative stabilities of alfa and beta analogs of various cyanostilbene derivatives by using the DFT method. This research can contribute to the design and synthesis of novel cyanostilbene based donor-acceptor system with intramolecular charge transfer, aggregation induced emission and photoswitching nature, which act as promising candidates for creating bright, emissive materials with the potential for diverse applications in the field of optoelectronics.

Chapter 8

Recommendations

7.1 Future recommendations

The organic π-conjugated cyanostyrene based materials have received paramount interest in the field of optoelectronics and material devices due to their excellent and unique properties. The cyanostyrene moiety can readily incorporate to the wide variety of organic system using simple organic synthetic procedures like Knoevenagel condensation. The systematic modifications of the system allow the fine tuning of the optical properties and make them potential candidate for the flexible optoelectronic applications (Figure 7.1.1). They are well known for their potential applications in devices such as OLEDs, OFETs, organic solar cells, photoswitching, bioimaging, and sensing devices.[1,2]

7.1.1 Development of advanced optoelectronic devices

The compounds discussed in chapter 3 and chapter 4 (Compounds named **CS 3.1**, **CS 3.2**, **CS 4.1**, **CS 4.2**, **CS 4.3**, **CS 4.4**) have got high thermal stability (300 °C <) as well as dual state emissive properties both in solid state and in the solution state. The enhanced thermal stability is very crucial for the maintenance of the improved efficiency and performance of various optoelectronic devices such as OLEDs, OFETs etc. It also imparts high flexibility and the capacity to withstand at high temperature during the manufacturing process without compromising its properties. The thermal stability ensures the longer lifespan of the devices as well as the reduced replacement choices. The dual state emissive (DSEgens) materials provide more robust and versatile platform for sensing and imaging.[3] The ability to produce strong luminescence, both in solution and solid state is the essential feature in the field of optoelectronics. Utilizing these properties of the synthesized compounds one can potentially integrate the properties to future optoelectronic devices and to the real-world applications.

7.1.2 Molecular design with varying donor unit

The synthesised compounds in chapter 4 were based on the effect of π-spacers in the D-π-A systems. In the future work one can incorporate different conjugated and non-conjugated spacers for tuning the photophysical properties by controlling the intramolecular charge transfer efficiency. The molecular designs that can be achieved by introducing groups of varying donor strength by maintaining the cyanostyrene as acceptor could produce molecular systems with tailor made photophysical properties. The new designs achieved by the fine tuning of the donor-acceptor strength could be explored in various optoelectronic devices and sensors.[4,5]

7.1.3 Systematic studies on weak interactions

Weak intermolecular interactions in the molecular systems reported in these thesis mainly includes π-π stacking and van der Waals interactions. The weak van der-Walls type of interactions are the key players in determining the photophysical properties in the solid state. These weak interactions facilitate the charge transfer between the adjacent molecules and may leads to the formation of charge transfer states which in turn significantly changes the emission behaviour and lifetime. Different crystallization conditions may leads to the formation of crystal with different packing structures and also results the development of polymorphs. A systematic exploration of various intermolecular interactions and molecular packing in the crystalline state of a similar class of molecules is essential for improving the photophysical properties with better tunability.

Figure 7.1 Future recommendations of the designed and synthesized compounds.

7.1.4 Enhanced NLO properties

The chapter 6 discusses the design and theoretical investigation of some novel D-π-A architectures with unique NLO properties. Among the compounds investigated the compounds **CS 6.6**, **CS 6.7**, **CS 6.8**, **CS 6.9** and **CS 6.10** exhibited strong NLO activity compared to the reference compound (**P$_0$a**) with scope for future applications. Therefore the synthesis and experimental investigation of the predicted properties provide scope for future exploration.[6,7]

7.2 References

(1) Kalita, N.; Kalita, K. J.; Borah, S. S.; Puschmann, H.; Nath, N. K.; Thakuria, R. Crystal Engineering-Based Approach to Introduce Mechanical Compliance in a Series of Highly Luminescent Substituted Distyrylbenzenes. *ACS Appl. Opt. Mater.* **2025**, *3* (5), 1078–1087.

(2) An, B.-K.; Gierschner, J.; Park, S. Y. π-Conjugated Cyanostilbene Derivatives: A Unique Self-Assembly Motif for Molecular Nanostructures with Enhanced Emission and Transport. *Acc. Chem. Res.* **2012**, *45*, 544.

(3) Ni, Y.; Yang, L.; Kong, L.; Wang, C.; Zhang, Q.; Yang, J. Highly Efficient Dual-State Emission and Two-Photon Absorption of Novel Naphthalimide Functionalized Cyanostilbene Derivatives with Finely Tuned Terminal Alkoxyl Groups. *Mater. Chem. Front.* **2022**, *6* (23), 3522–3530.

(4) Pei, Q.; Wang, X.; Hu, W.; Nie, L.; Shi, Y.; Ding, A.; Tang, F. Phenothiazine-Cyanostilbene Conjugates with Dual-State Emission for Mechanofluorochromism and Live-Cell Imaging. *Colloids Surfaces A Physicochem. Eng. Asp.* **2023**, *677*, 132347.

(5) Lv, T.; Wu, S.; Jin, Y.; Ma, J.; Jiang, S.; Xue, Y.; Wang, F. Enhancing the Circularly Polarized Luminescence of Self-Assembled Cyanostilbenes through Extended π-Conjugation. *Chinese J. Chem.* **2024**, *42* (2), 135–141.

(6) Mahmood, A.; Abdullah, M. I.; Khan, S. U.-D. Enhancement of Nonlinear Optical (NLO) Properties of Indigo through Modification of Auxiliary Donor, Donor and Acceptor. *Spectrochim. Acta Part A Mol. Biomol. Spectrosc.* **2015**, *139*, 425–430.

(7) Aslam, S.; Haroon, M.; Akhtar, T.; Arshad, M.; Khalid, M.; Shafiq, Z.; Imran, M.; Ullah, A. Synthesis, Characterization, and DFT-Based Electronic and Nonlinear Optical Properties of Methyl 1-(Arylsulfonyl)-2-Aryl-1H-Benzo[d]Imidazole-6-Carboxylates. *ACS Omega* **2022**, *7* (35), 31036–31046.

LIST OF PUBLICATIONS

Based on the Thesis Work:

1. **Femina, C**.; Shanthil, M.; Sajith, P. K.; Thomas, R. Anthracene-Incorporated Cyanostilbene Based Donor–Acceptor Systems: Intramolecular Charge Transfer and Aggregation Induced Emission. *New J. Chem.* **2023**, *47* (29), 13810–13819. https://doi.org/10.1039/D3NJ00478C.
2. **Femina, C**.; Sajith, P. K.; Remya, K.; Thomas, R.; Solomon, R. V. Theoretical Insights into the Structural and Optical Properties of D−π–A-Based Cyanostilbene Systems of α and β Variants. *ACS Omega* **2024**, *9* (21), 22764–22776. https://doi.org/10.1021/acsomega.4c00850.
3. **Femina, C**.; Yamamoto, N.; Ramya, N. K.; Sajith, P. K.; Thomas, R. Photophysical Divergence Driven by π-Spacer Variations in the Anthracene–Cyanostilbene Architecture. *Phys. Chem. Chem. Phys.* **2025**, *27* (45), 24641–24654. https://doi.org/10.1039/D5CP03033A.

Other Works:

4. **Femina, C**.; Yamagami, T.; Yamamoto, N.; Thomas, R.; Sajith, P. K. Theoretical Insights into Aggregation-Induced Emission of Bis(Cyanostyryl)Pyrrole Derivatives. *Phys. Chem. Chem. Phys.* **2025**. https://doi.org/10.1039/D4CP01291G.
5. Ramya, N. K.; **Femina, C**.; Suresh, S.; Mohanakumari, D. S.; Krishnan, R.; Thomas, R. Dicyanodistyrylbenzene Based Positional Isomers: A Comparative Study of AIEE and Stimuli Responsive Multicolour Fluorescence Switching. *New J. Chem.* **2022**, *46* (3), 1339–1346. https://doi.org/10.1039/D1NJ04489C.
6. Dar, A. A.; Ahangar, A. A.; **Femina, C**.; Malik, A. A.; Parambil, J. V; Sajith, P. K. Combined Experimental and Theoretical Investigations of a Photoswitching Dimorphic Chlorinated Schiff Base. *J. Phys. Chem. C* **2024**, *128* (44), 18901–18912. https://doi.org/10.1021/acs.jpcc.4c04437.
7. Lohithakshamenon, R.; Prasanthkumar, K. P.; **Femina, C**.; Sajith, P. K. Bond Strength and Interaction Energies in Togni Reagents: Insights from Molecular Electrostatic Potential-Based Parameters. *J. Phys. Chem. A* **2024**, *128* (4), 727–737. https://doi.org/10.1021/acs.jpca.3c06378.
8. Dar, A. A.; Lone, S. H.; Ahmad, I.; Ahangar, A. A.; Ganie, A. A.; **Femina, C**. Engineering the Solid-State Luminescence of Organic Crystals and Cocrystals. *Mater. Adv.* **2024**, *5* (3), 1056–1064. https://doi.org/10.1039/D3MA00853C.

Appendix 1

Tables showing torsions, bond length and bond angles of the molecules CS-3.1, CS-4.1b, and CS-4.2b

Appendix 1

CS-3.1

Table 1. Table showing torsions.

Atoms	Angle (°)	Atoms	Angle (°)
C(7)#1-C(1)-C(2)-C(3)	-0.7(2)	C(4)-C(8)-C(13)-C(12)	179.30(16)
C(1)-C(2)-C(3)-C(4)	-178.93(14)	C(10)-C(11)-C(14)-C(15)	164.8(2)
C(1)-C(2)-C(3)-C(5)#1	2.1(2)	C(12)-C(11)-C(14)-C(15)	-13.7(3)
C(2)-C(3)-C(4)-C(5)	-177.65(13)	C(11)-C(14)-C(15)-C(22)	0.1(3)
C(5)#1-C(3)-C(4)-C(5)	1.3(2)	C(11)-C(14)-C(15)-C(16)	-176.82(18)
C(2)-C(3)-C(4)-C(8)	6.3(2)	C(14)-C(15)-C(16)-C(21)	167.6(2)
C(5)#1-C(3)-C(4)-C(8)	-174.71(12)	C(22)-C(15)-C(16)-C(21)	-9.5(3)
C(3)-C(4)-C(5)-C(6)	179.27(13)	C(14)-C(15)-C(16)-C(17)	-10.1(3)
C(8)-C(4)-C(5)-C(6)	-4.8(2)	C(22)-C(15)-C(16)-C(17)	172.8(2)
C(3)-C(4)-C(5)-C(3)#1	-1.3(2)	C(21)-C(16)-C(17)-C(18)	1.5(4)
C(8)-C(4)-C(5)-C(3)#1	174.64(12)	C(15)-C(16)-C(17)-C(18)	179.4(2)
C(4)-C(5)-C(6)-C(7)	179.32(14)	C(16)-C(17)-C(18)-C(19)	0.4(4)
C(3)#1-C(5)-C(6)-C(7)	-0.1(2)	C(17)-C(18)-C(19)-C(20)	-2.9(5)
C(5)-C(6)-C(7)-C(1)#1	-1.3(2)	C(17)-C(18)-C(19)-O(1)	179.6(3)
C(5)-C(4)-C(8)-C(13)	72.5(2)	C(18)-C(19)-C(20)-C(21)	3.3(5)
C(3)-C(4)-C(8)-C(13)	-111.56(18)	O(1)-C(19)-C(20)-C(21)	-179.0(3)
C(5)-C(4)-C(8)-C(9)	-108.61(17)	C(17)-C(16)-C(21)-C(20)	-1.1(4)
C(3)-C(4)-C(8)-C(9)	67.4(2)	C(15)-C(16)-C(21)-C(20)	-179.0(3)
C(13)-C(8)-C(9)-C(10)	0.5(3)	C(19)-C(20)-C(21)-C(16)	-1.3(5)
C(4)-C(8)-C(9)-C(10)	-178.53(15)	O(1)-C(23)-C(24)-C(25)	179.1(3)
C(8)-C(9)-C(10)-C(11)	-1.0(3)	C(23)-C(24)-C(25)-C(26)	179.4(4)
C(9)-C(10)-C(11)-C(12)	0.6(3)	C(24)-C(25)-C(26)-C(27)	177.6(5)
C(9)-C(10)-C(11)-C(14)	-178.00(16)	C(25)-C(26)-C(27)-C(28)	178.7(8)
C(10)-C(11)-C(12)-C(13)	0.2(3)	C(20)-C(19)-O(1)-C(23)	176.1(3)
C(14)-C(11)-C(12)-C(13)	178.65(17)	C(18)-C(19)-O(1)-C(23)	-6.3(4)
C(11)-C(12)-C(13)-C(8)	-0.7(3)	C(24)-C(23)-O(1)-C(19)	-174.4(2)

Table 2. Table showing bond length and bond angles.

Bond Length	Bond Angle (°)	Bond Length	Bond Angle (°)	Bond Length	Bond Angle (°)
C(1)-C(2)	1.360(2)	C(19)-O(1)	1.362(3)	C(3)-C(4)-C(8)	119.11(13)
C(1)-C(7)#1	1.411(2)	C(20)-C(21)	1.382(3)	C(4)-C(5)-C(6)	121.90(14)
C(1)-H(1)	0.9300	C(20)-H(20)	0.9300	C(4)-C(5)-C(3)#1	120.05(13)
C(2)-C(3)	1.428(2)	C(21)-H(21)	0.9300	C(6)-C(5)-C(3)#1	118.05(14)
C(2)-H(2)	0.9300	C(22)-N(1)	1.143(3)	C(7)-C(6)-C(5)	121.42(15)
C(3)-C(4)	1.414(2)	C(23)-O(1)	1.401(3)	C(7)-C(6)-H(6)	119.3
C(3)-C(5)#1	1.439(2)	C(23)-C(24)	1.517(3)	C(5)-C(6)-H(6)	119.3
C(4)-C(5)	1.408(2)	C(23)-H(23A)	0.9700	C(6)-C(7)-C(1)#1	120.60(14)
C(4)-C(8)	1.493(2)	C(23)-H(23B)	0.9700	C(6)-C(7)-H(7)	119.7
C(5)-C(6)	1.433(2)	C(24)-C(25)	1.467(5)	C(1)#1-C(7)-H(7)	119.7
C(6)-C(7)	1.352(2)	C(24)-H(24A)	0.9700	C(13)-C(8)-C(9)	117.47(14)
C(6)-H(6)	0.9300	C(24)-H(24B)	0.9700	C(13)-C(8)-C(4)	123.54(13)
C(7)-H(7)	0.9300	C(25)-C(26)	1.518(5)	C(9)-C(8)-C(4)	118.98(13)
C(8)-C(13)	1.389(2)	C(25)-H(25A)	0.9700	C(10)-C(9)-C(8)	121.09(15)
C(8)-C(9)	1.389(2)	C(25)-H(25B)	0.9700	C(10)-C(9)-H(9)	119.5
C(9)-C(10)	1.377(2)	C(26)-C(27)	1.520(9)	C(8)-C(9)-H(9)	119.5
C(9)-H(9)	0.9300	C(26)-H(26A)	0.9700	C(9)-C(10)-C(11)	121.73(15)
C(10)-C(11)	1.394(2)	C(26)-H(26B)	0.9700	C(9)-C(10)-H(10)	119.1
C(10)-H(10)	0.9300	C(27)-C(28)	1.458(12)	C(11)-C(10)-H(10)	119.1
C(11)-C(12)	1.397(2)	C(27)-H(27A)	0.9700	C(10)-C(11)-C(12)	117.19(15)
C(11)-C(14)	1.463(2)	C(27)-H(27B)	0.9700	C(10)-C(11)-C(14)	116.08(15)
C(12)-C(13)	1.382(2)	C(28)-H(28A)	0.9600	C(12)-C(11)-C(14)	126.71(15)
C(12)-H(12)	0.9300	C(28)-H(28B)	0.9600	C(13)-C(12)-C(11)	120.76(15)
C(13)-H(13)	0.9300	C(28)-H(28C)	0.9600	C(13)-C(12)-H(12)	119.6
C(14)-C(15)	1.344(2)	C(2)-C(1)-C(7)#1	120.36(15)	C(11)-C(12)-H(12)	119.6
C(14)-H(14)	0.9300	C(2)-C(1)-H(1)	119.8	C(12)-C(13)-C(8)	121.76(15)
C(15)-C(22)	1.437(3)	C(7)#1-C(1)-H(1)	119.8	C(12)-C(13)-H(13)	119.1
C(15)-C(16)	1.486(2)	C(1)-C(2)-C(3)	121.42(15)	C(8)-C(13)-H(13)	119.1
C(16)-C(21)	1.375(3)	C(1)-C(2)-H(2)	119.3	C(15)-C(14)-C(11)	132.22(17)
C(16)-C(17)	1.377(3)	C(3)-C(2)-H(2)	119.3	C(15)-C(14)-H(14)	113.9
C(17)-C(18)	1.386(3)	C(4)-C(3)-C(2)	121.76(14)	C(11)-C(14)-H(14)	113.9
C(17)-H(17)	0.9300	C(4)-C(3)-C(5)#1	120.11(14)	C(14)-C(15)-C(22)	120.55(16)

C(18)-C(19)	1.360(3)	C(2)-C(3)-C(5)#1	118.12(13)	C(14)-C(15)-C(16)	123.78(17)
C(18)-H(18)	0.9300	C(5)-C(4)-C(3)	119.83(14)	C(22)-C(15)-C(16)	115.61(15)
C(19)-C(20)	1.360(4)	C(5)-C(4)-C(8)	120.94(13)	C(21)-C(16)-C(17)	115.79(19)
C(21)-C(16)-C(15)	121.80(19)	C(16)-C(21)-H(21)	119.0	C(24)-C(25)-C(26)	114.0(4)
C(17)-C(16)-C(15)	122.37(17)	C(20)-C(21)-H(21)	119.0	C(24)-C(25)-H(25A)	108.8
C(16)-C(17)-C(18)	122.4(2)	N(1)-C(22)-C(15)	177.6(2)	C(26)-C(25)-H(25A)	108.8
C(16)-C(17)-H(17)	118.8	O(1)-C(23)-C(24)	108.2(2)	C(24)-C(25)-H(25B)	108.8
C(18)-C(17)-H(17)	118.8	O(1)-C(23)-H(23A)	110.1	C(26)-C(25)-H(25B)	108.8
C(19)-C(18)-C(17)	120.3(2)	C(24)-C(23)-H(23A)	110.1	H(25A)-C(25)-H(25B)	107.7
C(19)-C(18)-H(18)	119.9	O(1)-C(23)-H(23B)	110.1	C(25)-C(26)-C(27)	113.6(6)
C(17)-C(18)-H(18)	119.9	C(24)-C(23)-H(23B)	110.1	C(25)-C(26)-H(26A)	108.8
C(20)-C(19)-C(18)	118.6(2)	H(23A)-C(23)-H(23B)	108.4	C(27)-C(26)-H(26A)	108.8
C(20)-C(19)-O(1)	116.4(2)	C(25)-C(24)-C(23)	113.1(3)	C(25)-C(26)-H(26B)	108.8
C(18)-C(19)-O(1)	125.0(2)	C(25)-C(24)-H(24A)	109.0	C(27)-C(26)-H(26B)	108.8
C(19)-C(20)-C(21)	120.8(2)	C(23)-C(24)-H(24A)	109.0	H(26A)-C(26)-H(26B)	107.7
C(19)-C(20)-H(20)	119.6	C(25)-C(24)-H(24B)	109.0	C(28)-C(27)-C(26)	107.9(9)
C(21)-C(20)-H(20)	119.6	C(23)-C(24)-H(24B)	109.0	C(28)-C(27)-H(27A)	110.1
C(16)-C(21)-C(20)	122.1(2)	H(24A)-C(24)-H(24B)	107.8	C(26)-C(27)-H(27A)	110.1
C(28)-C(27)-H(27B)	110.1	C(27)-C(28)-H(28A)	109.5	C(27)-C(28)-H(28C)	109.5
C(26)-C(27)-H(27B)	110.1	C(27)-C(28)-H(28B)	109.5	H(28A)-C(28)-H(28C)	109.5
H(27A)-C(27)-H(27B)	108.4	H(28A)-C(28)-H(28B)	109.5	H(28B)-C(28)-H(28C)	109.5
C(19)-O(1)-C(23)	119.2(2)				

CS-4.1b

Table 1. Table showing torsions.

Atoms	Angle (°)	Atoms	Angle (°)
C(1)-C(2)-C(3)-C(4)	179.43(13)	C(12)-C(15)-C(16)-C(17)	-179.28(12)
C(2)-C(3)-C(4)-C(5)	179.45(12)	C(15)-C(16)-C(17)-C(18)	112.95(15)
C(3)-C(4)-C(5)-C(6)	179.44(12)	C(15)-C(16)-C(17)-C(21)	-64.85(18)
C(4)-C(5)-C(6)-C(7)	178.49(11)	C(21)-C(17)-C(18)-C(19)	-178.60(12)
C(5)-C(6)-C(7)-C(8)	-178.50(11)	C(16)-C(17)-C(18)-C(19)	3.59(19)
C(6)-C(7)-C(8)-O(1)	178.00(11)	C(21)-C(17)-C(18)-C(21)#1	2.7(2)
O(1)-C(9)-C(10)-C(11)	179.01(12)	C(16)-C(17)-C(18)-C(21)#1	-175.08(12)
C(14)-C(9)-C(10)-C(11)	-1.0(2)	C(17)-C(18)-C(19)-C(20)	-177.07(14)
C(9)-C(10)-C(11)-C(12)	-0.3(2)	C(21)#1-C(18)-C(19)-C(20)	1.6(2)
C(10)-C(11)-C(12)-C(13)	1.5(2)	C(18)-C(19)-C(20)-C(23)#1	1.8(2)
C(10)-C(11)-C(12)-C(15)	-177.36(12)	C(18)-C(17)-C(21)-C(22)	174.95(12)
C(11)-C(12)-C(13)-C(14)	-1.5(2)	C(16)-C(17)-C(21)-C(22)	-7.3(2)
C(15)-C(12)-C(13)-C(14)	177.33(12)	C(18)-C(17)-C(21)-C(18)#1	-2.7(2)
C(12)-C(13)-C(14)-C(9)	0.3(2)	C(16)-C(17)-C(21)-C(18)#1	175.03(12)
O(1)-C(9)-C(14)-C(13)	-179.02(12)	C(17)-C(21)-C(22)-C(23)	179.83(14)
C(10)-C(9)-C(14)-C(13)	1.0(2)	C(18)#1-C(21)-C(22)-C(23)	-2.4(2)
C(13)-C(12)-C(15)-C(16)	-14.3(2)	C(21)-C(22)-C(23)-C(20)#1	-0.9(2)
C(11)-C(12)-C(15)-C(16)	164.57(14)	C(10)-C(9)-O(1)-C(8)	-179.73(11)
C(13)-C(12)-C(15)-C(24)	169.27(12)	C(14)-C(9)-O(1)-C(8)	0.3(2)
C(11)-C(12)-C(15)-C(24)	-11.91(18)	C(7)-C(8)-O(1)-C(9)	178.13(11)
C(24)-C(15)-C(16)-C(17)	-2.9(2)		

Table 2. Table showing bond length and bond angles.

Bond Length	Bond Angle (°)	Bond Length	Bond Angle (°)	Bond Length	Bond Angle (°)
C(1)-C(2)	1.524(2)	C(13)-H(13)	0.9500	H(3A)-C(3)-H(3B)	107.9
C(1)-H(1A)	0.9800	C(14)-H(14)	0.9500	C(5)-C(4)-C(3)	114.02(11)
C(1)-H(1B)	0.9800	C(15)-C(16)	1.344(2)	C(5)-C(4)-H(4A)	108.7
C(1)-H(1C)	0.9800	C(15)-C(24)	1.4525(19)	C(3)-C(4)-H(4A)	108.7
C(2)-C(3)	1.5272(19)	C(16)-C(17)	1.4836(18)	C(5)-C(4)-H(4B)	108.7
C(2)-H(2A)	0.9900	C(16)-H(16)	0.9500	C(3)-C(4)-H(4B)	108.7
C(2)-H(2B)	0.9900	C(17)-C(18)	1.4099(19)	H(4A)-C(4)-H(4B)	107.6
C(3)-C(4)	1.5286(19)	C(17)-C(21)	1.4107(19)	C(4)-C(5)-C(6)	113.04(11)
C(3)-H(3A)	0.9900	C(18)-C(19)	1.4326(19)	C(4)-C(5)-H(5A)	109.0
C(3)-H(3B)	0.9900	C(18)-C(21)#1	1.4366(18)	C(6)-C(5)-H(5A)	109.0
C(4)-C(5)	1.5255(18)	C(19)-C(20)	1.360(2)	C(4)-C(5)-H(5B)	109.0
C(4)-H(4A)	0.9900	C(19)-H(19)	0.9500	C(6)-C(5)-H(5B)	109.0
C(4)-H(4B)	0.9900	C(20)-C(23)#1	1.423(2)	H(5A)-C(5)-H(5B)	107.8
C(5)-C(6)	1.5290(18)	C(20)-H(20)	0.9500	C(7)-C(6)-C(5)	111.82(11)
C(5)-H(5A)	0.9900	C(21)-C(22)	1.4334(19)	C(7)-C(6)-H(6A)	109.3
C(5)-H(5B)	0.9900	C(22)-C(23)	1.357(2)	C(5)-C(6)-H(6A)	109.3
C(6)-C(7)	1.5256(18)	C(22)-H(22)	0.9500	C(7)-C(6)-H(6B)	109.3
C(6)-H(6A)	0.9900	C(23)-H(23)	0.9500	C(5)-C(6)-H(6B)	109.3
C(6)-H(6B)	0.9900	C(24)-N(1)	1.1448(19)	H(6A)-C(6)-H(6B)	107.9
C(7)-C(8)	1.5151(18)			C(8)-C(7)-C(6)	113.46(11)
C(7)-H(7A)	0.9900	C(2)-C(1)-H(1A)	109.5	C(8)-C(7)-H(7A)	108.9
C(7)-H(7B)	0.9900	C(2)-C(1)-H(1B)	109.5	C(6)-C(7)-H(7A)	108.9
C(8)-O(1)	1.4362(16)	H(1A)-C(1)-H(1B)	109.5	C(8)-C(7)-H(7B)	108.9
C(8)-H(8A)	0.9900	C(2)-C(1)-H(1C)	109.5	C(6)-C(7)-H(7B)	108.9
C(8)-H(8B)	0.9900	H(1A)-C(1)-H(1C)	109.5	H(7A)-C(7)-H(7B)	107.7
C(9)-O(1)	1.3666(16)	H(1B)-C(1)-H(1C)	109.5	O(1)-C(8)-C(7)	106.19(11)
C(9)-C(10)	1.3927(19)	C(1)-C(2)-C(3)	114.08(12)	O(1)-C(8)-H(8A)	110.5
C(9)-C(14)	1.396(2)	C(1)-C(2)-H(2A)	108.7	C(7)-C(8)-H(8A)	110.5
C(10)-C(11)	1.3840(19)	C(3)-C(2)-H(2A)	108.7	O(1)-C(8)-H(8B)	110.5
C(10)-H(10)	0.9500	C(1)-C(2)-H(2B)	108.7	C(7)-C(8)-H(8B)	110.5
C(11)-C(12)	1.4038(19)	C(3)-C(2)-H(2B)	108.7	H(8A)-C(8)-H(8B)	108.7
C(11)-H(11)	0.9500	H(2A)-C(2)-H(2B)	107.6	O(1)-C(9)-C(10)	115.21(12)
C(12)-C(13)	1.3929(19)	C(2)-C(3)-C(4)	112.18(12)	O(1)-C(9)-C(14)	124.82(12)
C(12)-C(15)	1.4825(18)	C(2)-C(3)-H(3A)	109.2	C(10)-C(9)-C(14)	119.97(12)
C(13)-C(14)	1.3920(19)	C(4)-C(3)-H(3A)	109.2	C(11)-C(10)-C(9)	119.95(12)

C(11)-C(10)-H(10)	120.0	C(17)-C(16)-H(16)	118.6	C(22)-C(23)-C(20)#1	120.67(14)
C(9)-C(10)-H(10)	120.0	C(18)-C(17)-C(21)	120.27(12)	C(22)-C(23)-H(23)	119.7
C(10)-C(11)-C(12)	121.11(13)	C(18)-C(17)-C(16)	118.99(12)	C(20)#1-C(23)-H(23)	119.7
C(10)-C(11)-H(11)	119.4	C(21)-C(17)-C(16)	120.70(12)	N(1)-C(24)-C(15)	178.31(15)
C(12)-C(11)-H(11)	119.4	C(17)-C(18)-C(19)	121.39(12)	C(9)-O(1)-C(8)	119.05(10)
C(13)-C(12)-C(11)	118.08(12)	C(17)-C(18)-C(21)#1	119.67(12)	C(22)-C(21)-C(18)#1	117.91(12)
C(13)-C(12)-C(15)	121.77(12)	C(19)-C(18)-C(21)#1	118.92(12)	C(23)-C(22)-C(21)	121.25(13)
C(11)-C(12)-C(15)	120.14(12)	C(20)-C(19)-C(18)	120.87(13)	C(23)-C(22)-H(22)	119.4
C(14)-C(13)-C(12)	121.49(13)	C(20)-C(19)-H(19)	119.6	C(21)-C(22)-H(22)	119.4
C(14)-C(13)-H(13)	119.3	C(18)-C(19)-H(19)	119.6	C(16)-C(15)-C(12)	126.88(12)
C(12)-C(13)-H(13)	119.3	C(19)-C(20)-C(23)#1	120.24(14)	C(24)-C(15)-C(12)	115.55(12)
C(13)-C(14)-C(9)	119.39(13)	C(19)-C(20)-H(20)	119.9	C(15)-C(16)-C(17)	122.82(12)
C(13)-C(14)-H(14)	120.3	C(23)#1-C(20)-H(20)	119.9	C(15)-C(16)-H(16)	118.6
C(9)-C(14)-H(14)	120.3	C(17)-C(21)-C(22)	122.05(12)	C(17)-C(21)-C(18)#1	120.00(12)
C(16)-C(15)-C(24)	117.48(12)				

CS-4.2b

Table 1. Table showing torsions.

Atoms	Angle (°)	Atoms	Angle (°)
C(7)-C(1)-C(2)-C(3)	-179.3(2)	C(10)-C(11)-C(14)-C(15)	-14.3(5)
C(6)-C(1)-C(2)-C(3)	2.3(4)	C(11)-C(14)-C(15)-C(16)	-0.1(5)
C(1)-C(2)-C(3)-C(4)	-0.4(4)	C(11)-C(14)-C(15)-C(17)	-176.3(3)
C(2)-C(3)-C(4)-C(5)	-1.6(4)	C(14)-C(15)-C(17)-C(22)	-14.8(5)
C(3)-C(4)-C(5)-C(6)	1.6(4)	C(16)-C(15)-C(17)-C(22)	168.7(3)
C(4)-C(5)-C(6)-C(7)#1	-179.4(2)	C(14)-C(15)-C(17)-C(18)	164.0(3)
C(4)-C(5)-C(6)-C(1)	0.4(4)	C(16)-C(15)-C(17)-C(18)	-12.4(4)
C(7)-C(1)-C(6)-C(7)#1	-0.8(4)	C(22)-C(17)-C(18)-C(19)	-0.2(5)
C(2)-C(1)-C(6)-C(7)#1	177.6(2)	C(15)-C(17)-C(18)-C(19)	-179.1(3)
C(7)-C(1)-C(6)-C(5)	179.4(2)	C(17)-C(18)-C(19)-C(20)	-1.0(6)
C(2)-C(1)-C(6)-C(5)	-2.3(3)	C(18)-C(19)-C(20)-C(21)	2.2(6)
C(2)-C(1)-C(7)-C(6)#1	-177.5(2)	C(18)-C(19)-C(20)-O(1)	-179.4(3)
C(6)-C(1)-C(7)-C(6)#1	0.8(4)	C(19)-C(20)-C(21)-C(22)	-2.2(6)
C(2)-C(1)-C(7)-C(8)	6.9(3)	O(1)-C(20)-C(21)-C(22)	179.5(3)
C(6)-C(1)-C(7)-C(8)	-174.8(2)	C(18)-C(17)-C(22)-C(21)	0.1(5)
C(6)#1-C(7)-C(8)-C(9)	72.2(3)	C(15)-C(17)-C(22)-C(21)	179.0(3)
C(1)-C(7)-C(8)-C(9)	-112.2(3)	C(20)-C(21)-C(22)-C(17)	1.1(6)
C(6)#1-C(7)-C(8)-C(13)	-109.3(3)	O(1)-C(23)-C(24)-C(25)	179.6(3)
C(1)-C(7)-C(8)-C(13)	66.3(3)	C(23)-C(24)-C(25)-C(26)	177.8(3)
C(13)-C(8)-C(9)-C(10)	1.0(4)	C(24)-C(25)-C(26)-C(27)	177.7(4)
C(7)-C(8)-C(9)-C(10)	179.5(3)	C(25)-C(26)-C(27)-C(28)	177.2(13)
C(8)-C(9)-C(10)-C(11)	-1.1(4)	C(25)-C(26)-C(27)-C(28')	178.1(10)
C(9)-C(10)-C(11)-C(12)	-0.2(4)	C(19)-C(20)-O(1)-C(23)	175.3(3)
C(9)-C(10)-C(11)-C(14)	178.7(3)	C(21)-C(20)-O(1)-C(23)	-6.4(5)
C(10)-C(11)-C(12)-C(13)	1.4(4)	C(24)-C(23)-O(1)-C(20)	-174.0(3)
C(14)-C(11)-C(12)-C(13)	-177.5(3)	C(26)-C(27)-C(28)-C(29)	-178(2)
C(11)-C(12)-C(13)-C(8)	-1.5(4)	C(27)-C(28)-C(29)-C(30)	178(2)
C(9)-C(8)-C(13)-C(12)	0.3(4)	C(26)-C(27)-C(28')-C(29')	-172(2)
C(7)-C(8)-C(13)-C(12)	-178.3(2)	C(27)-C(28')-C(29')-C(30')	-27(6)
C(12)-C(11)-C(14)-C(15)	164.6(3)		

Table 2. Table showing bond length and bond angles.

Bond Length	Bond Angle (°)	Bond Length	Bond Angle (°)	Bond Length	Bond Angle (°)
C(1)-C(7)	1.405(3)	C(29)-C(30)	1.419(10)	C(17)-C(18)-C(19)	121.7(3)
C(1)-C(2)	1.429(3)	C(28')-C(29')	1.434(17)	C(20)-C(19)-C(18)	121.0(3)
C(1)-C(6)	1.436(3)	C(29')-C(30')	1.410(10)	C(19)-C(20)-C(21)	118.8(3)
C(2)-C(3)	1.353(3)			C(19)-C(20)-O(1)	116.7(3)
C(3)-C(4)	1.408(4)	C(7)-C(1)-C(2)	122.0(2)	C(21)-C(20)-O(1)	124.5(3)
C(4)-C(5)	1.345(4)	C(7)-C(1)-C(6)	120.5(2)	C(20)-C(21)-C(22)	120.0(3)
C(5)-C(6)	1.428(3)	C(2)-C(1)-C(6)	117.5(2)	C(17)-C(22)-C(21)	122.4(3)
C(6)-C(7)#1	1.399(3)	C(3)-C(2)-C(1)	121.9(2)	O(1)-C(23)-C(24)	109.2(3)
C(7)-C(8)	1.495(3)	C(2)-C(3)-C(4)	120.2(3)	C(23)-C(24)-C(25)	111.7(3)
C(8)-C(9)	1.379(3)	C(5)-C(4)-C(3)	120.5(3)	C(26)-C(25)-C(24)	115.4(4)
C(8)-C(13)	1.389(3)	C(4)-C(5)-C(6)	121.6(2)	C(27)-C(26)-C(25)	116.4(4)
C(9)-C(10)	1.384(3)	C(7)#1-C(6)-C(5)	122.0(2)	C(28)-C(27)-C(26)	126.7(9)
C(10)-C(11)	1.396(4)	C(7)#1-C(6)-C(1)	119.8(2)	C(26)-C(27)-C(28')	106.4(8)
C(11)-C(12)	1.384(4)	C(5)-C(6)-C(1)	118.2(2)	C(20)-O(1)-C(23)	118.3(3)
C(11)-C(14)	1.457(3)	C(6)#1-C(7)-C(1)	119.7(2)	C(27)-C(28)-C(29)	129.0(16)
C(12)-C(13)	1.370(3)	C(6)#1-C(7)-C(8)	121.0(2)	C(30)-C(29)-C(28)	117.2(17)
C(14)-C(15)	1.340(4)	C(1)-C(7)-C(8)	119.1(2)	C(29')-C(28')-C(27)	114.8(16)
C(15)-C(16)	1.432(4)	C(9)-C(8)-C(13)	117.4(2)	C(30')-C(29')-C(28')	120.8(19)
C(15)-C(17)	1.490(4)	C(9)-C(8)-C(7)	123.7(2)	C(26)-C(27)	1.492(6)
C(16)-N(1)	1.141(4)	C(13)-C(8)-C(7)	118.9(2)	C(27)-C(28)	1.415(15)
C(17)-C(22)	1.374(4)	C(8)-C(9)-C(10)	121.7(3)	C(27)-C(28')	1.60(2)
C(17)-C(18)	1.377(4)	C(9)-C(10)-C(11)	120.8(3)	C(28)-C(29)	1.444(16)
C(18)-C(19)	1.381(4)	C(12)-C(11)-C(10)	117.0(2)	N(1)-C(16)-C(15)	177.9(3)
C(19)-C(20)	1.355(4)	C(12)-C(11)-C(14)	116.4(2)	C(22)-C(17)-C(18)	116.1(3)
C(20)-C(21)	1.361(4)	C(10)-C(11)-C(14)	126.6(3)	C(22)-C(17)-C(15)	122.0(3)
C(20)-O(1)	1.370(3)	C(13)-C(12)-C(11)	122.0(3)	C(18)-C(17)-C(15)	121.9(3)
C(21)-C(22)	1.387(4)	C(12)-C(13)-C(8)	121.1(3)	C(24)-C(25)	1.508(5)
C(23)-O(1)	1.412(4)	C(15)-C(14)-C(11)	132.5(3)	C(25)-C(26)	1.492(5)
C(23)-C(24)	1.503(4)	C(14)-C(15)-C(16)	120.7(3)	C(16)-C(15)-C(17)	115.3(2)
C(14)-C(15)-C(17)	123.9(3)				

Appendix II

Copyrights and Permissions

CCC Marketplace

Order Confirmation

Thank you, your order has been placed. An email confirmation has been sent to you. Your order license details and printable licenses will be available within 24 hours. Please access Manage Account for final order details.

This is not an invoice. Please go to manage account to access your order history and invoices.

CUSTOMER INFORMATION

Payment by invoice: You can cancel your order until the invoice is generated by contacting customer service.

Billing Address

Ms. FEMINA CHERUMANNIL
Farook College
Farook College
Kozhikode, Kerala 673632
India

+91 9995990602
femi.fana@gmail.com

Customer Location

Ms. FEMINA CHERUMANNIL
Farook College
Farook College
Kozhikode, Kerala 673632
India

PO Number (optional)

N/A

Payment options

Invoice

PENDING ORDER CONFIRMATION

Confirmation Number: Pending

Order Date: 17-Sep-2025

1. Journal of materials chemistry. C, Materials for optical and electronic devices

0.00 USD

Article: Cyanostilbene-based intelligent organic optoelectronic materials

Order License ID	Pending	**Publisher**	Royal Society of Chemistry
ISSN	2050-7534	**Portion**	Image/photo/illustration
Type of Use	Republish in a thesis/dissertation		

LICENSED CONTENT

Publication Title	Journal of materials chemistry. C, Materials for optical and electronic devices	**Publication Type**	e-Journal
		Start Page	1059
Article Title	Cyanostilbene-based intelligent organic optoelectronic materials	**End Page**	1065
		Issue	6
Author / Editor	Royal Society of Chemistry (Great Britain)	**Volume**	1
Date	01/01/2013	**URL**	http://pubs.rsc.org/en/journals/journalissues/tc#
Language	English		
Country	United Kingdom of Great Britain and Northern Ireland		
Rightsholder	Royal Society of Chemistry		

REQUEST DETAILS

Portion Type	Image/photo/illustration	**Distribution**	Worldwide
Number of Images / Photos / Illustrations	1	**Translation**	Original language of publication
		Copies for the Disabled?	Yes
Format (select all that apply)	Print, Electronic	**Minor Editing Privileges?**	No
Who Will Republish the Content?	Academic institution	**Incidental Promotional Use?**	No
Duration of Use	Life of current edition	**Currency**	USD
Lifetime Unit Quantity	Up to 499		
Rights Requested	Main product		

NEW WORK DETAILS

Title	Experimental and Theoretical Investigation of Optical Properties on Cyanostyrene Based Donor-Acceptor Systems	**Institution Name**	Farook College
		Expected Presentation Date	2025-09-20
Instructor Name	Dr. Reji Thomas		

ADDITIONAL DETAILS

Order Reference Number	N/A	**The Requesting Person / Organization to Appear on the License**	Femina C

REQUESTED CONTENT DETAILS

Title, Description or Numeric Reference of the Portion(s)	Figure 1.3	**Title of the Article / Chapter the Portion Is From**	Cyanostilbene-based intelligent organic optoelectronic materials
Editor of Portion(s)	Zhu, Liangliang; Zhao, Yanli	**Author of Portion(s)**	Zhu, Liangliang; Zhao, Yanli
Volume / Edition	1		

Page or Page Range of Portion	1059-1065	Issue, if Republishing an Article From a Serial	6
		Publication Date of Portion	2013-01-17

Total Items: 1

Total Due: 0.00 USD

Accepted: Marketplace Permissions General Terms and Conditions and any applicable Publisher Terms and Conditions

AMERICAN CHEMICAL SOCIETY LICENSE
TERMS AND CONDITIONS

Sep 17, 2025

This Agreement between Femina C ("You") and American Chemical Society ("American Chemical Society") consists of your license details and the terms and conditions provided by American Chemical Society and Copyright Clearance Center.

License Number	6111470161798
License date	Sep 17, 2025
Licensed Content Publisher	American Chemical Society
Licensed Content Publication	Journal of Chemical Education
Licensed Content Title	Fluorescence Aggregation-Caused Quenching versus Aggregation-Induced Emission: A Visual Teaching Technology for Undergraduate Chemistry Students
Licensed Content Author	Xiaofeng Ma, Rui Sun, Jinghui Cheng, et al
Licensed Content Date	Feb 1, 2016
Licensed Content Volume	93
Licensed Content Issue	2
Volume number	93
Issue number	2
Type of Use	Thesis/Dissertation
Requestor type	Non-profit
Format	Print and Electronic
Portion	Table/Figure/Micrograph
Number of Table/Figure/Micrographs	1
Title of new work	Experimental and Theoretical Investigation of Optical Properties on Cyanostyrene Based Donor-Acceptor Systems
Institution name	Farook College
Expected presentation date	Sep 2025
Portions	Figure 1.4
The Requesting Person / Organization to Appear on the License	Femina C
Requestor Location	Ms. FEMINA CHERUMANNIL Farook College Kozhikode, Kerala 673632 India
Billing Type	Invoice
Billing Address	Farook College Farook College Kozhikode, India 673632

Total 0.00 USD

Terms and Conditions

American Chemical Society's Policy on Thesis and Dissertations

If your university requires you to obtain permission, you must use the RightsLink permission system.
See RightsLink instructions at http://pubs.acs.org/page/copyright/permissions.html.

This is regarding request for permission to include **your** paper(s) or portions of text from **your** paper(s) in your thesis.
Permission is now automatically granted; please pay special attention to the **implications** paragraph below. The Copyright Subcommittee of the Joint Board/Council Committees on Publications approved the following:

> Copyright permission for published and submitted material from thesis and dissertations
> ACS extends blanket permission to students to include in their thesis and dissertations their own articles, or portions thereof, that have been published in ACS journals or submitted to ACS journals for publication, provided that the ACS copyright credit line is noted on the appropriate page(s).
>
> Publishing implications of electronic publication of thesis and dissertation material
> Students and their mentors should be aware that posting of thesis and dissertation material on the Web prior to submission of material from that thesis or dissertation to an ACS journal may affect publication in that journal. Whether Web posting is considered prior publication may be evaluated on a case-by-case basis by the journal's editor. If an ACS journal editor considers Web posting to be "prior publication", the paper will not be accepted for publication in that journal. If you intend to submit your unpublished paper to ACS for publication, check with the appropriate editor prior to posting your manuscript electronically.

Reuse/Republication of the Entire Work in Thesis or Collections: Authors may reuse all or part of the Submitted, Accepted or Published Work in a thesis or dissertation that the author writes and is required to submit to satisfy the criteria of degree-granting institutions. Such reuse is permitted subject to the ACS' "Ethical Guidelines to Publication of Chemical Research" (http://pubs.acs.org/page/policy/ethics/index.htmlb); the author should secure written confirmation (via letter or email) from the respective ACS journal editor(s) to avoid potential conflicts with journal prior publication*/embargo policies. Appropriate citation of the Published Work must be made. If the thesis or dissertation to be published is in electronic format, a direct link to the Published Work must also be included using the ACS Articles on Request author-directed link - see http://pubs.acs.org/page/policy/articlesonrequest/index.html

* Prior publication policies of ACS journals are posted on the ACS website at http://pubs.acs.org/page/policy/prior/index.html

If your paper has not yet been published by ACS, please print the following credit line on the first page of your article: "Reproduced (or 'Reproduced in part') with permission from [JOURNAL NAME], in press (or 'submitted for publication'). Unpublished work copyright [CURRENT YEAR] American Chemical Society." Include appropriate information.

If your paper has already been published by ACS and you want to include the text or portions of the text in your thesis/dissertation, please print the ACS copyright credit line on the first page of your article: "Reproduced (or 'Reproduced in part') with permission from [FULL REFERENCE CITATION.] Copyright [YEAR] American Chemical Society." Include appropriate information.

Submission to a Dissertation Distributor: If you plan to submit your thesis to UMI or to another dissertation distributor, you should not include the unpublished ACS paper in your thesis if the thesis will be disseminated electronically, until ACS has published your paper. After publication of the paper by ACS, you may release the entire thesis (**not the individual ACS article by itself**) for electronic dissemination through the distributor; ACS's copyright credit line should be printed on the first page of the ACS paper.

v1.4

Questions? customercare@copyright.com.

AMERICAN CHEMICAL SOCIETY LICENSE
TERMS AND CONDITIONS

Sep 17, 2025

This Agreement between Femina C ("You") and American Chemical Society ("American Chemical Society") consists of your license details and the terms and conditions provided by American Chemical Society and Copyright Clearance Center.

License Number	6111471397751
License date	Sep 17, 2025
Licensed Content Publisher	American Chemical Society
Licensed Content Publication	Chemical Reviews
Licensed Content Title	Aggregation-Induced Emission: Together We Shine, United We Soar!
Licensed Content Author	Ju Mei, Nelson L. C. Leung, Ryan T. K. Kwok, et al
Licensed Content Date	Nov 1, 2015
Licensed Content Volume	115
Licensed Content Issue	21
Volume number	115
Issue number	21
Type of Use	Thesis/Dissertation
Requestor type	Non-profit
Format	Print and Electronic
Portion	Table/Figure/Micrograph
Number of Table/Figure/Micrographs	1
Title of new work	Experimental and Theoretical Investigation of Optical Properties on Cyanostyrene Based Donor-Acceptor Systems
Institution name	Farook College
Expected presentation date	Sep 2025
Portions	Figure 1.6
The Requesting Person / Organization to Appear on the License	Femina C
Requestor Location	Ms. FEMINA CHERUMANNIL Farook College Kozhikode, Kerala 673632 India
Billing Type	Invoice
Billing Address	Farook College Farook College Kozhikode, India 673632
Total	0.00 USD

Terms and Conditions

American Chemical Society's Policy on Thesis and Dissertations

If your university requires you to obtain permission, you must use the RightsLink permission system.

See RightsLink instructions at http://pubs.acs.org/page/copyright/permissions.html.

This is regarding request for permission to include **your** paper(s) or portions of text from **your** paper(s) in your thesis.
Permission is now automatically granted; please pay special attention to the **implications** paragraph below. The Copyright Subcommittee of the Joint Board/Council Committees on Publications approved the following:

> Copyright permission for published and submitted material from thesis and dissertations
> ACS extends blanket permission to students to include in their thesis and dissertations their own articles, or portions thereof, that have been published in ACS journals or submitted to ACS journals for publication, provided that the ACS copyright credit line is noted on the appropriate page(s).
>
> Publishing implications of electronic publication of thesis and dissertation material
> Students and their mentors should be aware that posting of thesis and dissertation material on the Web prior to submission of material from that thesis or dissertation to an ACS journal may affect publication in that journal. Whether Web posting is considered prior publication may be evaluated on a case-by-case basis by the journal's editor. If an ACS journal editor considers Web posting to be "prior publication", the paper will not be accepted for publication in that journal. If you intend to submit your unpublished paper to ACS for publication, check with the appropriate editor prior to posting your manuscript electronically.

Reuse/Republication of the Entire Work in Thesis or Collections: Authors may reuse all or part of the Submitted, Accepted or Published Work in a thesis or dissertation that the author writes and is required to submit to satisfy the criteria of degree-granting institutions. Such reuse is permitted subject to the ACS' "Ethical Guidelines to Publication of Chemical Research" (http://pubs.acs.org/page/policy/ethics/index.htmlb); the author should secure written confirmation (via letter or email) from the respective ACS journal editor(s) to avoid potential conflicts with journal prior publication*/embargo policies. Appropriate citation of the Published Work must be made. If the thesis or dissertation to be published is in electronic format, a direct link to the Published Work must also be included using the ACS Articles on Request author-directed link - see http://pubs.acs.org/page/policy/articlesonrequest/index.html

* Prior publication policies of ACS journals are posted on the ACS website at http://pubs.acs.org/page/policy/prior/index.html

If your paper has not yet been published by ACS, please print the following credit line on the first page of your article: "Reproduced (or 'Reproduced in part') with permission from [JOURNAL NAME], in press (or 'submitted for publication'). Unpublished work copyright [CURRENT YEAR] American Chemical Society." Include appropriate information.

If your paper has already been published by ACS and you want to include the text or portions of the text in your thesis/dissertation, please print the ACS copyright credit line on the first page of your article: "Reproduced (or 'Reproduced in part') with permission from [FULL REFERENCE CITATION.] Copyright [YEAR] American Chemical Society." Include appropriate information.

Submission to a Dissertation Distributor: If you plan to submit your thesis to UMI or to another dissertation distributor, you should not include the unpublished ACS paper in your thesis if the thesis will be disseminated electronically, until ACS has published your paper. After publication of the paper by ACS, you may release the entire thesis (**not the individual ACS article by itself**) for electronic dissemination through the distributor; ACS's copyright credit line should be printed on the first page of the ACS paper.

v1.4

Questions? customercare@copyright.com.

CCC Marketplace

Order Confirmation

Thank you, your order has been placed. An email confirmation has been sent to you. Your order license details and printable licenses will be available within 24 hours. Please access Manage Account for final order details.

This is not an invoice. Please go to manage account to access your order history and invoices.

CUSTOMER INFORMATION

Payment by invoice: You can cancel your order until the invoice is generated by contacting customer service.

Billing Address

Ms. FEMINA CHERUMANNIL
Farook College
Farook College
Kozhikode, Kerala 673632
India

+91 9995990602
femi.fana@gmail.com

Customer Location

Ms. FEMINA CHERUMANNIL
Farook College
Farook College
Kozhikode, Kerala 673632
India

PO Number (optional)

N/A

Payment options

Invoice

PENDING ORDER CONFIRMATION

Confirmation Number: Pending

Order Date: 17-Sep-2025

1. CrystEngComm

0.00 USD

Article: Dimesitylboryl-functionalised cyanostilbene derivatives of phenothiazine: distinctive polymorphism-dependent emission and mechanofluorochromism

Order License ID	Pending	**Publisher**	ROYAL SOCIETY OF CHEMISTRY
ISSN	1466-8033		
Type of Use	Republish in a thesis/dissertation	**Portion**	Image/photo/illustration

LICENSED CONTENT

Publication Title	CrystEngComm	**Publication Type**	e-Journal
Article Title	Dimesitylboryl-functionalised cyanostilbene derivatives of phenothiazine: distinctive polymorphism-dependent emission and mechanofluorochromism	**Start Page**	3162
		End Page	3166
		Issue	23
		Volume	20
Author / Editor	Royal Society of Chemistry (Great Britain)	**URL**	http://www.rsc.org/Publishing/Journals/ce/index.asp
Date	01/01/1999		
Language	English		
Country	United Kingdom of Great Britain and Northern Ireland		
Rightsholder	Royal Society of Chemistry		

REQUEST DETAILS

Portion Type	Image/photo/illustration	**Distribution**	Worldwide
Number of Images / Photos / Illustrations	1	**Translation**	Original language of publication
		Copies for the Disabled?	No
Format (select all that apply)	Print, Electronic	**Minor Editing Privileges?**	No
Who Will Republish the Content?	Academic institution	**Incidental Promotional Use?**	No
Duration of Use	Life of current edition	**Currency**	USD
Lifetime Unit Quantity	Up to 499		
Rights Requested	Main product		

NEW WORK DETAILS

Title	Experimental and Theoretical Investigation of Optical Properties on Cyanostyrene Based Donor-Acceptor Systems	**Institution Name**	Farook College
		Expected Presentation Date	2025-09-17
Instructor Name	Dr. Reji Thomas		

ADDITIONAL DETAILS

Order Reference Number	N/A	**The Requesting Person / Organization to Appear on the License**	Femina C

REQUESTED CONTENT DETAILS

Title, Description or Numeric Reference of the Portion(s)	Figure 1.8

Editor of Portion(s)	Arivazhagan, C.; Malakar, Partha; Jagan, R.; Prasad, Edamana; Ghosh, Sundargopal	Title of the Article / Chapter the Portion Is From	Dimesitylboryl-functionalised cyanostilbene derivatives of phenothiazine: distinctive polymorphism-dependent emission and mechanofluorochromism
Volume / Edition	20	Author of Portion(s)	Arivazhagan, C.; Malakar, Partha; Jagan, R.; Prasad, Edamana; Ghosh, Sundargopal
Page or Page Range of Portion	3162-3166	Issue, if Republishing an Article From a Serial	23
		Publication Date of Portion	2018-01-01

Total Items: 1

Total Due: 0.00 USD

CCC Marketplace

Order Confirmation

Thank you, your order has been placed. An email confirmation has been sent to you. Your order license details and printable licenses will be available within 24 hours. Please access Manage Account for final order details.

This is not an invoice. Please go to manage account to access your order history and invoices.

CUSTOMER INFORMATION

Payment by invoice: You can cancel your order until the invoice is generated by contacting customer service.

Billing Address

Ms. FEMINA CHERUMANNIL
Farook College
Farook College
Kozhikode, Kerala 673632
India

+91 9995990602
femi.fana@gmail.com

Customer Location

Ms. FEMINA CHERUMANNIL
Farook College
Farook College
Kozhikode, Kerala 673632
India

PO Number (optional)

N/A

Payment options

Invoice

PENDING ORDER CONFIRMATION

Confirmation Number: Pending

Order Date: 17-Sep-2025

1. Organic Chemistry Frontiers

0.00 USD

Article: Pyrene and triphenylamine substituted cyanostyrene and cyanostilbene derivatives with dual-state emission for high contrast mechanofluorochromism and cell imaging

Order License ID	Pending	**Publisher**	Royal Society of Chemistry
ISSN	2052-4129	**Portion**	Image/photo/illustration
Type of Use	Republish in a thesis/dissertation		

LICENSED CONTENT

Publication Title	Organic Chemistry Frontiers	**Rightsholder**	Royal Society of Chemistry
Article Title	Pyrene and triphenylamine substituted cyanostyrene and cyanostilbene derivatives with dual-state emission for high contrast mechanofluorochromism and cell imaging	**Publication Type**	e-Journal
		Start Page	5118
		End Page	5124
		Issue	19
Author / Editor	Royal Society of Chemistry (Great Britain), Shanghai you ji hua xue yan jiu suo,, Zhongguo hua xue hui (Beijing, China),	**Volume**	9
Date	01/01/2014		
Language	English		
Country	United Kingdom of Great Britain and Northern Ireland		

REQUEST DETAILS

Portion Type	Image/photo/illustration	**Distribution**	Worldwide
Number of Images / Photos / Illustrations	1	**Translation**	Original language of publication
		Copies for the Disabled?	No
Format (select all that apply)	Print, Electronic	**Minor Editing Privileges?**	No
Who Will Republish the Content?	Academic institution	**Incidental Promotional Use?**	No
Duration of Use	Life of current edition	**Currency**	USD
Lifetime Unit Quantity	Up to 499		
Rights Requested	Main product		

NEW WORK DETAILS

Title	Experimental and Theoretical Investigation of Optical Properties on Cyanostyrene Based Donor-Acceptor Systems	**Institution Name**	Farook College
		Expected Presentation Date	2025-09-17
Instructor Name	Dr. Reji Thomas		

ADDITIONAL DETAILS

Order Reference Number	N/A	**The Requesting Person / Organization to Appear on the License**	Femina C

REQUESTED CONTENT DETAILS

Title, Description or Numeric Reference of the Portion(s)	Figure 1.8

Editor of Portion(s)	Huang, Ze; Tang, Fang; He, Felicia; Kong, Lin; Huang, Jianyan; Yang, Jiaxiang; Ding, Aixiang	Title of the Article / Chapter the Portion Is From	Pyrene and triphenylamine substituted cyanostyrene and cyanostilbene derivatives with dual-state emission for high contrast mechanofluorochromism and cell imaging
Volume / Edition	9	Author of Portion(s)	Huang, Ze; Tang, Fang; He, Felicia; Kong, Lin; Huang, Jianyan; Yang, Jiaxiang; Ding, Aixiang
Page or Page Range of Portion	5118-5124	Issue, if Republishing an Article From a Serial	19
		Publication Date of Portion	2022-01-01

Total Items: 1

Total Due: 0.00 USD

AMERICAN CHEMICAL SOCIETY LICENSE
TERMS AND CONDITIONS

Sep 17, 2025

This Agreement between Femina C ("You") and American Chemical Society ("American Chemical Society") consists of your license details and the terms and conditions provided by American Chemical Society and Copyright Clearance Center.

License Number	6111490427092
License date	Sep 17, 2025
Licensed Content Publisher	American Chemical Society
Licensed Content Publication	Applied Materials
Licensed Content Title	Multi-Stimuli-Responsive Fluorescence Switching from a Pyridine-Functionalized Tetraphenylethene AIEgen
Licensed Content Author	Jianbo Xiong, Kai Wang, Zhaoquan Yao, et al
Licensed Content Date	Feb 1, 2018
Licensed Content Volume	10
Licensed Content Issue	6
Volume number	10
Issue number	6
Type of Use	Thesis/Dissertation
Requestor type	Non-profit
Format	Print and Electronic
Portion	Table/Figure/Micrograph
Number of Table/Figure/Micrographs	1
Title of new work	Experimental and Theoretical Investigation of Optical Properties on Cyanostyrene Based Donor-Acceptor Systems
Institution name	Farook College
Expected presentation date	Sep 2025
Portions	1.11
The Requesting Person / Organization to Appear on the License	Femina C
Requestor Location	Ms. FEMINA CHERUMANNIL Farook College Kozhikode, Kerala 673632 India
Billing Type	Invoice
Billing Address	Farook College Farook College Kozhikode, India 673632
Total	0.00 USD

Terms and Conditions

American Chemical Society's Policy on Thesis and Dissertations

If your university requires you to obtain permission, you must use the RightsLink permission system.

See RightsLink instructions at http://pubs.acs.org/page/copyright/permissions.html.

This is regarding request for permission to include **your** paper(s) or portions of text from **your** paper(s) in your thesis.
Permission is now automatically granted; please pay special attention to the **implications** paragraph below. The Copyright Subcommittee of the Joint Board/Council Committees on Publications approved the following:

> Copyright permission for published and submitted material from thesis and dissertations
> ACS extends blanket permission to students to include in their thesis and dissertations their own articles, or portions thereof, that have been published in ACS journals or submitted to ACS journals for publication, provided that the ACS copyright credit line is noted on the appropriate page(s).
>
> Publishing implications of electronic publication of thesis and dissertation material
> Students and their mentors should be aware that posting of thesis and dissertation material on the Web prior to submission of material from that thesis or dissertation to an ACS journal may affect publication in that journal. Whether Web posting is considered prior publication may be evaluated on a case-by-case basis by the journal's editor. If an ACS journal editor considers Web posting to be "prior publication", the paper will not be accepted for publication in that journal. If you intend to submit your unpublished paper to ACS for publication, check with the appropriate editor prior to posting your manuscript electronically.

Reuse/Republication of the Entire Work in Thesis or Collections: Authors may reuse all or part of the Submitted, Accepted or Published Work in a thesis or dissertation that the author writes and is required to submit to satisfy the criteria of degree-granting institutions. Such reuse is permitted subject to the ACS' "Ethical Guidelines to Publication of Chemical Research" (http://pubs.acs.org/page/policy/ethics/index.htmlb); the author should secure written confirmation (via letter or email) from the respective ACS journal editor(s) to avoid potential conflicts with journal prior publication*/embargo policies. Appropriate citation of the Published Work must be made. If the thesis or dissertation to be published is in electronic format, a direct link to the Published Work must also be included using the ACS Articles on Request author-directed link - see http://pubs.acs.org/page/policy/articlesonrequest/index.html

* Prior publication policies of ACS journals are posted on the ACS website at http://pubs.acs.org/page/policy/prior/index.html

If your paper has not yet been published by ACS, please print the following credit line on the first page of your article: "Reproduced (or 'Reproduced in part') with permission from [JOURNAL NAME], in press (or 'submitted for publication'). Unpublished work copyright [CURRENT YEAR] American Chemical Society." Include appropriate information.

If your paper has already been published by ACS and you want to include the text or portions of the text in your thesis/dissertation, please print the ACS copyright credit line on the first page of your article: "Reproduced (or 'Reproduced in part') with permission from [FULL REFERENCE CITATION.] Copyright [YEAR] American Chemical Society." Include appropriate information.

Submission to a Dissertation Distributor: If you plan to submit your thesis to UMI or to another dissertation distributor, you should not include the unpublished ACS paper in your thesis if the thesis will be disseminated electronically, until ACS has published your paper. After publication of the paper by ACS, you may release the entire thesis (**not the individual ACS article by itself**) for electronic dissemination through the distributor; ACS's copyright credit line should be printed on the first page of the ACS paper.

v1.4

Questions? customercare@copyright.com.

CCC Marketplace

Order Confirmation

Thank you, your order has been placed. An email confirmation has been sent to you. Your order license details and printable licenses will be available within 24 hours. Please access Manage Account for final order details.

This is not an invoice. Please go to manage account to access your order history and invoices.

CUSTOMER INFORMATION

Payment by invoice: You can cancel your order until the invoice is generated by contacting customer service.

Billing Address

Ms. FEMINA CHERUMANNIL
Farook College
Farook College
Kozhikode, Kerala 673632
India

+91 9995990602
femi.fana@gmail.com

Customer Location

Ms. FEMINA CHERUMANNIL
Farook College
Farook College
Kozhikode, Kerala 673632
India

PO Number (optional)

N/A

Payment options

Invoice

PENDING ORDER CONFIRMATION

Confirmation Number: Pending

Order Date: 18-Sep-2025

1. Journal of materials chemistry. C, Materials for optical and electronic devices

0.00 USD

Article: Stimuli-responsive chiral aggregation-induced emission luminogens and their circularly polarized luminescence †

Order License ID	Pending	**Publisher**	Royal Society of Chemistry
ISSN	2050-7534	**Portion**	Image/photo/illustration
Type of Use	Republish in a thesis/dissertation		

LICENSED CONTENT

Publication Title	Journal of materials chemistry. C, Materials for optical and electronic devices	**Publication Type**	e-Journal
Article Title	Stimuli-responsive chiral aggregation-induced emission luminogens and their circularly polarized luminescence †	**Start Page**	19140
		End Page	19147
		Issue	47
		Volume	12
Author / Editor	Royal Society of Chemistry (Great Britain)	**URL**	http://pubs.rsc.org/en/journals/journalissues/tc#
Date	01/01/2013		
Language	English		
Country	United Kingdom of Great Britain and Northern Ireland		
Rightsholder	Royal Society of Chemistry		

REQUEST DETAILS

Portion Type	Image/photo/illustration	**Distribution**	Worldwide
Number of Images / Photos / Illustrations	1	**Translation**	Original language of publication
		Copies for the Disabled?	No
Format (select all that apply)	Print, Electronic	**Minor Editing Privileges?**	No
Who Will Republish the Content?	Academic institution	**Incidental Promotional Use?**	No
Duration of Use	Life of current edition	**Currency**	USD
Lifetime Unit Quantity	Up to 499		
Rights Requested	Main product		

NEW WORK DETAILS

Title	Experimental and Theoretical Investigation of Optical Properties on Cyanostyrene Based Donor-Acceptor Systems	**Institution Name**	Farook College
		Expected Presentation Date	2025-09-22
Instructor Name	Dr. Reji Thomas		

ADDITIONAL DETAILS

Order Reference Number	N/A	**The Requesting Person / Organization to Appear on the License**	Femina C

REQUESTED CONTENT DETAILS

Title, Description or Numeric Reference of the Portion(s)	Figure 1.12	**Title of the Article / Chapter the Portion Is From**	Stimuli-responsive chiral aggregation-induced emission luminogens and their circularly polarized luminescence †
Editor of Portion(s)	Liang, Junhao; Fu, Shiwei; Wu, Qi; Wang, Pengbo; Liu, Xiaoqing; Wang, Lei; Liu, Yi		

Volume / Edition	12	Author of Portion(s)	Liang, Junhao; Fu, Shiwei; Wu, Qi; Wang, Pengbo; Liu, Xiaoqing; Wang, Lei; Liu, Yi
Page or Page Range of Portion	19140-19147	Issue, if Republishing an Article From a Serial	47
		Publication Date of Portion	2024-12-05

Total Items: 1

Total Due: 0.00 USD

Accepted: Marketplace Permissions General Terms and Conditions and any applicable Publisher Terms and Conditions

JOHN WILEY AND SONS LICENSE
TERMS AND CONDITIONS

Sep 17, 2025

This Agreement between Femina C ("You") and John Wiley and Sons ("John Wiley and Sons") consists of your license details and the terms and conditions provided by John Wiley and Sons and Copyright Clearance Center.

License Number	6111491208349
License date	Sep 17, 2025
Licensed Content Publisher	John Wiley and Sons
Licensed Content Publication	ChemPhotoChem
Licensed Content Title	Tuning Electronic Structures of Carbazole-Cyanostyrene Molecules to Achieve Dual-State Emission for Trace Water Analysis, Picric Acid Sensing, and Reversible Mechanofluorochromism
Licensed Content Author	Jie Xue, Fang Tang, Chengyuan Wang, et al
Licensed Content Date	Sep 27, 2022
Licensed Content Volume	6
Licensed Content Issue	12
Licensed Content Pages	12
Type of use	Dissertation/Thesis
Requestor type	University/Academic
Format	Print and electronic
Portion	Figure/table
Number of figures/tables	1
Will you be translating?	No
Title of new work	Experimental and Theoretical Investigation of Optical Properties on Cyanostyrene Based Donor-Acceptor Systems
Institution name	Farook College
Expected presentation date	Sep 2025
Portions	1.14
The Requesting Person / Organization to Appear on the License	Femina C
Requestor Location	Ms. FEMINA CHERUMANNIL Farook College Kozhikode, Kerala 673632 India
Publisher Tax ID	EU826007151
Total	0.00 USD
Terms and Conditions	

- The failure of either party to enforce any term or condition of this Agreement shall not constitute a waiver of either party's right to enforce each and every term and condition of this Agreement. No breach under this agreement shall be deemed waived or excused by either party unless such waiver or consent is in writing signed by the party granting such waiver or consent. The waiver by or consent of a party to a breach of any provision of this Agreement shall not operate or be construed as a waiver of or consent to any other or subsequent breach by such other party.

- This Agreement may not be assigned (including by operation of law or otherwise) by you without WILEY's prior written consent.

- Any fee required for this permission shall be non-refundable after thirty (30) days from receipt by the CCC.

- These terms and conditions together with CCC's Billing and Payment terms and conditions (which are incorporated herein) form the entire agreement between you and WILEY concerning this licensing transaction and (in the absence of fraud) supersedes all prior agreements and representations of the parties, oral or written. This Agreement may not be amended except in writing signed by both parties. This Agreement shall be binding upon and inure to the benefit of the parties' successors, legal representatives, and authorized assigns.

- In the event of any conflict between your obligations established by these terms and conditions and those established by CCC's Billing and Payment terms and conditions, these terms and conditions shall prevail.

- WILEY expressly reserves all rights not specifically granted in the combination of (i) the license details provided by you and accepted in the course of this licensing transaction, (ii) these terms and conditions and (iii) CCC's Billing and Payment terms and conditions.

- This Agreement will be void if the Type of Use, Format, Circulation, or Requestor Type was misrepresented during the licensing process.

- This Agreement shall be governed by and construed in accordance with the laws of the State of New York, USA, without regards to such state's conflict of law rules. Any legal action, suit or proceeding arising out of or relating to these Terms and Conditions or the breach thereof shall be instituted in a court of competent jurisdiction in New York County in the State of New York in the United States of America and each party hereby consents and submits to the personal jurisdiction of such court, waives any objection to venue in such court and consents to service of process by registered or certified mail, return receipt requested, at the last known address of such party.

WILEY OPEN ACCESS TERMS AND CONDITIONS

Wiley Publishes Open Access Articles in fully Open Access Journals and in Subscription journals offering Online Open. Although most of the fully Open Access journals publish open access articles under the terms of the Creative Commons Attribution (CC BY) License only, the subscription journals and a few of the Open Access Journals offer a choice of Creative Commons Licenses. The license type is clearly identified on the article.

The Creative Commons Attribution License

The Creative Commons Attribution License (CC-BY) allows users to copy, distribute and transmit an article, adapt the article and make commercial use of the article. The CC-BY license permits commercial and non-

Creative Commons Attribution Non-Commercial License

The Creative Commons Attribution Non-Commercial (CC-BY-NC)License permits use, distribution and reproduction in any medium, provided the original work is properly cited and is not used for commercial purposes.(see below)

Creative Commons Attribution-Non-Commercial-NoDerivs License

The Creative Commons Attribution Non-Commercial-NoDerivs License (CC-BY-NC-ND) permits use, distribution and reproduction in any medium, provided the original work is properly cited, is not used for commercial purposes and no modifications or adaptations are made. (see below)

Use by commercial "for-profit" organizations

Use of Wiley Open Access articles for commercial, promotional, or marketing purposes requires further explicit permission from Wiley and will be subject to a fee.

Further details can be found on Wiley Online Library
http://olabout.wiley.com/WileyCDA/Section/id-410895.html

Other Terms and Conditions:

v1.10 Last updated September 2015

Questions? customercare@copyright.com.